UNIVERSIDAD DE CHILE
FACULTAD DE CIENCIAS FÍSICAS Y MATEMÁTICAS
DEPARTAMENTO DE GEOLOGÍA

INSIGHTS INTO THE TECTONOSTRATIGRAPHIC EVOLUTION OF THE SOUTHERN MAGALLANES BASIN, SOUTHERN CHILE, DURING THE CENOZOIC

TESIS PARA OPTAR AL GRADO DE MAGÍSTER EN CIENCIAS
MENCIÓN GEOLOGÍA

HUBER ALBERTO RIVERA ROSADO

PROFESOR GUÍA:
Dr. JACOBUS LE ROUX

MIEMBROS DE LA COMISIÓN:
Dr. MARCELO FARÍAS THIERS
Dr. REYNALDO CHARRIER GONZÁLEZ

Proyecto Fondecyt 1130006: Tertiary Successions in Chile

SANTIAGO DE CHILE
2017

RESUMEN DE LA TESIS PARA OPTAR AL TÍTULO DE: MAGÍSTER EN CIENCIAS, MENCIÓN GEOLOGÍA
POR: HUBER ALBERTO RIVERA ROSADO
FECHA: 19/04/2017
PROFESOR GUÍA: Dr. JACOBUS LE ROUX

INSIGHTS INTO THE TECTONOSTRATIGRAPHIC EVOLUTION OF THE SOUTHERN MAGALLANES BASIN, SOUTHERN CHILE, DURING THE CENOZOIC

El relleno sedimentario de las cuencas de antepaís, es uno de los más usados y efectivos registros disponibles para comprender la dinámica de los frentes cordilleranos adyacentes y los diferentes procesos evolutivos ocurridos en los márgenes de placas convergentes. En éste sentido, la cuenca Magallanes (51°15”S y 53°39”S) ofrece una oportunidad única para evaluar >48 Ma de la historia tectónica de los Andes Sur-Patagónicos, arrojar luz sobre el marco temporal de la progradación de la deformación del frente orogénico y su relación con el estilo de relleno estratigráfico y patrón de dispersión de los sedimentos durante el Cenozoico. Por lo tanto, esta tesis examina la configuración y evolución tectono-estratigráfica de la cuenca de antepaís de retroarco cenozoica de Magallanes, resaltando la interacción entre los procesos tectónicos y sedimentarios, especialmente en una cuenca donde descifrar la evolución sedimentaria puede ser desafiante, dada la dificultad de afloramientos con buena preservación de la estratigrafía, por su complejidad en términos de configuración de placas tectónicas y por la alta variabilidad de eventos tectónicos ocurridos a lo largo del tiempo que han dejado su legado en el registro estratigráfico. Mediante la aplicación de diversas técnicas y herramientas como el análisis de facies a partir de información sedimentológica de afloramientos, estratigrafía física, bioestratigrafía, petrología sedimentaria y geocronología U-Pb en circón detrítico, se pretende obtener un mejor entendimiento de la evolución de los ambientes sedimentarios y su contexto paleogeográfico, los controles o mecanismos de depositación, entender las variaciones de la dispersión de los sedimentos a gran escala y establecer las bases para futuros análisis estratigráficos secuenciales a escala de afloramientos. La problemática abordada, la hipótesis de trabajo y la metodología empleada son presentadas en el capítulo I de la presente tesis, posteriormente en el capítulo II, se realiza una revisión y síntesis de la literatura previamente publicada respecto a la evolución geológica cenozoica de la cuenca y además se propone un nuevo marco cronoestratigráfico y modelo sedimentológico evolutivo, resaltando la identificación de discordancias regionales y la relación a eventos tectónicos regionales y globales. El capítulo III provee una síntesis de las principales conclusiones de la investigación de las cuales vale resaltar que el inicio de la sedimentación en la cuenca de Magallanes durante el Cenozoico estuvo dominado por depositación turbidítica de aguas profundas durante el Paleoceno que durante el Eoceno dio lugar a un periodo de agradación hemipelágica que posteriormente se relevaría por sistemas deltaicos de margen de plataforma. Desde el Oligoceno los ambientes predominantes son continentales, los cuales perduraron hasta el Mioceno inferior. Cada uno de estos ciclos sedimentarios fue interrumpido por 5 discordancias regionales relacionadas a la reorganización de las placas tectónicas y dinámica de las dorsales oceánicas.

"El conocimiento geológico de una región o de un país depende casi exclusivamente de los investigadores; pero no olvidar, frente al progreso de la ciencia cada generación de éstos descansa sobre los hombros, en el esfuerzo y en el sacrificio, de toda generación anterior"

Dr. Juan Keidel (1877-1954)

A Dios este triunfo, porque sin ti nada en mí vida sería posible, gracias por la fortaleza y las abundantes bendiciones que me has obsequiado en este proceso.

A mis padres, Huber Rivera Lindarte y Ada Rosado Mendinueta. Gracias por conducirme por un camino lleno de valores, amor y temor a Dios.

AGRADECIMIENTOS

En primer lugar, quiero extender mi devoción y agradecimientos a Dios porque fue quien me dio la fortaleza y calma en momentos de adversidades, me guió durante todas las etapas de este proceso y me bendijo de múltiples formas aún sin merecerlo.

Agradezco a mis padres por su apoyo constante, a mis hermanas que son mi orgullo. Especial reconocimiento a mi abuela Magaly Mendinueta, a mi tía Nayibe Rosado y tío Edward, por su apoyo e interés en mí bienestar durante mi estadía en Chile. Al resto de mi familia por su apoyo constante y amor latente.

A Jacobus Le Roux, mi profesor guía, pero también mi ejemplo, mi amigo y mentor. Junto con su esposa, Petrysia Le Roux, han sido ángeles que Dios ha puesto en mi camino. Solamente tengo palabras de agradecimientos, admiración y respeto para ustedes.

A Marcelo Farías, por su confianza en mí trabajo y capacidades, también por su guía sobre aspectos tectónicos de esta tesis. Igualmente, a Reynaldo Charrier por su buena disposición, amabilidad e invaluables discusiones acerca de la cuenca. Quiero agradecer a cada una de las personas de Enap-Sipetrol que contribuyeron directa e indirectamente al desarrollo de la tesis: Lisandro Rojas, Jorge Arriagada, Pablo Mella, Jesús Pinto, Álvaro Pérez, Danilo González.

Agradezco la colaboración y paciencia de Maritza Acuña en lo relacionado al Magíster. Agradezco a la Escuela de Postgrados de la FCFM por la beca arancelaria para cursar mis estudios. Asimismo, extiendo mis agradecimientos al Proyecto Fondecyt 1130006 por el soporte económico para el desarrollo de la tesis.

A mis amigos en Chile, especialmente a Mauricio Gutiérrez, Viviana Pedroza por su apoyo y guía al momento de aterrizar en tierras australes; a mis compadres Andrés Aguilar y William Nader por los buenos momentos, buenas charlas, pateadas (pichangas), compañía y apoyo mutuo. Agradecimientos especiales a mis compañeros de oficina, pichangas y amigos (o conocidos) en general de la uchile, por hacer más ameno y agradable la estadía: Camila Arróspide, Lissett Celle, Sebastián Herrera, Sebastián Bascuñán, Matías (Ataxia), David Calixto, Roberto Valles, Matías Taucare, Javier (Estrella), Manu García, Alejandra Serey, Benjamín Bahamondes, Pablo Molina y a Carla Barbosa por su ayuda en cosas varias de la tesis.

Finalmente, pero no menos importante, quiero resaltar y expresar mis agradecimientos a Katherine Sánchez, no sólo por su compañía, amor, comprensión, apoyo constante y por ser uno de los motores de mi vida, sino también por brindarme toda su colaboración en las jornadas de terreno y cuidar de mí en todo momento. Eres otro de los ángeles que Dios ha puesto en mi vida y mi camino (I Lava U).

TABLA DE CONTENIDO

INDICE DE TABLAS

INDICE DE ILUSTRACIONES

CAPÍTULO I

CAPÍTULO II

CAPÍTULO I.

INTRODUCCIÓN

1.1 Presentación y estructuración de la tesis

La presente tesis de Maestría persigue como finalidad, una mejor comprensión de la relación existente entre la orogénesis de los Andes Patagónicos y los procesos sedimentarios que dieron lugar al relleno o historia evolutiva de la cuenca de Magallanes-Austral durante el Cenozoico, en la XII Región de Magallanes y la Antártica Chilena, entre los 51°15”S y 53°39”S (Fig. 1.1b). Así pues, se investiga la configuración y la evolución tectono-estratigráfica de la cuenca de antepaís de retroarco, abarcando aspectos que han sido objeto de intenso estudio en las ciencias de la tierra, como los análisis evolutivos de rellenos de cuencas ligadas a orógenos, periodicidad de propagación del frente de deformación orogénico y la respuesta sedimentaria al mismo, basados en técnicas interdisciplinares como la sedimentología de afloramientos, estratigrafía física y secuencial, petrología sedimentaria y geocronología U-Pb en circón detrítico.

La tesis está basada en *papers* y se estructura en tres capítulos. El Capítulo I, introduce al lector en los aspectos concernientes a la motivación de la investigación y a la problemática del estudio, además presenta la hipótesis de investigación, los objetivos y la metodología planteada para alcanzarlos.

El Capítulo II, presenta una revisión y síntesis de la literatura previamente publicada acerca de la evolución geológica de la cuenca de Magallanes-Austral durante el Cenozoico, complementada con datos propios sedimentológicos y geocronológicos con el fin de interpretar los ambientes sedimentarios, calcular las edades máximas de depositación (MDA), identificar discordancias regionales, proponer un nuevo marco cronoestratigráfico y modelo sedimentológico evolutivo de la cuenca que permita resaltar la interacción entre el crecimiento de los Andes Patagónicos y la configuración de la

cuenca y su relleno sedimentario. El trabajo presentado en el Capítulo II ha sido sometido para publicación en *Earth-Science Reviews* (Rivera et al., en revisión).

El Capítulo III, provee una síntesis de cada capítulo de la tesis, resaltando las principales conclusiones del trabajo y además plantea algunas preguntas científicas que aún faltan por resolver y que han surgido a partir de la presente investigación, dando una breve dirección de cómo deberían ser abordadas.

Finalmente, en la sección de Anexos, se encuentra el material suplementario del artículo del Capítulo II, el cual consta de los datos analíticos y la estimación de las edades máximas de depositación (MDA) de cada una de las dataciones U-Pb en circón detrítico (Anexo A1 y A2), adicionalmente se adjunta la información batimétrica de cada uno de los foraminíferos bentónicos registrados en las formaciones estudiadas del Cenozoico en la Cuenca de Magallanes-Austral (Anexo B1). El Anexo C1 y C2, se relaciona a publicaciones como co-autor en la cuenca de Magallanes-Austral y a publicaciones de resúmenes en Congresos, respectivamente.

1.2 Motivación y Formulación del Problema

El entendimiento de la evolución tectónica de la Cuenca de Magallanes-Austral, ha sido un tópico que por más de 6 décadas ha interesado a geocientíficos alrededor del mundo, dado su origen estrechamente vinculado con la ruptura de Gondwana a comienzos del Jurásico, cuya fase extensional habría desarrollado una cuenca marginal de corteza oceánica (Cuenca de Rocas Verdes) hacia el extremo SSO de Sudamérica a finales del Jurásico e inicios del Cretácico (Katz, 1963; Dalziel, et al., 1974; Suárez y Pettigrew, 1976; Suárez, 1977; Bruhn, et al., 1978; Stern, et al., 1992; Pankhurst, et al., 2000). El cierre de dicha cuenca en el Cretácico medio-tardío permitió la formación de la Cuenca de Magallanes-Austral y marca el inicio del alzamiento de la Cordillera Patagónica en el extremo sur del continente (Wilson, 1991; Fildani y Hessler, 2005, Mpodozis y Rojas, 2006).

Es indudable que el estudio de la evolución de la cuenca de Magallanes-Austral, especialmente durante el Cenozoico, provee una oportunidad única para evaluar la historia tectónica de la Cordillera Patagónica y a su vez constreñir el tiempo de ocurrencia de otros eventos tectónicos de primer orden relacionados a la dinámica de subducción

entre placas litosféricas, que no solo condicionan la arquitectura tectónica de los Andes Patagónicos, sino que controlan procesos climáticos de significancia más global con una influencia muy acentuada en todas las formas de vida. Los principales eventos en orden cronológico de ocurrencia son: (1) la colisión y subducción de la dorsal oceánica sísmica Farallón-Aluk durante el Paleógeno (Cande y Leslie, 1986); (2) la apertura del pasaje Drake a fines del Eoceno, lo cual permitió la iniciación de la corriente circumpolar Antártica, la que a su vez aisló a la Antártida de la afluencia de corrientes cálidas intensificando su glaciación (Barker y Burrell, 1977; Barker, 2001; Barker y Thomas, 2004; Le Roux, 2012b); (3) la ruptura de la placa Farallón a finales del Oligoceno (Herron y Heirtzler, 1967); (4) la colisión y subducción de la dorsal sísmica de Chile durante el Mioceno temprano (Malumián y Ramos, 1984; Cande y Leslie, 1986) y (5) el establecimiento de una sombra de lluvia en la Patagonia en respuesta a la elevación de los Andes Patagónicos, a partir de los 16 Ma (Blisniuk et al., 2005).

Desde el punto de vista económico, la Cuenca de Magallanes-Austral alberga importantes reservas de hidrocarburos convencionales, de las cuales más de 6.5 BBOE (Billones de Barriles Equivalentes de Petróleo) han sido extraídos en Argentina (Belotti et al., 2013) y 5.9 BBOE en la porción Chilena (Enap-Cifras del Negocio 2016) mediante la explotación de la Formación Springhill (Cretácico inferior), principal reservorio convencional de la cuenca. Así mismo, posee gran potencial de recursos de hidrocarburos no convencionales (tight gas) en la denominada informalmente “Zona Glauconítica” que comprende la sucesión transgresiva de areniscas y limolitas ricas en glauconita (Zurita et al., 2013) del Maastrichtiano tardío a Eoceno temprano, alcanzando recursos de hasta 8.3 BCFG (billones de pies cúbicos de gas) y 83 MMBNGL (millones de barriles de gas natural líquido) aunque con una gran incertidumbre geológica asociada (Schenk et al., 2016).

A pesar de la reconocida importancia de la Cuenca de Magallanes-Austral y la información que pueden proveer las rocas del Cenozoico acerca de la evolución de la Cordillera Patagónica – entre otros tópicos –, existe una evidente escasez de trabajos científicos dentro de la porción Chilena de la cuenca enfocados en la evolución sedimentaria durante el cenozoico. La mayoría de los estudios que se han efectuado, se concentran en Argentina y en la Provincia de Última Esperanza en Chile, mientras que en la Provincia de Magallanes (Skyring-Península Brunswick) destacan los trabajos

pioneros de Felsch (1912), Bonarelli (1917), Decat y Pomeyrol (1931), Keidel y Hemmer (1931), Hemmer (1935), Ruby (1945), Barwick (1949), Kniker (1949), Thomas (1949), González (1952), Todd y Kniker (1952), von Goetsche (1953), Robles y Gómez (1956), Martínez-Pardo et al. (1965), Charrier y Lahsen (1969), Fasola (1969), Lahsen y Charrier (1972), Natland et al. (1974), Cañón y Ernst (1975) cuya vocación fue hacia la formalización de la estratigrafía, determinación de su edad a partir de micropaleontología con énfasis en la búsqueda de recursos petrolíferos, pero que bien hoy constituyen las bases sobre las que descansan los pocos trabajos que tratan acerca de la interpretación de ambientes y evolución tectono-estratigráfica de la cuenca durante el cenozoico, i.e. Biddle et al. (1986), Mella (2001) Mpodozis et al. (2011), Otero et al. (2012) y este trabajo. Lo anterior, conduce a un conocimiento limitado de su evolución y la posiciona como una de las áreas peor conocidas de Sudamérica en términos evolutivos y en cuanto al levantamiento de los Andes (Fildani y Hessler, 2005). De este modo, es común encontrar diversas nomenclaturas estratigráficas con erróneas definiciones en cuanto a descripciones litológicas, relaciones estratigráficas, edades y ambientes depositacionales, que en conjunto dificulta establecer acertadas correlaciones lito- y cronoestratigráficas entre formaciones coetáneas a ambos lados de la cuenca (Argentina y Chile) y comprender de una mejor forma la variación espacial de facies. Este hecho cobra mayor importancia, si se piensa en una integración del conocimiento a nivel más local entre las diferentes provincias Chilenas que conforman la cuenca, donde además se ve impedida la integración entre la geología de superficie y la del subsuelo, incidiendo directamente en los aspectos energéticos de la región.

Aunque los trabajos micropaleontológicos de Natland et al. (1974) y Cañón y Ernst (1975), intentaban establecer correlaciones estratigráficas, estas fueron de uso muy limitado debido a su baja resolución estratigráfica y ausencia del reconocimiento de discontinuidades (Malumián et al., 2013), además de los problemas inherentes que supone la notable ausencia de foraminíferos planctónicos en los sedimentos cenozoicos en la cuenca de Magallanes-Austral, lo que dificulta las correlaciones y asignación de edades tanto en la parte chilena como en la argentina (Herm, 1966; Cañón y Ernst, 1975; Malumián, 1993). Lo anterior, establece una arista más a la problemática estratigráfica resultando necesario la búsqueda de otros métodos de datación para las unidades

geológicas terciarias de la cuenca, que no sólo permita una asignación más precisa de la edad, sino también la identificación de discordancias de carácter regional.

Recientemente, el interés suscitado por tratar de entender la evolución del levantamiento de los Andes Patagónicos durante el cenozoico sin perder de vista los subsecuentes ciclos de relleno de la cuenca de Magallanes-Austral, ha motivado investigaciones mayormente abocadas a la parte norte de la cuenca (Provincia de Última Esperanza en Chile y sector de Lago Argentino en Argentina) (Fig. 1.1b), y a la parte más sur (costa atlántica de Tierra del Fuego en Argentina), permaneciendo la parte central de la cuenca (Provincia de Magallanes y Tierra del Fuego) con un conocimiento más limitado. Estos trabajos son los de Olivero y Malumián (1999), Olivero y Martinioni (2001), Ghiglione y Ramos (2005), Olivero et al. (2003), Hervé (2005), Olivero y Malumián (2008), Ponce et al. (2008), Torres-Carbonell et al. (2008a), Barbeau Jr. et al. (2009), Torres-Carbonell et al. (2009), Sánchez et al. (2010), Le Roux (2010), Mpodozis et al. (2011), Cuitiño et al. (2013a), Fosdick et al. (2015a), Ghiglione (2015), Ghiglione et al. (2016), Gutiérrez et al. (2017) y Rivera et al. (en revisión), los cuales han contribuido a establecer modelos sedimentarios más completos incluyendo aspectos de paleoambientes, proveniencia, correlaciones y edad de depositación, mientras que otros autores paralelamente han trabajado en temas más orientados a la paleontología, bioestratigrafía e icnología como Quatrocchio (2009), Malumián y Jannou (2010), Otero et al. (2012), Pearson et al. (2012), Bostelman et al. (2013), Malumián et al. (2013), Carrillo-Berumen et al. (2013) y Cuitiño et al. (2013b, 2016). No obstante a los importantes avances, la configuración exacta de la cuenca, el patrón de dispersión de los sedimentos derivados de los Andes Patagónicos y las correlaciones estratigráficas así como variaciones de facies a lo largo de la cuenca aún es muy incierta, inhibiendo el reconocimiento de las principales etapas evolutivas que ha experimentado la región más austral del continente Sudamericano.

1.3 Localización del área de estudio

La Cuenca de Magallanes-Austral es una cuenca de antepaís de retroarco que se encuentra ubicada en el extremo sur de Sudamérica, limitada al oeste por la faja plegada y corrida de la Cordillera Patagónica Austral (porción sur de la cordillera de los Andes); hacia el norte y este, por el arco de Río Chico-Dungeness; en el sudeste se fusiona con

la cuenca de las Malvinas (Fig. 1.1a). Posee una extensión de 230.000 Km^2 y puede ser dividida en cuatro áreas bien diferenciadas estratigráficamente, como se enumeran a continuación (Malumián et al., 2013): 1). Corresponde a la costa Atlántica Fueguina; 2). La región Fueguina de Chile; 3). Península de Brunswick e Isla Riesco; 4). El área de Ultima Esperanza- Rio Turbio.

El área de estudio del proyecto comprende la tercera y cuarta región estratigráfica de la cuenca dentro del límite político chileno, entre los 51°15”S y 53°09”S en la XII Región de Magallanes y la Antártica Chilena. Los trabajos de terreno se desarrollan principalmente en el monoclinal frontal entre Cerro Castillo, perteneciente a la Provincia de Última Esperanza, y en las zonas circundantes a Punta Arenas incluyendo los Cerros Palomares (Fig. 1.1b), pertenecientes a la Provincia de Magallanes. La localidad de Cerro Castillo (Fig. 1.1b), representa la sección donde se levantó información del Cretácico Superior, mientras que las secciones de Península Brunswick y costa norte de Seno Skyring-Isla Riesco (Fig. 1.1b), se levantó la información sedimentológica y estratigráfica correspondiente a la sucesión del Paleógeno-Neógeno y donde se concentran la mayoría de muestras para dataciones U-Pb en circón detrítico.

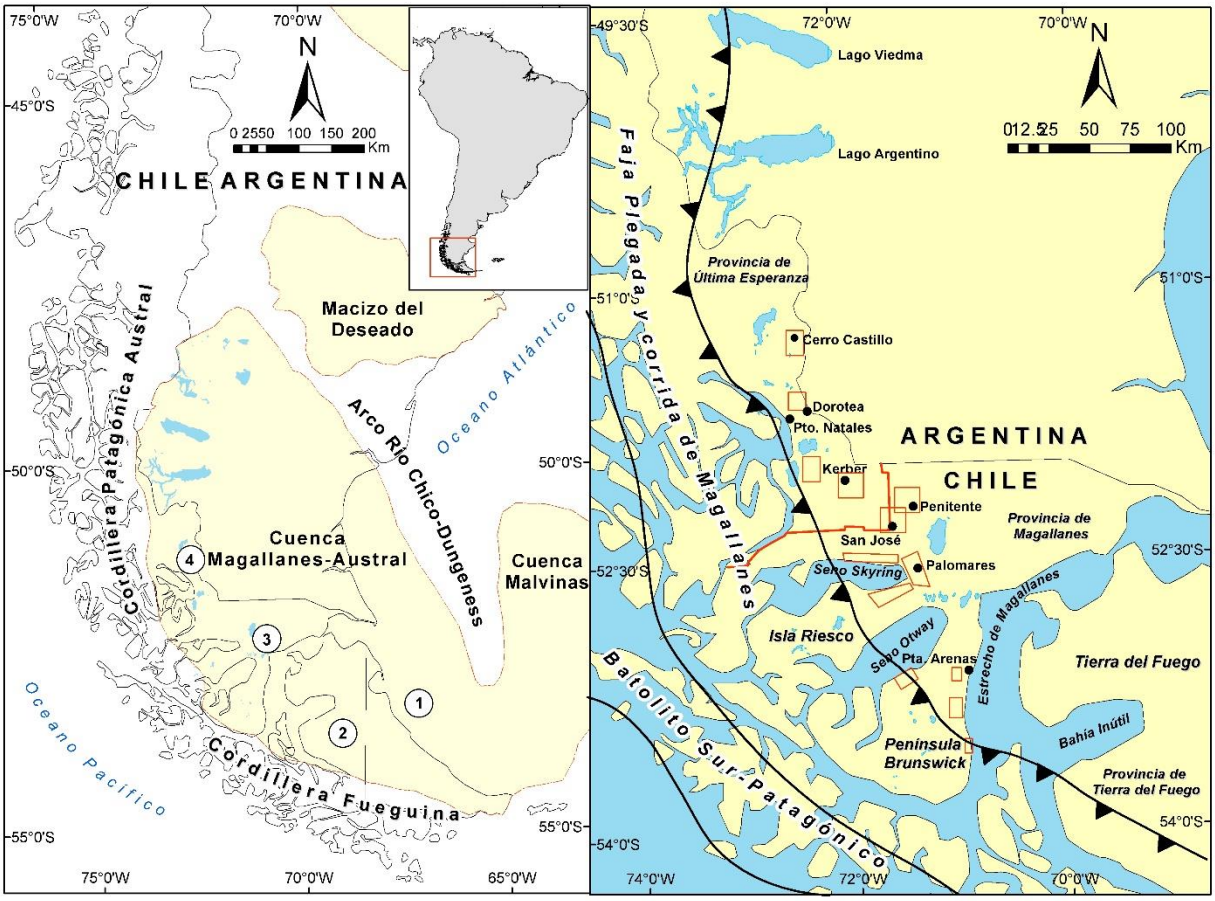

Figura 1.1 Localización geográfica de la Cuenca de Magallanes-Austral y de las secciones estratigráficas estudiadas (área de estudio) indicado por recuadros rojos. La numeración corresponde a las 4 zonas estratigráficas diferenciadas.

1.4 Hipótesis de trabajo y Objetivos del estudio

1.4.1 Hipótesis

Los rellenos sedimentarios de cuencas de antepaís han sido por mucho tiempo usados para inferir la paleogeografía y evolución del dinámico cinturón orogénico adyacente (e.g. Dickinson y Suczek, 1979; Schwab, 1986; Jordan et al., 1988; Jordan 1995; Bayona et al., 2008). De este modo, conocer la evolución sedimentaria de la cuenca de Magallanes-Austral, interpretar los mecanismos de relleno y los controles en el patrón de dispersión de sedimentos durante el Cenozoico, permitirá inferir los cambios y procesos evolutivos de las fuentes de proveniencia en las áreas emergidas de la faja plegada y corrida de Magallanes.

La poca deformación tectónica de las rocas cenozoicas en el área estudiada, manifestada en los suaves pliegues de gran amplitud permitirán registrar sin mayor

complicación las sucesiones verticales de facies existentes que conducirá a interpretar los eventos sedimentarios a los cuales ha estado sometida la cuenca, incluyendo la identificación y génesis de las diversas discontinuidades que autores como Ghiglione et al., (2011) y Malumián et al., (2013) mencionan por lo menos para la sucesión Paleógena.

Como es normal desde el punto de vista sedimentológico, cambios en altura de los relieves impactarán en los flujos de corrientes de sedimentación de una cuenca (Bossi et al., 2000), en éste orden de ideas, la interpretación detallada de los ambientes sedimentarios y el análisis de cómo éstos variaron a lo largo del tiempo, permitirá dilucidar los eventos tectónicos que influyeron en el momento de su sedimentación, resaltando la inherente relación entre los procesos sedimentarios y el levantamiento de los Andes que dieron lugar a la sucesión cenozoica.

La nueva información sedimentológica y las relaciones estratigráficas que se establezcan entre las unidades cenozoicas dentro del lado Chileno de la cuenca, permitirá comprender mejor cómo se relacionan con las unidades equivalentes del lado argentino, facilitando el establecimiento de cartas cronoestratigráficas bien fundamentadas y la correlación de formaciones tanto en superficie como en subsuelo. Lo anterior, consecuentemente contribuirá a documentar de manera más fehaciente los procesos tectono-sedimentarios de la cuenca y a establecer su vínculo con el frente orogénico en el mejor de los casos. En adición, el estudio cuidadoso y de alta resolución sedimentológica alcanzará finalmente el objetivo de establecer secuencias sedimentarias de bajo rango (Alta frecuencia e.g: 3^{er} – 5^{to} orden) complementando y detallando de mejor manera las megasecuencias de 1^{er} orden propuesta por Mpodozis, et al., (2011).

1.4.2 Objetivos generales

Evaluar la relación existente entre los mecanismos y estilo de relleno del depocentro (foredeep) y la dinámica de los bloques alzados dentro de la faja plegada y corrida adyacente de la cuenca de antepaís Magallanes-Austral (51°15” S – 53°09”S) durante el Cenozoico.

1.4.3 Objetivos específicos

1. Establecer la relación existente entre la evolución sedimentaria de la cuenca y las posibles etapas orogénicas de los Andes Sur-Patagónicos, definiendo a una escala más detallada la cronología de la deformación.
2. Esclarecer las relaciones estratigráficas entre las unidades geológicas del Cenozoico y aportar en la formalización de la estratigrafía.
3. Interpretar los ambientes de depositación y el modelo arquitectural de cada una de las unidades geológicas estudiadas.
4. Evaluar preliminarmente las diferentes áreas de proveniencia sedimentaria e interpretar los controles en el patrón de dispersión de los sedimentos.
5. Definir un cuadro cronoestratigráfico con mayor resolución estratigráfica, destacando las principales discordancias regionales durante el Cenozoico a partir de dataciones U-Pb en circón detrítico e información bioestratigráfica.
6. Proveer un contexto paleogeográfico a escala de cuenca y establecer las bases para un posterior desarrollo de un modelo de estratigrafía secuencial predictivo.

1.5 Metodología de la investigación

El desarrollo del proyecto consta de tres fases o etapas, las cuales se plantearon de esta manera con el fin de realizar un trabajo bien estructurado, óptimo y sistemático que permita reducir los riesgos a pérdidas de información y contratiempos. A continuación se presenta una breve descripción:

Fase I. Preliminar de Gabinete. Esta fase cumplió con el propósito de realizar una síntesis de la información existente principalmente con base a información pública como artículos científicos, tesis de maestría, trabajos de pregrado, trabajos inéditos, dataciones radiométricas previas, información micropaleontológica (anexo 2), obtención de planos topográficos y mapas geológicos del área estudiada. El objeto de esta síntesis fue el de conocer a grandes rasgos la geología regional de la zona de estudio y tener una idea clara acerca del estado del arte de las investigaciones en la cuenca. De manera simultánea durante ésta etapa, se desarrolló un Scouting del área con una duración de 8 días en el mes de Enero de 2015, donde se colectaron 10 muestras de roca para datación U-Pb en circón detrítico y elaboración de secciones delgadas,

adicionalmente se establecieron la ubicación de secciones estratigráficas para el posterior levantamiento a detalle durante la etapa de terreno y se solicitaron los permisos correspondientes para el acceso a los fundos donde se localizaban los mejores afloramientos.

Fase II. Pre-terreno y Terreno. La fase de pre-terreno consistió en la preparación del mapa geológico preliminar a escala 1:100.000 a partir de fotografías aéreas a escala 1:70.000, modelos digitales de terreno de 30m de resolución espacial e imágenes satelitales y además se realizó la descripción de las secciones delgadas de las muestras colectadas durante el Scouting. La etapa de terreno propiamente, tuvo una duración de 28 días realizada en el mes de enero de 2016, en esta fase se realizó el levantamiento de 16 secciones estratigráficas la cual se vio parcialmente dificultada por la espesa cobertura vegetal, por los afloramientos aislados y de difícil acceso y por el importante relleno de sedimentos glaciaricos y post-glaciaricos que obliteran la geología cenozoica de nuestro interés, sin embargo, la descripción de las secciones y sus perfiles sedimentológicos se realizó a detalle (cm/dm) con el bastón de Jacob en donde los afloramiento eran de mejor calidad y con cinta y brújula en los afloramientos más complejos, en todos los casos identificando estructuras sedimentarias, geometrías de los litosomas, contactos y contenido fósil e icnológico y medición de paleocorrientes. En determinadas zonas de interés, se colectaron muestras de rocas para dataciones y análisis petrográficos, además de fósiles para una identificación más precisa.

Fase III. Análisis e Interpretación de la Información. Esta fase consistió en el procesamiento y análisis de toda la información levantada en terreno, digitalización de columnas estratigráficas, identificación de fósiles, elaboración de ilustraciones, análisis de facies, definición y asociaciones de facies, interpretación de los ambientes de depósito de las asociaciones de facies, estratigrafía de secuencias (definición de ciclos y superficies limitantes), análisis de subsidencia. Paralelamente, se realizaron 9 dataciones U-Pb en circón detrítico usando el método LA-MC-ICP-MS en el Departamento de Geología de la Universidad de Chile y en el Sernageomin, previamente separadas y concentradas en el laboratorio de preparación de muestras del Departamento de Geología de la Universidad de Chile, una vez obtenidos los resultados se procedió a calcular las edades máximas de depositación (MDA) cuyos resultados

analíticos se presentan en el anexo 1. Finalmente se realizó la integración de toda la información previamente descrita en el informe final de tesis.

CAPÍTULO II.

SEDIMENTARY EVOLUTION OF THE CENOZOIC MAGALLANES-AUSTRAL FORELAND BASIN: IMPLICATIONS FOR PATAGONIAN ANDES OROGENY

ABSTRACT

The evolution of the Magallanes-Austral Basin records crucial information related to the break-up of Gondwana and the development of the Southern Patagonian Andes. Nevertheless, there has been a lack of adequate data and most of the literature concerning to Cenozoic deposits is outdated, so that there is still considerable controversy regarding the stratigraphic nomenclature, facies changes and evolutional history of the basin. We present a review of the published literature and our own sedimentological and geochronological studies of the Cenozoic deposits in the Chilean part of the Magallanes-Austral Basin to propose a new sedimentological model in which the onset of the Cenozoic foreland basin reached bathyal depths with prograding turbidite lobes (Chorrillo Chico Formation) during the Paleocene, followed by a second period of basin infill dominated by aggradation of (hemi-)pelagic sediments (Agua Fresca Formation) in the middle Eocene. This was succeeded by prograding and aggrading delta facies (Tres Brazos Formation) representing the establishment of a continental shelf system that prevailed until the Priabonian (Loreto Formation). Thereafter, a pulse of tectonic uplift between the

Oligocene and early Miocene, gave rise to continental conditions (Río Leona, El Salto and Palomares Formations), interrupted by periods of volcanic activity and tectonic events that caused the local emplacement of basalts. Five regional unconformities are recognized, related to an increase/decrease of mid-ocean ridge spreading rates, the opening of the Drake Passage, and mountain building. These events were manifested by five orogenic stages that are clearly reflected in the sedimentary system: (1) Between 68 – 56 Ma the basement domain was uplifted, which led to turbidite lobe progradation; (2) Between 43 – 42 Ma the previously deposited foreland strata were cannibalized; (3) Between 37.8 – 33.9 Ma the late Cretaceous volcanic arc was reactivated and the deformation front advanced eastward; (4) Between 26.4 – 19.6 Ma the most prominent growth of the Patagonian Andes wedge took place; (5) From 18 Ma collision of the Chilean Ridge beneath the South American Plate took place. This integrated assessment allows us, at least partially, to overcome the present lack of knowledge regarding the geological evolution and enhances our understanding of the basin configuration, providing valuable insights into the growth of the Patagonian Andes and its sedimentary response in the adjacent foreland basin.

Keywords: Patagonian Andes; Chilean Ridge; Drake Passage; Magallanes-Austral Basin; Sedimentary evolution.

2.1 Introduction

The tectonic evolution and infill of the Magallanes-Austral Basin of Chile and Argentina (Fig. 2.1) has been studied for more than 50 years by researchers from both academia and industry. These studies have focused on three approaches: (1) Economic, as the basin hosts important oil and gas resources, from which more than 6.5 billion BOE have been recovered in Argentina alone (Belotti et al., 2013). Most of the hydrocarbons are hosted by Cretaceous to early Tertiary strata, with the result that these successions have received most of the attention to date. However, other Cenozoic deposits also

constitute potential hosts. (2) Stratigraphy, paleontology and basin architecture, as it contains some of the best preserved outcrops in the world that allow study of deep-water turbidite systems and slope systems (including associated shelf-edge deltas) (Katz, 1963; Scott, 1966; Sohn, et al., 2002; Schultz et al., 2005; Crane and Lowe, 2008; Dott et al., 1982; Fildani et al., 2009; Hubbard et al., 2008; Hubbard et al., 2010; Covault et al., 2009; Romans et al., 2011; Schwartz and Graham, 2015; Beaubouef, 2004) also its paleontological heritage has a lower taxonomic diversity and controversial ages than same latitude counterparts but also reveals connections between the Antarctic and South America (Lahsen and Charrier, 1972; Crame, 1999; Reguero et al., 2002; Otero et al., 2012; Leppe et al., 2012) and because its architecture cannot be characterized by that of a classic foreland basin (Romans et al., 2010; Fosdick et al., 2014; Malkowski et al., 2017). (3) Plate tectonics, given that the basin origin was closely linked to the breakup of Gondwana in the Middle to Late Jurassic, resulting in an extensional backarc basin (Bruhn et al., 1978; Dalziel, 1981; Pankhurst et al., 2000; Fildani and Hessler, 2005; Klepeis et al., 2010; McAtamney et al., 2011; Malkowski et al., 2016). The latter gradually changed into a compressional retroarc foreland basin (Wilson, 1991). It is important to understand the post-Jurassic stratigraphic, sedimentological and tectonic setting of the Magallanes-Austral Basin, especially during the Late Cretaceous to Miocene, where a continuous stratigraphic record hosts critical information about the tectonic evolution and orogenic cycles of the Southern Patagonian Andes (Feruglio, 1949-50; Dessanti, 1972; Ramos, 1982).

Cenozoic strata in the Magallanes-Austral Basin have been investigated since the middle of the 19th Century, the best known early studies being those of d'Orbigny (1842), Darwin (1846), Hatcher (1897), Ameghino (1906) and Quensel (1911) which were focused mostly on the eastern part of Patagonia in Argentinian territory. The first attempts to formalize the stratigraphy of the basin were carried out by Felsch (1912), Bonarelli (1917), Decat and Pomeyrol (1931), Keidel and Hemmer (1931), Hemmer (1935), Fossa Mancini (1938), Ruby (1945), Barwick (1949) and Feruglio (1949-50), with the main objective to evaluate the hydrocarbon potential of the basin. These studies formed the basis of subsequent research by Thomas (1949) and Von Goetsche (1953), who established the stratigraphic subdivision for at least the Brunswick Peninsula and Skyring Sound. This was slightly modified by Cecioni (1955, 1957) and Katz (1961) (cf. Charrier and Lahsen,

1969). In the Penitente and Cordillera Vidal areas (Fig. 2.2), González (1953) also revised the earlier work of Keidel and Hemmer (1931). Likewise, important advances were reached in micropaleontology studies by Todd and Kniker (1952), Robles y Gómez (1956).

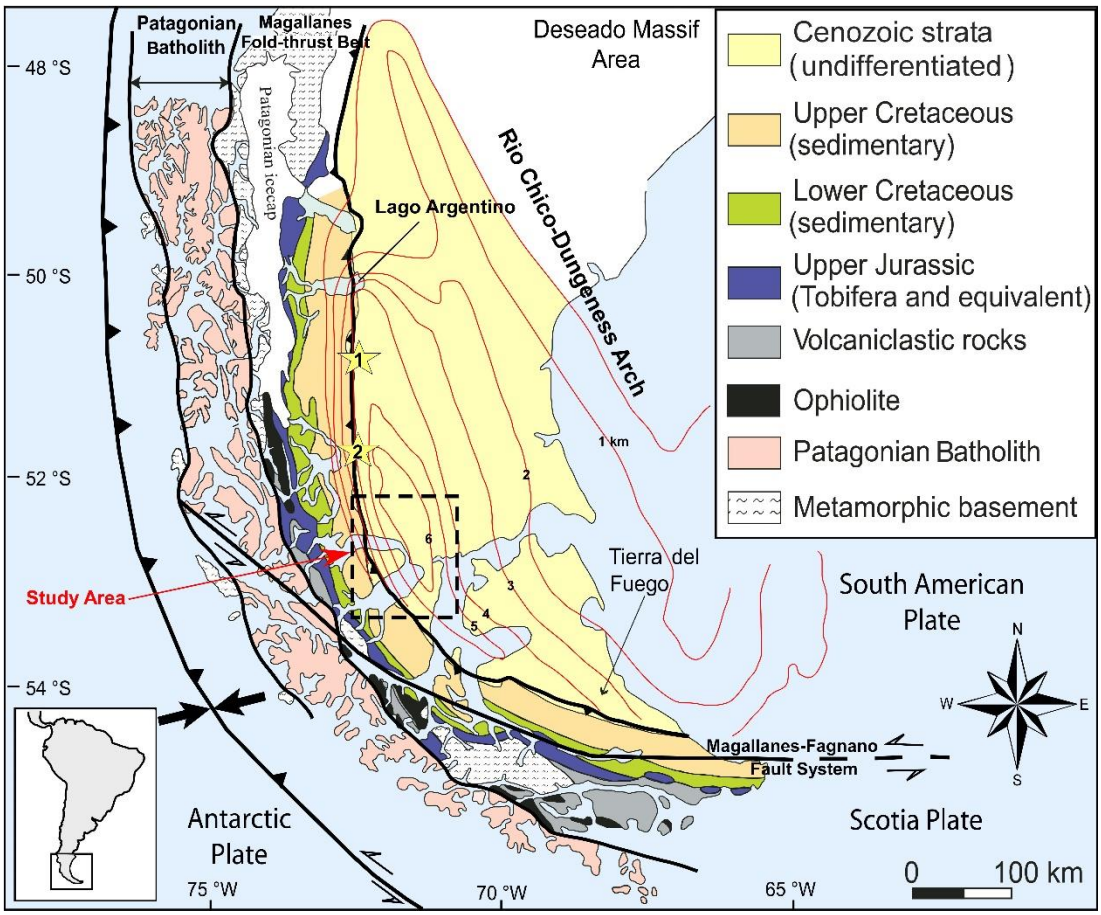

Figure 2. 1. Simplified morphotectonic map of the Magallanes-Austral Basin (modified from Fildani et al., 2008). Contours indicate foreland sediment thickness (after Ghiglione et al., 2009). The location of the study area is indicated by the black dashed-line box. The yellow star numbered 1 indicates the location of Sierra Baguales (Última Esperanza Province) and the yellow star numbered 2 indicates the location of Rio Turbio (Argentina) and Cerro Castillo, which are areas of geological observations.

After the middle of the previous century, several decades passed without any significant contributions, with the exception of those of Charrier and Lahsen (1969) and Lahsen and Charrier (1972) on the attempts to determinate paleontologically the K-T boundary; Malumián (1968), Malumián et al. (1971) and Bertels (1977) on the first foraminiferal studies revealing transgressive peaks and unconformities in the Argentinian portion of the basin; and finally, those of Natland et al. (1974) and Cañón and Ernst (1975) on stratigraphic correlations, widely used by the Petroleum industry, but holding some limitations due to the exclusive use of benthic foraminifers, their stratigraphic resolution

and the non-recognition of discontinuities (Malumián et al., 2013). Nevertheless, the scarcity of good-stratigraphic indicator planktonic foraminifers and the exact age of each foraminiferal association highly prevented more accurate dating at the time (Herm, 1966; Cañón and Ernst, 1975; Malumián, 1993).

Since the ending of the 20st Century and mainly beginning of the 21st, interest in the basin was renewed in attempts to understand not only the Late Cretaceous tectonic evolution of the Southern Patagonian Andes and its adjacent retroarc basin (Biddle et al., 1986; Ramos and Aguirre-Urreta, 1994; Fildani and Hessler, 2005; Fildani et al., 2008; Romans et al., 2010; McAtamney et al., 2011; Fosdick et al., 2013; Fosdick et al., 2014; Schwartz et al., 2016; Malkowski et al., 2015; Malkowski et al., 2016; Malkowski et al., 2017, *inter alia*), but also, to get insights into their evolution during the Cenozoic, motivating authors such as Olivero and Malumián (1999), Suárez et al., 2000; Olivero and Martinioni (2001), Ghiglione and Ramos (2005), Olivero et al. (2003), Hervé (2005), Olivero and Malumián (2008), Ponce et al. (2008), Torres-Carbonell et al. (2008a), Barbeau Jr. et al. (2009), Torres-Carbonell et al. (2009), Cuitiño and Scasso (2010), Sánchez et al. (2010), Le Roux (2010), Mpodozis et al. (2011), Cuitiño and Scasso (2013), Fosdick et al. (2015a, 2015b), Ghiglione (2015), Ghiglione et al. (2016), Gutiérrez et al. (2017) to establish more detailed depositional models, including the paleoenvironments, provenance areas, stratigraphic correlations and ages of the different units. At the same time, others worked on related topics such as paleontology, biostratigraphy, and ichnology (Quatrocchio, 2009; Malumián y Jannou 2010; Otero et al., 2009, 2012, 2015; Pearson et al., 2012; Bostelmann et al., 2013; Carrillo-Berumen et al., 2013; Cuitiño et al., 2013, 2016; Malumián et al., 2013). Nevertheless, in spite of these important advances, there is still a very acute lack of knowledge on the distribution, correlation, facies changes and sediment dispersal patterns of the different Cenozoic stratigraphic units and their tectonic settings. The Magallanes-Austral Basin is in fact among the least understood regions of South America in terms of tectonic evolution and Andean mountain building (Fildani and Hessler, 2005).

In this paper, we present a review of the published literature and our own sedimentological and geochronological studies of the Cenozoic deposits in the Chilean part of the Magallanes-Austral Basin (Fig. 2.1), in order to interpret the sedimentary environments, assess the maximum depositional ages (MDA), propose litho- and

chronostratigraphic correlations, and highlight regional unconformities and their relationship to Cenozoic tectonic plate reconfigurations. This integrated assessment strategy allows us, at least partially, to overcome the lack of knowledge with regard to the geological evolution and enhances our understanding of basin configuration and the sedimentary response to the growth of the Patagonian Andes.

2.2 Geological background

The Magallanes-Austral Basin located in the southernmost end of South America (Fig. 2.1) has an elongated NNW-SSE trend which toward south in Tierra del Fuego gradually change to a ~ESE-WNW orientation, accompanying in its shape the Patagonian Orocline. Its geological units follow a similar, sub-parallel outcrop pattern. Their age and the intensity of deformation decrease progressively eastward, passing from an internal fold-and-thrust belt to a slightly deformed westward verging frontal monocline in the external fold-and-thrust domain (Castelli et al., 1993; Farfán, 1997; Ghiglione et al., 2009, 2014). The western and southern basin limits are represented by plutons of the Patagonian Batholith, while its eastern margin corresponds to the Dungeness-Río Chico Granitic Arc (Fig. 2.1). The oldest known geological unit is Jurassic, porphyritic tuff and volcanic breccia interbedded with black shales and limestones, belonging to the Tobífera Formation (Figs. 2.1, 2.2) which record the onset of the lithospheric extension in the back-arc rift Rocas Verdes Basin. This early filling stage of the Rocas Verdes Basin is overlain by transgressive Cretaceous sandstones of the Springhill Formation, which are in turn succeeded by a thick succession of black shales of the Zapata/Erezcano Formation. The transition from back-arc extension to compression and onset of the Magallanes-Austral foreland basin development is represented by the medium-grained sandstone, shale and siltstone of the Punta Barrosa/Latorre, representing the onset of turbiditic sedimentation. This deep-water succession continue with the ~2500 m thick overall shales and conglomeratic beds of the Cerro Toro/Escarpada Formations (Fig. 2.2). During the Late Cretaceous, this succession was capped by continental slope and delta deposits of the Tres Pasos/Fuentes and Dorotea/Rocallosa Formations, respectively. The subsequent Cenozoic sequence is characterized by thick shales, siltstones and clay-rich, glauconitic sandstones reflecting a deep marine environment from the Paleocene until at least the early Eocene, represented by the Chorrillo Chico and Agua Fresca Formations in the Brunswick Peninsula-Skyring Sound area (Magallanes Province) (Fig. 2.2) and their

correlative units in Tierra del Fuego. Towards the north in the Última Esperanza Province, a prolonged hiatus from the Paleocene to early Eocene indicates either an interruption in sedimentation or cannibalization of these deposits.

Subsequently, during the late early to late Eocene, the development of deltaic complexes reflects a close relationship between deposition and orogenic pulses linked to the growth of the Southern Patagonian Andes. The continuous migration of the basin depocenter towards the east is manifested in a thick succession of sandstones and calcareous claystones with interbedded siltstones, coal seams, and shales. A continental environment was established in the Oligocene, as reflected by the conglomerates and pebbly sandstones of the Río Leona/El Salto Formations, which continued at least until the early Miocene (Fig. 2.2). These continental conditions were briefly interrupted by the Patagonian Transgression during the early Miocene, when the Estancia 25 de Mayo Formation was deposited in the central-northern part of the basin. However, continental conditions returned soon thereafter with the fluvial conglomerates, sandstones and rhyodacitic tuffs of the Santa Cruz and Palomares Formations. Finally, during the Plio-Pleistocene, glacial and fluvio-glacial sediments were deposited discordantly throughout the basin, these outcrops being especially prominent in the eastern section.

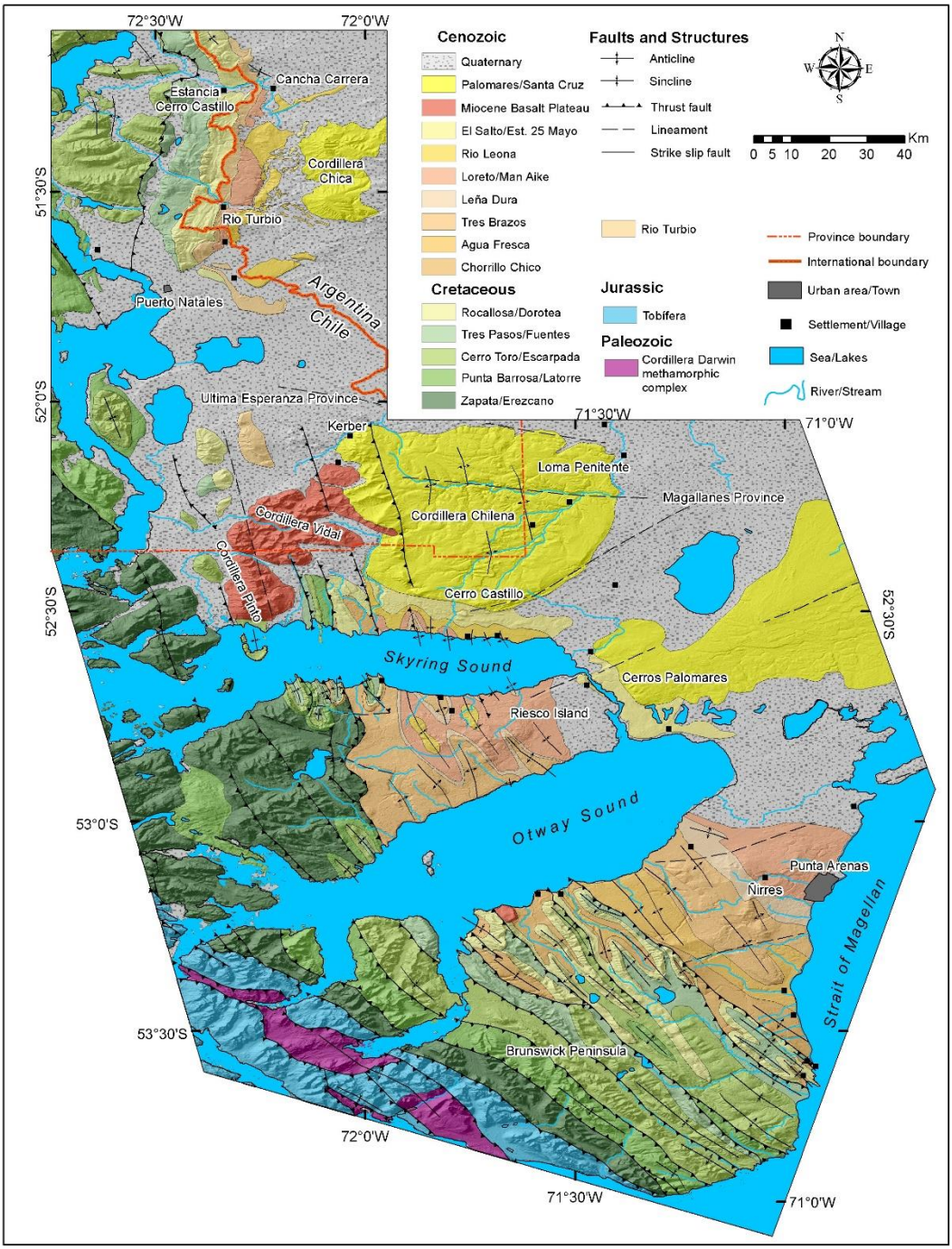

Figure 2. 2. Integrated geological map of area between Cerro Castillo (Última Esperanza Province) and Skyring Sound-Brunswick Peninsula (Magallanes Province) showing the distribution of Cenozoic deposits, based on collected field data and modified from Mella (2001), Sernageomin (2003), Fosdick, et al. (2011) and Ghiglione et al. (2009).

2.3 Study area and methodology

This study was focused primarily on the Brunswick Peninsula and the coastal area to the north and east of the Skyring Sound (Fig. 2.2), belonging to the Magallanes Province. Here, stratigraphic and sedimentological studies were carried out in greater

detail and more samples were collected for detrital zircon dating. However, other localities within the Magallanes-Austral Basin (like Última Esperanza) were also investigated to establish the geological context and to carry out additional dating. Stratigraphically, the study encompasses units ranging from the Upper Cretaceous to lower Miocene. At Cerro Castillo (Fig. 2.3), a stratigraphic column was measured in the Upper Cretaceous Dorotea Formation, whereas the Brunswick Peninsula (Fig. 2.5) and northern coastal area around the Skyring Sound and Riesco Island (Fig. 2.4) yielded information on the sedimentology and stratigraphy of the Paleogene succession, mainly at the localities of Cerros Palomares, Las Vacas-Penitente and Kerber (Fig. 2.4). Although investigation of these Mesozoic-Cenozoic rocks was hampered by a cover of dense vegetation and glacial to post-glacial deposits (Fig. 2.2) causing a scarcity of outcrops and difficult access, stratigraphic sections could be measured in sufficient detail along river valleys and rocky hillsides. The columns were measured at a cm-dm scale using the best available exposures, in which lithosome geometries, lithologies, types of contacts, sedimentary structures, fossils, and trace fossils were recorded. Samples were collected for detrital zircon dating and petrographic studies. Sandstones with a medium grain-size were used preferentially for zircon separation in the Sample Preparation Laboratory of the Geology Department at the University of Chile following standard density and magnetic concentration techniques, to be dated by U-Pb using laser ablation multicollector inductively coupled plasma mass spectrometry (LA-MC-ICP-MS) in the same department and using laser ablation inductively coupled plasma mass spectrometry (LA-ICP-MS) in the Servicio Nacional de Geología y Minería (SERNAGEOMIN).

In Table 2.1, the geographic locations of samples, stratigraphic units, estimated ages, and author(s) are indicated for the present study as well as previous detrital zircon dates reported in the literature.

Table 2. 1. Compiled U-Pb geochronological detrital age data from the Late Cretaceous through the Miocene in the Magallanes and Última Esperanza Provinces of the Magallanes-Austral Basin, indicating the sample locations, author(s), formation sampled, and proposed new nomenclature for the different formations based on this study. YDZ: Youngest detrital zircon (isoplot); YSG: Youngest single grain; YP: Youngest peak.

Location	Sample	Author	Lithology	Formation according each author	Formation in this work	MDA (2σ Ma)
N Cordillera Vidal	Kerber	This work	Sandstone	Palomares	Palomares	18.6±0.1
Morro Bayo	Zr-LF-001	Gutiérrez et al., 2017	Sandstone	Santa Cruz	Santa Cruz	16.8±0.2
Cordillera Chica	09-235A	Fosdick et al., 2011	Volcanic ash	Santa Cruz		18.1±0.8ΨΦ
Rio Baguales	09-207	Fosdick et al 2015a	Sandstone	Santa Cruz		18.9±0.4Ψ
E. Fitz Roy Channel	RV1	This work	Sandstone	El Salto	El Salto	19.6±0.9
South Sierra Baguales	09-206	Fosdick et al., 2011	Dacite	Rio Guillermo (Intrusion)		19.8±0.4ΨΦ
Ruta40/Cancha Carrera	09-237A	Fosdick et al., 2011	Volcanic ash	Rio Guillermo	Río Leona	21.8±0.3ΨΦ
Seno Skyring	FO0322	Hervé et al., 2004	Sandstone	El Salto		YDZ: 21.8±1.5Φ
Ruta40/Cancha Carrera	RT28DZ5	Fosdick et al., 2015b	Sandstone	Rio Guillermo		23.5±0.3
Seno Skyring	SK2	This work	Sandstone	(Mb. Las Coles of El Salto)		26.4±0.7
Ruta40/Cancha Carrera	RT28DZ6	Fosdick et al., 2015b	Sandstone	Upper Rio Turbio		26.6±0.2
Chorrillo Las Flores	Zr-BAG-25	Gutiérrez et al., 2017	Sandstone	Rio Leona		32.8±0.7
Chorrillo Jabón	Zr-PTO-81	Gutiérrez et al., 2017	Sandstone	Rio Leona		33±2.8
Ruta40/Cancha Carrera	RT28DZ8	Fosdick et al., 2015b	Sandstone	Upper Rio Turbio	Man Aike	33.4±0.5
Ruta40/Cancha Carrera	RT28DZ7	Fosdick et al., 2015b	Sandstone	Upper Rio Turbio		33.8±0.4
Cordillera Chica	09-230	Fosdick et al., 2015a	Sandstone	Rio Turbio		38.6±1.5Ψ
Chorrillo Jabón	Zr-PTO-77	Gutiérrez et al., 2017	Sandstone	Man Aike		40.3±0.5
3R Ravine	-	Le Roux 2012	Sandstone	Man Aike		40.5±0.4
Seno Skyring	SK1	This work	Sandstone	Loreto	Loreto	36.2±0.4

Isla Riesco	IR1	This work	Sandstone	Loreto		37.2±0.6
Chorrillo Lynch	RL1	This work	Sandstone	Loreto		37.1±0.3
Rio Las Minas	LMIN2008-1	Otero et al., 2012	Sandstone	Loreto		36.48±0.47
Rio Las Minas	LMIN2008-2	Otero et al., 2012	Sandstone	Loreto		36.73±0.5
Ruta40/Cancha Carrera	LdCDZ2	Fosdick et al., 2015b	Sandstone	Lower Rio Turbio	Rio Turbio	46.3±1.3
Ruta40/Cancha Carrera	LdCDZ4	Fosdick et al., 2015b	Sandstone	Lower Rio Turbio		47.1±2.7
Punta Pratt	FO0325	Hervé et al., 2004	Sandstone	Chorrillo Chico	Chorrillo Chico	YDZ: 58±2.2φ
Punta Canelo	PB1	This work	Sandstone	Chorrillo Chico		67.0±1.7
Blanco River	RB1	This work	Sandstone	Chorrillo Chico		65.2±0.5
Cabo Nariz	CN06-1	Sánchez et al., 2010	Sandstone	Upper Cabo Nariz Beds		57.6±1φ
Chorrillo Santiago	CN05-1	Sánchez et al., 2010	Sandstone	Lower Cabo Nariz Beds		76.5±0.7φ
Punta Prat	TO-25	Alvarez et al., 2006	Sandstone	Chorrillo Chico		YSG: 56; YP:73
Punta Rocallosa	FO0323	Hervé et al., 2004	Sandstone	Rocallosa	Rocallosa	YDZ: 78±2.5φ
Punta Eulogio	TO-24	Alvarez et al., 2006	Sandstone	Rocallosa		YPP: 62
Sierra Dorotea	FO0319	Hervé et al., 2004	Sandstone	Dorotea	Dorotea	YDZ: 67.4±1.5φ
Limite Intnal-C. Castillo	AVDZ2	Fosdick et al., 2015b	Sandstone	Dorotea		60.5±0.8
Limite Intnal-C. Castillo	AVDZ1	Fosdick et al., 2015b	Sandstone	Dorotea		61.9±0.3
Cerro Castillo Belt	CC1	This work	Sandstone	Dorotea		88.5±1.3
Cordillera Chica	09-226	Fosdick et al., 2015a	Sandstone	Dorotea		68.6±1.4
Cerro Guido	Zr-PTO-123	Gutiérrez et al., 2017	Sandstone	Dorotea		92.8±0.8
Las Tetas de las Chinas	Zr-FB-2	Gutiérrez et al., 2017	Sandstone	Dorotea		93.7±1.2
Las Tetas de las Chinas	Zr-FB-1	Gutiérrez et al., 2017	Sandstone	Dorotea		95.1±1.5

Río de las Chinas	Several samples	Schwartz et al., 2016	Sandstone	Dorotea		82-69

The $^{\Psi}$ indicates 1σ level of uncertainty; $^{\varphi}$ indicates SHRIMP-RG analysis.

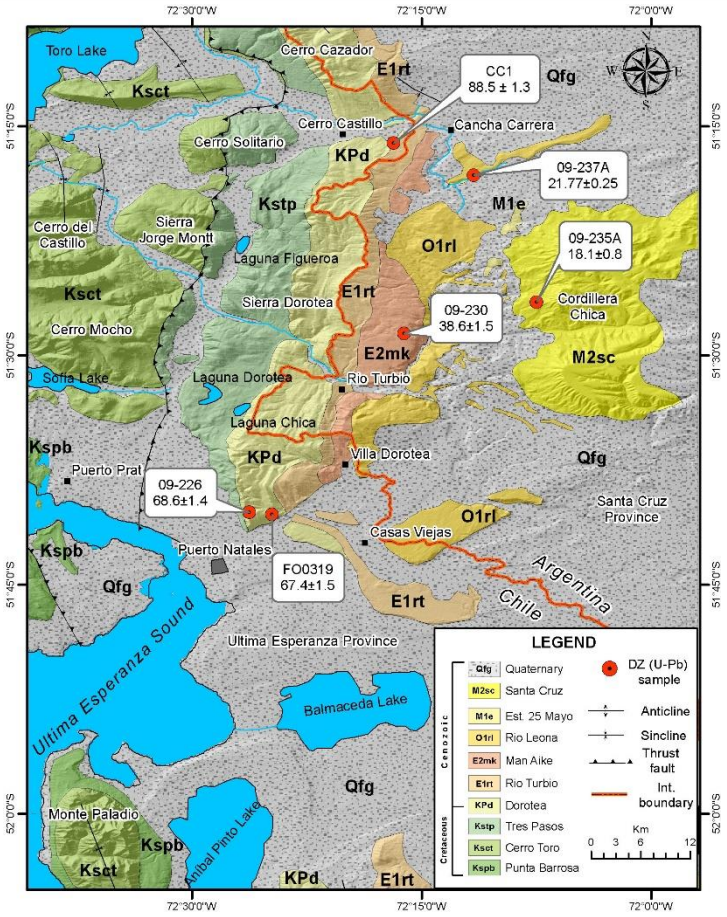

Figure 2. 3. Detailed geological map of the Cerro Castillo-Puerto Natales area (Última Esperanza Province) showing the distribution of the studied geological units and U-Pb detrital zircon sample locations (red circles).

Figures 2.3, 2.4 and 2.5 show the distribution of the samples that were used to establish the maximum depositional ages (MDA's) of the Cenozoic units and refine the regional chronostratigraphic model. The MDA's were calculated utilizing five different well-known metrics, namely the Youngest Single Grain (YSG), Youngest Detrital Zircon age (YDZ), Weighted Mean Average Age (YC1σ) (+2), Weighted Mean Average Age (YC2σ) (+2) and Weighted Average (+2) (Dickinson and Gehrels, 2009; Tucker et al., 2013; Schwartz et al., 2016) in order to obtain the most accurate representation of the MDA. Analytical data of MDA's are reported in Appendix A1 and A2. A compilation of the micro-fossiliferous content is presented in Appendix B, which was used to constrain the ages and bathymetric ranges of each formation. To compile the regional geological map (Fig. 2.2), Landsat-TM and Google Earth images, as well as topographic maps at a scale of 1:250,000 and previous published geological maps were initially used. This was subsequently refined by an ASTER-GDEM digital elevation model with a resolution of 1

arc-second (approximately 30 m, resampled to 12 m) and aerial photographs at a scale of 1:70,000. The final geological map (Fig. 2.2) was produced at a scale of 1:100,000 for the study area between Última Esperanza Province and the Brunswick Peninsula (Magallanes Province).

2.4 Stratigraphy and sedimentology

Cenozoic stratigraphic units that crop out in the Brunswick Peninsula-Skyring Sound area are described below, in each case formalizing its rank and providing its known thickness range, lithological and petrographic characteristics, age, and sedimentological interpretation.

2.4.1 Chorrillo Chico Formation

Originally defined by Thomas (1949) as the Chorrillo Chico Siltstone, the type locality of this unit is east of Punta Rocallosa (Fig. 2.4). It was subsequently raised to formation status by geologists of the Empresa Nacional de Petróleo (ENAP) (Hoffstetter et al., 1957). Thomas (1949) described the formation as consisting of hard, clay- and glauconite-rich siltstones with thin beds of limestone and $CaCO_3$ concretions. Charrier and Lahsen (1969) amplified this description, referring to very hard, light brown, clay-rich siltstones with many thin intercalations of glauconitic arenites, sometimes clay-rich and normally graded, as well as local coarse lenses of glauconitic sandstone. They also referred to the characteristic presence of large, irregular (up to 1.6 m thick and 6 m long) $CaCO_3$ concretions. The formation has a transitional contact with the underlying Rocallosa Formation and is about 275 m thick.

Thomas (1949) considered this unit to be of Cretaceous age based on its foraminifer content, but did not provide any details. Charrier and Lahsen (1969), using stratigraphic relationships and evidence of a micropaleontological overturn, assigned it a late Maastrichtian – early Paleocene age. The K/T boundary is located in the upper part of this formation according to these authors. Subsequently, Quattrocchio and Sarjeant (2003) reported a middle to late Paleocene (late Selandian) age on the basis of dinoflagellates recorded in the western part of the Brunswick Peninsula. On the other hand, the youngest detrital zircons reported are 58±2.2 Ma (Hervé, et al., 2004) and ~56 Ma (Álvarez et al., 2006), i.e. Thanetian, dated at Punta Prat (Fig. 2.5). We also dated the

lower part of the Chorrillo Chico Formation at Punta Canelos and Río Blanco valley (Fig. 5), in the former sample the second youngest zircon yielded an age of 59.2±3.1 Ma and in the latter sample the youngest zircon yielded an age of 64.4±1.3 Ma, but none of these detrital zircon ages is considered to represent a robust measure of the MDA. Nevertheless, it is important to note that Chorrillo Chico is progressively younger towards NW. A statistically more reliable MDA's of 67±1.7 Ma and 65.2±0.5 Ma were assigned to each sample respectively of the Chorrillo Chico Formation, which is consistent with fossil ages. However, bearing in mind that benthonic foraminifers of the Midway type, which include *Spiroplectamina beccariiformis* and *S. spectabilis* (Robles and Gómez, 1956) reported from the formation, have a Last Appearance Date (LAD) representing the Paleocene/Eocene limit (van Morkhoven et al., 1986) this constrains the age to be between 67±1.7 and ca.56.2 Ma.

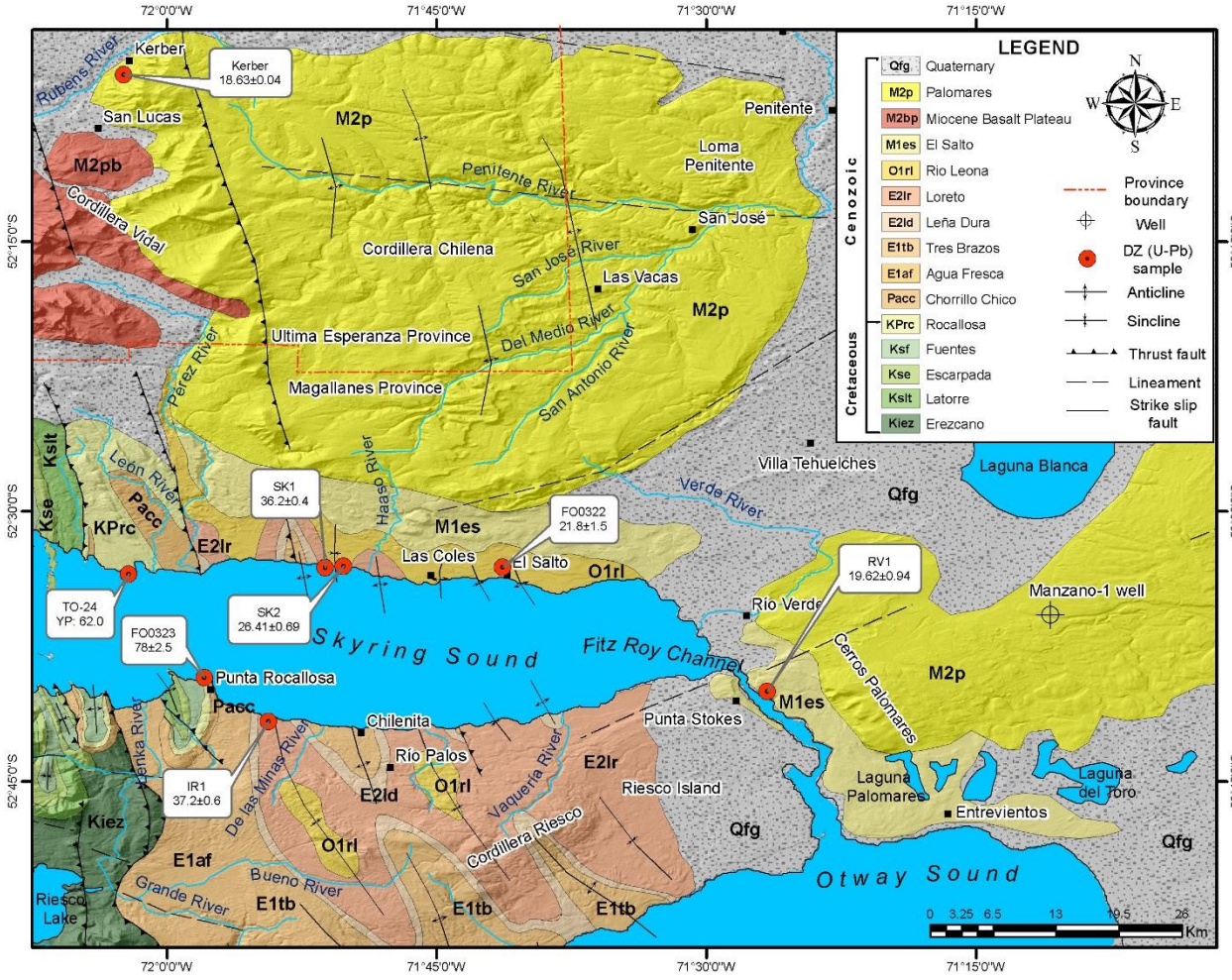

Figure 2. 4. Detailed geological map of the north coast of Skyring Sound and Riesco Island (Magallanes Province) showing the distribution of the studied geological units, ENAP wells (Celtic cross), and U-Pb detrital zircon sample locations (red circles).

Along the lower part of the Río Blanco valley (Fig. 2.5) in the eastern part of the Brunswick Peninsula, and at Punta Canelos (Fig. 2.5) in the western part of the same peninsula, the sandstones of the Chorrillo Chico Formation are composed mainly of monocrystalline quartz, followed in minor proportion by sedimentary rock fragments (including chert) and potassium feldspar, together with some plagioclase (Fig. 2.6). Fractured, rounded glauconite grains which underwent pervasive micro-spar cementation are common. At the localities mentioned above, we observed a facies association of prograding, middle turbidite lobes (FA1) and a more proximal submarine fan (FA2), characterized by a coarsening-upward succession with thickening-upward strata (Fig. 2.7). The basal part is dominated by poorly stratified, massive, light grey, glauconitic siltstones interbedded with ~7 cm thick, grey, coarsening-upward siltstones, and 5 – 68 cm thick, dark mudstones. This part of the succession shows contorted bedding, load casts, and turboglyphs indicating a north-northwesterly transport direction. The intensive bioturbation is dominated by ichnogenera such as *Thalassinoides*, *Neonereites* (Fig. 2.7c), *Scolicia (Laminites)* (Fig. 2.7d), *Asterosoma*, *Zoophycos*, and local occurrences of *Skolithos*. With the exception of the latter ichnogenus, these indicate a Zoophycos ichnofacies association (Hubbard et al., 2012). The upper part of the succession is more arenaceous, being characterized by 60 – 90 cm thick beds of massive siltstones with fine, sandy, glauconitic concretions (mean diameter 50 cm) and fine- to medium-grained, massive, poorly sorted, glauconitic sandstones with sub-angular grains. Bioturbation in this part of the succession is very rare, with only *Thalassinoides* isp. recognized locally. The graphoglyptic ichnofauna and clear coarsening-upward trend with thickening-upward strata, reflect the existence of actively prograding turbidite lobes in deep water, i.e. the distal continental slope and bathyal environment (Buatois and Mángano, 2011; Hubbard, et al., 2012). This is supported by benthonic foraminifera typical of bathyal depths such as *Cyclammina*, *Allomorphina*, and *Ammobaculites* (Encyclopedia of Life: http://eol.org/pages/62458/overview; http://eol.org/pages/62476/overview; http://eol.org/pages/6815624/overview; Akers, 1954; Bandy, 1964; Marchant, 2011). The abundance of glauconite, generally considered to characterize moderately shallow marine environments with a very low sedimentation rate, together with the presence of foraminifer genera such as *Trochammina*, *Haplophragmoides*, *Spiroplectamina spectabilis* and *Alabamina wilcoxensis*, which normally inhabit the internal continental shelf within the

photic zone (Charrier and Lahsen, 1969; Murray, 1979; Marchant, 2011) apparently contradicts a deep marine environment. Nevertheless, Mesquita (1998) reported *Trochammina* and *Haplophragmoides* associated with paleobathymetric conditions of 500 – 1,000 m depth in turbidite facies, whereas Valchev (2003) also suggests that foraminifer associations typical of bathyal depths include *Trochammina*, *Haplophragmoides* and *S. spectabilis*. Although glauconite is more typical of shallow marine shelves, it has been reported in waters exceeding 2,500 m depth in the Indian Ocean (Collet, 1908). The presence of the genus *Alabamina wilcoxensis* and the abundance of glauconite in the Chorillo Chico Formation could also be explained by the reworking of shelf sediments down submarine canyons by turbidity currents that fed the more distal lobes, as is in fact supported by the rounded and fractured nature of the glauconite grains (Fig. 2.6c). Although the optimum depth for glauconite generation is between 100 and 1,000 m, once formed, it is stable in sea water and can survive transport in a marine environment (Selley, 1976). This mechanism could therefore satisfactorily explain the two apparently contrasting sedimentary environments.

2.4.2 Agua Fresca Formation

Decat and Pomeyrol (1931) originally included part of the Chorrillo Chico Formation in the basal part of this unit, referred to by Von Goetsche (1953) as the San Jorge Formation. Subsequently, this was considered by ENAP geologists to be the basal part of the Agua Fresca Formation. However, Thomas (1949) redefined the Agua Fresca Formation after Hollister (1944) included it as part of the Skyring Formation along the southern coast of the Skyring Sound (Fig. 2.4), which was especially inappropriate due to the fact that numerous stratigraphic units are present in this area and outcrops are very incomplete. The type locality, according to the original definition, is situated along the lower valley of the Agua Fresca River in the eastern part of the Brunswick Peninsula (Fig. 2.5). Its basal part, also referred to as the San Jorge Formation by Charrier and Lahsen (1969), consists of maroon claystones with many $CaCO_3$ concretions, some glauconite-rich strata, and abundant thin beds of sandstone and siltstone interbedded with normally graded claystone. This basal part corresponds very well to what was named by Mohr (in Todd and Kniker, 1952) as the lower Skyring Formation, characterized by abundant $CaCO_3$ concretions within clay-rich beds and calcareous siltstones, as well as local

conglomeratic beds. Higher up the succession becomes less calcareous and more clay-rich with scarce concretions that are characteristically flat and thin, with better defined stratification. The overlying strata become less well defined and concretions much smaller, while the uppermost interval typically shows “wormhole” concretions, tubular structures about 15 cm long in the core of which abundant mm-scale tubes are observed that were made by polychaetes (serpulids) (Fig. 2.7e). This interval was also found by us in the easternmost part of the Agua Fresca River, where it is characterized by dark grey, fissile, siliceous shales with calcareous concretions reaching 90 cm in diameter, as well as abundant calcite veins. The thickness of the Agua Fresca Formation reported by Mohr (in Todd and Kniker, 1952) in the Brunswick Peninsula is 2,180 m, whereas Thomas (1949) recorded a thickness of 2,100 m. Its basal contact with the Chorillo Chico Formation is gradual (Charrier and Lahsen, 1969).

Figure 2. 5. Detailed geological map of the Brunswick Peninsula (Magallanes Province) showing the distribution of the studied geological units, ENAP wells (Celtic cross), and U-Pb detrital zircon sample locations (red circles).

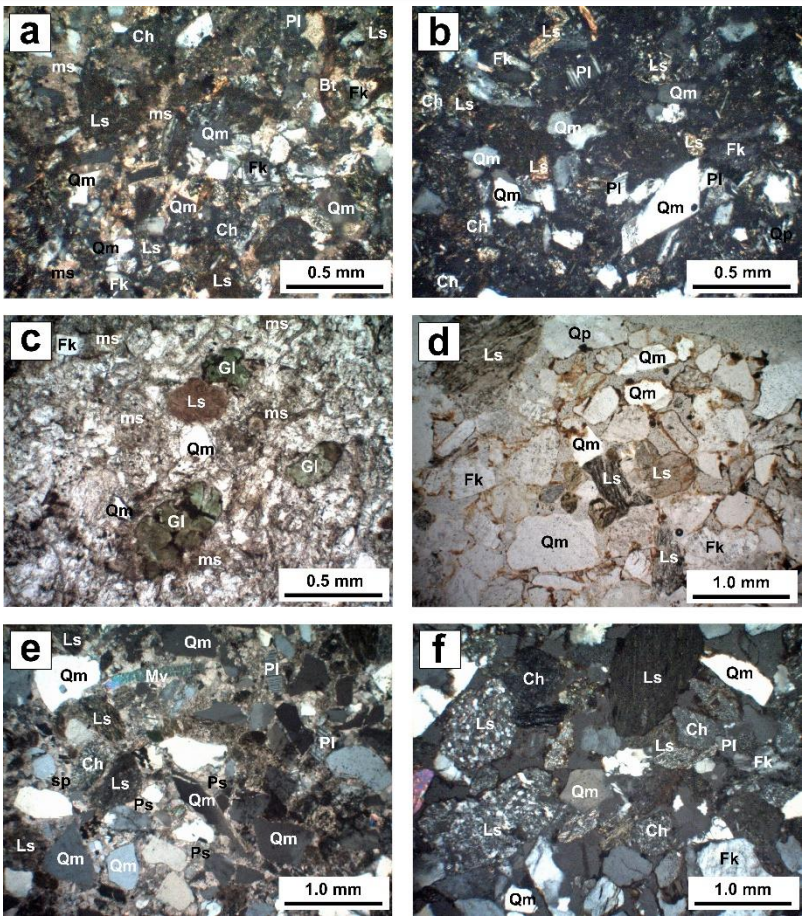

Figure 2. 6. Thin-section photomicrograph showing the major components of the Chorrillo Chico Formation (a, b, c) and the Tres Brazos Formation (d, e, f) in their type locality (see Fig. 2.5 for location). (a), (b) Note the abundance of quartz and feldspar in Chorrillo Chico Formation samples from the Blanco River valley section (see Fig. 2.5 for location), XPL. (c) Rounded and fractured glauconite grains, suggesting reworking. Note the pervasive micro-spar cementation. Sample from Punta Canelos (see Fig. 2.5 for location), PPL. (d) Ferruginous rimmed cementation around lithoclasts of sandstones from the Tres Brazos Formation, PPL. (e), (f) Note the reduction of feldspar and increase in sedimentary rock fragments. Selected diagnostic grains are labelled as follows: Ch: Chert, Fk: potassium feldspar, Pl: plagioclase, Qm: monocrystalline quartz, Qp: polycrystalline quartz, ms: micro-spar cement, Gl: glauconite, Ls: lithic sedimentary fragment, Mv: detrital muscovite, Ps: pseudo-spar cement.

Thomas (1949) considered an age not older than the latest early Eocene, whereas Todd and Kniker (1952) assigned the formation a late Eocene age based on its faunal affinity with the Kreyenhagen Shale of California. On the other hand, Charrier and Lahsen (1969) proposed a late Paleocene to early Eocene age, although the presence of *Globanomalina australiformis* apparently rules out the former possibility (Malumián et al., 2013). *G. australiformis* has a FAD of 55.5 Ma (in Malumián et al., 2013) and LAD of 44.2 Ma (Huber and Quillévéré, 2005). Given that *Acarinina esnaensis* (LAD of 51 Ma; Berggren et al., 2006) and *G. index* are present in the overlying Tres Brazos Formation

(FAD of 43.7 Ma; Malumián et al., 2013) this confines the age of the Agua Fresca Formation to 53.25 – 43.7 Ma.

In spite of the fact that the complete Agua Fresca Formation could not be surveyed in this study, the stratigraphic information provided by Charrier and Lahsen (1969) and Mohr (in Todd and Kniker, 1952), allows the general depositional environment to be identified as an association of prograding turbidite lobes (FA2) for the lower part. These were more proximal than the FA1 lobes of the Chorrillo Chico Formation, given the frequent intercalations of sandstones and siltstones, as well as conglomeratic beds that probably filled lobe feeder channels and submarine canyons. The good stratification developed towards the top of the formation suggests that this facies association accumulated in deep water below storm wave base, where early diagenetic processes gave rise to $CaCO_3$ concretions. The succeeding interval represents an aggrading, external shelf to upper continental slope association (FA3) in which the main sedimentation mechanism was from suspension and vertical accretion on a muddy ocean floor. That the energy level and sedimentation rate were low is attested by the presence of serpulids and well-stratified shales (Fig. 2.7) in conjunction with benthonic foraminifers such as *Globigerina triloculinoides* Plummer, *G. spiralis* Bolli, *Globorotalia compressa* Plummer, *G. membranácea* (ehrenbergii), *G. quadrata*, *Acarinina triplex subbotina, Dorothia principensis*, *Achilleodinium biformoides*, *Allomorphina conica*, and *Globanomalina australiformis*, which are typical of depths between 92 – 967 m (http://eol.org/pages/6813341/overview; http://eol.org/pages/6998677/overview; http://eol.org/pages/6998404/overview; http://eol.org/pages/6998087/overview; http://eol.org/pages/6999003/overview; http://eol.org/pages/6991658/overview; http://eol.org/pages/6817131/overview; http://eol.org/pages/6999128/overview; http://eol.org/pages/6815629/overview; http://eol.org/pages/20577911/overview; Valchev, 2003). The presence of shallow water (<30 m) benthic foraminifers such as *Globigerina aquiensis, Elphidium, Alterbidinium distinctum*, and *Acarinina esnaensis* (http://eol.org/pages/6992137/overview; Charrier and Lahsen, 1969; Marchant, 2011 http://eol.org/pages/6999484/overview; http://eol.org/pages/6992127/overview) probably resulted from their reworking into deeper environments by offshore and turbidity currents. A minimum depth of about 100 m can therefore be inferred for the uppermost strata of the

Agua Fresca Formation, and the general environment is envisaged as an external shelf to upper continental slope.

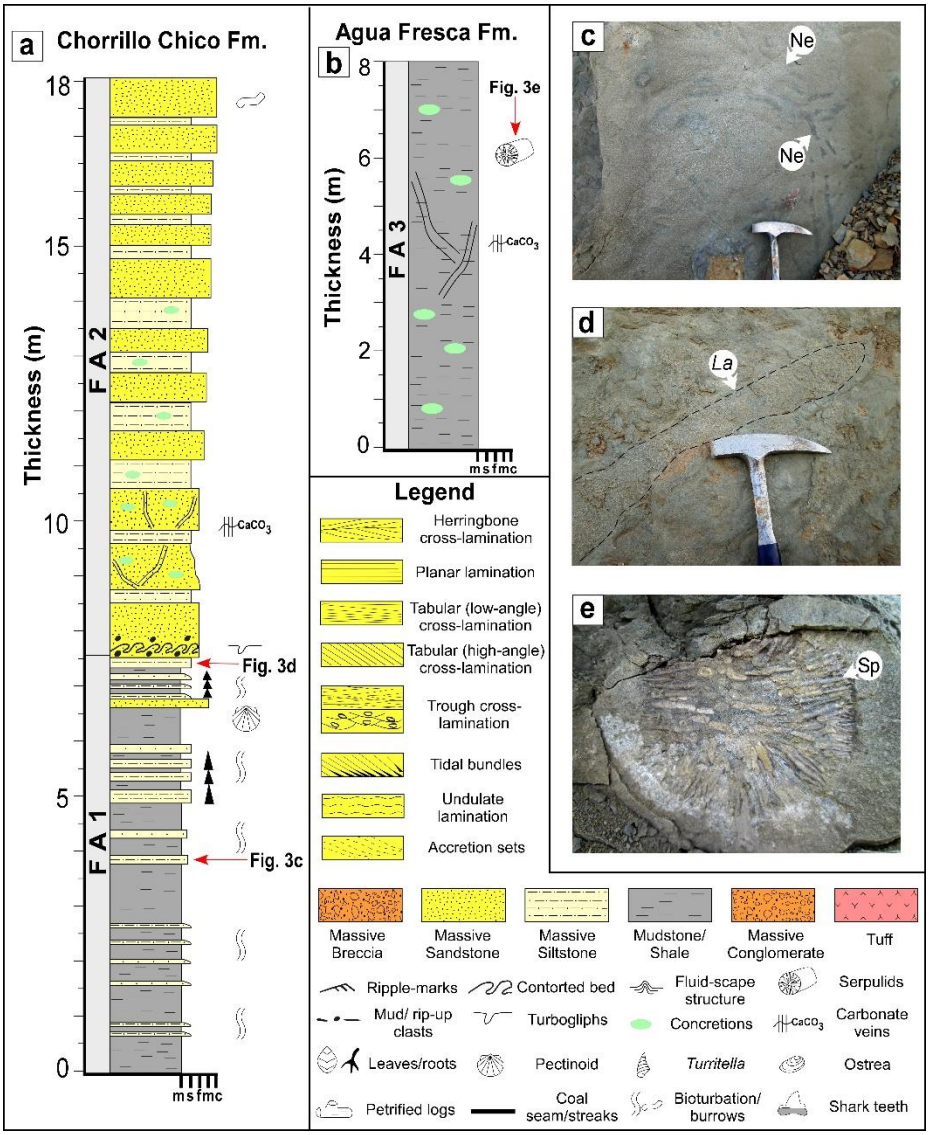

Figure 2. 7. Stratigraphic columns of the Chorrrillo Chico Formation and upper part of the Agua Fresca Formation illustrating the facies associations and some paleontological and ichnological features. (a) Prograding character of the deep marine turbidites of the Chorrillo Chico Formation. (b) Vertical accretion of pelagic and hemi-pelagic deposits of the Agua Fresca Formation. (c) Neonereites (Ne) traces and (d) Scolicia (Laminites) traces (La) in the distal turbidites of the Chorrillo Chico Formation. (e) Serpulids (Sp) in well stratified shales from the Agua Fresca Formation.

2.4.3 Tres Brazos Formation

Defined originally by Decat and Pomeyrol (1931) as the Río Grande Sandstone, it was redefined by Ruby (1945) as the Tres Brazos Sandstone, because the name Río Grande was considered to be too common and also due to the fact that the outcrops occur

north of the homonymous river and not along it. In this manner, its type locality was changed to the outcrops along the Tres Brazos River in the eastern part of the Brunswick Peninsula (Fig. 2.5). Here, unfortunately, the basal contact is poorly exposed northeast of the ENAP P-7 test well, and its upper contact is not present in this valley but in that of the Leña Dura River to the north (Fig. 2.5), where the outcrops are of poor quality. Thomas (1949) described the formation as consisting of medium-grained, well-sorted, glauconitic sandstones hosting large, spherical, siliceous concretions in addition to smaller, calcareous, fossiliferous concretions. Barwick (1949) described the formation as consisting of intercalated thin, fine-grained, glauconitic sandstones, siltstones and silty shales in the basal part, followed by massive, medium- to coarse-grained, glauconitic sandstones with calcareous concretion horizons. This sub-unit is overlain by thin intercalations of fine-grained sandstones, glauconitic siltstones, organic-rich shale and thin coal streaks. The uppermost part consists of medium- to coarse-grained, glauconitic sandstones with elongated, calcareous concretions (described as “ledges”) as well as thin pebbly lenses. The thickness is variable, from 1,500 m in the vicinity of the Grande River to 160 m in the Mina Rica Well northwest of Punta Arenas (Thomas, 1949). On the other hand, along the Tres Brazos River, Barwick (1949) reported 1,280 m without the base or top being exposed. The type of basal contact has not been defined clearly until now, being apparently transitional according to surface observations. However, Todd and Kniker (1952, p. 2) mentioned that the underlying Agua Fresca Formation is separated by an unconformity from the Tres Brazos Formation, probably based on micropaleontological data. A paraconformable contact can therefore be inferred.

Thomas (1949) assigned a late Eocene age to the Tres Brazos Formation, whereas Malumián et al. (2013) proposed a Lutetian – Bartonian range due to the similarity of its benthic foraminifer association with that of the Leticia Formation in Tierra del Fuego, where *G. index* (FAD = 43.7 Ma) and *Acarinina* sp. (LAD = 39 Ma) occur. However, the presence of *Acarinina bullbrooki* in the overlying Leña Dura Formation, which has a LAD of 41.8 Ma, led them to conclude that the Tres Brazos Formation cannot be younger. Therefore, considering that the basal contact of this formation with the Agua Fresca Formation is probably a paraconformity, it should be significantly younger than 43.7 Ma. Therefore, the formation probably has a latest Lutetian age.

The sandstone compositional data from the Tres Brazos Formation display a dominance of monocrystalline quartz, followed by chert, argillaceous sedimentary rock fragments, potassium feldspar, plagioclase and detrital muscovite (Fig. 2.6d, e, f) in order of abundance. The former components are well cemented by pseudo-spar and ferruginous, rimmed cement.

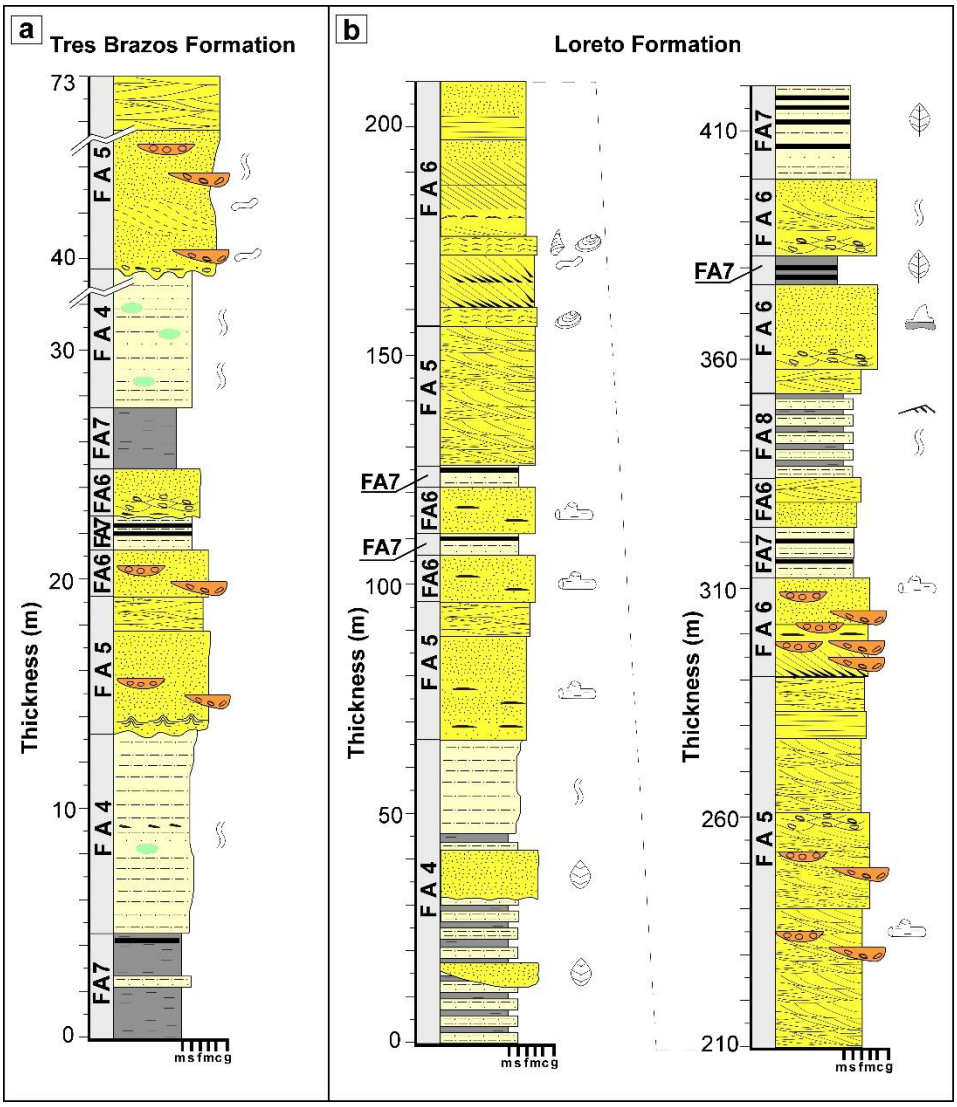

Figure 2. 8. Stratigraphic columns of the Tres Brazos and Loreto Formations, showing the distinctive facies associations of deltaic systems. (a) Note the aggradational pattern of the Tres Brazos deltaic system indicated by thick shale/siltstone-rich sequence. (b) The opposite is observed in the Loreto deltaic system, where high sedimentation rates led to the development of gullies and intense erosion in the prodelta facies (FA4), preventing the proliferation of benthic organisms. Note also, the tidal bundles and herringbone-cross lamination indicating tidal influence. Legend as indicated in Fig. 2.7.

At the type locality of the Tres Brazos Formation, 4 facies associations characteristic of prograding delta systems were recognized by us (Fig. 2.8a). This progradation took place towards the north-north-northeast, as shown by the inclination of

clinoforms, while pulses of aggradation also occurred. The prodelta facies association (FA4) is characterized by brown to grey, clay-rich siltstones. These are well stratified, ferruginous, slightly micaceous, and locally carbonaceous. Calcareous concretions are locally observed. The bioturbation index is moderate, represented by tubular structures parallel to the bedding and filled by fine-grained sand. The distributary mouth bar facies association (FA5) consists of fine- to coarse-grained, massive sandstones with poor to moderate sorting, showing marked erosional relief at their basal contacts. They show common fluid escape structures, undulate lamination, *Skolithos* and *Arenicolites* traces indicating a Skolithos ichnofacies association, as well as medium- to coarse-grained channels throughout the succession and medium- to large-scale trough cross-lamination towards the top. The latter indicate stronger current flow as the water became shallower with bar growth. The distributary channel facies (FA6) is represented by fine- to medium-grained sandstones with an erosional basal relief and troughs filled with small pebbles at the base. Upward, this facies becomes mainly massive, with coarse-grained sandstone filling the channels. Spherical concretions also occur. Separating the different units of facies association FA6 are deposits representing interdistributary bays and marshes (FA7), consisting of light grey, silty mudrock with vague stratification (occasionally fissile bedding) and coal lenses. Calcareous concretions with calcite-filled synaeresis cracks also occur. The scarcity of bioturbation and fossils suggests a fairly high sedimentation rate. The stacking pattern is progradational, as shown by the coarsening- and shallowing-upward trend, the latter indicated by the presence of *Elphidium patagonicum* (Marchant, 2011). Some vertical aggradation took place during the deeper water cycles before new deltaic lobes migrated over the area, as suggested by the occurrence of *Globigerinatheka index*, *Acarinina* spp. and *Globigerina triloculinoides* Plummer (http://eol.org/pages/7008444/overview; http://eol.org/pages/6960468/overview; http://eol.org/pages/6813341/overview). Overall, the facies are typical of river-dominated deltas.

2.4.4 Leña Dura Formation

This unit was referred to by Decat and Pomeyrol (1931) as the Leña Dura Shales, its type locality being the valley of the Leña Dura River south of Punta Arenas in the eastern part of the Brunswick Peninsula (Fig. 2.5). The basal contact is poorly exposed

and therefore incompletely described, whereas its upper contact is visible in the valley of the Los Ciervos River (Fig. 2.5). The formation consists of grey, hard shales with large (>1 m), spheroidal, fossiliferous, calcareous concretions concentrated along certain horizons. Abundant foraminifers are present (Thomas, 1949). Barwick (1949) described the shales as silty, glauconitic and poorly stratified. The concretions according to this author occur in clay-rich shale and are mainly flattened. The upper part of the formation has grey, silty shales with abundant calcareous, baseball- to football-sized concretions, with the shales turning more clay-rich and the concretions becoming more flattened and scarcer towards the top. Barwick (1949) reported a thickness of 825 m without observing the base, but this thickness is doubtful seeing that covered intervals of up to 370 m were identified in the present study, while structural data are too limited for tilt-corrections. It is important to note that the thickness increases markedly towards the SE (reaching between 1,500 m and 2,500 m in Tierra del Fuego), whereas it wedges out towards the NW, where 210 m was recorded. The formation is absent in the vicinity of the Pérez River north of the Skyring Sound. Although the basal contact is not clearly visible, it appears to be sharp. Due to the marked wedging out of the underlying Tres Brazos Formation, Thomas (1949) proposed an unconformity between the two formations, but this could also be due to lateral facies changes that are typical of the Cenozoic units in the Magallanes-Austral Basin.

Thomas (1949) assigned a late Eocene age to this formation, as did Fasola (1969) and Cookson and Cranwell (1967), based on palynomorphs and marine invertebrates. On the other hand, Biddle et al. (1986) included this unit in their so-called “Glauconitic Zone”, to which they assigned a middle Eocene to early Oligocene age. The presence of *Testacarinata inconspicua* (Malumián et al., 2013), whose biozone ranges from the FAD of *Chiloguembelina cubensis* to the LAD of *Globorotalia aculeata* (*sensu* Jenkins, 1966), restricts its biochron to between 44 Ma and ~38 Ma, so that we propose a Bartonian age (41.2 – 37.8 Ma) due to the presence of an unconformity between the Leña Dura and Tres Brazos Formations.

No stratigraphic sections were measured by us in the Leña Dura Formation. However, based on the stratigraphic descriptions of Thomas (1949) and Barwick (1949), we conclude an FA3 facies association, similar to the upper interval of the Agua Fresca Formation. The presence of *Acarinina bullbrooki*, *Spiroplectammina* and *Plectina elongata*, with bathymetric ranges between 180 and 1,132 m

(http://eol.org/pages/6991652/overview; http://eol.org/pages/62459/overview; http://eol.org/pages/7000281/overview) suggests an external shelf to upper continental slope environment.

2.4.5 Loreto Formation

The name “Loreto Strata” was originally given to this succession by Keidel and Hemmer (1931), but included the present Tres Brazos Formation. Decat and Pomeyrol (1931) separated the latter unit from the present Loreto Formation and divided it into the Lynch Sandstone and “Formation with Lignite”, with its type locality around the Loreto Mine in the valley of the Las Minas River (Fig. 2.5). Ruby (1945) in turn, restricted the name Loreto to the sandstones above the uppermost shale of the Leña Dura Formation. Afterwards, Kniker (1949) identified a basal member which he named the Los Ciervos Siltstone, based on the abundant presence of foraminifers, which was subsequently elevated to formation status by Martínez-Pardo et al. (1965). Thomas (1949) proposed the terms “Marine Loreto” referring to the Lynch Sandstone, and “Coal-bearing Loreto” referring to the “Formation with Lignite”. Finally, ENAP geologists (in Hoffstetter et al., 1957), redefined and formalized the Loreto Formation based on the original stratigraphic subdivision of Felsch (1912), which they corrected in certain aspects to establish the three formal subdivisions as they are currently known (from base to top): Los Ciervos, Lynch, and Carbonoso Members. The type locality of the Los Ciervos Member is in the lower valley of the Los Ciervos River (Fig. 2.5), where its contact with the underlying Leña Dura Formation can be observed. This member is composed of a basal unit of glauconite-rich siltstones and silty shale, followed by grey siltstones with thin, very fine-grained sandstone beds. There are also some silty and fine-grained sandstone intervals with concretions. The total thickness of this member is 540 m (Barwick, 1949). The Lynch Member has its type locality in the Chorillo Lynch valley (Fig. 2.5), one of the main tributaries of the Las Minas River. It consists of grey, clay-rich, medium- to coarse-grained sandstones that are well sorted with cross-lamination. Coal is absent from this member (Barwick, 1949). The Carbonoso Member is similar to the Lynch Member, the only difference being the presence of coal seams, beds with abundant plant fossils, and more abundant shale (Thomas, 1949). The top of this member has not been observed to date at any of the localities where the Loreto Formation crops out, due to glacial erosion and deposition.

Thomas (1949) estimated a thickness of 500 – 800 m for his "Marine Loreto" unit, where he apparently included the Los Ciervos Member of Kniker (1949). Therefore, considering the thickness of the Los Ciervos Member reported by Barwick (1949), the Lynch Member should have a thickness of around 260 m. Similarly, a thickness of 225 m has been attributed to the Carbonoso Member, although Hoffstetter et al. (1957) reported a thickness of 350 m. The basal contact is sharp to transitional, being marked by the first glauconite-rich sandy siltstone.

Kniker (1949) assigned a late Eocene age to the Loreto Formation based on microfossils, whereas Martínez-Pardo et al. (1965) proposed a Burdigalian age based on the presence of the foraminifers *Candeina nítida* d'Orbigny, *G. falconensis* Blow, and *Globigerinoides triloba* Le Roy. However, Malumián et al. (2013) could not confirm the existence of these species in the collection of ENAP. Although Thomas (1949) also favored a Miocene age, Fasola (1969) proposed an Oligocene age based on palynomorphs, as did Biddle et al. (1986) for the basal part of the formation. Subsequently, Martínez-Pardo and Martínez (1989) reiterated their Miocene age for the Los Ciervos Member, pointing to the co-existence of *Boltovskoyella* and *Virgulinella severini* Cañón and Ernst, in its upper part. The first genus, however, is considered as an endemic taxon characteristic of the late middle Eocene Atlantic transgression (Malumián et al., 2013). Finally, Otero et al. (2012) reported radiometric U-Pb ages for detrital zircons of two samples from the upper part of the Loreto Formation, which gave dates of 36.5±0.5 and 36.7±0.5 Ma, respectively. We dated three samples from the same formation collected from the northern coast of the Skyring Sound, the northern coast of Riesco Island and the Chorrillo Lynch corresponding to the upper part of the Los Ciervos Member (Fig. 4), which yielded ages of 36.2±0.4, 37.2±0.6 and 37.1±0.3 Ma, respectively. The youngest zircons dated at 35.3±1.0, 36.0±1.0 and 35.4±0.7 Ma, respectively. This allows us to assign the upper part of the Loreto Formation to the Priabonian and possibly earliest Rupelian, and its basal part to the Priabonian/Bartonian boundary according to its stratigraphic relationships.

Petrographically, the Loreto Formation shows two major compositional tendencies. The lower part is dominated by volcanic rock fragments with microlitic and lathwork textures, followed by plagioclase, potassium feldspar, quartz and some argillaceous rock

fragments (Fig. 2.9a). The upper part (Fig. 2.9b), displays a more equal proportion among mono- and polycrystalline quartz, sedimentary rock fragments, and volcanic rock fragments. Some plagioclase and fractured potassium feldspars are present. Replacing, fibrous calcite cement is conspicuous in the upper part of the Loreto Formation.

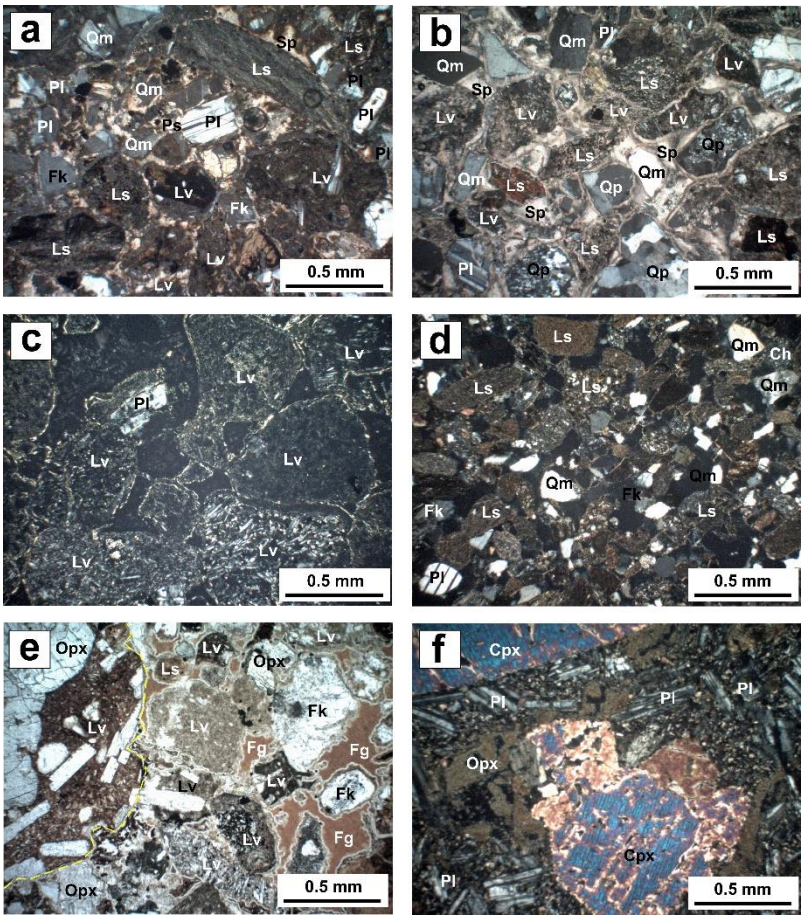

Figure 2. 9. Thin-section photomicrograph showing the major components of the Loreto (a, b), Rio Leona (c), El Salto (d) and the Palomares Formations (e, f). (a) Lower part of the Loreto Formation at Chorrillo Lynch (see Fig. 2.5 for location), showing a dominance of andesitic volcanic rock fragments and plagioclase over quartz and sedimentary rock fragments. Note microlitic texture of the andesitic volcanic rock fragments, XPL. (b) Well cemented sandstone of the upper part of the Loreto Formation (at Ñirres, see Fig.2. 5 for location), showing an equal proportion of the major components. Note the fibrous-radial spar cement, representing a mixed marine-meteoric diagenetic zone, XPL. (c) Abundance of volcanic rock fragments with characteristic microlitic texture and Illite-smectite as rim cement, XPL. (d) Increasing of the argillaceous and fine-grained sandstone fragment rocks, XPL. (e) Sample from Cerros Palomares (see Fig. 2.4 for location). Note the abundance of basaltic-andesitic volcanic rock fragments, large clasts of orthopyroxene and some sedimentary rock fragments and potassium feldspar, all surrounded by ferruginous cement. (f) Vidal conglomerate sample (at Kerber, see Fig. 2.4 for location) showing abundant clasts of clino- and orthopyroxene immersed in plagioclase groundmass moderately sericitized. Selected diagnostic grains are labelled as follows: Fk: potassium feldspar, Pl: plagioclase, Qm: monocrystalline quartz, Qp: polycrystalline quartz, Lv: volcanic lithic fragment, Ls: sedimentary lithic fragment, Ps: pseudo-spar cement, Sp: spar cement, Opx: orthopyroxene, Cpx: Clinopyroxene.

The Loreto Formation has facies associations typical of northeastward prograding deltas according to our own observations (Fig. 2.8b). However, there are important differences with the deltaic systems of the Tres Brazos Formation. The prodelta facies association, which shows rare bioturbation (FA4), is frequently cut by gullies and small submarine canyons, whereas the subaqueous delta platform (FA5) shows ample evidence of tidal action. The interdistributary bay and marsh association (FA7) is better developed with draining worse than in the Tres Brazos Formation, which led to the accumulation of thick and extensive peat deposits. The distributary channels (FA6) display anastomosing and braided patterns, as indicated by multiple channels with trough cross-stratified sandstone and fine conglomerate. Glossifungites ichnofacies is concentrated in the trough cross-stratified sandstone packages, representing active accretion processes (Pearson et al., 2012). Subaerial delta plain deposits (overbank sediments and crevasse splays) are also common (FA8), being represented by siltstones and massive to laminated claystones with abundant organic material and evidence of bioturbation. In the last two facies associations, branching tidal creeks, as well as tabular, tangential, and herringbone cross-lamination were recognized, suggesting a strong tidal influence. The deltas of the Loreto Formation were therefore mixed fluvial- and tidal-dominated systems (Fig. 2.8b). A bathymetric interpretation based on microfossils is complex, however, due to the scarcity of foraminifers in the upper two members, although the Los Ciervos Member yielded Marginulina, Virgulina, Elphidium, and Cibicides spp. Unfortunately, these represent very wide bathymetric ranges, from 3.5 m – 3,354 m (http://eol.org/pages/62346/overview; http://eol.org/pages/62159/overview; http://eol.org/pages/62244/overview; Marchant, 2011), so that they are inconclusive.

2.4.6 El Salto Formation

The El Salto Formation was defined as such by González and Tapia (1952). Its type locality is the Estancia El Salto northeast of the Skyring Sound (Fig. 2.4). Keidel and Hemmer (1931) previously included these strata in the basal part of the Palomares Formation, but there is a marked lithological difference and also an unconformity between the two successions. A year later, González (1953) referred to these strata as the “El Salto Group” in order to accommodate three recognized lithological subdivisions. The type locality of the basal unit (“Las Coles Stage”) is situated in the vicinity of the Las Coles

section (Fig. 2.4), where its base is well defined but not its top. Here it consists of greenish grey, well cemented, clay-rich conglomerates and pebbly sandstones, siltstones, and greyish brown to greenish grey, carbonaceous claystones, with some high-reflectivity coal seams. There are abundant remains of monocotyledonous and dicotyledonous plants and rare volcanic glass fragments. The middle unit ("Río Verde Stage") has its type locality around Estancia Río Verde (Fig. 2.4) and along the homonymous valley, consisting mainly of dark grey to greenish, poorly sorted, clay-rich conglomerates and pebbly sandstones, greenish, fine-grained sandstones, and green siltstones to claystones with some calcareous concretions. The type locality of the upper lithological unit ("San Antonio Stage") is in the vicinity of the San Antonio Anticline and valley of the homonymous river (Fig. 2.4), where it consists of bluish grey conglomerates and pebbly sandstones, white, fine breccias composed of pumice and volcanic ash, light grey claystone rich in volcanic ash with Nothofagus impressions, and grey, hard tuffs. It is important to note that we visited the type locality of the "San Antonio Stage" and consider all the outcrops to belong to the lower member of the Palomares Formation. In fact, in their original report, González and Tapia (1952) also assigned the first volcaniclastic beds to the Palomares Formation. The thickness of the El Salto Formation varies between 700 and 1,200 m (including the "San Antonio Stage"). González (1953), in each of the type localities, reported a thickness of 370 m for the "Las Coles Stage" (without observing the top), 220 m for the "Río Verde Stage" (also without the top), and 100 m or 150 m for the "San Antonio Stage" from outcrop and well data, respectively. González and Tapia (1952) proposed the existence of a hiatus or erosional unconformity at the base of the "El Salto Group", based on the strong wedging out of the underlying Loreto Formation between the Pérez River and Cordillera Pinto (Fig. 2.4), as well as the notable absence of the Brush Lake Formation that underlies this formation in Tierra del Fuego, in the Manzano No. 1 Well (Fig. 2.4) and to the west thereof.

González (1953) proposed a late Oligocene to early Miocene age for the El Salto Formation, and although he did not encounter fossils characteristic of the "Patagonian", suggested that it could be correlated with that informal chronostratigraphic unit. Curiously, this assignation was probably the most accurate of those reported during this early period for Cenozoic successions in the Brunswick Peninsula-Skyring Sound area, as it was confirmed by later radiometric U-Pb dates. Hervé et al. (2004) reported an age of 21.8±1.5 Ma for the El Salto Formation along the northeastern coast of the Skyring Sound, while

we obtained ages of 26.4±0.7 and 19.6±0.9 Ma, respectively, in the same area and eastern coast of the Fitz Roy Channel in the vicinity of Estancia Río Verde (Fig. 2.4). A detailed analysis of the age, subdivision and correlations of this formation is presented in the next section.

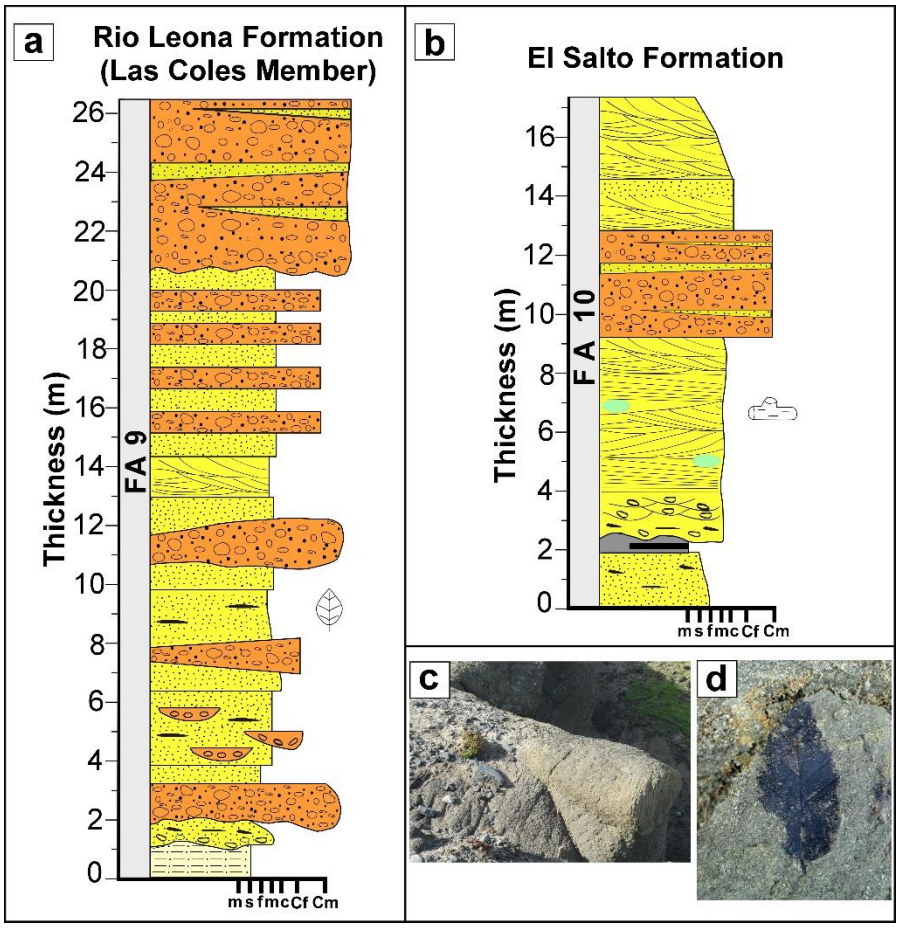

Figure 2. 10. Stratigraphic columns of the Río Leona and El Salto Formations. (a) Stratigraphic column measured at Las Coles section (see Fig. 2.4 for location). (b) Stratigraphic column measured at Río Verde (see Fig. 2.4 for location). (c) Petrified log in the El Salto Formation. (d) Moderately well-preserved Nothofagus leaf, characteristic of the Río Leona Formation. Legend as indicated in Fig. 2.7.

In the "Las Coles" section, the sandstones of the El Salto Formation are composed mainly of volcanic rock fragments with a microlitic texture (Fig. 2.9c). On the other hand, at Estancia Rio Verde, they records an increasing of argillaceous fragments poorly cemented by micro-spar and Illite-Smectite, regards to the volcanic rock fragments content (Fig. 2.9d).

The El Salto Formation marks the first appearance of continental environments within the Magallanes-Austral Basin. Our investigation suggests that the "Las Coles Stage" represents a proximal, high-energy, braided river system of gravel and sand (FA9),

where sediment gravity-flows occurred occasionally (Fig. 2.10a), whereas the "Rio Verde Stage" represents a more distal, braided, arenaceous fluvial system (FA10) (Fig. 2.10b). The FA9 facies association is composed of clast-supported, polymictic conglomerates with small to medium-sized, poorly to moderately sorted clasts and a sandy matrix. Lenses of medium to coarse-grained sandstone with sharp to slightly erosional bases probably represent partially abandoned channels, whereas polymictic conglomerates with strongly eroded basal contacts and lobe-shaped terminations suggest high-density debris flows along pre-existing channels. Massive, medium-grained, well sorted sandstones with sub-rounded grains and small-pebble conglomerate lenses were probably deposited in shifting channels and bars. Facies FA10, on the other hand, is dominated by medium-grained, low-angle tabular and trough cross-laminated sandstones, some of the troughs being lined with small pebbles. These sedimentary structures indicate strong, channelized flow. Abandoned channels and poorly drained interchannel deposits are represented by massive, very fine-grained sandstones and ferruginous siltstones associated with carbonaceous mudstones and small lignite lenses. Similar deposits are also found subordinately in the FA9 facies association of the "Las Coles Stage".

2.4.7 Palomares Formation

Keidel and Hemmer (1931) originally referred to this unit, with its type locality in the Cerros Palomares east of the Fitz Roy Channel (Fig. 2.4), as the "Palomar Beds". It included what is known today as the El Salto Formation. Decat and Pomeyrol (1931) also adopted this name in their description of the Brunswick Peninsula geology, but it still included the El Salto Formation. Subsequently González (1953) redefined the succession as the Palomares Formation, separating it from the latter. Although geologists of CORFO and ENAP used this definition sensu González (1953), Hoffstetter et al. (1957) referred to it as the Palomares Group, as it contains two easily distinguishable lithological units. The lower unit ("San José Stage") has its type locality in the valley of the San José River near Estancia San José (Fig. 2.4), where both the base and top are well exposed. It consists of fine conglomerates, pebbly sandstones, bluish, fine-grained, poorly sorted sandstones with cross-lamination and a pyroclastic matrix, and white tuff. Towards the west and southwest, the formation shows a facies change to coarse breccia, constituting the Vidal Conglomerate. The upper unit ("Penitente Stage") is well exposed in its type locality in the

homonymous valley close to the mouth of the San José River (Fig. 2.4), except for the top that has been eroded by glacial action. It consists of whitish yellow, fine- to coarse-grained, poorly sorted tuffs. These porous, relatively hard rocks are formed by volcanic ash, pumice grains, volcanic glass, zeolites, feldspars and quartz. In some horizons, which are up to 80 cm thick, are silicified, semi-carbonized wood fragments. The reported thicknesses of the Palomares Formation are 170 m for the "San José Stage" and 200 m for the "Penitente Stage". Its lower contact, according to González (1953), is apparently an erosional unconformity, poorly expressed east of the Cordillera Vidal (Fig. 2.4), but better defined west of this mountain range.

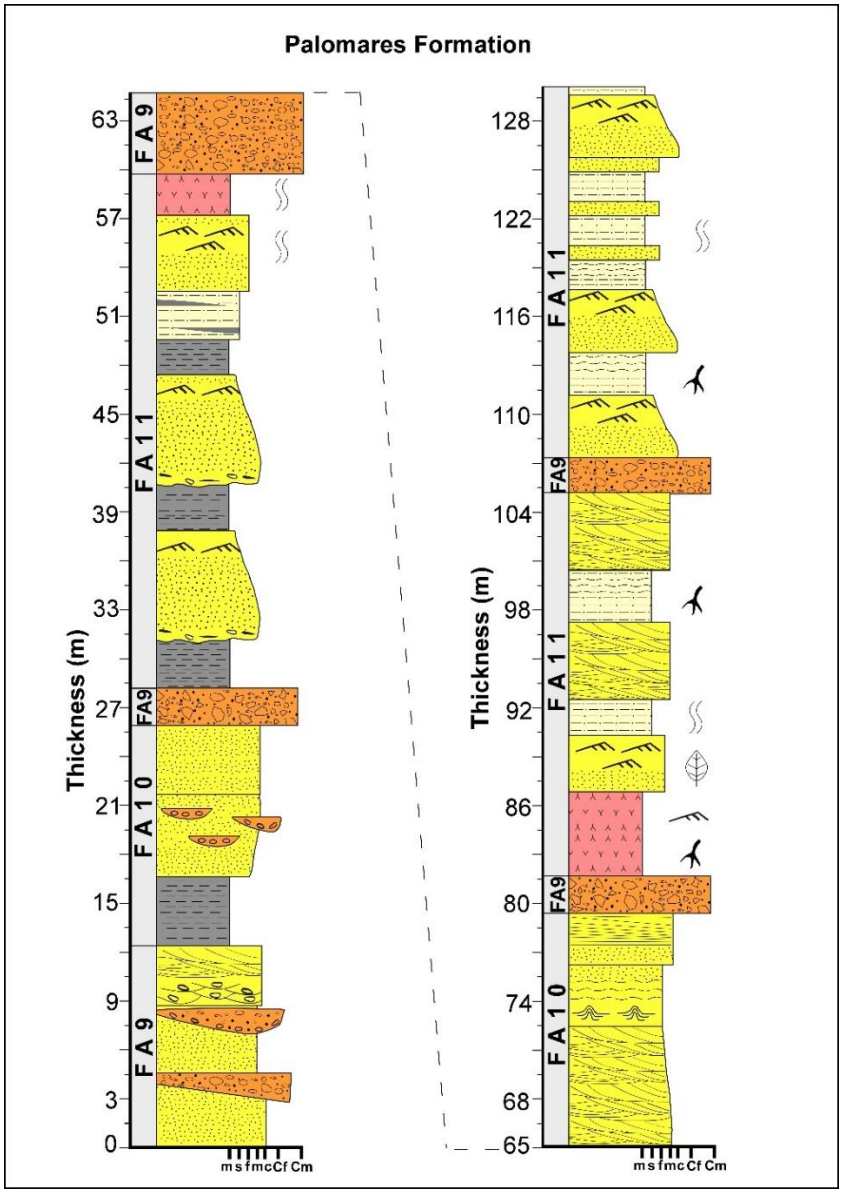

Figure 2. 11. Stratigraphic columns of the Palomares Formation measured at Cerros Palomares (see Fig. 2.4 for location). Legend as indicated in Fig. 2.7.

González (1953) proposed a middle to late Miocene age for this unit, based on paleontological and lithological relationships at that time attributed to the Santacrucian mammals. This was supported by the presence of *Astrapotherium magnum* and *Nematherium birdi* reported by Hammer and Bird, respectively (in González, 1953), which had been identified in many outcrops of Argentinian Patagonia in strata attributed to the Santacrucian. We dated the lower member of the Palomares Formation (Vidal Conglomerate) at Kerber (Fig. 2.4), which gave a well-defined age of 18.6±0.1Ma, i.e. Burdigalian. This is coeval with the Santa Cruz Formation in the Última Esperanza Province, dated by Bostelmann et al. (2013) at 18.23±0.26 Ma and characterized by terrestrial vertebrate fossils biostratigraphically equivalent to a post-Colhuehuapian, pre-Santacrucian South American Land Mammal Age.

Compositional data from the Palomares Formation sandstones reflect the direct influence of a volcanic source. The lower part (Vidal Conglomerate) exhibits a dominance of clinopyroxenes and basaltic volcanic rock fragments, some olivine and orthopyroxene crystals also being present (Fig. 2.9f). At the Cerros Palomares section, the formation is composed mainly of basaltic volcanic rock fragments with microlitic, lathwork and felsitic textures and some sedimentary rock fragments, orthopyroxene and potassium feldspar crystals in a conspicuous ferruginous cement (Fig. 2.9e).

The Palomares Formation in its type locality shows facies associations already described for the underlying El Salto Formation, with high-energy, proximal braided streams (FA9) as well as more distal braided streams (FA10). However, the succession is dominated by facies associations of low-energy, meandering rivers (FA11) interrupted by volcanic eruptions (Fig. 2.11). The FA11 association is characterized by a high proportion of massive siltstone and volcaniclastic mudstone, with abundant plant fragments including roots and herbaceous plants that represent overbank flood plains. Fine-grained, thin, tabular sandstones within these mudstones are interpreted as crevasse splay deposits. Fining-upward cycles of intraformational clay-pebble conglomerate and medium- to fine-grained sandstone with trough cross-lamination overlying sharp to erosional contacts, represent point bars in sinuous channels. Frequent intercalations of tuff, tuffaceous mudstone lenses, and tuffaceous sandstone beds with sharp basal and upper contacts, show traction structures such as straight-crested and linguoid ripple marks, suggesting slow-moving currents. Rhizocretions, trace fossils

representing the ichnofacies Scoyenia (including insect burrows), and mud-cracks indicate the subaerial emergence of point bar tops or overbank sediments in the case of muddy tuffs (Cuitiño and Scasso, 2013). In the proximity of Estancia San José, these tuffaceous beds show imprints of ferns, Fuscospora and Lophozonia, the last two genera belonging to Nothofagacea family. Paleocurrent directions in the Palomares Formation, mainly derived from trough cross-lamination and lateral facies changes, indicating a northeastward transport direction.

2.5 Correlations and unconfomities

2.5.1 Stratigraphic nomenclature and chronostratigraphic correlations

The Cenozoic nomenclature in the Magallanes-Austral Basin of Chile and Argentina is complicated, as similar units in different locations have been given different names independent of their age and lithological characteristics. This derives from a lack of integration of the stratigraphic knowledge acquired through time on both sides of the border (Malumián et al., 2013), one of the problems in this regard being the absence of Committees for Stratigraphy as present in many other countries. Additionally, the majority of geological units lacked a clear and complete description of their lithological nature, paleontology, contact relationships, thicknesses, and ages. For the Paleocene and middle Eocene in Chile, there is a remarkable absence of stratigraphic information, especially in the northern part of the Magallanes-Austral Basin (Última Esperanza Province), but in the southern area (Brunswick Peninsula, Skyring Sound, and Tierra del Fuego) the stratigraphic register has been maintained more or less intact. The stratigraphic nomenclature, as well as lithological and geochronological correlations of the Paleocene to middle Eocene units discussed below, is therefore applicable mainly to the Brunswick Peninsula-Skyring sound-Tierra del Fuego area, but as from this epoch until the Miocene both areas (Magallanes and Última Esperanza Provinces) have been integrated more fully (Fig. 2.12). The changes in stratigraphic nomenclature, terminology and correlations proposed here obey the established concepts of the International Stratigraphic Guide (Hedberg, 1976). However, it is important to highlight some of the present difficulties in the correlation, mainly due to our still incomplete knowledge of the geology of the sector between Cordillera Vidal and Puerto Natales (Fig. 2.2) north of the Skyring Sound, where access is very restricted.

2.5.1.1 Maastrichtian to Upper Paleocene

Two roughly contemporaneous Cretaceous successions in the Magallanes-Austral Basin are the Dorotea Formation (Hünicken, 1955), with its type locality at Cerro Dorotea just outside Puerto Natales (Fig. 2.3), and the Rocallosa Formation (Hollister, 1943-1944, in Hoffstetter et al., 1957) of the Brunswick Peninsula-Skyring Sound area. For the northernmost Chilean outcrops of the Dorotea Formation in Sierra Baguales (Fig. 2.2), Gutiérrez et al. (2017) reported youngest zircon ages of 74.9±2.1, 71.0±1.2, and 71.7±1.2 Ma. The latter dates are supported by the presence of *Gunnarites* sp., *Pachydiscus* aff. *gollevilensis*, and *Pachydiscus cazadoriana* (González, 2015), the first two being of Maastrichtian age (Martínez-Pardo, 1965), while the last is from the Campanian-Maastrichtian (Otero et al., 2009). A vertebrate fragment of an *Aristonectes* sp. (Plesiosauria, Elasmosauridae) reported by Otero et al. (2015) at the same locality also indicates a late Maastrichtian age, while the presence of *Hoplitoplacenticeras* ammonite species at Cerro Cazador (Fig. 2.3) suggests a Campanian age for the basal part of the Dorotea Formation (Macellari et al., 1989). Further south at its type locality, an age of 67.4±1.5 Ma was reported for the 5 youngest zircons (Hervé et al., 2004), whereas Fosdick et al. (2015b) obtained a detrital zircon date of 60.5±0.8 Ma for this formation at the Chile-Argentina border east of Cerro Castillo (Fig. 2.3). This indicates that the gradual southward decrease in age for the Dorotea Formation reported by Hubbard et al. (2010), Romans et al. (2010), Bernhardt et al. (2011), Schwartz and Graham (2015) and Schwartz et al. (2016) is in fact more irregular but maintains the general trend. Mpodozis (in Álvarez et al. 2006) reported an age of 62 Ma for the six youngest zircons from the Rocallosa Formation at the Skyring Sound (Fig. 2.4).

Lithological correlation between the Dorotea and Rocallosa Formations is somewhat confuse, however, due to the facies diversity in both successions. In the north, the Dorotea Formation represents a deltaic to estuarine complex influenced by tides (Schwartz and Graham, 2015; Gutiérrez et al., 2017), whereas in the Brunswick Peninsula the dominant facies vary from the lower shoreface to neritic shelf, with some local exceptions such as the area between Río Turbio (Fig. 2.3) and Skyring Sound, where lower shoreface facies as well as distributary mouth bars of an estuarine/deltaic system are common (Mpodozis, in Álvarez et al., 2006). Due to these lithostratigraphic and

paleoenvironmental differences, it is convenient to maintain the names Dorotea Formation in the Última Esperanza Province and Rocallosa Formation in the Brunswick Peninsula-Skyring Sound area (Magallanes Province) (Fig. 2.12). For both formations the lithostratigraphic, biostratigraphic and sedimentological information is sufficiently detailed to substantiate this proposal (Charrier and Lahsen, 1969; Lahsen and Charrier, 1972; Malumián and Caramés, 1997; Mpodozis en Álvarez et al., 2006; Mpodozis et al., 2011; Schwartz and Graham, 2015; Schwartz et al., 2016; Gutiérrez et al., 2017).

The Chorrillo Chico Formation was the first unit to be deposited during the Cenozoic in the Brunswick Peninsula-Skyring Sound area (Magallanes Province), and has no clear counterpart in the Última Esperanza Province. However, in the Chilean Tierra del Fuego, the "Cabo Nariz Beds" (dated at 57.6±1 Ma by Sánchez et al., 2010, using detrital zircons) are both geochronologically and lithologically similar to the Chorrillo Chico Formation. The facies distribution indicates that, in the Chilean Tierra del Fuego, the "Cabo Nariz Beds" represent the proximal part of a submarine marine fan system of turbidites that prograded towards the north-northwest (Sánchez et al., 2010; Gutiérrez et al., 2017), whereas the Chorrillo Chico Formation in the Brunswick Peninsula represents the medium and more distal part of the same system. Therefore, because the name "Cabo Nariz Beds" was used only informally for this succession by Céspedes (1971) and moreover was introduced after the name "Chorillo Chico Formation" had been given to these beds by Thomas (1949), the latter name has preference and should be retained.

2.5.1.2 Eocene

The Agua Fresca Formation represents the first Eocene deposits in the Brunswick Peninsula-Skyring Sound area, whereas the last Eocene stratigraphic unit is the Loreto Formation. Although the top of the latter is not exposed, we believe that its upper contact still lies within the Eocene. The Agua Fresca Formation was also mentioned in the Chilean Tierra del Fuego by Céspedes (1971), but he placed it within the Paleocene. Previously, others such as Felsch (1912) and Keidel and Hemmer (1931) described the "Boquerón Beds" in Tierra del Fuego as the first succession deposited after the Cenomanian. They mentioned that it culminated with the deposition of the Loreto Formation, thus also including the Tres Brazos and Leña Dura Formations. Cecioni and Wenzel (in Hoffstetter et al., 1957) correlated the Loreto Formation with the Río Bautismo and Santa Clara

Formations of the Bahía Inútil Group, but did not clearly define the limits of these units nor gave sufficiently detailed stratigraphic descriptions. We therefore recommend that the name “Boquerón Beds” be discarded and that the Bahía Inútil Group be used only for the subsurface, for the time being. Where possible, the nomenclature of the Brunswick Peninsula-Skyring Sound area (Agua Fresca, Tres Brazos, Leña Dura and Loreto Formations) should be applied to outcrops until more precise correlations can be established.

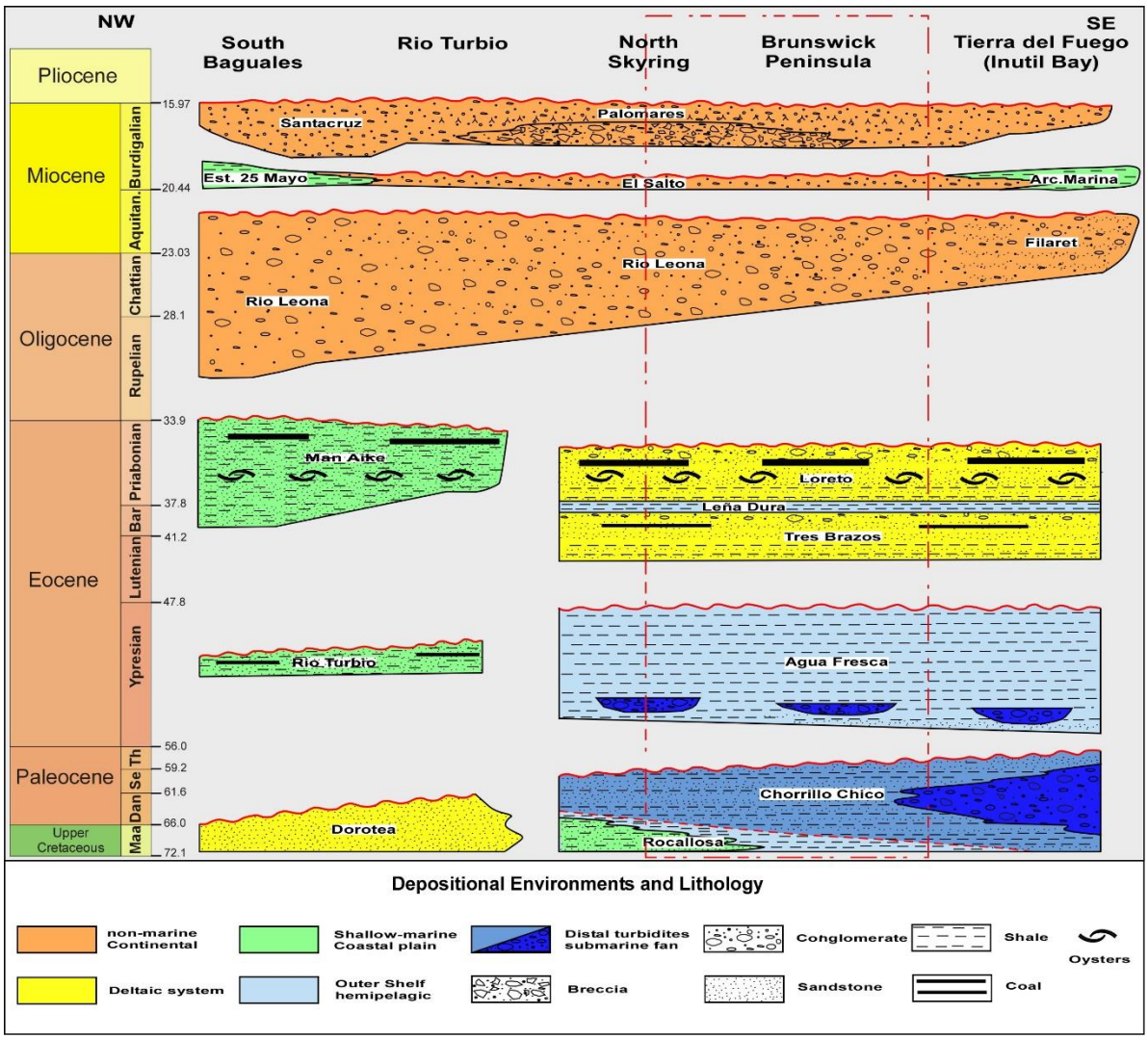

Figure 2. 12. Generalized NW-SE chronostratigraphic section of the Magallanes-Austral Basin between Sierra Baguales-Rio Turbio (Última Esperanza Province), Skyring Sound-Brunswick Peninsula, and Inútil Bay, Tierra del Fuego (Magallanes Province), indicating the distribution and duration of the five major unconformities identified in this study, facies changes and the stratigraphic nomenclature for different regions throughout the basin. Red dashed box represents the study area; wavy line represents unconformities; red dash line represents correlative conformity.

Together, the Tres Brazos and Leña Dura Formations could be lithologically comparable with part of the "Lower Member" of the Río Turbio Formation (Hünicken, 1955) further to the north. However, in our opinion attempts to correlate these units from a lithostratigraphic point of view should rather be avoided, as they apparently represent local depositional events without evidence for interfingering or lateral facies changes between them (Fig. 2.12). A more accurate correlation could in fact be made from a chronostratigraphic point of view. Chronostratigraphically and paleontologically, the Loreto Formation can be correlated with parts of both the "Lower" and "Upper" members of the Río Turbio Formation. Nevertheless, accurate lithostratigraphic correlations between the Loreto and Río Turbio Formations could not be established, as the "Upper Member" of the Río Turbio Formation represents an isolated, tidally dominated estuarine to open marine system within a transgressive context (Manassero et al., 1990; Pearson et al., 2012; Rodríguez-Raising et al., 2014), whereas the Loreto Formation reflects a fluvially dominated delta system influenced by tides within a regressive context.

The similarities of facies and depositional environments between the Man Aike Formation in the Última Esperanza Province and the "Upper Member" of the Río Turbio Formation allow a lithostratigraphic correlation to be proposed (Camacho et al., 1998, 2000; Casadío et al., 2009), as both were deposited in a shallow marine, tidally dominated estuarine environment during a transgressive event (Casadío et al., 2009; Le Roux et al., 2010; Pearson et al., 2013; Gutiérrez et al., 2017). In addition, their micropaleontological content and $^{87}Sr/^{86}Sr$ isotope data support a chronostratigraphic equivalency (Casadío et al., 2009) (Fig. 2.12). On the other hand, U-Pb dating of detrital zircons in the Man Aike Formation confirmed a maximum depositional age of 40.30±0.47 and 40.48±0.37 Ma at Chorrillo Jabón and the 3R Ravine in the Baguales Mountain Range, respectively (Le Roux, 2012a; Gutiérrez et al., 2017) suggesting that it could also be chronostratigraphically correlated with part of the "Lower Member" of the Río Turbio Formation. From a stratigraphic nomenclature point of view, an additional problem is presented as to which name (Man Aike or Río Turbio) should prevail. We propose that the name Río Turbio Formation be restricted to its previous "Lower Member" and that the name Man Aike Formation be applied to the "Upper Member" throughout the Última Esperanza and Río Turbio areas in Chile and Argentina, respectively (Fig. 2.2). This would also be in compliance with the International Stratigraphic Code, as according to Fosdick

et al. (2015b) there is a hiatus between the two former “members” of the Río Turbio Formation. This will be analyzed in more detail in section 2.5.2.

2.5.1.3 Oligocene to Miocene

The Las Coles Member of the El Salto Formation reflects the start of continental sedimentation in the region and has been dated at 26.41±0.69 Ma (peak of youngest zircons) along the northeastern coast of the Skyring Sound. The overlying Río Verde Member was dated in the same area (Hervé et al., 2004) as well as east of the Fitz Roy Channel, yielding ages between 21.8±1.5 and 19.2±0.9 Ma (peak of youngest zircons), respectively. This suggests a possible hiatus between the two members, which would imply that a stratigraphic redefinition is required. Following this idea, the Las Coles Member could be correlated both litho- and chronostratigraphically with the Río Leona Formation (Fig. 2.12) present in the Sierra Baguales and defined around Lago Argentino in Argentina (Fig. 2.1), which represents the first non-marine sedimentation in the Magallanes-Austral Basin during the Cenozoic. The Río Verde Member, on the other hand, can only be correlated chronostratigraphically with the Estancia 25 de Mayo Formation, as they have very different lithological and paleoenvironmental characteristics. The equivalent of the Palomares Formation in geochronological terms would be the Santa Cruz Formation (Fig. 2.12) (defined in the Santa Cruz Province of Argentina), given the presence of pre-Santacrucian fauna in both units and their equivalent ages yielded by detrital zircons, in both cases not exceeding 19 Ma. However, the lithostratigraphic correlation is not clear, as there are important differences in their lithofacies. The Santa Cruz Formation is dominated by flood plain mudstones with meandering river deposits, whereas at least the basal part of the Palomares Formation reflects a braided system with much coarser facies.

As far as the stratigraphic nomenclature is concerned, therefore, we propose that the name Río Leona Formation be used instead of the Río Guillermo Formation in the Río Turbio area (Fig. 2.3), because the latter unit presents the last stages of the former, as already pointed out by Robbiano et al. (1996), Camacho et al. (1998), Nullo and Combina (2002), and Bostelmann et al. (2013). Therefore, given that the Río Leona Formation reflects the start of high-energy, continental sedimentation similar to that reflected by the Las Coles Member of the El Salto Formation, we propose that only the former name be

used for the area between Lago Argentino, Última Esperanza-Río Turbio and the Brunswick Peninsula-Skyring Sound, whereas in Chilean Tierra del Fuego, the Brush Lake Formation possibly represents its chronostratigraphic equivalent. As a result, the El Salto Formation is restricted to the outcrop areas of its former Río Verde Member, with the latter name being discarded. The name El Salto is retained for the southern outcrops as it does not correspond lithologically to the Estancia 25 de Mayo Formation, representing a distal fluvial, arenaceous system in comparison with the shallow marine deposits of the latter. In Chilean Tierra del Fuego it is also convenient to continue using the name Filaret Formation for its chronostratigraphic equivalent (*sensu lato*) (Fig. 12), because lithologically the two formations are not completely comparable.

2.5.2 Major unconformities

For the Cenozoic, four to five major unconformities are well recognized that can be followed throughout the basin, as derived from paleontological, seismic-stratigraphic, facies distribution, and detrital zircon data. However, from subsurface studies in Tierra del Fuego, an unconformity can be recognized, marked by onlaps above of the marker G7 (Harambour, 1965) which separates the Cenozoic from Cretaceous strata, but in Skyring-Brunswick Peninsula area this unconformity cannot be identified nor lithostratigraphically as Rocallosa Formation gradually pass to Chorrillo Chico Formation (Charrier and Lahsen, 1969) nor chronostratigraphically as Rocallosa Formation yielded an age of Maastrichtian-Danian (YP: 62 Ma and second YP: 66 Ma) (Mpodozis in Álvarez et al., 2006) in Skyring Sound and Chorrillo Chico Formation yielded an age of Maastrichtian-Thanetian in Brunswick Peninsula. Therefore, the contact between Rocallosa and Chorrillo Chico Formation in Skyring-Brunswick Peninsula area (Fig. 12) represents the correlative conformity of the G7 unconformity in Tierra del Fuego.

The first well recognized unconformity is located between the Chorrillo Chico and Agua Fresca Formations close to the Paleocene-Eocene boundary (Fig. 12), based on the different lines of evidence presented below:

- Carrillo-Berumen et al. (2013) noted the absence of dinoflagellate cysts of the genus *Apectodinum*, which characterizes the Paleocene-Eocene boundary; their absence suggests the presence of a hiatus or stratigraphic gap.

- Malumián et al. (2013) recognized a marked faunal change at the Paleocene-Eocene boundary, where the cosmopolitan association of Midway-type foraminifers that characterizes the Paleocene is replaced by another strongly endemic association of Austral character during the early Eocene. Although this change could be of global significance, it could also indicate the existence of a regional gap in the sedimentary record.

- Biddle et al. (1986), based on an analysis of seismic facies, observed an erosional truncation at the top of the Chorrillo Chico Formation, located in the middle Thanetian, and also noted that this erosional surface has a regional extent. It was subsequently linked to a prominent unconformity between the Selandian and middle Eocene by other authors (Thomas, 1949; Malumián et al., 2000; Fosdick et al., 2011, *inter alia*).

- Gutiérrez et al. (2017) noted that the contact between the Dorotea (~70 Ma) and Man Aike (~40 Ma) Formations in Sierra Baguales is paraconformable to unconformable, with an age difference of almost 30 Ma between these two formations.

- In the distribution of detrital zircon ages presented in this study, a prominent gap between 40-60 Ma can be observed (Fig. 2.13). In Sierra Baguales, Gutiérrez et al. (2017) reported a gap in the ages of zircons derived from a predominantly eastern source area, between 75 – 50 Ma. Together, this suggests a general gap between 60 and 50 Ma, which is confirmed by a gap around 50 Ma in zircons from the Río Turbio and “Río Guillermo” Formations of Fosdick et al. (2015b). Although this gap could be due to a change in paleocurrent directions, it could also be related to a hiatus in the source areas.

The presence of a gap in the sedimentary record between the middle Thanetian and early Ypresian can be dated more accurately by the micropaleontological content of both the Chorillo Chico and Agua Fresca Formations between ~56.2 and ~53.25 Ma. This discontinuity can be correlated with the well-established Selandian – middle Eocene hiatus in the Última Esperanza Province (Fig. 2.12) (Malumián et al, 2000; Fosdick et al., 2011), which according to detrital zircon ages from the Dorotea and Río Turbio Formations had a range of 60.5±0.8 to 47.1±2.7 Ma (Fosdick et al., 2015b).

A second unconformity is possibly situated between the Agua Fresca and Tres Brazos Formations close to the Lutetian-Bartonian limit (Fig. 2.12). This is supported by the following evidence:

- Todd and Kniker (1952) mentioned a discordant contact between these formations, probably based on micropaleontological data, but did not provide any details.
- Malumián et al. (2013) recorded an unconformity between turbiditic, anaerobic and shallower, oxidised environments in the Agua Fresca and Tres Brazos Formations, respectively, which agrees with our environmental interpretation of these formations. However, a marked facies change does not always indicate the existence of an unconformity.
- The existence of a break in sedimentation between the lower and upper members of the Río Turbio Formation as tentatively proposed by Fosdick et al. (2015b). This is suggested by the ages of detrital zircons, which can be analyzed in two ways: first, if the MDA ages of the lower (46.3±1.3 Ma) and upper (33.8 ±0.4 Ma) members are considered, they indicate a hiatus of 12.5 Ma; second, if considering only the youngest individual zircon ages in both members (46.3±1.3 Ma and 43.75 Ma, respectively), they suggest a hiatus of ~2.55 Ma.

Although this is the least certain of the 5 unconformities recorded by us in the basin, we believe that a short hiatus existed between the Agua Fresca and Tres Brazos Formations close to the Lutetian-Bartonian limit (41.2 Ma), with a duration of about 2 – 3 Ma.

A third prominent unconformity is present between the Loreto and Río Leona Formations (Fig. 2.12) (old Las Coles Member of the El Salto Formation) close to the Rupelian-Chattian boundary. The evidence in this case can be summarized as follows:

- Malumián et al. (2013) registered an abrupt variation in depositional environment in formations of the Atlantic coast of Tierra del Fuego, changing from below the carbonate compensation depth (~4000 m) to very shallow environments as suggested by the appearance of a conglomerate wedge. This was coeval with uplift of the region between Última Esperanza-Rio Turbio and the Brunswick Peninsula.

- Several authors recorded an unconformity between the Man Aike and Río Leona Formations (Malumián and Caramés, 1997; Camacho et al., 2000; Marenssi et al., 2002; Casadío et al., 2009) for the Lago Argentino and Río Turbio areas.

- Gutiérrez et al. (2017) reported a difference in age of around 8 Ma between the Man Aike and Río Leona Formations.

- González (1953) refers to the studies of Floreal García in the Río Pérez-Cordillera Pinto area (Fig. 2.2), where a pronounced angular unconformity was observed between the El Salto Formation (*sensu lato*) and the Loreto Formation. There is also a marked change in facies and thickness in both units towards the east and northeast. In addition, it was noted that this unconformity becomes less prominent east of Cordillera Vidal and that it can be traced into northeastern Tierra del Fuego. The El Salto Formation (here referred to as the Río Leona Formation) wedges out strongly between Pérez River and Cordillera Pinto.

- The ages reported here for the Loreto Formation (sample SK1, Table 2.1) and Río Leona Formation (sample SK2, Table 2.1), geographically separated by less than 1.5 km, suggest a marked interruption in sedimentation with a duration of at least 10 Ma, along the northern coast of the Skyring Sound.

- There is a gap in detrital zircon ages between 30 and 25 Ma (Fig. 2.13), between Sierra Baguales (Última Esperanza Province) and the Brunswick Peninsula (Magallanes Province). This could either result from an unconformity or an abrupt change in paleocurrent directions, which in both cases could be related to a tectonic uplift.

The fourth unconformity is present between the Río Leona Formation (former Las Coles Member) and the El Salto Formation (equivalent to the Estancia 25 de Mayo Formation) close to the Chattian-Aquitanian boundary (Fig. 2.12). This is indicated by the following evidence:

- Results of a palynological analysis by Barreda et al. (2009) of the Río Leona Formation showed substantial differences with the overlying Estancia 25 de Mayo (ex-Centinela) Formation, suggesting a temporal gap between these units embracing the late Oligocene-early Miocene.

- Furque and Camacho (1972) confirmed that the base of the Estancia 25 de Mayo Formation is an erosional unconformity.

The ages reported in this study for the El Salto Formation (sample RV1, Table 2.1) and the Río Leona Formation (sample SK2, Table 2.1) clearly indicate a temporal gap of at least 6 Ma between 26.41 and 19.0 Ma in the area between the Brunswick Peninsula and the Skyring Sound. On the other hand, ages reported by Fosdick et al. (2011) in the Última Esperanza area for what they denominated the Río Guillermo Formation (here divided into the El Salto and Río Leona Formations) indicate a more restricted and also younger gap between 21.7 and 19.8 Ma.

The last major unconformity corresponds to the contact between the El Salto Formation (equivalent to the Estancia 25 de Mayo Formation) and the Palomares Formation (equivalent to the Santa Cruz Formation) close to 18 Ma (Fig. 2.12), as evidenced by the following:

- North of the Skyring Sound, in the foothills of Cordillera Vidal (Fig. 2.4), González and Tapia (1952) and González (1953) described the Palomares Formation as overlying strongly folded and fractured strata of the El Salto Formation (*sensu lato*). Similarly, Ramos (1982) recognized an angular unconformity between the Estancia 25 de Mayo and Santa Cruz Formations in the Lago Cardiel area of Argentina.

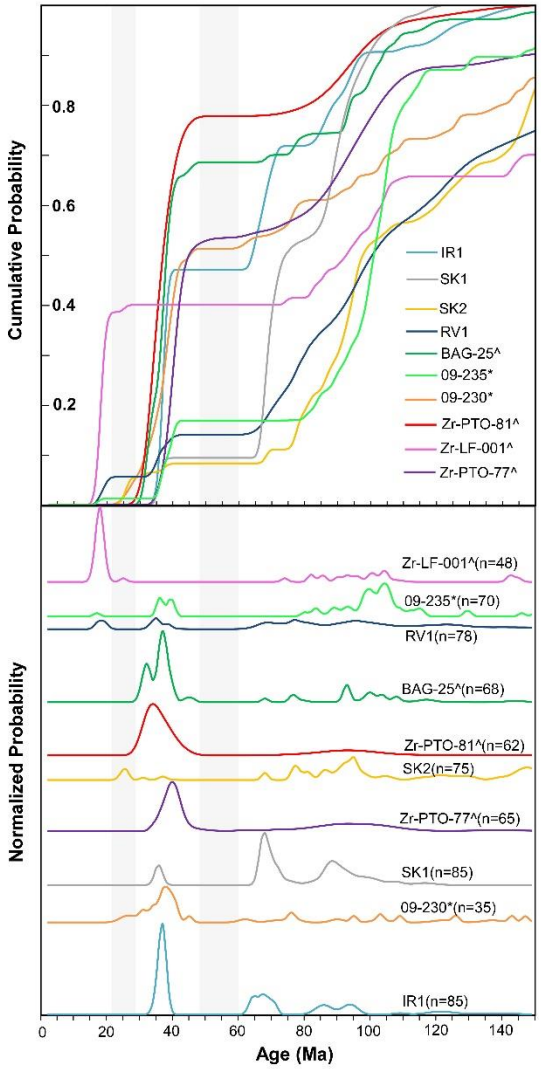

Figure 2. 13. Integrated Normalized Probability and Cumulative Probability plots, highlighting the two gaps in the population of the detrital zircon ages (grey shading). Note the prominent peak between ca. 32 – 40 Ma, indicating reactivation of the magmatic arc. The peak at ca. 18 Ma represents the last orogenic pulse identified in this study. The ^ indicates samples from Gutiérrez et al., 2017; the * from Fosdick et al., 2015a.

- An abrupt facies change in the San José Member of the Palomares Formation, which towards the west (Cordillera Vidal) is represented by the Vidal Conglomerate (a coarse volcanic breccia) and towards the east by ever more distal fluvial facies, indicates marked volcanic and tectonic activity during deposition of the Palomares Formation.

Although these data support the existence of an unconformity, it must be emphasized that its regional extent is still debatable, as Cuitiño (2011) mentioned a gradual transition between the Estancia 25 de Mayo and Santa Cruz Formations in the Santa Cruz Province of Argentina. Bostelmann et al. (2013) did not report an unconformity

between these two formations in the Sierra Baguales just south of the Argentinian border, but the contact zone is in fact obscured by loose talus and vegetation. Detrital zircon ages do not support the existence of a long-lived hiatus between these two units, although the locally observed angular disconformities and evidence of tectonic activity at the start of the Palomares Formation indicate that it does exist, at least in the southern part of Patagonia.

2.6 Discussion and conclusions

2.6.1 Evolution of basin-filling

Cenozoic infilling of the Magallanes-Austral foreland basin in the Peninsula Brunswick-Skyring Sound area (Fig. 2.4, 2.5) started with deeper environments compared with the neritic internal shelf to lower shoreface environment as manifested in the Rocallosa Formation (Mpodozis, in Álvarez et al., 2006). The Cenozoic foreland basin progressively deepened to reach bathyal depths in which the prograding turbidite lobes of the Chorrillo Chico Formation were deposited. This initial sedimentary infilling marks an abrupt change with respect to the southerly and southwesterly direction of paleocurrents that dominated the basin until the Late Cretaceous (Gutiérrez et al., 2017). At this time detritus began to be delivered from the south and south-southeast, as evidenced by the facies distribution and paleocurrent directions measured by us as well as the latter authors. The gravelly to coarse sandy facies overlying the finer, deeper marine sediments deposited by turbidity currents in Tierra del Fuego (Sánchez et al., 2010), represent the wedge top depozone of an advancing deformational front that continually disturbed sedimentation in the proximal part of the foredeep. In this way, the facies identified by us in the Chorillo Chico Formation in the eastern and western parts of the Brunswick Peninsula represent the most distal and deepest parts of a submarine fan, which showed a clear north-northwesterly progradation affected by uplift episodes as the orogenic wedge advanced. This advance is reflected by conglomerates and other proximal facies in the lower part of the Agua Fresca Formation. The first cycle of sedimentation thus reveals the existence of ample accommodation space (underfilled foreland basin) at least until the late Ypresian, when the upper part of the Agua Fresca Formation began to be deposited.

The second period of basin infill is characterized by a change in the stacking pattern, now dominated by aggradation or vertical accretion of pelagic and hemi-pelagic sediments corresponding to the uppermost parts of the Agua Fresca Formation. This indicates a near-equilibrium phase between accommodation space and sediment input, which was succeeded by the prograding and aggrading delta facies of the Tres Brazos Formation. This shallow marine accumulation was related to a normal regressive cycle in which sediment input outstripped a relative rise in sea-level (Fig. 2.14). At the same time, a change in paleocurrent directions towards the north-northeast is observed throughout the entire basin, which is concordant with the paleocurrent data observed by Gutiérrez et al. (2017) in the Sierra Baguales area. Although more detailed sedimentological studies in the Agua Fresca Formation and its relationship with the overlying Tres Brazos Formation are required, we can tentatively infer that the facies succession between these units represents the establishment of a continental shelf system in which the deltaic facies of the Tres Brazos Formation constituted the topsets of slope clinoforms in the Agua Fresca Formation. If this is correct, it would indicate the existence of a shelf-edge delta in the Tres Brazos Formation during the onset of a sea-level lowstand, and could explain the contrasting geometry between the deepwater ramp system that dominated during deposition of the Chorrillo Chico Formation and the basal terminations of the Agua Fresca Formation.

A short-lived marine flooding event interrupted the sedimentary systems above, allowing the hemi-pelagic, outer shelf deposition of the Leña Dura Formation (Fig. 2.12) and the establishment of much shallower shelf-margin deltaic systems that prograded towards the northeast. Paleocurrents indicate an additional westerly mode attributed to flood-tidal currents. The facies changes recorded towards the north, between the Loreto Formation and the estuarine facies of the chronostratigraphically equivalent Man Aike Formation (Fig. 2.12), suggest an irregular coastline with local bays, rivers and deltas. Tectonic uplift in the south also caused detritus to be contributed from this area, but the uplift focus gradually migrated towards the northern part of the basin. The Loreto Formation thus appears to have had a synorogenic character, which together with a sea-level fall between the Bartonian and Oligocene (Dingle y Lavelle, 1998; Le Roux, 2012a) caused forced regression that ended in continental sedimentation. There is no doubt that this pulse of tectonic uplift that reached its peak in the Oligocene and lasted until the early

Miocene, gave rise to the high-energy fluvial environments of the Río Leona and El Salto Formations (Fig. 2.10) in the Brunswick Peninsula-Skyring Sound area. Although the uplift and associated thrust faulting caused basin subsidence in the foreland that allowed the incursion of the Patagonian Sea towards the north and northwest, giving rise to the deposition of the Estancia 25 de Mayo Formation, in the areas proximal to the orogen (Brunswick Peninsula-Skyring Sound), this marine incursion is absent. In this context, the El Salto Formation would thus represent the most proximal or continental facies of the Estancia 25 de Mayo Formation, with sediment sourced from the southwest as indicated by northeastward-directed paleocurrents. This southwestern provenance already prevailed since the Oligocene, as suggested by the facies change in the Río Leona Formation, which in the Brunswick Peninsula-Skyring Sound area partly reflects a high-energy fluvial system and towards Lago Argentino was dominated by meandering rivers and marshy floodplains (Barreda et al., 2009).

A period of volcanic activity followed that deposited tuffaceous beds at the top of the El Salto Formation and in the Palomares Formation, which can also be observed in the volcanic ash layers of the Estancia 25 de Mayo and Santa Cruz Formations in the northern part of the basin (Cuitiño and Scasso, 2013, Gutiérrez et al., 2017). A tectonic event subsequently gave rise to the local emplacement of basalts, which were strongly eroded and reworked into the basaltic breccias known as the Vidal Conglomerate (Fig. 2.9e). The latter grades laterally into a high-energy, braided fluvial system (Fig. 2.11) representing the proximal facies of the Santa Cruz Formation, which in the northern and northeastern part of the basin reflects lower-energy meandering channels. The latter were coeval with volcanic activity as shown by the intercalated tuffs in the upper member of the Palomares Formation. The source area remained in the southwest, however, as shown by facies relationships and northeast-directed paleocurrents in the latter unit.

2.6.2 Influence of basin configuration on stratigraphic architecture

Our overview of sedimentological, paleontological, ichnological, and geochronological data shows that coeval Cenozoic formations of the Magallanes Basin have contrasting stratigraphic and sedimentological architectures in the southern and northern parts of the basin. This confirms but also contrasts some conclusions of other authors working in different parts of the basin. Charrier and Lahsen (1969) proposed the

existence of a northeast-southwest-striking topographic high between the Skyring Sound and the Strait of Magallanes, which separated two depocenters with contrasting geochemical signatures and opposite paleocurrent directions (south-to-north vs. northwest-to-southeast) in successions that preceded the Chorrillo Chico Formation. For the Upper Cretaceous units, Mpodozis (in Álvarez et al., 2006) and Mpodozis et al. (2007) recognized a regional facies contrast between the Última Esperanza region (deep-marine turbidites) and the Peninsula Brunswick-Skyring Sound area (shallow marine associations). Locally, between the Brunswick Peninsula and Skyring Sound, they also recorded marked differences between facies and paleocurrent directions. Ghiglione et al. (2009), from a structural more than stratigraphic point of view, suggested that the area between Lago Viedma (Argentina) and Última Esperanza Province exhibits along-strike changes in the fold-and-thrust belt of the Southern Patagonian Andes, which together with north-south thickness and facies variations of the Late Cretaceous to early Tertiary deposits could reflect an inheritance of the paleobathymetry-topography of the Late Jurassic extensional depocenters.

The age of the Dorotea Formation generally increases northward, which reflects southward progradation from a topographically elevated area (or local basin margin) that existed in the north during the Campanian-Maastrichtian. The same configuration probably influenced the well-documented transgressive-regressive pulse in Última Esperanza Province and Lago Argentino (Mpodozis et al., 2011) during the Maastrichtian-Danian, which is hardly recognized in the Brunswick Peninsula and Tierra del Fuego. This trend had already been established in the underlying, Cenomanian-Campanian Tres Pasos Formation (Gutiérrez et al., 2017), and also persisted until at least the Eocene, as shown by the fact that the Paleocene-Eocene unconformity represents a much wider sedimentation gap in Última Esperanza than in the Brunswick Peninsula (Fig. 2.12). During the middle to late Eocene interval, significant facies differences are displayed between the Río Turbio/Man Aike Formations (Fig. 2.12) (old “upper” and “lower” members of the Río Turbio Formation) around Lago Argentino and Última Esperanza, and the coeval Tres Brazos, Leña Dura and Loreto Formations in the Brunswick Peninsula-Skyring Sound areas. However, coastal, deltaic to estuarine facies are common to both the northern and southern deposits, which indicates that the basin had become less depth-differentiated at this stage. The early Burdigalian Patagonian Transgression subsequently

affected only the northern part of the basin, whereas the southern areas exhibited coarser, more proximal fluvial facies (Palomares Formation) than their coeval northern facies (Santa Cruz Formation) during the middle to late Burdigalian. This can be ascribed to intensified uplift in the Southern Patagonian Andes at this time (Bostelmann et al., 2013, Gutiérrez et al., 2017). The basin thus exhibited a "see-saw" depositional pattern starting with shallow areas in the north and deeper areas in the south until the Eocene, and ending with the opposite configuration by the Miocene.

2.6.3 Link with global tectonic events

The distinct gap between 60 – 50 Ma in detrital zircon ages of the Cenozoic succession could be associated with a period of tectonic quiescence or reduced magmatic activity, which in turn could possibly be related to lithospheric stagnation characteristic of an episode of regimen change in the mantle (O'Neill et al., 2007). Such episodes are manifested as a decrease in the volume of oceanic crust production at the ocean ridges and accompanying cooling, which allow a deepening of the ocean basins and global sea-level falls (Moucha et al., 2008). The latter cause a lowering of the erosional base level of the continents, leading to widespread erosion and the development of extensive unconformities in the stratigraphic record, as clearly recorded in our studied succession. However, increased tectonic activity along the mid-ocean ridges should also lead to the development of unconformities on the adjacent continents, due to increased spreading rates and mountain building.

The first two unconformities reported here at the Chorrillo Chico-Agua Fresca and Agua Fresca-Tres Brazos contacts, coincide very well with the start of the Ypresian and Bartonian-Rupelian climatic cooling periods identified by Le Roux (2012a) (see Fig.2.14). The first unconformity (Chorrillo Chico-Agua Fresca limit) formed simultaneously with the initial decrease in oceanic crust production along the East Pacific Ridge (Conrad and Lithgow-Bertelloni, 2007). The same process was repeated along the South Pacific Ridge, which coincided with the second major unconformity (Fig. 2.14) (Agua Fresca-Tres Brazos limit) and was also coeval with the first incursion of Pacific Ocean waters into the Atlantic Ocean along the Drake Passage (Scher and Martin, 2006; Barbeau et al., 2009; Le Roux, 2012a; Gutiérrez et al., 2017) and the Oi-1 sea-level fall (Zachos et al., 1996).

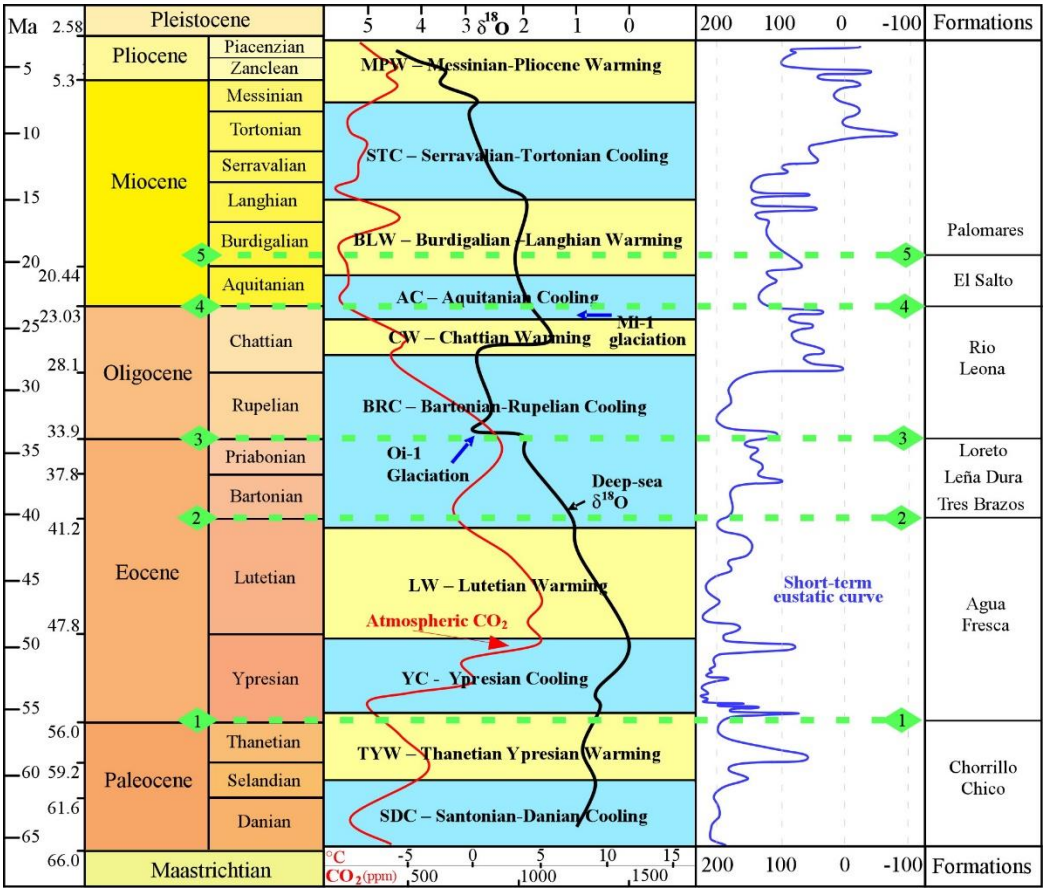

Figure 2. 14. Major unconformities related to long-term global trends in ocean and air temperatures from Le Roux (2012) and short-term eustatic curve from Abreu and Anderson (1998). Note how the unconformities fit well with cooling and warming episodes, as well as with short pulses of sea level fall.

The fourth unconformity (Río Leona-El Salto contact) was in turn coeval with the Aquitanian cooling episode (Le Roux, 2012) (Fig. 2.14), which coincided with a decrease in the spreading rate of the Southwest Indian Ocean (Patriat et al., 2008) as well as the North Pacific (Cande and Kent, 1992), increased deep circulation of the Antarctic Circum-polar Current (Lyle et al., 2007), and the Mi-1 sea-level fall (Miller et al., 1991; Naish et al., 2008). Although the third and fifth unconformities between the Loreto-Río Leona and El Salto-Palomares Formations, respectively, do not coincide with periods of marine cooling (Fig. 2.14), they seem to have been linked to the Chattian and Burdigalian-Langhian Warming Episodes (Le Roux, 2012) between 28 – 24 Ma and 21 – 15 Ma, respectively. The former coincided with the breakup of the Farrellon Plate (Herron and Heirtzler, 1967), commencement of spreading in West Scotia Ridge (Barker, 2001), opening of Bransfield Basin (Sell et al., 2004), an increase in the South Pacific spreading rate, and global sea-floor production (Somoza, 1998; Conrad and Lithgow-Bertelloni,

2007), whereas the second was simultaneous with a high convergence rate between the South American-Nazca Plates (Pardo-Casas and Molnar, 1987), the Quechua Phase of deformation in the central Andes (Malumián and Ramos, 1984; Ramos, 2002) and prominent uplift of the Southern Patagonian Andes (Blisniuk et al., 2005; Gutiérrez et al., 2017).

2.6.4 Growth of the Patagonian Andes inferred by the sedimentary response

The evolution of the entire Cenozoic Magallanes-Austral foreland basin has been strongly controlled by different factors, among which were both regional and global tectonic events, magmatic processes intimately associated with uplift of the Southern Patagonian Andes, and climate changes related to the latter. These have left a clear imprint on the sedimentary processes.

To date, three orogenic and deformational episodes have been documented in the basin (Coutand et al., 1999; Suárez et al., 2000a; Ghiglione and Ramos, 2005; Fildani et al., 2008; Ghiglione et al., 2016), namely during the Late Cretaceous, Eocene-Oligocene, and post-Miocene. However, these have been imprecisely defined due to the scarcity of reliable dates for the Cenozoic units and deformational events (Suárez et al., 2000a). Proof of the first of these orogenic episodes has been based on the closure of the Rocas Verdes Marginal Basin and the initiation of Cretaceous turbidite deposition (Wilson, 1991; Fildani and Hessler, 2005; Ghiglione et al., 2016). The second was based on the hiatus in the Paleocene-middle Eocene (Thomas, 1949; Malumián et al., 2000; Fildani et al., 2008; Fosdick et al., 2011, *inter alia*) and the subsequent progressive unconformities and growth strata documented in the Río Turbio Formation (Malumián et al., 2000; Álvarez et al., 2006), in addition to synorogenic deposition of the Río Leona Formation during the early Oligocene. The last episode is largely based on the extrusion of plateau basalts (Ramos, 1989) associated with collision of the Chile Ridge and eastward tilting of the craton (Fildani et al., 2008; Ghiglione et al., 2016).

Our geochronological data and identification of depositional environments encompassing the complete Cenozoic succession in the Brunswick Peninsula-Skyring Sound, allow us to distinguish five stages of orogen emergence uplift in the foreland related to uplift of the Andes during the Maastrichtian-Burdigalian transition. These stages mark the most active phases of the basin from both tectonic and depositional perspective,

where tectonic uplift in the fold-thrust belt is expected to peak which lead high sedimentation rates.

The first stage (68 – 56 Ma) marks the initiation of deposition in the Cenozoic foreland basin, characterized by the progradation of deep-marine, distal turbidite lobes over the base of the continental slope (Chorrillo Chico Formation), in response to an incipient orogenic uplift phase towards the south. The clastic composition of the Chorrillo Chico Formation, rich in quartz, indicates that it was derived mainly from a metamorphic provenance, and in minor proportion from silica-rich volcanic sources or quartz-rich sedimentary units (Fig. 2.6a, b, c). The NNW transport direction indicated by paleocurrents suggests that the sources could have been situated towards the SSE where the Darwin Metamorphic Complex and volcaniclastic succession of the Tobífera Formation are widely exposed (Figs. 2.1 and 2.2). However, the distribution of detrital zircon ages in the Chorrillo Chico Formation shows that they do not exceed 130 Ma, indicating that the most likely source was the Patagonian Batholith (of Hervé et al. 2007) (Fig. 2.15a). This first stage also can be recognized in Última Esperanza Province, where the upper Dorotea Formation (Maastrichtian-Selandian *sensu* Fosdick et al. 2015b) exhibits felsic to intermediate (meta-) volcanic clastic composition (Schwartz and Graham, 2015) indicating unroofing of thrust sheets containing upper Jurassic volcanic rocks of the late-stage Rocas Verdes volcanism and South Patagonian Batholith (Schwartz et al., 2016).

The progress of this orogenic uplift, manifested by the unconformity that separates the Agua Fresca and Tres Brazos Formations, reflects a new tectonic pulse or second orogenic phase (43 – 42 Ma) that gave rise to a reactivation of the depositional system and produced an abrupt change in sedimentary environments as well as paleocurrent directions, passing from semi-pelagic to deltaic systems (Tres Brazos Formation) and from sources in the SSE to SW. Although the clastic composition of the Tres Brazos Formation shares certain characteristics with the Chorrillo Chico Formation, such as an abundance of quartz, the presence of lithic sedimentary fragments in the latter is important (Fig. 2.6d, e, f), suggesting the exhumation and erosion of an emerging orogen situated more towards the west. Although the TB2 sample cannot be used for a MDA estimation because of the detrital zircon population was skewed, but can be a good indicator for provenance studies. Therefore, the distribution of detrital zircon ages in the Tres Brazos Formation shows unroofing of thrust sheets containing Chorrillo Chico and Rocallosa

Formations (Fig. 2.15b), which in turns, explains the similarity of the clastic composition of the Tres Brazos and Chorrillo Chico Formations.

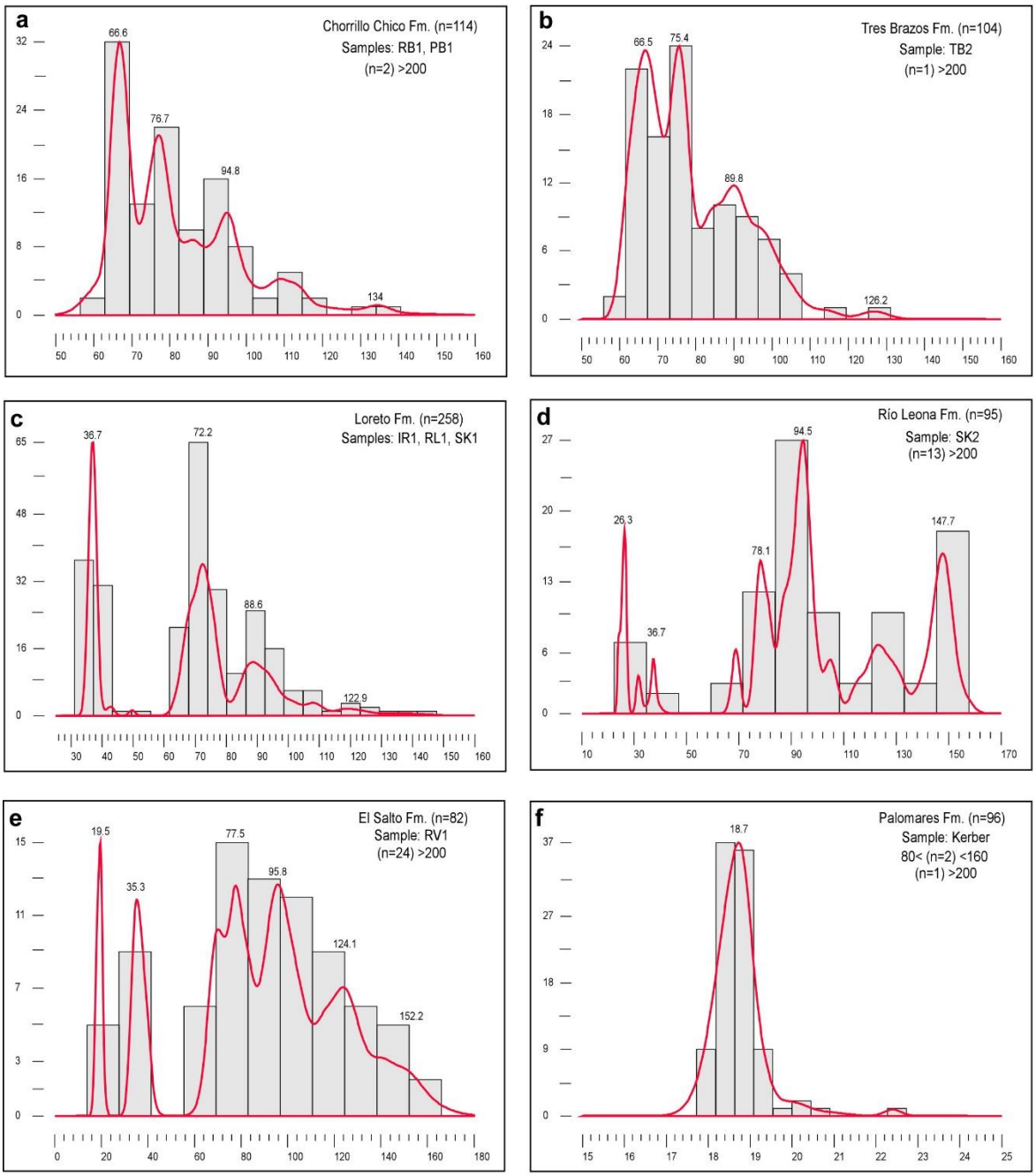

Figura 2. 15. Composite histograms and probability density plots for detrital zircons grouped by lithostratigraphic formations. Lower case "n" beside the formation name refers to total number of grains younger than 200 Ma. Grains > 200 Ma not shown in plot but indicated by "n" in parentheses; only for Palomares Formation grains older than 80 Ma but younger than 160 Ma not shown in plot.

The third phase (37.8 – 33.9 Ma) is revealed by the synorogenic nature of the Loreto Formation, in which a deltaic system was established after a short deepening of the environments. The paleocurrent directions remained constant although a certain

contribution from the east can be identified, possibly related to the existence of a forebulge in this area. The clastic composition of the basal part of the Loreto Formation indicates a contribution from the magmatic arc towards the west, which continued supplying detritus until the end of this formation. However, the uppermost part shows a similar proportion between lithic volcanic and sedimentary fragments, monocrystalline quartz, and feldspar (Fig. 2.9a, b), suggesting that the early Cenozoic and latest Cretaceous rocks were already exhumed and provided an additional source of detritus (Fig. 2.15c). This stage marks the reactivation of active volcanism that started during the Late Cretaceous and the initiation of the most prominent uplift of the Patagonian Andes, as indicated by the prominent, laterally extensive unconformity between the Man Aike/Loreto and Río Leona Formations.

The transition to a continental environment reflected by the Río Leona-El Salto Formations indicates the fourth orogenic stage (26.4 – 19.6 Ma), during which a marked change in the source areas occurred, this time located mainly towards the SW and associated with the volcanic arc, given the abundance of lithic volcanic fragments (Fig. 2.9c, d). The unconformity that separates both units and the appearance of sedimentary fragments in the clastic composition of the Río Leona and El Salto Formations suggests that sedimentation was interrupted by tectonic uplift that exposed to erosion previously deposited sedimentary rocks as Loreto Formation and older units (Fig. 2.15d, e). This stage is the most representative of the Patagonian Andes uplift, as indicated by strong folding of the Río Leona-El Salto succession, which represents the growth of the orogenic wedge.

Finally, the fifth orogenic stage after 18.7 Ma, is manifested by the deposition of the Vidal Conglomerate at the base of the Palomares Formation and the unconformity that separates it from the underlying El Salto Formation. The clastic composition indicates a mafic volcanic source (Fig. 2.9 e, f) not far to the west, probably in the vicinity of the Pinto Cordillera (Figs. 2.2 y 2.4). If this is correct, this orogenic pulse could be related to the subduction of the seismic Chile Ridge during the Miocene.

The Paleogene orogenic stages apparently affected mainly the basement, with part of the deformation transferred to the cover rocks. This can be related to the reorganization of tectonic plates, in which the collision of the Farallon-Aluk (Phoenix) Ridge with the

South American Plate started approximately between 52 and 50 Ma (Ghiglione et al., 2016) and its progressive migration towards the south allowed the reactivation of the orogenic front (Cande and Leslie, 1986; Gorring et al., 1997; Ghiglione and Ramos, 2005; Ghiglione et al., 2016). On the other hand, the orogenic stages that took place during the Miocene could be related to subduction of the seismic Chile Ridge beneath the South American Plate, conditioned by changes in the subduction dynamics that probably reflect growth of the orogenic wedge in response to compressive forces transmitted from the deep-sea trough towards the foreland (Ramos, 1989; Fosdick et al., 2011; Ghiglione et al., 2016).

Acknowledgements

This study was financially and logistically supported by Project Fondecyt 1130006 under the auspices of Project CONICYT/FONDAP 15090013. CONAF-Magallanes kindly gave permission to work in the Magallanes and Laguna Parrillar National Reserves. L. Sánchez is thanked for her invaluable assistance during field campaigns. We gratefully acknowledge L. Rojas (Enap-Sipetrol) for permission to review unpublished reports and collaboration in this research, as well as J. Arriagada (Enap-sipetrol) for his assistance in searching through the Enap technical files database. We thank L. Buatois for his very kind and helpful assistance in the identification of some ichnological traces. Some detrital zircon dating was carried out by Mathieu Leisen in the Mass Spectometry Laboratory of the Andean Geothermal Centre of Excellence. The clarity of this manuscript has benefited greatly from comments and suggestions of Reynaldo Charrier and Marcelo Farías.

CAPÍTULO III.

CONCLUSIONES

El relleno sedimentario de cuencas de antepaís es el resultado de una compleja interacción entre procesos tectónicos y sedimentarios. La cuenca de Magallanes-Austral no es la excepción y provee un registro extraordinario de la variabilidad de los procesos alocíclicos ocurridos en las áreas fuente de aporte de sedimentos y de los autocíclicos dominantes en la cuenca de sedimentación por sí misma.

El desarrollo de la cuenca de antepaís sobre una litosfera fuertemente atenuada durante el Jurásico y Cretácico temprano, que durante la inversión, antiguas fallas normales fueron reactivadas como fallas inversas de alto ángulo, contribuyendo al desarrollo de una faja orogénica relativamente estrecha que permitiría la interacción del arco volcánico con el depocentro de la cuenca en distancias relativamente cortas en comparación con las demás cuencas de antepaís a nivel mundial, favoreció el gran aporte de detritos derivados del arco en las sucesiones sedimentarias tanto Cretácicas como Cenozoicas. La paleobatimetría-topografía heredada de la fase extensional antes mencionada, pudo condicionar el estilo de relleno y la compartimentalización de la cuenca favoreciendo una paleogeografía irregular y compleja con enbahiamientos locales, ríos, deltas y estuarios. De este modo se puede explicar las contrastantes arquitecturas estratigráficas entre las formaciones del Cenozoico en la parte norte (Provincia de Última Esperanza) y la parte sur (Provincia de Magallanes), sugiriendo que hasta fines del Paleógeno, prevaleció en la cuenca Magallanes-Austral dos depocentros independientes con procesos y mecanismos de sedimentación disímiles.

Durante el Cretácico tardío (Maastrichtiano) el patrón altamente progradacional registrado por la Formación Rocallosa (=Dorotea en Última Esperanza) de ambiente deltaico, da lugar a la depositación de lóbulos turbidíticos progradantes de profundidades batiales correspondiente a la Formación Chorrillo Chico, marcando así el inicio del relleno de la cuenca de antepaís Cenozoica. Este cambio pudo estar relacionado con actividad

del arco magmático y de la faja plegada del Cretácico tardío, donde un periodo de cabalgamiento habría iniciado desde el Campaniano temprano, soportado por la composición clástica predominante félsica a intermedia observada en la Formación Chorrillo Chico y en la Formación Dorotea (equivalente a Formación Rocallosa), lo cual sugiere el destechamiento de cuñas de cabalgamiento con presencia de rocas del Jurásico superior en conjunto con aportes provenientes del Batolito Patagónico. Posteriormente, la cuña progradante de la Formación Chorrillo Chico es reemplazada por un periodo de agradación de depósitos hemipelágico durante el Eoceno medio, este estadío queda representado por la Formación Agua Fresca. El siguiente estadío de relleno de la cuenca estaría dominado por condiciones cada vez más someras durante el Lutetiano, donde el espacio de acomodación y la sedimentación estarían casi en equilibrio dando lugar a la depositación del sistema deltaico progradante-agradante de la Formación Tres Brazos representando el inicio del establecimiento de un sistema de plataforma continental que prevaleció hasta el Priaboniano. Este sistema deltaico sería el resultado de la exhumación de las unidades del Cretácico tardío y Paleoceno temprano mediante otra etapa de corrimiento de la faja plegada y corrida de Magallanes (MFTB), lo cual se sustenta por la composición clástica típica de orógeno reciclado y la distribución de circones detríticos entre 75 y 65 Ma. Un corto pulso de inundación marina interrumpió la sedimentación anterior, permitiendo la depositación hemipelágica de plataforma externa de la Formación Leña Dura que luego dio paso al dominio de sistemas deltaicos de margen de plataforma de la Formación Loreto, el cual progradó hacia el NE, pero también recibió detritos desde el E, transportados por corrientes mareales las cuales estuvieron presentes durante mayor parte del sistema. La depositación de la Formación Loreto se relaciona con un periodo de exhumación de la MFTB y reactivación del arco volcánico al W. A partir del Oligoceno y por lo menos hasta el Mioceno inferior (Burdigaliano), la sedimentación en toda la cuenca cambia de marina a predominantemente continental producto del alzamiento más prominente de los Andes Patagónicos, donde las Formaciones Rio Leona, El Salto y Palomares representarían esta etapa cúspide de sedimentación de la cuenca de antepaís. No obstante, es importante puntualizar que la carga tectónica de los Andes Patagónicos, promovió una subsidencia flexural que permitió la transgresión marina del *Patagoniano* que dio lugar a la sedimentación marina somera de la Formación Estancia 25 de Mayo (Provincia de

Última Esperanza) y a las Formaciones Brush Lake y Filaret (definidas tanto en subsuelo como en superficie en la Provincia de Tierra del Fuego), sin embargo, esta transgresión no quedó registrada en la Provincia de Magallanes, donde sedimentos de abanicos aluviales y sistemas fluviales de alta energía correspondientes a las Formaciones Río Leona y El Salto, respectivamente, sugieren que estuvo emergida a causa de una mayor influencia de la progradación del frente de deformación de la MFTB, impidiendo así el ingreso de las aguas del atlántico.

El nuevo modelo evolutivo propuesto para la cuenca de antepaís Cenozoica, plantea marcadas diferencias con los modelos sedimentarios anteriormente conocidos para los depósitos terciarios, donde el inicio de la fase de relleno de la cuenca es dominado por depositación de turbiditas de agua profunda que pertenece a un gran sistema de abanicos submarinos que prograda hacia el NW desde el SE de Tierra del Fuego. Este sistema queda representado en su parte más proximal por la unidad informalmente definida “Estratos de Cabo Nariz” en Bahía Inútil (Tierra del Fuego) y en su parte media y distal, por la Formación Chorrillo Chico al Este y Oeste de la Península Brunswick, respectivamente. Esta etapa inicial de relleno, está estrechamente relacionada al crecimiento y migración de la Faja Plegada y Corrida de Magallanes (MFTB) en la conformación del sistema de cabalgamiento frontal de los Andes Patagónicos, donde la sedimentación del sistema de abanicos submarinos se enmarca dentro de depocentros de techo de cuña (Wedgetop depozone).

El entendimiento de los procesos sedimentarios que dominaron en la cuenca, integrado con el conjunto de datos geocronológicos y con la identificación de 5 discordancias regionales principales relacionadas a eventos tectónicos tanto locales como globales, ha permitido el establecimiento de un marco cronoestratigráfico que provee con la mayor precisión alcanzada hasta ahora, la cronología de los principales pulsos orogénicos de la cuenca durante el Cenozoico. Así mismo se ha clarificado de gran manera la nomenclatura estratigráfica, las correlaciones lito y cronoestratigráficas dentro de las diferentes Provincias Chilenas y entre la porción Argentina y Chilena de la cuenca, permitiendo una visión integrada de las fases evolutivas del relleno de la cuenca Magallanes-Austral y resaltando la relación intrínseca entre el tectonismo y la sedimentación.

Las etapas orogénicas ocurridas durante el Paleógeno parecen haber afectado mayormente el dominio del basamento, donde la deformación se pudo haber transferido hacia la cobertera sedimentaria. Estas pueden ser atribuidas a procesos relacionados a la reorganización de las placas tectónicas mayormente, donde la colisión del ridge Farallon-Aluk (Phoenix) contra los Andes Sur Patagónicos iniciada probablemente entre los 52-50 Ma y su progresivo desplazamiento hacia el sur permitió la reactivación del frente orogénico. Por otra parte, las etapas orogénicas que tomaron lugar durante el Mioceno pueden estar relacionados con la subducción del ridge sísmico de Chile por debajo de la Placa Sudamericana, condicionado por cambios en la dinámica de subducción y probablemente refleja el crecimiento de la cuña orogénica en respuesta a esfuerzos compresivos transmitidos desde la fosa hacia el antepaís. El inicio de la colisión del ridge sísmico de Chile *ca.* 18 Ma pudo ser la responsable del emplazamiento de los basaltos que dieron origen al miembro basal “Conglomerado Vidal” de la Formación Palomares, resaltando así la interacción tectónica-sedimentación en la cuenca.

El notable gap entre los 48-56 Ma en la actividad magmática del arco volcánico y escasez de emplazamientos del Batolito Sur-Patagónico a lo largo de la cuenca, en un contexto donde inicia la subducción del ridge Farallón-Aluk bajo la placa Sudamericana y junto con el descenso de la velocidad de generación de corteza oceánica en la dorsal del Pacífico Oriental a los *ca.* 56 Ma, podría hipotetizar la ocurrencia de un proceso de subducción sub-horizontal (flat slab) en la Cuenca de Magallanes, hacia fines del Paleoceno e inicio del Eoceno. Así mismo, la presencia de lavas de geometría tabular en la Cordillera Vidal, rodeadas por unidades de brecha gruesa inmersas en matriz arenosa parduzca del miembro Conglomerado Vidal de la Formación Palomares, asemeja la conformación morfoestructural del Morro Philippi y Morro Domeyko, para los cuales se ha propuesto anteriormente un origen relacionado a procesos de delaminación (slab window). El inicio de la colisión del Ridge Chileno *ca.* 18 Ma a lo largo del margen Pacífico del extremo sur de Sudamérica, podría ser el mecanismo gatillador de la delaminación en el Mioceno temprano (Burdigaliano).

Finalmente, en cuanto al potencial de recursos económicos, el análisis sedimentológico llevado a cabo en las formaciones del Cenozoico, abre la posibilidad a nuevos conceptos exploratorios de hidrocarburos y permite entender la complejidad de

otros. Como ejemplo, las turbiditas de la Formación Chorrillo Chico en las zonas proximales del depocentro, constituyen por una parte, un buen análogo para el estudio de sistemas turbidíticos de aguas profundas en respuesta al avance de la deformación en fajas plegadas (donde la inherente complejidad estratigráfica y estructural representa un factor de riesgo geológico en los proyectos de exploración), y por otra parte, constituyen un prospecto interesante de reservorio, en donde el avance de la deformación pudo haber creado y/o mejorado las trampas estratigráficas y estructurales para gas. Así mismo, la influencia mareal en el sistema deltaico de margen de plataforma de la Formación Loreto, desestima las características como reservorio de hidrocarburos, pero su carácter orogénico en patrón de apilamiento degradacional favorece el desarrollo de reservorios turbidíticos y de transporte de masa en las zonas baja del talud.

BIBLIOGRAFÍA

Álvarez, P., Elgueta, S., Mpodozis, C., Briceño, M., Vieytes, H., Radic, J.P., Mella, P., 2006. Proyecto Tranquilo-Otway, Informe Final. Informe Archivo Técnico ENAP, Santiago, (Inédito).

Akers, W., 1954. Ecologic aspects and stratigraphic significance of the foraminifera *cyclamina cancellata* Brady. Journal of Paleontology 28, 132-152.

Ameghino, F., 1906. Las Formaciones sedimentarias del Cretácico superior y del Terciario de Patagonia, con un paralelo entre sus faunas mastológicas y las del Antiguo Continente. Anales del Museo Nacional de Historia Natural de Buenos Aires, serie 3 (8), 1-568.

Bandy, O.L., 1964. General correlation of foraminiferal structure with environments. In: Imbrie, J., Newell, N. (Eds.), Approaches to paleoecology. John Wiley and Sons, New York, 238-27.

Barbeau Jr., D.L., Olivero, E.B., Swanson-Hysell, N.L., Zahid, K.M., Murray, K.E., Gehrels, G.E., 2009. Detrital-zircon geochronology of the eastern Magallanes foreland basin: Implications for Eocene kinematics of the northern Scotia Arc and Drake Passage. Earth and Planetary Letters 284, 489-503.

Bayona, G., Cortés, M., Jaramillo, C., Ojeda, G., Aristizábal, J.J., Reyes-Harker, A., 2008. An integrated analysis of an orogen-sedimentary basin pair: Latest Cretaceous-Cenozoic evolution of the linked Eastern Cordillera orogen and the Llanos foreland basin of Colombia. Gological Society Bulletin 120, 1171-1197.

Barker, P.F., Burell, J., 1977. The opening of the Drake Passage. Marine Geology 25, 15–34.

Barker, P.F., 2001. Scotia regional tectonic evolution: implication for the mantle flow and paleocirculation. Earth-Science Reviews 55, 1-39.

Barker, P. F., Thomas, E., 2004. Origin, signature and palaeoclimatic influence of the Antarctic Circumpolar Current. *Earth-Science Reviews 66*, 143-162.

Barwick, J., 1949. Tertiary stratigraphic studies in Eastern Peninsula Brunswick. Informe Archivo Técnico ENAP, Santiago, (Inédito).

Barreda, V. D., Palazzesi, L., Marenssi, S., 2009. Palynological record of the Paleogene Río Leona Formation (southernmost South America): Stratigraphical and paleoenvironmental implications. Review of Palaeobotany and Palynology 151, 22-33.

Beaubouef, R.T., 2004. Deep-water leveed-channel complexes of the Cerro Toro Formation, Upper Cretaceous, southern Chile. AAPG Bulletin 88, 1471-1500.

Belotti, H., Pagan, F., Perez Mazas, A., Agüera, M., Rodriguez, J., Porras, J., Köhler, G. Weiner, G. Conforto, G., Cagnolatti, M., 2013. Geologic Interpretation and Assessment of

Early Cretaceous Shale Oil and Gas Potential in Austral Basin, Santa Cruz, Argentina. Unconventional Resources Technology Conference, Denver, No. 1579691.

Berggren, W.A., Pearson, P.N., Huber, B.T., Wade, B.S., 2006. Taxonomy, biostratigraphy and phylogeny of Acarinina. Cushman Foundation Special Publication 41, 257-326.

Bernhardt, A., 2011. Paleogeography and sedimentary development of two deep-marine foreland basins: The Cretaceous Magallanes Basin, southern Chile, and the Tertiary Molasse Basin, Austria. Unpublished Ph.D. thesis, Stanford University, pp 218.

Bertels, A., 1977. Estratigrafía y micropaleontología de la Formación San Julián en su area tipo, Provincia de Santa Cruz, República Argentina. Ameghiniana, 14, 233-293.

Biddle, K.T., Uliana, M.A., Mitchum, R.M., Fitzgerald, M.G., Wright, R.G., 1986. The stratigraphic and structural evolution of the Central and Eastern Magallanes Basin, southern South America. Foreland Basins. Blackwell Publishing Ltd., 41-61.

Blisniuk, P.M., Stern, L.A., Chamberlain, C.P., Idleman, B., Zeitler, P.K., 2005. Andes climatic and ecologic changes during Miocene surface uplift in the southern Patagonian Andes. Earth and Planetary Science Letters 230, 125–142.

Bonarelli, G., 1917. Informe Geológico sobre exploraciones Petrolíferas en Magallanes. Santiago, Chile, Ministerio de Fomento, Dept. Minas y Petróleo.

Bossi, G.E., Vides, M.E., Ahumada, A.L., Georgieff, S.M., Muruaga, C.M., Ibáñez, L.M., 2000. Análisis de las paleocorrientes y de la varianza de los componentes a tres niveles, Neógeno del valle del cajón de Catamarca, Argentina. Revista Asociación Argentina de Sedimentología 7, 23-47.

Bostelmann, J.E., Le Roux, J.P., Vásquez, A., Gutiérrez, N.M., Oyarzún, J.L., Carreño, C., Torres, T., Otero, R., Llanos, A., Fanning, M., Hervé, F., 2013. Burdigalian deposits of the Santa Cruz Formation in the Sierra Baguales, Austral (Magallanes) basin: age, depositional environment and vertebrate fossil. Andean Geology 40, 458-489.

Buatois, L.A., Mángano, G., 2011. Ichnology: organism-substrate interactions in space and time. Cambridge University Press, pp 358.

Bruhn, R.L., Stern, C.R., De Wit, M.J., 1978. Field and geochemical data bearing on the development of a Mesozoic volcano–tectonic rift zone and back–arc basin in southernmost South America. Earth and Planetary Science Letters 41, 32–46.

Camacho, H. H., Chiesa, J. O., Parma, S. G., 1998. Relaciones estratigráficas entre formaciones terciarias en el occidente de la Provincia de Santa Cruz. Revista de la Asociación Geológica Argentina 53, 273-281.

Camacho, H. H., Chiesa, J. O., Parma, S. G., Reichler, V., 2000. Invertebrados marinos de la Formación Man Aike (Eoceno medio), Provincia de Santa Cruz, Argentina. Boletín de la Academia Nacional de Ciencias 64, 187-208.

Cande, S.C., Leslie, R.B., 1986. Late Cenozoic tectonics of the southern Chile trench. Journal of Geophysical Research 91, 471–496.

Cande, S.C., Kent, D.V., 1992. A new geomagnetic timescale for the Late Cretaceous and Cenozoic. Journal of Geophysical Research 97, 917–951.

Cañón, A., Ernst, M., 1975. Cuadro de correlaciones estratigráfica de la Provincia de Magallanes. Informe Archivo Técnico ENAP, Santiago, (Inédito).

Carrillo-Berumen, R.; Quattrocchio, M.E.; Helenes, J., 2013. Palinomorfos continentales del Paleógeno de las Formaciones Chorrillo Chico y Agua Fresca, Punta Prat, Región de Magallanes, Chile. Andean Geology 40, 539 -560.

Casadío, S., Griffin, M., Marenssi, S., Net, L., Parras, A., Rodríguez-Raising, M., Santillana, S., 2009. Paleontology and sedimentology of middle Eocene rocks in Lago Argentino area, Santa Cruz Province, Argentina. Ameghiniana 46, 27-48.

Castelli, J.C., Robertson, R., Harambour, S., 1993. Evaluación geológica y Petrolera de los bloques Ultima Esperanza sur e Isla Riesco. Informe Archivo Técnico ENAP, Santiago, (Inédito).

Cecioni, G., 1955. Distribuzione verticale de alcuniKosmmaticeratidae nella Patagonia cilena. Italia Servizio Geol. Boll. 74, 141-149.

Cecioni, G., 1957. Cretaceous flysch and molasse in Departamento Ultima Esperanza, Magallanes Province, Chile. Am. Association of Petroleum Geologist Bulletin 11, 111-120.

Céspedes, S., 1971. Estudio Geológico de la zona de Cabo Nariz y Tierra del Fuego. Informe Archivo Técnico ENAP, Santiago, (Inédito).

Charrier, R., Lahsen, A., 1969. Stratigraphy of Late Cretaceous-Early Eocene, Seno Skyring –Strait of Magellan Area, Magallanes Province, Chile. Am. Association of Petroleum Geologist Bulletin 53, 568-590.

Collet, L.W., 2008. Les dépôts marins. Paris, 1908.

Cookson, I.C., Cranwell, L.M., 1967. Lower Tertiary micro-plankton, spores and pollen grains from southernmost Chile. Micropaleontology 13, 204-216.

Conrad, C.P., Lithgow-Bertelloni, C., 2007. Faster sea floor spreading and lithosphere production during the mid-Cenozoic. Geology 35, 29–32.

Coutand, I., Diraison, M., Cobbold, P.R., Gapais, D., Rossello, E.A., Millar. M., 1999. Structure and kinematics of a foothills transect, Lago Viedma, southern Andes (49° 30`S). J. S. Am. Earth Science 12, 1–15.

Covault, J.A., Romans, B.W., Graham, S.A., 2009. Outcrop expression of a continental margin-scale shelf-edge delta from the Cretaceous Magallanes Basin, Chile. Journal of Sedimentary Research 79, 523–539, doi:10.2110/jsr.2009.053

Crame, J.A., 1999. An evolutionary perspective on marine faunal connection between southernmost South America and Antarctica. Scientia Marina 63, 1-14

Crane, W.H., Lowe, D.R., 2008. Architecture and evolution of the Paine channel complex, Cerro Toro Formation (Upper Cretaceous), Silla Syncline, Magallanes basin, Chile. Sedimentology 55, 979–1009.

Cuitiño, J.I., Scasso, R., 2010. Sedimentología y paleoambientes del Patagoniano y su transición a la Formación Santa Cruz al sur del Lago Argentino, Patagonia Austral. Revista de la Asociación Geológica Argentina 66, 406-417.

Cuitiño, J.I., 2011. Registro sedimentológico e isotópico de paleoambientes marinos y transicionales en el Patagoniano (mioceno) del Lago Argentino. Facultad de Ciencias Exactas y Naturales, Universidad de Buenos Aires, Tesis Doctoral (Inédita).

Cuitiño, J.I., Scasso, R., 2013a. Reworked pyroclastic beds in the early Miocene of Patagonia: reaction in response to high sediment supply during explosive volcanic events. Sedimentary Geology 289, 194-209.

Cuitiño, J.I., Ventura, R., Scasso, R., 2013b. Insights into the distribution of shallow-marine to estuarine early Miocene oysters from Southwestern Patagonia: sedimentological and stable isotope constraints. PALAIOS 28, 583-598.

Cuitiño, J.I., Fernicola, J.C., Kohn, M., Trayler, R., Naipauer, M., Bargo, M.S., Kay, R.F., Vizcaíno, S.F., 2016. U-Pb geochronology of the Santa Cruz Formation (early Miocene) at the Río Bote and Río Santa Cruz (southernmost Patagonia, Argentina): implications for the correlation of fossil vertebrate localities. J. of South American Earth Sciences 70, 198-210.

Dalziel, I.W.D., de Wit, M.F., Palmer, K.F., 1974. Fossil marginal basin in the southern Andes. Nature 250, 291–294.

Dalziel, I.W.D., 1981. Back-arc extension in the southern Andes: A review and critical reappraisal. Philosophical Transactions of the Royal Society London A, 300, 319–335, doi:10.1098/rsta.1981.0067.

Darwin, C., 1846. Geological observations on South America, pt. III, The Geology of the Voyage of the Beagle. London. Smith Elder and Co., pp 279.

Decat, J., Pomeyrol, R., 1931. Informe Geológico sobre las posibilidades petrolíferas de la Región de Magallanes. Boletín del Departamento de Minas y Petróleo, Ministerio de Fomento, Santiago, Chile, 69-77.

Dessanti, R.M., 1972. Andes Patagónicos septentrionales. 7th Symposio de Geología Regional Argentina, Academia Nacional de Ciencias, Córdoba, 655-688.

Dickinson, W.R., Suczek, C.A., 1979. Plate tectonics and sandstone compositions. AAPG Bulletin 63, 2164-2182.

Dickinson, W.R., Gehrels, G.E., 2009. Use of U-Pb ages of detrital zircon to infer maximum depositional ages of strata: A test against a Colorado Plateau Mesozoic database. Earth and Planetary Science Letters 288, 115-125.

Dingle, R, and Lavelle, M., 1998. Late Cretaceous-Cenozoic climatic variations of the northern Antarctic Peninsula: new geochemical evidence and review. PALAIOS 107, 79-101.

d'Orbigny, A., 1842. Voyage dans l'Amerique Méridionale (le Brésil, la République Orientale de l'Uruguay, la République Argentine, la Patagonie, la République du Chili, la République du Bolivia, la République du Pereou), exécuté pendant les anneés 1827,

1828, 1829, 1830, 1831, 1832 et 1833. P. Bertrand. París, V. Levrault, Strasbourg, vol. 3, 4.

Dott, R.H., Winn Jr., R.D., Smith, C.H.L., 1982. Relationship of Late Mesozoic and Early Cenozoic sedimentation to the tectonic evolution of the southernmost Andes and Scotia Arc, in Antarctic Geoscience, edited by C. Craddock, pp. 193–201, Univ. of Wisconsin Press, Madison.

Farfán, L., 1997. Sección estructural en la península Brunswick, extremo sur de Chile. 6th Simposio Bolivariano ACGGP-Exploración Petrolera en las cuencas subandinas.

Fasola, A., 1969. Estudio palinológico de la Formación Loreto (Terciario Medio), Provincia de Magallanes, Chile. Ameghiniana 6, 3-49.

Felsch, J., 1912. Informe sobre el conocimiento geológico en los alrededores de Punta Arenas y de la parte noroeste de Tierra del Fuego con el objeto de encontrar posibles yacimientos de petróleo. Boletín Sociedad Nacional de Minería, Santiago, Chile.

Feruglio, E., 1949-50. Descripción Geológica de la Patagonia. Dirección General de Yacimientos Petrolíferos Fiscales. Ministerio de Industria y Comercio de la República de la Argentina. Buenos Aires. v.1, 1-334.

Fildani, A., Hessler, A.M., 2005. Stratigraphic record across a retroarc basin inversion: Rocas Verdes-Magallanes Basin, Patagonian Andes, Chile. GSA Bulletin 117, 1596-1614.

Fildani, A., Romans, B.W., Fosdick, J.C., Crane, W.H., Hubbard, S.M., 2008. Orogenesis of the Patagonian Andes as reflected by basin evolution in southernmost South America. In Spencer, J.E., Titley, S.R., /eds), Ores and orogenesis: Circum-Pacific tectonics, geologic evolution, and ore deposits. Arizona Geological Society Digest 22, 259-268.

Fildani, A., Hubbard, S.M., Romans, B.W., 2009. Stratigraphic Evolution of Deep-Water Architecture: Examples of Controls and Depositional Styles From the Magallanes Basin, Southern Chile, SEPM Field Trip Guide., vol. 10, 73 pp., Soc. for Sediment. Geol., Tulsa, Okla.

Fossa Mancini, E., Feruglio, E., Yausen de Campana, J.C., 1938. Una reunión de Geólogos de YPF y el problema de la Terminología Estratigráfica. Boletín de Informaciones Petroleras. v.15, 31-95.

Fosdick, J.C., Romans, B.W., Fildani, A., Bernhardt, A., Calderón, M., Graham, S.A., 2011. Kinematic evolution of the Patagonian retro-arc fold-and-thrust belt and Magallanes foreland basin, Chile and Argentina, 51°30'S. Geological Society of America Bulletin 123, 1679-1698.

Fosdick, J.C., Grove, M., Hourigan, J.K., Calderón, M. 2013. Retroarc deformation and exhumation near the end of the Andes, Southern Patagonia. Earth and Planetary Science Letters 361, 504-517.

Fosdick, J.C., Graham, S.A., Hilley, G.E., 2014. Influence of attenuated lithosphere and sediment loading on flexure of the deep-water Magallanes retroarc foreland basin, Southern Andes, Tectonics, 33, 2505–2525, doi: 10.1002/2014TC003684.

Fosdick, J.C., Grove, M., Graham, S.A., Hourigan, J.K., Lovera, O., Romans, B.W., 2015a. Detrital thermochronologic record of burial heating and sediment recycling in the Magallanes foreland basin, Patagonian Andes. Basin Research 27, 546-572.

Fosdick, J.C., Bostelmann, E., Leonard, J., Ugalde, R., Oyarzún, J.L., Griffin, M., 2015b. Timing and rates of foreland sedimentation: new detrital zircon U/Pb geochronology of the Cerro Dorotea, Río Turbio and Río Guillermo Formations, Magallanes basin. XIV Congreso Geológico Chileno, La Serena, Chile.

Furque, G., Camacho, H.H., 1972. El Cretácico Superior y terciario de la región austral del Lago Argentino (Provincia de Santa Cruz). Actas 4º Jornadas Geológicas Argentinas, Buenos Aires, 61-75.

Ghiglione, M.C., Ramos, V.A., 2005. Chronology of deformation in the Southernmost Andes of Tierra del Fuego. Tectonophysics 405, 25–46.

Ghiglione, M.C., Suárez, F., Ambrosio, A., Da Poian, G., Cristallini, E.O., Pizzio, M.F., Reinoso, R.M., 2009. Structure and evolution of the Austral Basin, Fold-Thrust Belt, Southern Patagonian Andes. Revista de la Asociación Geológica Argentina 65, 215-226.

Ghiglione, F. A., Minniti, S., Gutiérrez-Pleimling, A., Ghiglione, M. C., 2011. Geología de la costa noreste del Skyring, Región de Magallanes, Chile. XVII Congreso Geológico Argentino, Neuquén, Abstract.

Ghiglione, M.C., Likerman, J., Barberón, V., Giambiagi, L.B., Aguirre-Urreta, B., Suárez, F., 2014. Geodynamic context for the deposition of coarse-grained deep-water axial channel systems in the Patagonian Andes. Basin Research, 1–20, doi: 10.1111/bre.12061.

Ghiglione, M.C., Ramos, V.A., Cuitiño, J., Barberón, V., 2016. Growth of the Southern Patagonian Andes (46–53°S) and their relation to subduction processes. In Folguera, A., Naipauer, M., Sagripanti, L., Ghiglione, M., Orts, D. y Giambiagi L. (eds.), Growth of the Southern Andes. Springer Earth System Sciences, Amsterdam, 201-240.

González, E., Tapia, G. 1952. Levantamiento geológico estructural en el área de Estancia El Salto y sección Las Coles. Informe Archivo Técnico ENAP, Santiago. (Inédito).

González, E. 1953. Estratigrafía y distribución de los grupos El Salto y Palomares en gran parte de la cuenca de Magallanes. Informe Archivo Técnico ENAP, Santiago. (Inédito).

González, E., 2015. Estratigrafía secuencial y sedimentología de la Formación Dorotea (Maastrichtiano), sector Río de las Chinas, Región de Magallanes y Antártica Chilena, Chile (50°S). Memoria, Departamento de Geología, Universidad de Chile.

Gorring, M.L., Kay, S.M., Zeitler, P.K., Ramos, V.A., Rubiolo, D., Fernandez, M.I., Panza, J.L., 1997. Neogene Patagonian plateau lavas: Continental magmas associated with ridge collision at the Chile Triple Junction. Tectonics 16, 1–17.

Gutiérrez, N.M., Le Roux, J.P., Vásquez, A., Carreño, C., Pedroza, V., Araos, J., Oyarzún, J.L., Pino, J.P., Rivera, H.A., Hinojosa, L.F., 2017. Tectonic events reflected by palaeocurrents, zircon geochronology, and palaeobotany in the Sierra Baguales of Chilean Patagonia. Tectonophysics 695, 76-99.

Harambour, S., 1965. Geología de los yacimientos petrolíferos del sector Cóndor-Dungeness, Provincia de Magallanes. Departamento de Geología, Universidad de Chile, Memoria de pregrado (Inédito).

Hatcher, J.B., 1897. On the Geology of the Southern Patagonia. American Journal of Sciences 9, 85-107.

Hedberg, H.D., 1976. International Stratigraphic Guide: A Guide to Stratigraphic Classification. Terminology and Procedure, by the International Subcommission on Stratigraphic Classification of IUGS Commission of Stratigraphy. Wiley Interscience Publication, New York, pp 200.

Hemmer, A., 1935. Geología de los terrenos petrolíferos de Magallanes y las exploraciones realizadas. Instituto de Ingenieros de Minas de Chile, Santiago, Chile.

Herm, D., 1966. Micropaleontological aspects of the Magellanese geosyncline, Southernmost Chile, South America. Proceedings of the second West African Micropaleontological Colloquium. Ibadan, 1, 72-85.

Herron, E., Heirtzler, J., 1967. Sea-floor spreading near the Galápagos. Science 158, 775-780.

Hervé, F., Godoy, E., Mpodozis, C., Fanning, M., 2004. Monitoring magmatism of the Patagonian Batholith through the U-Pb SHRIMP dating of detrital zircons in sedimentary units of the Magallanes Basin. In: Carcione, J.; Donda, F.; Lodolo, E. (Eds.), International Symposium on the Geology and Geophysics of the Southernmost Andes, the Scotia Are and the Antarctic Península, GEOSUR. Bolletino di Geofísica Teórica ed Applicata 45, 113-117.

Hervé, F., 2005. Estudio de la cronología y proveniencia de las Formaciones Terciarias de la cuenca de Magallanes mediante la datación U/Pb de sus poblaciones de circones detríticos. Informe Archivo Técnico ENAP, Santiago. (Inédito).

Hervé, F., Pankhurst, R.J., Fanning, C.M., Calderón, M., Yaxley, G.M., 2007. The South Patagonian batholith: 150 my of granite magmatism on a static plate margin. Lithos 97, 373-394.

Hoffstetter, R., Fuenzalida, H., Cecioni, G. 1957. Chile. In: Lexique Stratigraphique International, Vol. 5. Centre National de la Recherche Scientifique V, Paris, pp 444.

Hollister, J.S., 1944. Report petroleum Survey. Informe Archivo Técnico ENAP, Santiago. (Inédito).

Hubbard, S.M., Romans, B.W., Graham, S.A., 2008. Deep-water foreland basin deposits of the Cerro Toro Formation, Magallanes basin, Chile: Architectural elements of a sinuous basin axial channel belt. Sedimentology 55, 1333–1359, doi:10.1111/j.1365-3091.2007.00948.x.

Hubbard, S.M., Fildani, A., Romans, B.W., Covault, J.A., McHargue, T.R., 2010. High-relief slope clinoform development : insights from outcrop, Magallanes Basin, Chile. Journal of Sedimentary Research 80, 357-375.

Hubbard, S.M., MacEachern, J.A., Bann, K.L., 2012. Slopes. In: Knaust, D., Bromley, R.G (Eds.), Trace fossils as indicators of sedimentary environments. Developments in Sedimentology 64, 607-642.

Huber, B.T., Quillévéré, F., 2005. Revised Paleogene foraminiferal biozonation for the Austral realm. Journal of Foraminifera Research 35, 299-314.

Hünicken, M., 1955. Depósitos neocretácicos y terciarios del extremo SSW de Santa Cruz. Cuenca carbonífera de Río Turbio. Revista del Instituto Nacional de Investigaciones de las Ciencias Naturales y Museo Argentino de Ciencias Naturales "Bernardino Rivadavia", Ciencias Geológicas 4, 1-164.

Jenkins, D.G., 1966. Planktonic foraminiferal zones and new taxa from the Danian to Lower Miocene of New Zealand. N.Z.J. Geology, Geophysics 8, 1088-1126.

Jordan, T.E., 1995. Retroarc foreland and related basins. In Busby, C.J., and Ingersoll, R.V (Eds.), Tectonics of Sedimentary Basins, Blackwell Science, Oxford. pp. 331-362.

Jordan, T.E., Flemings, P.B., Beer, J.A., 1988. Dating of thrust-fault activity by use of foreland basin strata. In Kleinspehn, K.K., and Paola, C., (Eds.), New Perspective in Basin Analysis, Springer-Verlag, New York, pp. 307-330.

Katz, H.R., 1961. Descubrimiento de una microflora neocomiana en la Formación Agua Fresca (Eocena) de Magallanes y su significado con respecto a la evolución tectónica de la zona. Universidad de Chile, Facultad de Ciencias Físicas y Matemáticas, Anales 21, 133–141.

Katz, H.R., 1963. Revision of Cretaceous stratigraphy in Patagonian cordillera of Ultima Esperanza, Magallanes Province, Chile. American Association of Petroleum Geologist Bulletin 47, 506-524.

Keidel, I., Hemmer, A., 1931. Informe preliminar sobre las investigaciones en la región petrolífera de Magallanes en los meses de verano de 1928-1929. Boletín del Departamento de Minas y Petróleo, Ministerio de Fomento, Santiago, Chile, 44-55.

Klepeis, K., Betka, P., Clarke, G., Fanning, M., Hervé, F., Rojas, L., Mpodozis, C., Thomson, S., 2010. Continental underthrusting and obduction during the Cretaceous closure of the Rocas Verdes rift basin, Cordillera Darwin, Patagonian Andes, Tectonics, 29, TC3014, doi: 10.1029/2009TC002610.

Kniker, H., 1949. Report of samples collected by J. S. Barwick on Peninsula Brunswick. Field season of 1948-49 to accompany his report on Tertiary stratigraphic studies in eastern Peninsula Brunswick, Tierra del Fuego. Informe Archivo Técnico ENAP, Santiago. (Inédito).

Lahsen, A., Charrier, R., 1972. Late Cretaceous ammonites from Seno Skyring-Strait of Magellan area, Magallanes Province, Chile. Journal of Paleontology 46, 520-532.

Leppe, M., Mihoc, M., Varela, N., Stinnesbeck, W., Mansilla, H., Bierma, H., Cisterna, K., Frey, E., Jujihara, T., 2012. Evolution of the Austral-Antartic flora during the Cretaceous: New insights from a paleobiogeographic perspective. Revista Chilena de Historia Natural 85, 369-392.

Le Roux, J.P., Puratich, J., Mourgues, F.A., Oyarzún, J.L., Otero, R.A., Torres, T., Hervé, F., 2010. Estuary deposits in the Río Baguales Formation (Chattian – Aquitanean), Magallanes Province, Chile. Andean Geology 37, 329-344.

Le Roux, J.P., 2012a. A review of Tertiary climate changes in southern South America and the Antarctic Peninsula. Part 1: Ocean conditions. Sedimentary Geology 247-248, 1-20.

Lyle, M., Gibbs, S., Moore, T.C., Rea, D.K., 2007. Late Oligocene initiation of the Antarctic Circumpolar Current: evidence from the South Pacific. Geology 35, 691–694.

Macellari, C.E., Barrio, C.A., Manassero, M.J., 1989. Upper Cretaceous to Paleocene depositional sequences and sandstone petrography of southwestern Patagonia (Argentina and Chile). Journal of South American Earth Sciences 2, 223-239.

Malkowski, M.A., Sharman, G.R., Graham, S.A., Fildani, A., 2015. Characterisation and diachronous initiation of coarse clastic deposition in the Magallanes-Austral foreland basin, Patagonian Andes. Basin Research, doi: 10.1111/bre.12150.

Malkowski, M.A., Grove, M., Graham, S.A., 2016. Unzipping the Patagonian Andes-long-lived influence of rifting history on foreland basin evolution. Lithosphere 8, 23-28, doi: 10.1130/L489.1.

Malkowski, M.A., Schwartz, T.M., Sharman, G.R., Sickmann, Z.T., Graham, S.A., 2017. Stratigraphic and provenance variations in the early evolution of the Magallanes-Austral foreland basin: Implications for the role of longitudinal versus transverse sediment dispersal during arc-continent collision. GSA Bulletin 129, 349-371, doi: 10.1130/B31549.1.

Malumián, N. 1968. Foraminíferos del Cretácico Superior y Terciario del subsuelo de la provincia de Santa Cruz. Ameghiniana 5, 191-227.

Malumián, N., Masiuk V., Riggi J.C. (1971). Micropaleontología y sedimentología de la perforación SC-1, Provincia de Santa Cruz, República Argentina. Su importancia y correlaciones. Revista de la Asociación Geológica Argentina *26*, 175-208.

Malumián, N., Ramos, V.A., 1984. Magmatic intervals, transgression cycles and oceanic events in the Cretaceous and Tertiary of Southern South America. Earth and Planetary Science Letters 67, 228-237.

Malumián, N., 1993. El Eoceno medio marino del cono sur. Paleogeografía y foraminíferos. 12º Congreso Geológico Argentino y 2º Congreso de Exploración de Hidrocarburos, Actas 2, 142-146.

Malumián, N., Caramés, A., 1997. Upper Campanian-Paleogene from Río Turbio coal measures in southern Argentina: micropaleontology and the Paleocene/Eocene boundary. Journal of South American Earth Sciences 10, 189-201.

Malumián, N., Panza, J.L., Parisi, C., Náñez, C., Caramés, A., Torres, A., 2000. Hoja Geológica 5172-III, Yacimiento Río Turbio (1:250.000). Servicio Geológico Minero Argentino, Boletín 247, pp 180.

Malumián, N., Jannou, G., 2010. Los Andes Fueguinos: el registro micropaleontológico de los mayores acontecimientos paleooceanográficos australes del Campaniano al Mioceno. Andean geology 37, 345-374.

Malumián, N., Hromic, T., Náñez, C., 2013. El paleógeno de la cuenca de Magallanes: bioestratigrafía y discontinuidades. Anales Instituto Patagonia 41, 29-52.

Manassero, M. J., Iñiguez Rodríguez, A. M., Decastelli, O. O., 1990. Estratigrafía y argilofacies del Cretácico superior y Terciario inferior en la Cuenca Austral Argentina. Revista de la Asociación Geológica Argentina 45, 37-46.

Marchant, M., 2011. Paleoecología mediante foraminíferos del Paleógeno del área Dorado Sur, de la Cuenca de Magallanes, Chile. Anales Instituto Patagonia 39, 5-16.

Marenssi, S.A., Casadío, S., Santillana, S. N., 2002. La Formación Man Aike al sur de El Calafate (Provincia de Santa Cruz) y su relación con la discordancia del Eoceno medio en la cuenca Austral. Revista de la Asociación Geológica Argentina 57, 341-344.

Martínez-Pardo, R., Osorio, R., Lillo, J., 1965. Edad de la Formación Ciervos. Resúmenes Sociedad Geológica de Chile 10, 5-6.

Martínez-Pardo, R., Martínez. R., 1989. Reinterpretation of Boltovskoyella (benthic foraminiferal genus) as Neogene TransAndean chronostratigraphic event in southern South America. The Pacific, bridge or barrier? In: Pacific Science Association Inter-Congress No. 6, Abstracts. Valparaíso.

McAtamney, J., Klepeis, K., Mehrtens, C., Thomson, S., Betka, P., Rojas, L., Snyder, S., 2011. Along-strike variability of back-arc basin collapse and the initiation of sedimentation in the Magallanes foreland basin, southernmost Andes (53-54.5°S). Tectonics 30, TC5001, doi:10.1029/2010TC002826.

Mella, P. 2001. Control tectónico de la Cuenca de antepaís de Magallanes, XII Región, Chile. Departamento de Ciencias de la Tierra, Universidad de Concepción, Memoria de pregrado (Inédito).

Mesquita, A., 1998. High-Resolution biostratigraphy and Paleoecology of Early Miocene foraminiferal assemblages from turbidite reservoirs in the Campos Basin. Abstract: AAPG International Conference and Exhibition, Rio de Janeiro, Brazil. AAPG Search and Discovery Article #90933.

Miller, K.G., Wright, J.D., Fairbanks, R.G., 1991. Unlocking the ice house: Oligocene–Miocene oxygen isotopes, eustasy, and margin erosion. Journal of Geophysical Research 96, 6829–6848.

Moucha, R., Forte, A.M., Mitrova, J.X., Rowley, D.B., Quere, S., Simmons, N.A., Grand, S.P., 2008. Dynamic topography and long-term sea-level variations: there is no such thing as a stable continental platform. Earth Planet. Sci. Lett. 271, 101– 108.

Mpodozis, C., Rojas, L., 2006. Orogénesis en los Andes Patagónicos Australes de Tierra del Fuego: cierre de una “cuenca marginal” o colisión intracontinental?. XI Congreso Geológico Chileno, Antofagasta, Actas, Vol. 2, 283-286.

Mpodozis, C. 2007, Tectonics of the southernmost Patagonian Andes: A critical review: Geosur 2007 International Congress on the Geology and Geophysics of the Southern Hemisphere, Santiago, Chile.

Mpodozis, C., Mella, P., Padva, D. 2011. Estratigrafía y megasecuencias sedimentarias en la cuenca Austral-Magallanes, Argentina y Chile. VIII Congreso de Exploración y desarrollo de Hidrocarburos.

Murray, J., 1979. Cenozoic biostratigraphy and paleoecology of sites 304 to 406 based on the foraminifers. Deep Sea Drilling Project reports 48, 415-430.

Naish, T.R., Wilson, G.S., Dunbar, G.B., Barrett, P.J., 2008. Constraining the amplitude of Late Oligocene bathymetry changes in western Ross Sea during orbitally induced oscillations in the East Antarctic Ice Sheet: (2) implications for global sea-level changes. Palaeogeography, Palaeoclimatology, Palaeoecology 260, 66-76.

Natland, M., Gonzalez, E., Cañón, A., Ernst, M., 1974. A System of stages for correlation of Magallanes basin sediments. The Geological Society of America Memoir 139, 1-57.

Nullo, F. y Combina, A., 2002. Sedimentitas terciarias continentales. En M. J. Haller (Ed.), Geología y Recursos naturales de Santa Cruz. Relatorio XV Congreso Geológico Argentino, El Calafate, I-16, 245-258.

Olivero, E.B., Malumian, N., 1999. Eocene stratigraphy of Southern Tierra del Fuego, Argentina. American Association Petroleum Geologist Bulletin 83, 295-313.

Olivero, E.B., Martinioni, D.R., 2001. A review of the geology of the Argentinian Fuegian Andes. Journal of South American Earth Sciences 14, 175-788.

Olivero, E.B., Malumian, N., 2008. Mesozoic-Cenozoic stratigraphy of the Fuegian Andes, Argentina. Geologica Acta 6, 5-18.

Olivero, E.B., Malumian, N., Palamarczuk, S., 2003. Estratigrafía del Cretácico Superior-Paleoceno del área de Bahía Thetis, Andes fueguinos, Argentina: acontecimientos tectónicos y paleobiológicos. Andean Geology 30, 245-263.

O'Neill, C., Lenardic, A., Moresi, L., Torsvik, T.H., Lee, C.-T.A., 2007. Episodic Precambrian subduction. Earth Planet. Sci. Lett. 262, 552–562.

Otero, R.A., Suárez, M.E., Le Roux, J.P., 2009. First record of elasmosaurid plesiosaurs (Sauropterygia: Plesiosauria) in upper levels of the Dorothea Formation, Late Cretaceous (Maastrichtian), Puerto Natales, Chiulean Patagonia. Andean Geology 36, 342-350.

Otero, R., Torres, T., Le Roux, J.P., Hervé, F., Fanning, M., Yury-Yáñez, R., Rubilar-Rogers, D., 2012. A Late Eocene age proposal for the Loreto Formation (Brunswick Peninsula, southernmost Chile), based on fossil cartilaginous fishes, paleobotany and radiometric evidence. Andean Geology 39, 180-200.

Otero, R.A., Soto-Acuña, S., Salazar, C., Oyarzún, J.-L., 2015. New elasmosaurids (Sauropterygia, Plesiosauria) from the Late Cretaceous of the Magallanes Basin, Chilean Patagonia: Evidence of a faunal turnover during the Maastrichtian along the Weddellian Biogeographic Province. Andean Geology 42, 237-267.

Pankhurst, R.J., Riley, T.R., Fanning, C.M., Kelley, S.P., 2000. Episodic silicic volcanism in Patagonia and the Antarctic Peninsula: chronology of magmatism associated with the break–up of Gondwana. Journal of Petrology 41, 605–625.

Pardo-Casas, F., Molnar, P., 1987. Relative motion of the Nazca (Farellon) and South American Plates since Late Cretaceous times. Tectonics 6, 233-248.

Patriat, P., Sloan, H., Sauter, D., 2008. From slow to ultraslow: a previously undetected event at the Southwest Indian Ridge at ca. 24 Ma. Geology 36, 207–210.

Pearson, N.J., Mángano, G., Buatois, L., Casadío, S., Rodríguez Raising, M., 2012. Ichnology, sedimentology and sequence Stratigraphy of outer-estuarine and coastal plain deposits: implications for the distinction between allogenic and autogenic expressions of the *Glossinfungites* ichnofacies. PALAEO 333: 192-217.

Pearson, N.J., Mángano, G., Buatois, L.A., Casadío, S., Raising, M.R., 2013. Environmental variability of *Macaronichnus* ichnofabrics in Eocene tidal-embayment deposits of Southern Patagonia, Argentina. Lethaia 46, 341-354.

Ponce, J.J., Olivero, E.B., Martinioni, D.R., 2008. Upper Oligocene-Miocene clinoforms of the foreland Austral Basin of Tierra del Fuego, Argentina: Stratigraphy, depositional sequences and architecture of the foredeep deposits. Journal of South American Earth Sciences 26, 36-54.

Quattrocchio, M.E., Sarjeant, W.A.S., 2003. Dinoflagellates from Chorrillo Chico Formation (Paleocene) of southern Chile. Ameghiniana 40, 129-153.

Quattrocchio, M.E., 2009. Paleogene dinoflagellate cysts from Punta Pratt, southern Chile. Palynology 33, 141-156.

Quensel, P.D., 1911. Geologische-petrographische studien in der Patagonischen Cordillera. Universidad de Upsala, Geological Institute Bulletin, 11, 1-114 pp.

Ramos, V.A., Aguirre–Urreta, M.B., 1994. Cretaceous evolution of the Magallanes Basin. In Salfity, J.A. (Ed.), Cretaceous Tectonics of the Andes. Earth Evolution Series, Fried. Vieweg & Sohn, Braunschweig/Wiesbaden, 315-345, doi: 10.1007/978-3-322-85472-8_7.

Ramos, V.A., 1982. Geología de la región del Lago Cardiel, provincia de Santa Cruz. Revista Asociación Geológica Argentina 37, 23-49.

Ramos, V.A., 2002. Evolución tectónica. In: Haller, M.J. (ed.), Geología y Recursos Naturales de Santa Cruz. Abstracts XV Congreso Geológico Argentino, Buenos Aires, Vol. I-23, 365–387.

Reguero, M.A., Marenssi, S.A., Santillana, S.N., 2002. Antarctic Peninsula and Patagonia Paleogene terrestrial environments: biotic and biogeographic relationships. Palaeogeography, Palaeoclimatology, Palaeoecology 179: 189-210.

Robbiano, J. A., Arbe, H. A., Gangui, A., 1996. Cuenca Austral Marina. En: Ramos, V. A., Turic, M. A. (Eds.), Geología y Recursos Naturales de la Plataforma Continental Argentina. XIII Congreso Geológico Argentino y III Congreso de Exploración de Hidrocarburos, Buenos Aires, Relatorio 17, 323-341.

Robles, M.L., Gómez, M., 1956. Foraminíferos del Cretácico superior y del Paleoceno de la Provincia de Magallanes, Chile. 20th International Geological Congress (México), Resúmenes, 184-185.

Rodríguez-Raising, M., Casadío, S., Pearson, N., Mángano, G., Buatois, L., Griffin, M., 2014. Paleoenvironmental setting and description of an estuarine oyster reef in the Eocene of Patagonia, southern Argentina. Journal of South American Earth Sciences 56, 242-250.

Romans, B.W., Fildani, A., Graham, S.A., Hubbard, S.M., Covault, J.A., 2010. Importance of predecessor basin history on sedimentary fill of a retroarc foreland basin: Provenance analysis of the Cretaceous Magallanes basin, Chile (50–52°S), Basin Res., 22, 640–658, doi:10.1111/j.13652117.2009.00443.x.

Romans, B.W., Fildani, A., Hubbard, S.M., Covault, J.A., Fosdick, J.C., Graham, S.A., 2011. Evolution of deep-water stratigraphic architecture, Magallanes Basin, Chile, Mar. Pet. Geol., 28,612–628, doi:10.1016/j.marpetgeo.2010.05.002.

Ruby, G., 1945. Mina Rica structure, Seno Otway, District Magallanes. Informe Archivo Técnico ENAP, Santiago, (Inédito).

Sánchez, A., Pavlishina, P., Godoy, E., Hervé, F., Fanning, M., 2010. On the presence of Upper Paleocene rocks in the foreland succession at Cabo Nariz, Tierra del Fuego, Chile: geology and new palynological and U-Pb data. Andean Geology 37, 413-432.

Sell, I., Poupeau, G., González-Casado, J.M., López-Martínez, J., 2004. A fission-track thermochronological study of King George and Livingston Islands, South Shetland Islands (West Antarctica). Antarctic Science 16, 191-197.

Schenk, C.J., Charpentier, R.R., Pitman, J.K., Tennyson, M.E., Brownfield, M.E., Gaswirth, S.B., Le, P.A., Leathers-Miller, H.M., and Marra, K.R., 2016. Assessment of unconventional tight-gas resources of the Magallanes Basin Province, Chile, 2015. U.S. Geological Survey Fact Sheet 2015–3085, http://dx.doi.org/10.3133/fs20153085.

Scher, H.D., Martin, E.E., 2006. Timing and climatic consequences of the opening of the Drake Passage. Science 312, 428–430.

Schultz, M.R., Fildani, A., Cope, T.D., Graham, S.A., 2005. Deposition and stratigraphic architecture of an outcropping ancient slope system: Tres Pasos Formation, Magallanes Basin, southern Chile. In Hodgson, D.M., and Flint, S.S., (eds.), Submarine slope systems: Processes and products: Geological Society Special Publication 244, p. 27–50.

Schwab, F. L., 1986. Sedimentary 'signatures' of foreland basin assemblages: real or counterfeit? In: Allen, P.A. and Homewood, P., (Eds.), Foreland Basins, Special Publications International Association of Sedimentologist 8, 395-410.

Schwartz, T.M., Graham, S.A., 2015. Stratigraphic architecture of a tide-influenced shelf-edge delta, Upper Cretaceous Dorotea Formation, Magallanes-Austral Basin, Patagonia. Sedimentology 62, 1039-1077.

Schwartz, T.M., Fosdick, J., Graham, S.A., 2016. Using detrital zircon U-Pb ages to calculate Late Cretaceous sedimentation rates in the Magallanes-Austral Basin, Patagonia, Basin Research. doi:10.1111/bre.12198

Scott, K.M., 1966. Sedimentology and dispersal pattern of a Cretaceous flysch sequence, Patagonian Andes, southern Chile. AAPG Bulletin 50, 72-107.

Selley, R.C., 1976. An Introduction to Sedimentology. Academic Press, London, 408 p.

Sernageomin., 2003. Mapa Geológico de Chile: versión digital, escala 1:1, 000,000. Servicio Nacional de Geología y Minería, Santiago, Chile.

Sohn, Y.K., Choe, M.Y., Jo, H.R., 2002. Transition from debris flow to hyperconcentrated flow in a submarine channel (the Cretaceous Cerro Toro Formation, southern Chile). Terra Nova 14, 405-415.

Somoza, R., 1998. Updated Nazca (Farallon)–South America relative motions during the last 40 Ma: implications for mountain building in the central Andean region. Journal of South American Earth Sciences 11, 211-215.

Stern, C.R., Mukasa, S.B., Fuenzalida, R., 1992. Age and petrogenesis of the Sarmiento ophiolite complex of southern Chile. Journal of South American Earth Sciences 6, 97–104.

Suárez, M., Pettigrew, T.H., 1976. An upper Mesozoic island–arc back–arc system in the southern Andes and South Georgia. Geological Magazine 113, 305–400.

Suárez, M., 1977. Aspectos geoquímicos del Complejo Ofiolítico Tortuga en la Cordillera Patagónica del sur de Chile. Andean Geology 4, 3–14.

Suárez, M., De la Cruz, R., Bell, C.M., 2000a. Timing and origin of deformation along the Patagonian fold and thrust belt. Geological Magazine 137, 345–353.

Thomas, C.R., 1949. Geology and petroleum exploration in Magallanes province, Chile. Am. Association of Petroleum Geologist Bull. 33, 1553-1578.

Todd, R., Kniker, H., 1952. An Eocene foraminiferal fauna from the Agua Fresca Shale of Magallanes Province, Southernmost, Chile. Cushman Foundation Foraminiferal Research Special Publication 1, pp 28.

Torres-Carbonell, P.J., Olivero, E.B., Dimieri, L.V., 2008a. Structure and evolution of the Fuegian Andes foreland thrust-fold belt, Tierra del Fuego, Argentina: paleo-geographic implications. Journal of South American Earth Sciences 25, 417-439.

Torres-Carbonell, P.J., Malumian, N., Olivero, E.B., 2009. El Paleoceno-Mioceno de Península Mitre: antefosa y depocentro de techo de cuña de la cuenca Austral, Tierra del Fuego, Argentina. Andean Geology 36, 197-235.

Tucker, R.T., Roberts, E.M., Hu, Y., Kemp, A., Salisbury, S.W., 2013. Detrital zircon age constraints for the Winton Formation, Queensland: Contextualizing Australia's Late Cretaceous dinosaur faunas. Gondwana Research 24, 767-779.

Valchev, B., 2003. On the potential of small benthic foraminifera as paleoecological indicators: recent advances. Abstract: 50 years University of Mining and Geology "St. Ivan Rilski" Annual, vol. 46, Part I, Geology and Geophysics, Sofia, 189-194.

Van Morkhoven, F.P.C.M., Berggren, W.A., Edwards, A.S., 1986. Cenozoic cosmopolitan deep-water benthic foraminifera. Elf-Aquitaine Mem. 11, pp 423.

Von Goetsche, G., 1953. Informe Geológico del área Tres Morros-Agua Fresca- San Isidro. Informe Archivo Técnico ENAP, Santiago. (Inédito).

Wilson, T.J., 1991. Transition from back-arc to foreland basin development in southernmost Andes: stratigraphic record from the Ultima Esperanza District, Chile. Geological Society of America Bulletin 103 98-111.

Zachos, J., Quinn, T.M., Salamy, K.A., 1996. High-resolution (104 yr) deep-sea foraminifer stable isotope records of the Eocene–Oligocene climate transition. Paleoceanography 11, 251-266.

Zurita, E., Carpinelli, A., Trejo, S., Saa, A., 2013. Gas Resource Potential from Maastrichtian–Eocene Reservoir in Magallanes Basin, Chile. AAPG International Conference and Exhibition, Cartagena, Colombia. Search and Discovery Article # 90166.

ANEXO A1

MÉTRICAS DE EDADES MÁXIMAS DE DEPOSITACIÓN

Compilation of the five metrics utilized within this study to calculate the MDA's

Analysis		09-235A*‡	09-207*^	Kerber	RV1	SK2	09-237A*‡	SK1
YSG		17.2 ± 0.9	15.4 ± 1.5	18.0 ± 0.2	18.0 ± 0.8	25.4 ± 0.6	21.3 ± 0.4	35.3 ± 1.0
YDZ		16.7 +0.8 -1.3	15.4 +0.8 -1.3	18.3 +0.1 -0.1	17.9 +0.1 -0.7	25.3 +0.6 -0.6	21.1 +0.4 -0.78	35.2 +0.7 -1.0
YC1σ (+2)	Final Age	18.2 ± 0.8 (4.3%)	19.6 ± 0.6 (2.8%)	18.9 ± 0.3 (1.5%)	20.0 ± 1.2 (5.8%)	26.6 ± 0.8 (3.1%)	22.0 ± 0.5 (2.5%)	36.2 ± 1.1 (2.9%)
	Weighted Mean Age	18.2 ± 0.8 (4.2%)	19.6 ± 0.5 (2.6%)	18.9 ± 0.2 (1.0%)	20.0 ± 1.1 (5.7%)	26.6 ± 0.8 (2.9%)	22.0 ± 0.5 (2.2%)	36.2 ± 1.0 (2.7%)
	Systematic error	1.1%	1.1%	1.1%	1.1%	1.1%	1.1%	1.1%
	MSWD	0.3	1.0	0.0	0.0	0.1	0.0	0.1
YC2σ (+2)	Final Age	18.1 ± 0.8 (4.2%)	18.2 ± 1.1 (5.9%)	18.6 ± 0.2 (1.2%)	19.4 ± 1.0 (5.0%)	26.1 ± 0.8 (2.9%)	21.7 ± 0.4 (1.7%)	36.1 ± 1.1 (2.9%)
	Weighted Mean Age	18.1 ± 0.7 (4.0%)	18.2 ± 1.0 (5.8%)	18.6 ± 0.1 (0.5%)	19.4 ± 0.9 (4.9%)	26.1 ± 0.7 (2.7%)	21.7 ± 0.3 (1.3%)	36.1 ± 1.0 (2.7%)
	Systematic error	1.1%	1.1%	1.1%	1.1%	1.1%	1.1%	1.1%
	MSWD	0.8	0.7	1.1	2.1	0.9	1.0	0.6
Weighted average (+2)	Age	18.1 ± 0.6 (3.3%)	18.9 ± 0.4 (2.4%)	18.6 ± 0.1 (0.21%)	19.6 ± 0.9 (4.8%)	26.4 ± 0.7 (2.6%)	21.8 ± 0.3 (1.1%)	36.2 ± 0.4 (1.1%)
	Rejection	0 of 5	0 of 8	0 of 35	0 of 5	0 of 4	0 of 9	0 of 6
	MSWD	0.42	0.92	1.05	1.80	1.60	0.64	0.82
	Probability	0.79	0.49	0.38	0.14	0.19	0.74	0.54
	Acceptable MSWD	0.166-2.560	0.277-2.188	0.560-1.567	0.166-2.560	0.121-2.775	0.300-2.111	0.207-2.400

Compilation of the five metrics utilized within this study to calculate the MDA's (Continued)

Analysis		RL-1	IR1	09-230*^	RB-1	PB1	CC1
YSG		35.4 ± 0.7	36.0 ± 1.0	27.5 ± 2.5	64.4 ± 1.3	59.2 ± 3.1	88.2 ± 1.9
YDZ		35.3 +0.5 -0.7	35.8 +0.4 -0.5	27.7 +3.8 -5.1	64.1 +0.8 -1.3	58.5 +3.1 -3.3	87.8 +1.8 -1.8
YC1σ (+2)	Final Age	36.8 ± 0.7 (2.0%)	37.7 ± 0.7 (1.7%)	39.8 ± 1.9 (4.8%)	64.9 ± 1.4 (2.2%)	77.6 ± 5.4 (7.0%)	96.4 ± 2.5 (2.6%)
	Weighted Mean Age	36.8 ± 0.6 (1.7%)	37.7 ± 0.5 (1.3%)	39.8 ± 1.8 (4.6%)	64.9 ± 1.2 (1.9%)	77.6 ± 5.4 (6.9%)	96.4 ± 2.3 (2.4%)
	Systematic error	1.1%	1.1%	1.1%	1.1%	1.1%	1.1%
	MSWD	0.1	0.1	0.2	0.1	0.1	0.2
YC2σ (+2)	Final Age	36.8 ± 0.6 (1.6%)	37.2 ± 0.6 (1.7%)	38.6 ± 1.5 (3.8%)	66.4 ± 1.1 (1.7%)	69.3 ± 2.9 (4.2%)	93.8 ± 1.8 (1.9%)
	Weighted Mean Age	36.8 ± 0.4 (1.2%)	37.2 ± 0.5 (1.2%)	38.6 ± 1.4 (3.6%)	66.4 ± 0.9 (1.3%)	69.3 ± 2.8 (4.1%)	93.8 ± 1.5 (1.6%)
	Systematic error	1.1%	1.1%	1.1%	1.1%	1.1%	1.1%
	MSWD	2.2	0.6	1.0	1.0	1.7	3.2
Weighted average (+2)	Age	37.1 ± 0.3 (0.9%)	37.4 ± 0.2 (0.51%)	36.1 ± 2.6 (7.3%)	65.2 ± 0.5 (0.7%)	67.0 ± 1.7 (2.6%)	88.5 ± 1.3 (1.5%)
	Rejection	0 of 10	0 of 37	0 of 7	0 of 9	1 of 15	0 of 2
	MSWD	1.50	1.30	2.30	0.61	1.40	0.17
	Probability	0.15	0.08	0.03	0.77	0.17	0.68
	Acceptable MSWD	0.325-2.050	0.560-1.567	0.241-2.286	0.300-2.111	0.417-1.833	0.025-3.690

^Fosdick et al., 2015a; ǂFosdick et al., 2011.
* Ages 1σ; in red color, selected MDA

ANEXO A2

DATOS ANALÍTICOS DE GEOCRONOLOGÍA U-Pb EN CIRCÓN DETRÍTICO

Table A2. Detrital zircon U-Pb geochronologic analyses by using LA-ICP-MS analysis

Analysis	U (ppm)	U/Th	Apparent ages (Ma) $^{206}Pb^*/^{238}U$	± 2σ (Ma)	$^{207}Pb^*/^{235}U$	± 2σ (Ma)	$^{207}Pb^*/^{206}Pb^*$	± 2σ (Ma)	Preferred age ± 2σ (Ma)		conc (%)
Sample Kerber-Palomares Formation											
KERBER_39	962	0.75	18.2	0.2	19.8	0.5	249.0	46.0	18.0	0.2	91.5
KERBER_86	280	0.84	18.1	0.3	17.9	0.9	69.0	94.0	18.0	0.3	101.1
KERBER_91	82	0.79	18.4	0.3	21.4	2.2	370.0	170.0	18.1	0.4	85.7
KERBER_56	97	0.76	18.3	0.3	19.8	1.9	130.0	160.0	18.2	0.3	92.3
KERBER_68	463	0.63	18.4	0.4	20.7	0.8	267.0	74.0	18.2	0.4	88.5
KERBER_74	367	0.77	18.2	0.2	17.5	0.6	-28.0	61.0	18.2	0.2	103.9
KERBER_98	71	0.65	18.4	0.3	19.7	2.2	70.0	180.0	18.3	0.4	93.2
KERBER_50	733	0.67	18.3	0.3	19.0	0.5	105.0	56.0	18.3	0.3	96.7
KERBER_87	312	0.61	18.4	0.2	18.9	0.8	135.0	76.0	18.3	0.2	97.1
KERBER_67	174	0.45	18.3	0.3	18.8	1.0	127.0	96.0	18.3	0.3	97.6
KERBER_73	74	0.80	18.5	0.3	20.2	2.3	150.0	190.0	18.3	0.4	91.4
KERBER_79	305	0.90	18.4	0.2	18.2	0.7	19.0	68.0	18.4	0.2	101.0
KERBER_93	392	0.96	18.4	0.2	18.3	0.6	40.0	61.0	18.4	0.2	100.7
KERBER_105	359	0.84	18.5	0.2	19.3	0.6	125.0	62.0	18.4	0.2	96.0
KERBER_99	104	0.71	18.5	0.3	18.2	2.0	10.0	170.0	18.5	0.3	101.5
KERBER_88	230	0.82	18.7	0.3	21.6	1.3	380.0	120.0	18.5	0.3	86.4
KERBER_80	336	0.87	18.6	0.3	21.2	0.8	292.0	73.0	18.5	0.3	88.0
KERBER_103	169	1.15	18.5	0.3	17.9	1.3	10.0	110.0	18.5	0.3	103.4
KERBER_101	286	0.81	18.5	0.2	19.3	0.7	134.0	72.0	18.5	0.2	96.3
KERBER_45	276	0.60	18.5	0.2	17.8	0.8	-9.0	77.0	18.5	0.2	103.8
KERBER_19	135	1.10	18.6	0.3	19.7	1.4	190.0	110.0	18.5	0.3	94.5
KERBER_66	275	0.60	18.7	0.3	21.4	0.9	278.0	73.0	18.5	0.3	87.3
KERBER_75	163	1.06	18.6	0.3	19.0	1.1	140.0	110.0	18.5	0.3	97.8
KERBER_102	85	0.65	18.6	0.4	20.3	2.3	150.0	190.0	18.6	0.4	91.8
KERBER_22	501	0.70	18.6	0.3	18.7	0.6	78.0	56.0	18.6	0.3	99.1

Table A2. Detrital zircon U-Pb geochronologic analyses by using LA-ICP-MS analysis (continued)

Analysis	U (ppm)	U/Th	Apparent ages (Ma) $^{206}Pb^*/^{238}U$	± 2σ (Ma)	$^{207}Pb^*/^{235}U$	± 2σ (Ma)	$^{207}Pb^*/^{206}Pb^*$	± 2σ (Ma)	Preferred age ± 2σ (Ma)		conc (%)
KERBER_72	413	0.78	18.6	0.2	18.9	0.6	79.0	61.0	18.6	0.2	98.2
KERBER_100	156	1.14	18.6	0.3	18.2	1.0	63.0	99.0	18.6	0.3	102.0
KERBER_76	215	1.16	18.5	0.3	17.8	1.0	9.0	90.0	18.6	0.3	103.9
KERBER_42	261	0.62	20.5	0.3	52.8	1.6	1964.0	53.0	18.6	0.3	38.9
KERBER_7	234	1.06	18.6	0.3	18.6	0.8	85.0	76.0	18.6	0.3	100.2
KERBER_4	305	0.74	18.6	0.2	18.6	0.7	76.0	70.0	18.6	0.2	100.2
KERBER_104	151	1.25	18.7	0.3	18.8	1.3	70.0	120.0	18.6	0.3	99.3
KERBER_90	229	0.80	18.6	0.2	18.3	0.9	51.0	85.0	18.6	0.2	101.7

KERBER_25	350	0.53	18.7	0.3	19.9	0.9	180.0	85.0	18.6	0.3	94.2
KERBER_20	293	0.85	18.7	0.3	19.1	0.8	172.0	81.0	18.7	0.3	98.0
KERBER_53	138	1.14	18.7	0.3	19.7	1.3	170.0	110.0	18.7	0.3	95.0
KERBER_21	391	0.85	18.7	0.3	18.7	0.6	52.0	57.0	18.7	0.3	99.9
KERBER_36	497	0.55	18.8	0.2	20.4	0.6	194.0	52.0	18.7	0.2	92.3
KERBER_13	333	0.68	18.8	0.3	19.5	0.9	121.0	83.0	18.7	0.3	96.3
KERBER_40	387	0.88	18.8	0.2	20.0	0.7	198.0	71.0	18.7	0.2	94.2
KERBER_97	205	0.47	18.8	0.3	18.6	1.0	83.0	92.0	18.7	0.3	100.6
KERBER_18	284	0.90	18.8	0.4	19.5	1.0	138.0	95.0	18.7	0.4	96.3
KERBER_41	187	0.94	18.8	0.2	19.7	1.1	157.0	98.0	18.7	0.2	95.6
KERBER_78	189	0.93	18.7	0.3	18.0	1.0	10.0	94.0	18.8	0.3	104.0
KERBER_2	253	0.82	18.8	0.3	18.8	0.9	92.0	83.0	18.8	0.3	99.9
KERBER_15	420	0.65	18.8	0.2	18.7	0.6	65.0	56.0	18.8	0.2	100.2
KERBER_8	295	0.81	18.8	0.2	18.8	0.7	51.0	71.0	18.8	0.2	100.1
KERBER_32	226	1.00	18.8	0.2	19.1	1.0	95.0	85.0	18.8	0.2	98.5
KERBER_62	551	0.39	18.8	0.2	19.2	0.5	97.0	49.0	18.8	0.2	97.9
KERBER_47	319	0.54	18.9	0.2	19.9	0.7	145.0	68.0	18.8	0.2	95.0
KERBER_96	315	0.76	18.8	0.2	18.3	0.7	5.0	65.0	18.8	0.2	102.8
KERBER_95	169	1.22	18.8	0.2	19.2	1.2	100.0	110.0	18.8	0.2	98.1

Table A2. Detrital zircon U-Pb geochronologic analyses by using LA-ICP-MS analysis (continued)

Analysis	U (ppm)	U/Th	Apparent ages (Ma) $^{206}Pb^*/^{238}U$	± 2σ (Ma)	$^{207}Pb^*/^{235}U$	± 2σ (Ma)	$^{207}Pb^*/^{206}Pb^*$	± 2σ (Ma)	Preferred age ± 2σ (Ma)		conc (%)
KERBER_48	333	0.84	18.9	0.3	19.0	0.8	60.0	78.0	18.9	0.3	99.3
KERBER_16	235	0.80	18.9	0.3	19.6	0.9	130.0	83.0	18.9	0.2	96.6
KERBER_14	388	0.57	18.9	0.2	18.3	0.6	42.0	62.0	18.9	0.2	102.8
KERBER_85	287	0.78	18.9	0.2	18.8	0.8	47.0	76.0	18.9	0.2	100.3
KERBER_34	280	0.79	18.9	0.2	19.3	0.8	87.0	78.0	18.9	0.2	98.2
KERBER_71	145	0.45	19.0	0.4	19.5	1.5	120.0	140.0	18.9	0.4	97.2
KERBER_5	280	0.74	18.9	0.3	17.5	0.8	-52.0	77.0	18.9	0.3	107.6
KERBER_6	331	1.10	19.0	0.2	19.7	0.8	135.0	71.0	18.9	0.2	96.3
KERBER_70	495	0.50	18.9	0.2	18.9	0.6	62.0	53.0	18.9	0.2	100.5
KERBER_89	701	0.62	19.0	0.2	19.6	0.4	106.0	42.0	18.9	0.2	96.8
KERBER_49	344	1.01	19.0	0.3	18.8	0.7	56.0	64.0	19.0	0.3	100.6
KERBER_61	444	0.62	19.0	0.2	19.5	0.6	118.0	55.0	19.0	0.2	97.5
KERBER_33	375	0.59	19.0	0.2	18.9	0.6	57.0	58.0	19.0	0.2	100.7
KERBER_77	152	1.20	19.1	0.3	19.2	1.1	90.0	100.0	19.1	0.3	99.3
KERBER_26	190	0.96	19.3	0.5	21.4	2.2	240.0	180.0	19.1	0.5	90.0
KERBER_24	77	1.33	19.1	0.6	18.8	3.1	-80.0	250.0	19.1	0.6	101.4
KERBER_23	215	0.73	19.1	0.3	19.1	0.9	107.0	88.0	19.1	0.3	100.0
KERBER_28	302	1.03	19.2	0.5	19.1	1.1	130.0	110.0	19.1	0.5	100.4
KERBER_35	507	0.72	19.3	0.2	19.1	0.5	68.0	53.0	19.3	0.2	100.8
KERBER_27	753	0.59	19.3	0.2	19.1	0.4	34.0	40.0	19.3	0.2	101.2

KERBER_11	515	0.78	19.3	0.2	19.6	0.5	87.0	50.0	19.3	0.2	98.5
KERBER_10	290	0.81	19.9	0.3	20.4	0.9	130.0	81.0	19.9	0.3	97.5
KERBER_43	126	0.61	20.2	0.3	23.1	1.5	290.0	120.0	20.0	0.3	87.4
KERBER_63	267	0.76	20.3	0.2	20.5	0.9	92.0	82.0	20.3	0.3	99.2
KERBER_31	309	0.58	21.0	0.4	21.1	1.2	120.0	100.0	20.9	0.4	99.4
KERBER_17	387	1.21	22.5	0.2	23.0	0.7	99.0	56.0	22.4	0.2	97.6

Table A2. Detrital zircon U-Pb geochronologic analyses by using LA-ICP-MS analysis (continued)

Analysis	U (ppm)	U/Th	Apparent ages (Ma) $^{206}Pb^*/^{238}U$	± 2σ (Ma)	$^{207}Pb^*/^{235}U$	± 2σ (Ma)	$^{207}Pb^*/^{206}Pb^*$	± 2σ (Ma)	Preferred age ± 2σ (Ma)		conc (%)
KERBER_84	104	1.22	82.7	1.0	91.6	3.2	322.0	72.0	82.2	1.0	90.3
KERBER_51	228	1.02	151.0	1.3	149.3	2.2	140.0	30.0	151.1	1.3	101.1
KERBER_69	207	0.95	529.2	4.9	528.3	4.4	508.0	19.0	529.7	5.0	100.2

Table A2. Detrital zircon U-Pb geochronologic analyses by using LA-ICP-MS analysis

Analysis	U (ppm)	U/Th	Apparent ages (Ma) $^{206}Pb^*/^{238}U$	± 2σ (Ma)	$^{207}Pb^*/^{235}U$	± 2σ (Ma)	$^{207}Pb^*/^{206}Pb^*$	± 2σ (Ma)	Preferred age ± 2σ (Ma)		conc (%)
Sample RV1-El Salto Formation											
RV1_38	303	1.26	17.3	1.0	17.3	1.2	60.0	100.0	17.3	1.0	99.7
RV1_12	87	0.73	18.0	0.9	19.3	2.2	100.0	180.0	18.0	0.8	93.2
RV1_76	48	0.96	19.0	1.1	20.9	4.4	0.0	300.0	18.8	1.1	91.0
RV1_16	145	0.79	19.2	0.9	18.5	1.8	100.0	140.0	19.2	0.8	104.0
RV1_93	124	0.87	19.9	1.2	18.3	2.0	-90.0	160.0	20.0	1.2	108.7
RV1_21	163	0.65	20.3	0.7	24.1	1.5	360.0	110.0	20.1	0.6	84.4
RV1_6	45	1.41	33.3	1.6	27.9	4.1	-220.0	190.0	33.6	1.6	119.2
RV1_97	44	1.26	34.3	1.7	37.5	4.5	100.0	190.0	34.0	1.7	91.4
RV1_44	32	1.39	35.8	1.9	35.5	5.6	10.0	220.0	35.3	1.9	100.7
RV1_110	139	1.62	35.6	2.0	37.3	2.3	250.0	110.0	35.4	2.0	95.6
RV1_102	254	0.69	36.3	1.9	38.9	2.1	210.0	89.0	36.0	1.9	93.4
RV1_23	29	1.00	36.4	1.9	39.0	7.5	-140.0	270.0	36.3	2.0	93.3
RV1_51	117	1.14	38.8	3.0	41.6	3.8	240.0	160.0	38.5	3.1	93.4
RV1_47	102	1.29	38.8	2.0	40.7	2.8	180.0	110.0	38.6	2.0	95.1
RV1_71	107	1.20	39.8	1.8	40.5	2.7	130.0	110.0	39.7	1.8	98.2
RV1_79	189	1.17	66.5	3.9	68.2	3.7	118.0	98.0	66.3	3.9	97.5
RV1_46	123	0.52	68.9	2.9	73.4	3.1	235.0	75.0	68.5	2.9	93.8
RV1_29	240	0.84	68.7	3.1	68.2	2.9	122.0	71.0	68.7	3.1	100.8
RV1_112	91	0.81	68.7	3.5	67.5	3.9	82.0	94.0	68.7	3.5	101.9
RV1_113	209	0.95	69.1	3.1	69.0	3.1	85.0	70.0	69.1	3.1	100.1
RV1_31	108	0.54	69.2	3.1	69.8	3.7	108.0	88.0	69.1	3.1	99.0
RV1_45	185	0.63	69.8	3.2	67.5	3.0	44.0	75.0	69.8	3.2	103.4

Table A2. Detrital zircon U-Pb geochronologic analyses by using LA-ICP-MS analysis (continued)

Analysis	U (ppm)	U/Th	Apparent ages (Ma) $^{206}Pb^*/^{238}U$	± 2σ (Ma)	$^{207}Pb^*/^{235}U$	± 2σ (Ma)	$^{207}Pb^*/^{206}Pb^*$	± 2σ (Ma)	Preferred age ± 2σ (Ma)		conc (%)
RV1_72	96	0.96	72.6	3.3	73.4	3.5	160.0	87.0	72.4	3.3	98.8
RV1_58	140	0.56	73.9	3.5	78.9	3.7	183.0	78.0	73.6	3.4	93.6

RV1_20	117	0.77	75.4	3.3	76.5	3.5	111.0	75.0	75.3	3.3	98.5
RV1_35	137	0.87	76.2	3.2	79.6	3.5	152.0	69.0	76.1	3.2	95.7
RV1_70	143	0.68	76.6	3.4	75.1	3.4	65.0	74.0	76.7	3.5	102.1
RV1_111	168	0.55	76.9	4.6	75.5	4.0	124.0	82.0	76.7	4.6	101.9
RV1_106	224	0.62	77.8	1.9	81.7	2.7	186.0	62.0	77.5	1.9	95.2
RV1_85	168	1.18	78.8	3.5	80.8	3.5	145.0	71.0	78.6	3.5	97.5
RV1_95	77	1.33	79.5	3.6	79.3	4.1	90.0	90.0	79.5	3.6	100.4
RV1_81	244	0.68	80.4	3.9	79.3	3.4	85.0	70.0	80.4	4.0	101.5
RV1_19	63	1.17	80.4	3.8	79.1	4.5	72.0	99.0	80.4	3.9	101.7
RV1_30	175	1.28	80.6	3.6	82.7	3.4	111.0	70.0	80.5	3.6	97.5
RV1_3	57	1.33	82.0	4.0	81.1	5.1	130.0	100.0	81.9	4.1	101.0
RV1_92	129	1.01	82.9	4.0	82.0	3.8	69.0	72.0	83.0	4.0	101.1
RV1_87	76	0.99	83.7	3.1	87.5	4.1	179.0	83.0	83.5	3.1	95.6
RV1_26	92	0.71	86.0	3.7	95.8	4.4	277.0	84.0	85.5	3.7	89.8
RV1_7	48	0.79	90.7	4.2	89.6	5.3	130.0	100.0	90.6	4.3	101.2
RV1_105	91	0.88	90.7	2.7	90.6	3.6	88.0	70.0	90.7	2.7	100.1
RV1_60	810	1.33	91.1	4.5	92.8	3.8	110.0	64.0	90.9	4.5	98.1
RV1_5	74	0.69	91.5	4.4	91.3	4.6	128.0	86.0	91.3	4.4	100.2
RV1_13	149	0.97	92.9	4.2	93.7	4.1	124.0	69.0	92.8	4.2	99.2
RV1_88	108	1.61	94.5	2.7	102.0	3.7	231.0	67.0	94.2	2.7	92.7
RV1_69	343	2.24	95.0	4.1	97.4	3.7	122.0	60.0	94.9	4.1	97.5
RV1_2	156	1.50	95.1	4.3	92.8	3.8	98.0	63.0	95.0	4.3	102.5
RV1_96	207	1.22	95.4	4.3	93.0	3.7	53.0	67.0	95.5	4.3	102.5
RV1_64	32	0.82	96.9	2.8	103.7	6.9	240.0	120.0	96.5	2.8	93.4
RV1_98	28	1.33	97.0	4.6	96.2	7.2	110.0	130.0	96.8	4.7	100.8
RV1_68	129	1.16	98.8	8.3	110.2	8.1	350.0	130.0	97.9	8.2	89.6
RV1_36	174	1.23	98.8	4.3	97.9	4.0	111.0	70.0	98.7	4.3	100.9
RV1_37	116	0.89	99.4	3.9	99.6	4.1	117.0	73.0	99.4	3.9	99.7
RV1_52	62	0.83	100.1	4.6	101.5	5.1	171.0	89.0	99.7	4.6	98.7

Table A2. Detrital zircon U-Pb geochronologic analyses by using LA-ICP-MS analysis (continued)

Analysis	U (ppm)	U/Th	Apparent ages (Ma) $^{206}Pb^*/^{238}U$	± 2σ (Ma)	$^{207}Pb^*/^{235}U$	± 2σ (Ma)	$^{207}Pb^*/^{206}Pb^*$	± 2σ (Ma)	Preferred age ± 2σ (Ma)		conc (%)
RV1_61	123	1.04	102.4	6.4	113.5	6.5	275.0	97.0	101.6	6.3	90.3
RV1_59	95	0.68	102.2	5.1	104.1	5.2	153.0	80.0	102.0	5.2	98.2
RV1_83	102	2.22	102.6	5.5	102.0	5.2	87.0	79.0	102.6	5.5	100.6
RV1_55	31	1.07	103.9	5.0	105.3	7.6	200.0	120.0	103.4	5.0	98.7
RV1_54	63	1.24	103.9	4.6	106.3	5.1	211.0	81.0	103.6	4.6	97.8
RV1_17	88	1.66	104.1	4.8	101.5	5.1	158.0	85.0	104.0	4.9	102.6
RV1_33	100	0.79	104.8	5.3	109.5	5.1	188.0	84.0	104.6	5.3	95.8
RV1_108	645	1.31	110.6	4.2	110.5	3.7	94.0	53.0	110.6	4.3	100.1
RV1_24	84	1.62	112.1	5.8	107.4	5.6	30.0	84.0	112.3	5.9	104.4
RV1_86	100	1.03	116.0	3.1	123.6	4.2	252.0	71.0	115.5	3.2	93.8
RV1_57	208	1.23	116.7	5.4	117.3	4.5	118.0	64.0	116.7	5.4	99.5
RV1_77	199	0.65	120.8	7.3	123.9	6.7	216.0	96.0	120.4	7.6	97.4
RV1_74	74	1.16	121.3	5.3	119.0	5.2	99.0	81.0	121.2	5.3	101.9
RV1_34	108	0.69	122.6	4.9	125.1	4.7	135.0	66.0	122.5	4.9	98.0
RV1_91	288	0.72	122.9	6.1	120.5	4.9	92.0	64.0	122.9	6.0	102.0
RV1_27	126	0.88	124.9	8.0	142.0	8.1	330.0	100.0	123.9	8.2	88.0

RV1_9	87	1.28	124.3	5.3	124.0	5.3	133.0	71.0	124.3	5.3	100.2
RV1_32	161	0.96	124.7	5.3	126.9	4.9	107.0	65.0	124.7	5.3	98.2
RV1_90	57	1.04	124.9	6.3	123.8	6.4	139.0	86.0	124.8	6.3	100.9
RV1_49	423	1.44	126.1	4.8	130.3	4.2	169.0	59.0	126.0	4.8	96.8
RV1_50	150	0.84	131.2	6.0	132.6	5.3	131.0	65.0	131.1	6.0	98.9
RV1_107	338	1.02	131.1	5.7	128.0	4.6	111.0	60.0	131.2	5.8	102.4
RV1_114	66	1.16	133.8	8.2	139.5	8.0	252.0	94.0	132.9	8.2	95.9
RV1_73	989	0.85	141.2	4.1	153.7	4.5	306.0	56.0	140.5	4.2	91.9
RV1_66	69	1.57	141.5	7.4	148.4	8.2	290.0	110.0	140.5	7.6	95.4
RV1_11	43	0.81	148.6	7.0	150.7	7.5	196.0	91.0	148.1	6.9	98.6
RV1_48	220	1.26	148.6	7.6	146.5	5.8	74.0	63.0	148.8	7.6	101.4
RV1_82	134	1.72	149.7	7.4	151.2	6.2	125.0	67.0	149.8	7.6	99.0
RV1_15	397	0.89	152.7	6.4	157.4	5.4	173.0	59.0	152.5	6.3	97.0
RV1_53	612	0.90	162.7	8.3	173.8	6.8	277.0	72.0	162.1	8.2	93.6
RV1_78	232	1.81	264.9	11.0	270.0	8.8	262.0	62.0	264.7	11.2	98.1

Table A2. Detrital zircon U-Pb geochronologic analyses by using LA-ICP-MS analysis (continued)

Analysis	U (ppm)	U/Th	Apparent ages (Ma) $^{206}Pb^*/^{238}U$	± 2σ (Ma)	$^{207}Pb^*/^{235}U$	± 2σ (Ma)	$^{207}Pb^*/^{206}Pb^*$	± 2σ (Ma)	Preferred age ± 2σ (Ma)		conc (%)
RV1_65	491	0.90	267.2	7.7	274.3	6.9	292.0	49.0	266.9	8.1	97.4
RV1_103	478	1.03	271.8	9.5	275.9	7.8	259.0	56.0	271.8	9.4	98.5
RV1_18	151	1.68	279.3	12.0	287.6	9.2	275.0	64.0	279.2	12.4	97.1
RV1_4	45	0.67	285.7	14.0	281.8	11.0	249.0	74.0	285.6	13.7	101.4
RV1_8	166	1.02	299.0	13.0	299.9	10.0	245.0	61.0	299.2	13.1	99.7
RV1_14	146	1.17	300.7	13.0	303.5	10.0	230.0	59.0	300.9	13.1	99.1
RV1_94	48	1.71	320.8	16.0	311.3	13.0	185.0	73.0	321.5	16.8	103.0
RV1_100	237	0.49	331.7	13.0	344.2	10.0	346.0	60.0	331.0	13.0	96.4
RV1_84	325	1.15	394.5	18.0	390.7	13.0	319.0	57.0	394.8	17.8	101.0
RV1_40	165	1.07	407.0	15.0	412.8	11.0	349.0	58.0	407.2	15.3	98.6
RV1_43	167	1.27	423.9	20.0	426.8	14.0	348.0	58.0	424.1	20.2	99.3
RV1_42	166	1.24	435.2	21.0	428.7	15.0	296.0	62.0	436.2	21.4	101.5
RV1_41	236	1.28	443.7	22.0	432.5	15.0	325.0	65.0	444.6	22.6	102.6
RV1_1	101	1.07	489.7	20.0	503.8	15.0	451.0	65.0	489.3	20.6	97.2
RV1_101	125	0.71	493.1	19.0	515.0	14.0	476.0	57.0	492.3	20.0	95.8
RV1_80	789	2.79	525.4	18.0	618.3	16.0	846.0	57.0	518.4	18.5	85.0
RV1_67	258	0.75	552.1	27.0	557.1	18.0	500.0	70.0	552.0	27.1	99.1
RV1_63	133	2.15	597.3	29.0	604.0	19.0	505.0	67.0	597.4	30.0	98.9
RV1_104	165	1.10	625.3	25.0	634.0	17.0	586.0	62.0	625.3	26.3	98.6
RV1_89	105	2.69	923.4	39.0	964.6	24.0	951.0	67.0	919.5	41.0	95.7
RV1_25	98	0.61	1001.4	44.0	1037.4	25.0	954.0	69.0	999.6	46.0	96.5
RV1_62	24	1.33	1019.5	57.0	1035.0	37.0	848.0	78.0	1014.4	57.3	98.5
RV1_75	57	1.19	1886.0	92.0	1818.8	44.0	1696.0	70.0	1696.0	70.0	103.7

Table A2. Detrital zircon U-Pb geochronologic analyses by using LA-ICP-MS analysis

Analysis	U (ppm)	U/Th	Apparent ages (Ma) $^{206}Pb^*/^{238}U$	± 2σ (Ma)	$^{207}Pb^*/^{235}U$	± 2σ (Ma)	$^{207}Pb^*/^{206}Pb^*$	± 2σ (Ma)	Preferred age ± 2σ (Ma)		conc (%)
Sample SK2-Río Leona Formation											
SK2_45	148	1.76	24.1	0.5	23.9	1.3	65.0	97.0	24.1	0.5	100.7

SK2_24	68	1.19	25.6	0.6	27.7	2.5	190.0	150.0	25.4	0.6	92.4
SK2_1	97	1.23	25.7	0.8	25.7	2.0	130.0	130.0	25.7	0.8	100.2
SK2_103	79	1.58	26.6	0.6	27.4	2.3	170.0	140.0	26.4	0.6	96.9
SK2_44	84	0.91	26.7	0.7	29.4	2.2	270.0	140.0	26.6	0.7	91.0
SK2_39	43	1.05	26.9	0.7	28.1	3.6	-40.0	200.0	26.8	0.7	95.7
SK2_81	54	2.57	31.7	0.9	29.7	3.4	-20.0	170.0	31.7	0.9	106.8
SK2_106	36	1.29	37.3	2.4	36.7	8.5	180.0	380.0	37.2	2.4	101.6
SK2_58	107	1.01	37.4	0.8	36.6	1.9	55.0	92.0	37.4	0.8	102.2
SK2_14	165	0.66	68.8	1.5	69.9	1.9	163.0	58.0	68.7	1.5	98.4
SK2_99	72	0.90	69.0	2.0	70.7	3.7	160.0	100.0	68.9	2.0	97.6
SK2_73	819	0.69	69.0	1.3	70.3	1.2	139.0	39.0	68.9	1.3	98.2
SK2_100	59	0.77	76.5	1.7	76.2	3.4	126.0	84.0	76.5	1.7	100.4
SK2_108	110	0.71	77.5	1.7	76.9	2.3	145.0	61.0	77.4	1.7	100.8
SK2_110	96	1.16	77.9	1.7	77.2	2.8	139.0	67.0	77.8	1.7	100.9
SK2_62	57	1.58	77.8	1.6	78.3	3.2	122.0	79.0	77.8	1.7	99.4
SK2_92	70	0.73	78.0	1.7	76.3	3.0	145.0	78.0	77.9	1.7	102.2
SK2_61	102	1.15	78.8	1.8	87.8	2.7	360.0	68.0	78.1	1.8	89.7
SK2_57	49	0.96	78.5	1.7	79.7	3.6	162.0	86.0	78.3	1.7	98.5
SK2_11	505	9.71	79.3	1.5	79.0	1.4	96.0	40.0	79.3	1.5	100.4
SK2_105	483	3.40	80.4	1.7	79.8	1.5	101.0	40.0	80.4	1.7	100.8
SK2_98	260	1.29	81.2	1.5	80.7	1.6	115.0	47.0	81.3	1.5	100.6
SK2_29	218	0.80	81.8	1.3	85.4	1.9	188.0	48.0	81.6	1.3	95.8
SK2_30	127	1.01	82.4	1.5	83.6	2.3	143.0	56.0	82.3	1.5	98.6
SK2_28	172	0.88	85.3	1.7	82.9	2.2	76.0	54.0	85.4	1.7	102.9
SK2_2	89	0.67	86.1	2.2	86.5	3.0	140.0	71.0	85.9	2.2	99.5
SK2_59	101	1.22	87.0	1.8	87.1	2.5	149.0	63.0	86.9	1.9	99.9
SK2_89	101	0.70	87.0	1.8	87.4	2.7	139.0	59.0	86.9	1.9	99.5
SK2_80	121	1.19	87.8	1.9	85.4	2.5	133.0	64.0	87.4	1.9	102.8
SK2_102	132	0.80	88.4	1.9	88.9	2.4	142.0	57.0	88.3	1.9	99.4
SK2_13	81	1.03	88.7	2.4	89.7	3.3	158.0	79.0	88.6	2.4	98.9
SK2_90	245	0.78	90.0	2.0	90.0	2.0	143.0	50.0	89.9	2.0	100.0
SK2_56	152	1.48	89.9	1.8	88.7	2.3	78.0	52.0	90.0	1.9	101.4
SK2_46	980	2.40	91.7	1.6	107.2	2.1	443.0	44.0	90.7	1.6	85.5
SK2_85	116	0.67	91.5	1.9	91.7	2.7	142.0	62.0	91.5	1.9	99.8
SK2_104	233	0.97	92.8	1.9	92.4	2.1	119.0	48.0	92.5	1.9	100.4
SK2_32	252	1.32	93.1	1.8	98.5	2.1	261.0	50.0	92.7	1.8	94.5
SK2_41	67	0.87	92.7	2.0	91.7	3.3	115.0	71.0	92.7	2.0	101.1

Table A2. Detrital zircon U-Pb geochronologic analyses by using LA-ICP-MS analysis (continued)

Analysis	U (ppm)	U/Th	Apparent ages (Ma) $^{206}Pb^*/^{238}U$	± 2σ (Ma)	$^{207}Pb^*/^{235}U$	± 2σ (Ma)	$^{207}Pb^*/^{206}Pb^*$	± 2σ (Ma)	Preferred age ± 2σ (Ma)		conc (%)
SK2_93	368	0.59	92.7	2.1	89.0	1.8	109.0	50.0	92.7	2.1	104.2
SK2_63	219	1.70	93.5	1.9	93.1	2.0	94.0	47.0	93.5	1.9	100.4
SK2_33	249	1.82	93.5	1.8	92.7	1.8	93.0	40.0	93.5	1.8	100.9
SK2_67	247	1.82	94.1	1.9	94.5	1.9	138.0	49.0	94.1	1.9	99.6
SK2_112	584	1.10	94.1	2.0	94.4	1.7	125.0	42.0	94.1	2.0	99.7
SK2_68	103	1.27	94.6	2.2	98.8	3.1	264.0	73.0	94.2	2.2	95.7
SK2_35	479	0.93	95.1	1.8	95.1	1.5	123.0	38.0	95.0	1.8	100.0
SK2_20	293	1.42	95.1	2.1	94.6	1.9	123.0	48.0	95.1	2.1	100.5

SK2_94	383	1.45	95.6	2.0	96.7	1.8	158.0	45.0	95.3	2.0	98.9
SK2_49	437	2.84	95.4	1.9	96.0	1.7	138.0	41.0	95.3	1.9	99.4
SK2_17	183	1.66	95.3	1.9	95.3	2.1	128.0	51.0	95.3	1.9	100.0
SK2_40	397	1.40	95.5	1.8	96.4	1.6	137.0	42.0	95.4	1.8	99.1
SK2_77	138	0.84	96.0	2.2	95.9	2.7	152.0	61.0	95.9	2.2	100.1
SK2_47	755	0.90	96.7	2.5	96.6	1.9	168.0	50.0	96.5	2.5	100.1
SK2_82	55	1.83	96.9	2.1	94.1	3.6	104.0	76.0	96.9	2.1	103.0
SK2_19	29	1.53	97.2	2.2	94.2	6.4	80.0	120.0	97.3	2.3	103.2
SK2_9	20	1.05	98.7	2.3	104.7	7.7	220.0	140.0	98.3	2.4	94.3
SK2_66	334	1.39	98.2	2.1	95.5	1.9	105.0	46.0	98.3	2.2	102.8
SK2_50	209	0.69	98.8	2.0	98.4	2.1	123.0	49.0	98.8	2.0	100.4
SK2_23	127	0.67	104.4	2.1	102.0	2.4	85.0	51.0	104.5	2.1	102.4
SK2_55	65	1.10	104.6	2.2	101.6	3.5	122.0	73.0	104.7	2.2	103.0
SK2_51	1112	7.08	105.1	3.0	105.4	2.8	186.0	58.0	104.8	3.0	99.7
SK2_4	105	0.97	106.7	2.5	113.1	3.4	261.0	66.0	106.2	2.5	94.3
SK2_26	611	0.27	114.3	2.2	115.2	2.0	181.0	42.0	114.2	2.2	99.2
SK2_12	122	0.94	117.5	2.8	128.1	3.5	341.0	70.0	116.5	2.8	91.7
SK2_95	54	1.08	118.2	2.6	116.8	3.8	180.0	68.0	118.0	2.5	101.2
SK2_70	80	1.18	121.8	2.6	124.4	3.5	176.0	59.0	121.6	2.5	97.9
SK2_88	68	0.83	122.1	2.5	126.5	3.8	208.0	65.0	121.8	2.5	96.5
SK2_69	71	1.34	121.9	2.7	120.6	3.6	119.0	64.0	122.0	2.7	101.1
SK2_64	129	1.19	125.4	2.5	141.1	3.5	442.0	60.0	124.1	2.5	88.9
SK2_16	119	0.99	125.0	3.6	125.6	5.3	175.0	85.0	124.8	3.6	99.5

Table A2. Detrital zircon U-Pb geochronologic analyses by using LA-ICP-MS analysis (continued)

Analysis	U (ppm)	U/Th	Apparent ages (Ma) $^{206}Pb^*/^{238}U$	± 2σ (Ma)	$^{207}Pb^*/^{235}U$	± 2σ (Ma)	$^{207}Pb^*/^{206}Pb^*$	± 2σ (Ma)	Preferred age ± 2σ (Ma)		conc (%)
SK2_84	228	1.11	126.4	2.6	127.2	2.6	207.0	48.0	126.1	2.6	99.4
SK2_53	184	0.80	127.6	3.0	126.8	2.8	172.0	54.0	127.5	3.0	100.6
SK2_60	65	0.83	129.2	2.8	131.0	3.5	191.0	63.0	129.1	2.9	98.6
SK2_3	139	0.73	131.4	3.0	135.5	3.4	221.0	56.0	131.1	3.0	97.0
SK2_22	136	1.01	131.9	2.7	131.6	2.9	141.0	49.0	132.0	2.7	100.2
SK2_87	331	0.49	139.5	3.0	142.3	2.5	206.0	41.0	139.3	3.0	98.0
SK2_5	181	0.63	140.3	3.0	140.7	2.9	155.0	45.0	140.3	3.0	99.7
SK2_97	465	0.50	142.6	3.1	139.8	2.3	141.0	44.0	142.7	3.1	102.0
SK2_38	100	1.37	145.6	2.1	148.4	3.2	176.0	47.0	145.4	2.1	98.1
SK2_37	78	0.83	146.1	3.7	153.6	5.1	300.0	75.0	145.4	3.7	95.1
SK2_65	188	2.44	145.8	3.2	144.5	3.0	187.0	53.0	145.5	3.3	100.9
SK2_21	363	0.83	146.1	2.8	151.6	2.5	221.0	43.0	145.8	2.8	96.4
SK2_8	954	0.87	146.6	3.5	150.5	3.2	192.0	37.0	146.5	3.5	97.4
SK2_48	45	0.87	147.0	3.4	142.1	5.0	119.0	70.0	147.2	3.4	103.4
SK2_42	250	0.87	147.9	2.8	148.8	2.7	165.0	43.0	147.6	2.8	99.4
SK2_6	517	1.11	147.9	3.2	153.1	3.2	196.0	40.0	147.8	3.2	96.6
SK2_96	104	0.98	147.9	3.1	148.2	3.6	187.0	55.0	147.9	3.1	99.8
SK2_71	560	0.84	148.0	2.5	148.0	2.3	147.0	33.0	148.0	2.5	100.0
SK2_7	264	0.98	148.5	3.2	148.9	2.8	155.0	44.0	148.5	3.3	99.7
SK2_25	2929	0.74	149.2	2.9	146.9	2.1	167.0	38.0	149.2	3.0	101.6
SK2_111	459	1.14	150.7	2.4	169.9	3.1	456.0	38.0	149.3	2.4	88.7
SK2_18	151	1.05	149.6	3.3	152.1	3.5	198.0	56.0	149.5	3.3	98.4

SK2_79	63	0.88	152.6	3.4	176.8	4.8	519.0	66.0	150.7	3.4	86.3
SK2_107	115	1.60	150.9	3.2	150.3	3.2	184.0	52.0	150.8	3.2	100.4
SK2_75	884	1.40	151.2	2.8	154.0	2.3	213.0	38.0	150.9	2.8	98.2
SK2_34	1278	0.90	156.6	2.7	156.8	2.2	161.0	34.0	156.6	2.8	99.9
SK2_43	322	0.61	254.7	5.4	277.3	4.2	436.0	45.0	252.9	5.5	91.8
SK2_31	85	0.67	285.1	5.6	292.1	5.7	318.0	46.0	284.6	5.7	97.6
SK2_54	516	1.42	298.3	5.6	296.6	4.1	289.0	43.0	298.5	5.7	100.6
SK2_52	110	1.26	372.8	7.2	375.9	5.8	407.0	46.0	372.4	7.4	99.2
SK2_78	260	1.24	490.0	10.0	489.7	7.0	502.0	44.0	489.7	10.9	100.1

Table A2. Detrital zircon U-Pb geochronologic analyses by using LA-ICP-MS analysis (continued)

Analysis	U (ppm)	U/Th	Apparent ages (Ma) $^{206}Pb^*/^{238}U$	± 2σ (Ma)	$^{207}Pb^*/^{235}U$	± 2σ (Ma)	$^{207}Pb^*/^{206}Pb^*$	± 2σ (Ma)	Preferred age ± 2σ (Ma)		conc (%)
SK2_83	393	1.51	582.0	11.0	579.1	6.8	573.0	44.0	582.1	11.4	100.5
SK2_109	237	1.88	599.0	12.0	589.4	6.8	584.0	43.0	599.0	12.0	101.6
SK2_101	189	1.34	615.0	12.0	606.2	7.5	602.0	42.0	613.0	12.0	101.5
SK2_91	110	1.15	657.0	14.0	662.0	11.0	709.0	44.0	654.2	14.9	99.2
SK2_27	627	2.31	993.0	17.0	1041.5	9.0	1143.0	38.0	982.3	17.8	95.3
SK2_36	126	0.95	1177.0	20.0	1171.4	9.8	1162.0	34.0	1178.3	21.6	100.5
SK2_74	246	1.43	2406.0	50.0	2446.0	19.0	2479.0	39.0	2479.0	39.0	98.4
SK2_76	37	0.12	2473.0	46.0	2472.0	16.0	2466.0	34.0	2466.0	34.0	100.0

Table A2. Detrital zircon U-Pb geochronologic analyses by using LA-MC-ICP-MS analysis

Analysis	U (ppm)	U/Th	Apparent ages (Ma) $^{206}Pb^*/^{238}U$	± 2σ (Ma)	$^{207}Pb^*/^{235}U$	± 2σ (Ma)	$^{207}Pb^*/^{206}Pb^*$	± 2σ (Ma)	Preferred age ± 2σ (Ma)		conc (%)
Sample RL1-Loreto Formation											
B530_34	432	2.44	34.5	0.7	35.9	0.8	123.0	26.0	34.5	0.7	95.9
B530_32	89	0.65	35.4	0.7	37.2	1.7	146.0	91.0	35.4	0.7	95.3
B530_4	188	0.42	35.7	0.7	39.1	1.0	256.0	38.0	35.7	0.7	91.4
B530_9	293	0.97	35.7	0.7	39.1	1.2	204.0	59.0	35.7	0.7	91.4
B530_30	117	0.62	35.9	0.7	37.1	1.2	117.0	54.0	35.9	0.7	96.7
B530_5	243	0.85	35.9	0.7	38.5	0.9	168.0	27.0	35.9	0.7	93.4
B530_31	848	1.19	36.2	0.7	38.7	0.9	200.0	23.0	36.2	0.7	93.6
B530_15	147	0.58	36.6	0.7	39.0	1.1	182.0	46.0	36.6	0.7	93.8
B530_1	165	0.69	36.6	0.8	39.9	1.1	255.0	39.0	36.6	0.8	91.8
B530_45	229	0.50	36.8	0.7	38.4	1.0	117.0	34.0	36.8	0.7	95.9
B530_46	265	0.56	36.8	0.7	39.7	0.9	191.0	33.0	36.8	0.7	92.7
B530_44	145	0.67	36.9	0.8	39.1	1.1	181.0	46.0	36.9	0.8	94.2
B530_72	319	0.49	37.1	0.8	38.2	1.0	92.0	36.0	37.1	0.8	97.1
B530_70	268	0.39	37.5	0.8	39.4	1.0	127.0	33.0	37.5	0.8	95.3
B530_53	244	0.47	37.6	0.8	38.7	0.9	103.0	28.0	37.6	0.8	97.0
B530_80	207	0.60	37.7	0.8	38.1	1.0	78.0	42.0	37.7	0.8	98.9
B530_78	107	0.73	37.8	0.8	39.8	1.5	164.0	69.0	37.8	0.8	94.9
B530_87	127	1.03	38.0	0.8	39.6	1.1	126.0	47.0	38.0	0.8	96.0
B530_73	306	0.83	38.4	0.8	39.5	0.9	112.0	28.0	38.4	0.8	97.1
B530_79	140	0.96	39.7	0.8	41.3	1.2	112.0	50.0	39.7	0.8	96.2
B530_23	206	0.77	42.1	0.8	43.1	1.1	99.0	38.0	42.1	0.8	97.7
B530_50	396	0.65	43.4	0.9	44.3	1.0	93.0	23.0	43.4	0.9	98.0

B530_20	113	0.55	49.7	1.0	53.4	1.5	226.0	45.0	49.7	1.0	93.0
B530_16	324	0.88	70.8	1.4	72.3	1.5	111.0	20.0	70.8	1.4	97.9

Table A2. Detrital zircon U-Pb geochronologic analyses by using LA-MC-ICP-MS analysis (continued)

Analysis	U (ppm)	U/Th	Apparent ages (Ma) $^{206}Pb^*/^{238}U$	± 2σ (Ma)	$^{207}Pb^*/^{235}U$	± 2σ (Ma)	$^{207}Pb^*/^{206}Pb^*$	± 2σ (Ma)	Preferred age ± 2σ (Ma)		conc (%)
B530_33	246	0.73	71.1	1.4	71.9	1.6	92.0	23.0	71.1	1.4	98.8
B530_8	589	0.80	71.2	1.4	73.4	1.5	124.0	15.0	71.2	1.4	97.0
B530_17	1903	0.35	71.2	1.4	72.2	1.5	87.0	14.0	71.2	1.4	98.7
B530_21	689	0.73	71.7	1.4	72.5	1.5	97.0	15.0	71.7	1.4	98.8
B530_13	401	0.76	71.7	1.4	73.9	1.6	120.0	21.0	71.7	1.4	97.0
B530_22	834	0.66	71.7	1.4	72.6	1.5	96.0	13.0	71.7	1.4	98.8
B530_14	543	0.75	71.7	1.4	74.0	1.5	120.3	12.0	71.7	1.4	96.9
B530_40	536	0.75	71.8	1.4	73.5	1.5	124.0	18.0	71.8	1.4	97.6
B530_7	536	0.66	72.1	1.4	73.9	1.6	108.0	16.0	72.1	1.4	97.6
B530_11	1449	0.30	72.1	1.4	74.3	1.5	103.1	12.0	72.1	1.4	97.1
B530_27	1146	0.60	72.2	1.4	73.1	1.6	77.0	13.0	72.2	1.4	98.8
B530_25	289	0.79	72.3	1.4	74.6	1.6	141.0	23.0	72.3	1.4	96.8
B530_52	1741	0.34	72.3	1.5	75.0	1.8	134.0	15.0	72.3	1.5	96.5
B530_19	617	0.81	72.4	1.4	74.3	1.5	116.0	15.0	72.4	1.4	97.5
B530_41	689	1.05	72.7	1.4	73.2	1.5	85.0	15.0	72.7	1.4	99.3
B530_36	592	0.92	72.9	1.5	73.5	1.6	94.0	15.0	72.9	1.5	99.2
B530_0	2886	0.20	73.1	1.6	74.4	1.7	104.9	9.3	73.1	1.6	98.3
B530_67	348	0.88	73.2	1.5	73.8	1.7	103.0	25.0	73.2	1.5	99.1
B530_86	634	0.70	73.3	1.5	74.0	1.5	98.0	15.0	73.3	1.5	99.1
B530_51	476	0.68	73.4	1.5	73.7	1.5	68.0	15.0	73.4	1.5	99.6
B530_39	425	0.76	73.5	1.5	75.0	1.7	113.0	17.0	73.5	1.5	98.0
B530_38	479	0.76	73.6	1.5	74.3	1.6	87.0	16.0	73.6	1.5	99.0
B530_47	310	0.77	73.6	1.5	75.0	1.6	96.0	20.0	73.6	1.5	98.2
B530_48	417	0.79	73.6	1.5	74.0	1.6	81.0	20.0	73.6	1.5	99.5
B530_37	506	1.02	73.7	1.5	74.9	1.6	111.0	15.0	73.7	1.5	98.4
B530_56	2259	0.28	73.8	1.5	74.8	1.5	88.1	10.0	73.8	1.5	98.6
B530_64	1159	0.37	73.8	1.5	74.2	1.5	81.0	16.0	73.8	1.5	99.4
B530_49	275	1.04	73.8	1.5	74.3	1.6	88.0	21.0	73.8	1.5	99.4
B530_75	263	1.07	73.9	1.5	75.6	1.9	133.0	37.0	73.9	1.5	97.7
B530_85	243	0.94	74.1	1.5	74.7	1.8	97.0	31.0	74.1	1.5	99.2
B530_6	435	0.80	74.2	1.5	76.1	1.6	123.0	21.0	74.2	1.5	97.5

Table A2. Detrital zircon U-Pb geochronologic analyses by using LA-MC-ICP-MS analysis (continued)

Analysis	U (ppm)	U/Th	Apparent ages (Ma) $^{206}Pb^*/^{238}U$	± 2σ (Ma)	$^{207}Pb^*/^{235}U$	± 2σ (Ma)	$^{207}Pb^*/^{206}Pb^*$	± 2σ (Ma)	Preferred age ± 2σ (Ma)		conc (%)
B530_24	481	1.23	74.5	1.5	75.2	1.6	88.0	17.0	74.5	1.5	99.0
B530_68	236	0.58	74.6	1.5	76.8	1.9	149.0	29.0	74.6	1.5	97.1
B530_29	307	0.85	74.7	1.5	75.8	1.6	109.0	20.0	74.7	1.5	98.5
B530_89	2519	0.41	74.7	1.5	76.5	1.6	86.0	13.0	74.7	1.5	97.7
B530_18	383	0.88	75.0	1.5	77.5	1.8	139.0	21.0	75.0	1.5	96.8
B530_54	379	0.88	75.2	1.5	76.0	1.6	93.0	16.0	75.2	1.5	98.9
B530_55	2184	0.03	75.4	1.5	76.9	1.6	105.5	11.0	75.4	1.5	98.0

B530_83	325	0.85	75.5	1.5	76.7	1.7	90.0	19.0	75.5	1.5	98.4
B530_2	440	0.74	75.5	1.4	78.8	1.6	189.0	16.0	75.5	1.4	95.9
B530_60	446	0.89	75.6	1.5	76.7	1.7	95.0	20.0	75.6	1.5	98.6
B530_77	440	0.85	75.8	1.5	76.6	1.6	89.0	20.0	75.8	1.5	98.9
B530_28	542	0.82	75.8	1.5	77.5	1.6	134.0	14.0	75.8	1.5	97.8
B530_84	241	0.81	75.8	1.5	77.2	1.7	107.0	24.0	75.8	1.5	98.1
B530_57	291	0.73	76.1	1.5	77.7	1.8	108.0	27.0	76.1	1.5	97.9
B530_71	772	0.71	76.3	1.5	77.8	1.6	98.0	15.0	76.3	1.5	98.0
B530_10	1283	0.64	76.3	1.5	78.9	1.6	125.0	13.0	76.3	1.5	96.7
B530_69	282	1.14	76.5	1.5	77.5	1.7	108.0	26.0	76.5	1.5	98.7
B530_76	291	0.88	76.8	1.5	78.4	1.7	109.0	20.0	76.8	1.5	98.0
B530_42	1538	0.83	76.9	1.5	78.8	1.6	134.0	14.0	76.9	1.5	97.6
B530_82	241	0.95	76.9	1.5	77.8	1.7	101.0	23.0	76.9	1.5	98.9
B530_65	805	0.62	77.0	1.5	77.7	1.6	88.0	16.0	77.0	1.5	99.1
B530_63	440	1.07	77.7	1.5	78.5	1.6	93.0	17.0	77.7	1.5	99.0
B530_88	276	0.83	78.1	1.5	79.1	1.8	102.0	24.0	78.1	1.5	98.7
B530_61	316	0.82	78.2	1.5	79.6	1.7	103.0	20.0	78.2	1.5	98.3
B530_3	649	0.44	78.3	1.6	80.2	1.8	138.0	16.0	78.3	1.6	97.6
B530_58	243	0.63	78.6	1.6	80.7	1.8	148.0	21.0	78.6	1.6	97.4
B530_26	815	0.91	81.5	1.7	83.1	1.9	110.0	21.0	81.5	1.7	98.1
B530_81	451	0.33	85.1	1.7	90.5	2.2	231.0	33.0	85.1	1.7	94.0
B530_66	86	0.78	85.5	1.7	90.4	2.8	231.0	60.0	85.5	1.7	94.5
B530_12	813	0.70	92.5	1.8	95.1	1.9	144.0	14.0	92.5	1.8	97.3
B530_43	168	0.48	101.9	2.0	105.5	2.3	173.0	22.0	101.9	2.0	96.6

Table A2. Detrital zircon U-Pb geochronologic analyses by using LA-MC-ICP-MS analysis (continued)

Analysis	U (ppm)	U/Th	Apparent ages (Ma) $^{206}Pb^*/^{238}U$	± 2σ (Ma)	$^{207}Pb^*/^{235}U$	± 2σ (Ma)	$^{207}Pb^*/^{206}Pb^*$	± 2σ (Ma)	Preferred age ± 2σ (Ma)		conc (%)
B530_74	330	0.43	106.7	2.1	107.0	2.3	119.0	15.0	106.7	2.1	99.7
B530_35	102	0.52	108.1	2.1	111.5	2.6	180.0	31.0	108.1	2.1	97.0
B530_59	657	0.43	109.9	2.3	111.2	2.4	97.0	14.0	109.9	2.3	98.8

Table A2. Detrital zircon U-Pb geochronologic analyses by using LA-MC-ICP-MS analysis

Analysis	U (ppm)	U/Th	Apparent ages (Ma) $^{206}Pb^*/^{238}U$	± 2σ (Ma)	$^{207}Pb^*/^{235}U$	± 2σ (Ma)	$^{207}Pb^*/^{206}Pb^*$	± 2σ (Ma)	Preferred age ± 2σ (Ma)		conc (%)
Sample SK1-Loreto Formation											
KR1_1	656	1.30	77.9	2.1	79.1	1.5	107	25	77.9	2.1	98.4
KR1_2	595	2.17	72.4	1.9	72.7	1.5	71	29	72.4	1.9	99.5
KR1_3	239	1.55	116.5	3.1	114.8	2.5	82	36	116.5	3.1	101.5
KR1_4	202	1.15	88.3	2.4	87.8	2.4	72	46	88.3	2.4	100.6
KR1_5	734	2.28	98.5	2.6	99.5	1.8	117	17	98.5	2.6	98.9
KR1_6	357	0.99	68.9	1.8	69.3	1.4	87	28	68.9	1.8	99.3
KR1_7	487	1.86	68.9	1.9	75.0	1.9	273	45	68.9	1.9	91.8
KR1_8	391	2.02	97.5	2.6	97.9	1.8	109	23	97.5	2.6	99.6
KR1_9	488	1.98	89.5	2.4	92.4	1.9	151	31	89.5	2.4	96.9
KR1_10	148	1.08	72.1	1.9	79.0	2.0	291	50	72.1	1.9	91.2
KR1_11	213	1.02	87.8	2.3	91.6	2.1	188	39	87.8	2.3	95.9
KR1_12	386	1.59	82.2	2.2	84.2	1.6	129	28	82.2	2.2	97.6

KR1_13	290	0.99	88.5	2.3	90.3	1.7	142	29	88.5	2.3	98.0
KR1_14	200	1.59	88.2	2.4	91.3	2.0	169	34	88.2	2.4	96.6
KR1_15	172	1.55	36.3	1.0	39.7	1.6	257	78	36.3	1.0	91.5
KR1_16	143	1.46	87.7	2.4	89.2	2.2	141	44	87.7	2.4	98.3
KR1_17	257	1.00	70.4	1.9	70.9	1.6	89	36	70.4	1.9	99.2

Table A2. Detrital zircon U-Pb geochronologic analyses by using LA-MC-ICP-MS analysis (continued)

Analysis	U (ppm)	U/Th	Apparent ages (Ma) $^{206}Pb^*/^{238}U$	± 2σ (Ma)	$^{207}Pb^*/^{235}U$	± 2σ (Ma)	$^{207}Pb^*/^{206}Pb^*$	± 2σ (Ma)	Preferred age ± 2σ (Ma)		conc (%)
KR1_18	613	1.75	70.3	1.9	71.6	1.3	129	21	70.3	1.9	98.2
KR1_19	1025	1.13	68.2	1.9	68.7	1.2	97	18	68.2	1.9	99.2
KR1_20	455	0.80	91.7	2.5	94.0	1.7	158	21	91.7	2.5	97.6
KR1_21	265	1.67	88.9	2.4	90.1	1.8	130	32	88.9	2.4	98.7
KR1_22	138	1.41	98.0	2.7	104.3	3.4	248	67	98.0	2.7	93.9
KR1_23	206	2.10	88.0	2.4	91.2	2.1	174	41	88.0	2.4	96.5
KR1_24	355	1.13	67.4	1.8	70.2	1.5	177	33	67.4	1.8	96.0
KR1_25	925	2.04	95.1	2.5	95.3	1.6	104	16	95.1	2.5	99.8
KR1_26	284	1.72	117.9	3.3	119.7	2.3	153	21	117.9	3.3	98.5
KR1_27	127	1.31	91.1	2.5	93.4	2.5	147	50	91.1	2.5	97.6
KR1_28	203	1.89	35.9	1.0	36.5	1.5	75	76	35.9	1.0	98.4
KR1_29	116	1.26	70.1	1.9	73.8	2.4	193	67	70.1	1.9	95.0
KR1_30	790	1.11	69.1	1.9	71.1	1.4	122	31	69.1	1.9	97.2
KR1_31	185	0.88	88.9	2.4	90.4	2.1	130	40	88.9	2.4	98.4
KR1_32	824	0.76	69.7	1.9	77.1	7.1	210	100	69.7	1.9	90.3
KR1_33	222	1.07	88.7	2.4	94.9	2.1	253	34	88.7	2.4	93.4
KR1_34	128	1.40	88.3	2.4	96.4	2.5	291	50	88.3	2.4	91.6
KR1_35	212	0.81	99.6	2.7	99.4	2.3	97	35	99.6	2.7	100.2
KR1_36	209	1.26	36.8	1.0	41.4	1.8	309	85	36.8	1.0	88.9
KR1_37	391	1.48	37.7	1.0	39.0	1.0	107	39	37.7	1.0	96.8
KR1_38	182	1.32	71.6	1.9	74.0	2.1	135	52	71.6	1.9	96.7
KR1_39	549	0.85	67.1	1.8	69.1	1.3	136	23	67.1	1.8	97.1
KR1_40	202	0.78	75.1	2.0	79.0	1.8	199	42	75.1	2.0	95.1
KR1_41	301	0.87	69.6	1.9	70.5	1.5	109	30	69.6	1.9	98.7
KR1_42	161	2.16	108.8	2.9	116.0	2.5	265	39	108.8	2.9	93.8
KR1_43	319	0.68	73.1	2.0	75.1	1.6	139	34	73.1	2.0	97.3
KR1_44	535	0.98	68.9	1.8	69.7	1.3	115	25	68.9	1.8	98.8
KR1_45	1558	2.19	94.8	2.6	94.7	1.7	99	16	94.8	2.6	100.1
KR1_46	220	1.10	70.7	1.9	70.8	1.8	77	46	70.7	1.9	99.8
KR1_47	500	1.60	67.9	1.8	68.0	1.3	75	21	67.9	1.8	99.9
KR1_48	326	1.48	100.1	2.7	101.2	1.9	121	28	100.1	2.7	98.9

Table A2. Detrital zircon U-Pb geochronologic analyses by using LA-MC-ICP-MS analysis (continued)

Analysis	U (ppm)	U/Th	Apparent ages (Ma) $^{206}Pb^*/^{238}U$	± 2σ (Ma)	$^{207}Pb^*/^{235}U$	± 2σ (Ma)	$^{207}Pb^*/^{206}Pb^*$	± 2σ (Ma)	Preferred age ± 2σ (Ma)		conc (%)
KR1_49	148	1.20	87.4	2.4	90.6	2.2	173	42	87.4	2.4	96.4
KR1_50	563	2.27	101.8	2.7	101.9	1.8	109	20	101.8	2.7	99.8
KR1_51	448	1.71	93.0	2.5	95.0	1.9	148	22	93.0	2.5	97.8
KR1_52	721	1.22	91.2	2.5	92.6	1.7	116	19	91.2	2.5	98.5

KR1_53	1094	1.02	68.1	1.8	68.2	1.2	68	17	68.1	1.8	99.8
KR1_54	1150	1.48	88.8	2.4	92.3	1.8	172	29	88.8	2.4	96.2
KR1_55	174	1.10	72.1	2.0	74.2	2.1	147	50	72.1	2.0	97.1
KR1_56	303	1.49	67.9	1.8	70.9	1.4	172	30	67.9	1.8	95.8
KR1_57	156	1.02	70.5	1.9	68.9	1.6	15	39	70.5	1.9	102.3
KR1_58	194	3.01	86.8	2.3	87.5	2.0	106	39	86.8	2.3	99.2
KR1_59	248	0.92	72.1	1.9	75.0	1.6	157	35	72.1	1.9	96.1
KR1_60	390	2.25	108.2	2.9	109.5	2.0	130	21	108.2	2.9	98.8
KR1_61	112	1.64	70.0	1.9	69.1	2.2	33	53	70.0	1.9	101.3
KR1_62	77	1.68	67.3	1.9	65.1	2.5	-3	69	67.3	1.9	103.4
KR1_63	373	4.01	93.4	2.5	94.3	1.7	116	20	93.4	2.5	99.1
KR1_64	681	1.91	68.0	1.8	69.8	1.2	128	18	68.0	1.8	97.4
KR1_65	596	1.41	66.9	1.8	67.7	1.2	88	24	66.9	1.8	98.9
KR1_66	247	2.26	90.2	2.4	94.2	1.8	198	27	90.2	2.4	95.8
KR1_67	567	1.13	104.3	2.8	105.1	1.9	107	19	104.3	2.8	99.2
KR1_68	74	1.95	36.7	1.0	42.9	2.4	410	110	36.7	1.0	85.5
KR1_69	221	1.70	92.0	2.5	95.8	1.8	181	26	92.0	2.5	96.1
KR1_70	1067	0.79	67.9	1.8	68.1	1.2	72	17	67.9	1.8	99.7
KR1_71	529	1.21	67.8	1.8	68.8	1.4	98	23	67.8	1.8	98.5
KR1_72	474	1.08	102.3	2.7	101.9	1.7	89	17	102.3	2.7	100.4
KR1_73	244	1.76	90.8	2.5	91.9	1.8	104	26	90.8	2.5	98.9
KR1_74	190	1.53	68.6	1.8	67.6	1.6	26	33	68.6	1.8	101.5
KR1_75	103	1.21	35.6	1.0	36.6	2.0	100	110	35.6	1.0	97.4
KR1_76	86	1.63	35.3	1.0	33.9	1.9	-50	110	35.3	1.0	104.0
KR1_77	433	1.13	68.3	1.8	68.8	1.3	98	22	68.3	1.8	99.3
KR1_78	629	1.87	68.3	1.8	69.7	1.2	105	17	68.3	1.8	98.0
KR1_79	53	2.35	94.1	2.5	101.8	3.1	275	61	94.1	2.5	92.4

Table A2. Detrital zircon U-Pb geochronologic analyses by using LA-MC-ICP-MS analysis (continued)

Analysis	U (ppm)	U/Th	Apparent ages (Ma) $^{206}Pb^*/^{238}U$	± 2σ (Ma)	$^{207}Pb^*/^{235}U$	± 2σ (Ma)	$^{207}Pb^*/^{206}Pb^*$	± 2σ (Ma)	Preferred age ± 2σ (Ma)		conc (%)
KR1_80	173	2.59	36.0	1.0	38.5	1.3	173	64	36.0	1.0	93.6
KR1_81	100	1.09	73.7	2.0	80.0	1.9	268	42	73.7	2.0	92.1
KR1_82	892	1.01	66.7	1.8	71.6	1.9	228	48	66.7	1.8	93.1
KR1_83	194	1.96	69.0	1.9	67.3	1.3	15	27	69.0	1.9	102.5
KR1_84	727	2.08	93.8	2.5	94.2	1.7	92	19	93.8	2.5	99.6
KR1_85	346	1.74	83.5	2.3	84.9	1.6	116	21	83.5	2.3	98.4

Table A2. Detrital zircon U-Pb geochronologic analyses by using LA-MC-ICP-MS analysis

Analysis	U (ppm)	U/Th	Apparent ages (Ma) $^{206}Pb^*/^{238}U$	± 2σ (Ma)	$^{207}Pb^*/^{235}U$	± 2σ (Ma)	$^{207}Pb^*/^{206}Pb^*$	± 2σ (Ma)	Preferred age ± 2σ (Ma)		conc (%)
Sample IR1-Loreto Formation											
IR1_1	86	1.61	37.4	1.0	40.0	2.6	210	110	37.4	1.0	93.5
IR1_2	108	1.63	36.2	1.0	37.8	1.4	128	60	36.2	1.0	95.8
IR1_3	450	0.42	64.2	1.6	65.7	1.6	122	21	64.2	1.6	97.7
IR1_4	168	1.60	36.9	0.9	37.8	1.3	90	56	36.9	0.9	97.6
IR1_5	1392	1.81	143.7	4.3	146.8	4.2	186	28	143.7	4.3	97.9
IR1_6	123	2.80	69.1	1.8	74.6	2.3	260	48	69.1	1.8	92.6

IR1_7	60	3.24	87.9	2.3	99.9	3.0	401	45	87.9	2.3	88.0
IR1_8	287	2.84	68.2	1.8	70.6	2.0	153	30	68.2	1.8	96.6
IR1_9	123	2.95	35.5	0.9	35.6	1.5	72	72	35.5	0.9	99.6
IR1_10	148	1.61	37.5	1.0	38.1	1.5	82	68	37.5	1.0	98.3
IR1_11	182	1.04	36.5	0.9	38.4	1.2	168	46	36.5	0.9	94.9
IR1_12	121	1.65	37.7	1.0	40.3	1.9	187	88	37.7	1.0	93.4
IR1_13	285	1.68	109.8	2.8	112.9	2.8	193	20	109.8	2.8	97.2
IR1_14	312	1.33	38.1	1.0	41.2	1.4	216	56	38.1	1.0	92.4
IR1_15	195	2.08	37.4	1.0	40.9	1.4	252	63	37.4	1.0	91.5
IR1_16	188	1.83	85.7	2.2	85.5	2.6	93	41	85.7	2.2	100.3
IR1_17	135	1.92	118.3	3.1	119.2	3.2	139	31	118.3	3.1	99.3
IR1_18	284	1.70	37.5	1.0	38.5	1.2	98	51	37.5	1.0	97.4
IR1_19	107	1.66	36.9	1.0	35.3	2.4	-10	120	36.9	1.0	104.6

Table A2. Detrital zircon U-Pb geochronologic analyses by using LA-MC-ICP-MS analysis (continued)

Analysis	U (ppm)	U/Th	Apparent ages (Ma) $^{206}Pb^*/^{238}U$	± 2σ (Ma)	$^{207}Pb^*/^{235}U$	± 2σ (Ma)	$^{207}Pb^*/^{206}Pb^*$	± 2σ (Ma)	Preferred age ± 2σ (Ma)		conc (%)
IR1_20	860	2.97	94.7	2.5	95.0	2.3	107	16	94.7	2.5	99.7
IR1_21	134	1.69	38.1	1.1	44.5	2.0	382	84	38.1	1.1	85.7
IR1_22	122	1.19	65.8	1.7	72.2	2.2	291	48	65.8	1.7	91.1
IR1_23	160	2.61	120.1	3.2	120.8	3.6	134	36	120.1	3.2	99.4
IR1_24	46	1.38	95.7	2.4	101.2	4.5	227	84	95.7	2.4	94.5
IR1_25	66	1.19	87.9	2.3	86.5	3.2	49	60	87.9	2.3	101.7
IR1_26	101	1.96	83.9	2.1	81.7	2.4	32	42	83.9	2.1	102.7
IR1_27	212	0.83	67.9	1.7	68.8	1.8	94	29	67.9	1.7	98.7
IR1_28	606	2.00	94.8	2.4	97.2	2.4	142	21	94.8	2.4	97.6
IR1_29	242	4.87	92.4	2.4	94.9	2.4	140	32	92.4	2.4	97.3
IR1_30	331	3.71	92.4	2.4	94.0	2.3	121	20	92.4	2.4	98.3
IR1_31	175	2.65	36.0	1.0	38.1	1.3	164	50	36.0	1.0	94.5
IR1_32	808	1.04	85.0	2.2	87.0	2.1	130	17	85.0	2.2	97.7
IR1_33	100	2.16	34.7	0.9	34.9	1.8	42	91	34.7	0.9	99.5
IR1_34	110	0.81	69.0	1.8	71.1	2.1	145	43	69.0	1.8	97.0
IR1_35	159	1.89	36.1	1.0	42.0	1.5	384	65	36.1	1.0	86.0
IR1_36	157	1.96	37.5	1.0	39.9	1.5	199	65	37.5	1.0	94.0
IR1_37	110	2.48	37.3	1.0	42.6	1.8	355	84	37.3	1.0	87.6
IR1_38	296	1.35	66.0	1.7	66.5	1.8	86	29	66.0	1.7	99.2
IR1_39	274	2.17	37.3	1.0	38.5	1.2	108	47	37.3	1.0	96.9
IR1_40	519	3.07	37.8	1.0	38.8	1.1	89	35	37.8	1.0	97.5
IR1_41	435	2.31	38.0	1.0	37.8	1.0	24	30	38.0	1.0	100.7
IR1_42	99	2.69	37.1	1.0	39.5	2.0	140	93	37.1	1.0	93.9
IR1_43	464	3.58	93.0	2.4	95.2	2.4	145	19	93.0	2.4	97.7
IR1_44	131	1.93	65.3	1.7	69.2	2.7	181	77	65.3	1.7	94.4
IR1_45	106	2.25	123.8	3.2	128.5	3.6	206	42	123.8	3.2	96.4
IR1_46	179	2.61	37.1	1.0	36.6	1.3	15	48	37.1	1.0	101.3
IR1_47	183	3.04	37.6	1.0	38.0	1.4	54	54	37.6	1.0	98.9
IR1_48	148	2.66	37.2	1.0	37.7	1.6	92	71	37.2	1.0	98.6
IR1_49	170	1.92	37.5	1.0	39.7	1.5	168	63	37.5	1.0	94.5
IR1_50	105	2.02	37.0	1.0	37.4	1.9	72	92	37.0	1.0	98.9

Table A2. Detrital zircon U-Pb geochronologic analyses by using LA-MC-ICP-MS analysis (continued)

Analysis	U (ppm)	U/Th	Apparent ages (Ma) $^{206}Pb^*/^{238}U$	± 2σ (Ma)	$^{207}Pb^*/^{235}U$	± 2σ (Ma)	$^{207}Pb^*/^{206}Pb^*$	± 2σ (Ma)	Preferred age ± 2σ (Ma)		conc (%)
IR1_51	141	1.74	38.2	1.0	39.3	1.6	84	72	38.2	1.0	97.3
IR1_52	327	1.77	37.7	1.0	37.9	1.1	25	37	37.7	1.0	99.6
IR1_53	495	2.01	36.3	1.0	36.4	1.0	33	24	36.3	1.0	99.8
IR1_54	676	2.10	36.7	1.0	37.4	1.0	60	23	36.7	1.0	98.2
IR1_55	201	2.44	95.5	2.5	98.5	2.5	158	26	95.5	2.5	97.0
IR1_56	502	2.88	88.7	2.3	89.9	2.2	114	19	88.7	2.3	98.7
IR1_57	108	2.04	37.4	1.0	39.7	1.9	170	94	37.4	1.0	94.2
IR1_58	781	0.55	124.5	3.3	124.8	3.0	138	17	124.5	3.3	99.8
IR1_59	773	1.54	71.6	1.9	72.4	1.8	108	16	71.6	1.9	98.8
IR1_60	211	1.42	65.0	1.7	68.2	1.9	186	34	65.0	1.7	95.3
IR1_61	230	1.79	35.8	0.9	36.1	1.3	72	64	35.8	0.9	99.3
IR1_62	200	1.77	36.2	1.0	38.4	1.8	166	93	36.2	1.0	94.2
IR1_63	881	1.35	67.7	1.7	67.8	1.7	72	17	67.7	1.7	99.8
IR1_64	188	1.88	38.0	1.0	40.2	1.5	180	58	38.0	1.0	94.5
IR1_65	100	1.36	86.2	2.2	87.6	2.5	126	39	86.2	2.2	98.4
IR1_66	155	1.59	131.0	3.5	132.9	3.5	171	32	131.0	3.5	98.6
IR1_67	479	0.83	137.1	3.5	137.7	3.2	148	15	137.1	3.5	99.5
IR1_68	217	1.49	95.8	2.5	95.7	2.7	111	33	95.8	2.5	100.1
IR1_69	121	2.01	36.9	1.0	35.5	1.7	-20	79	36.9	1.0	104.0
IR1_70	64	1.42	69.3	1.8	74.6	3.2	256	83	69.3	1.8	92.9
IR1_71	104	2.34	37.7	1.0	38.3	1.9	90	84	37.7	1.0	98.5
IR1_72	168	1.25	69.7	1.8	69.3	2.0	59	34	69.7	1.8	100.6
IR1_73	626	1.35	67.8	1.7	68.2	1.6	79	21	67.8	1.7	99.4
IR1_74	355	1.64	70.6	1.8	73.6	1.9	175	29	70.6	1.8	95.9
IR1_75	425	1.37	64.9	1.7	66.0	1.7	111	26	64.9	1.7	98.3
IR1_76	382	1.69	63.3	1.7	63.5	1.9	59	32	63.3	1.7	99.7
IR1_77	197	1.42	66.3	1.7	68.6	2.0	133	40	66.3	1.7	96.6
IR1_78	119	1.23	71.3	1.8	78.7	2.6	295	55	71.3	1.8	90.5
IR1_79	156	1.06	71.8	1.9	69.9	2.4	12	50	71.8	1.9	102.6
IR1_80	1157	2.09	67.6	1.8	68.3	1.7	98	17	67.6	1.8	98.9
IR1_81	325	2.17	37.4	1.0	40.3	1.4	197	55	37.4	1.0	92.9

Table A2. Detrital zircon U-Pb geochronologic analyses by using LA-MC-ICP-MS analysis (continued)

Analysis	U (ppm)	U/Th	Apparent ages (Ma) $^{206}Pb^*/^{238}U$	± 2σ (Ma)	$^{207}Pb^*/^{235}U$	± 2σ (Ma)	$^{207}Pb^*/^{206}Pb^*$	± 2σ (Ma)	Preferred age ± 2σ (Ma)		conc (%)
IR1_82	399	1.52	38.1	1.0	40.4	1.2	154	47	38.1	1.0	94.1
IR1_83	152	1.45	85.9	2.3	86.8	2.7	76	37	85.9	2.3	99.0
IR1_84	420	2.08	37.2	1.0	38.5	1.2	109	56	37.2	1.0	96.7
IR1_85	174	1.77	37.5	1.0	42.0	1.7	318	85	37.5	1.0	89.3

Table A2. Detrital zircon U-Pb geochronologic analyses by using LA-ICP-MS analysis

Analysis	U (ppm)	U/Th	Apparent ages (Ma) $^{206}Pb^*/^{238}U$	± 2σ (Ma)	$^{207}Pb^*/^{235}U$	± 2σ (Ma)	$^{207}Pb^*/^{206}Pb^*$	± 2σ (Ma)	Preferred age ± 2σ (Ma)		conc (%)
Sample PB1-Chorrillo Chico Formation											

PB1_38	116	0.97	53.7	4.8	49.5	4.6	170.0	120.0	53.6	4.8	108.5
PB1_42	88	0.99	59.4	3.0	61.5	4.0	210.0	110.0	59.2	3.1	96.6
PB1_16	108	0.80	61.4	4.4	76.9	5.7	610.0	120.0	60.2	4.4	79.8
PB1_12	57	1.14	65.7	4.8	68.6	6.3	300.0	150.0	65.1	4.8	95.8
PB1_62	56	0.81	73.8	6.3	182.0	15.0	1920.0	150.0	65.5	5.7	40.5
PB1_51	91	0.73	67.4	5.3	91.1	6.9	820.0	120.0	65.6	5.2	74.0
PB1_2	85	0.92	69.0	4.6	101.1	6.7	890.0	110.0	66.7	4.4	68.2
PB1_9	79	0.80	67.3	4.7	62.6	4.8	90.0	120.0	67.3	4.8	107.5
PB1_37	92	0.82	70.8	5.1	114.1	8.2	1150.0	120.0	67.6	4.9	62.1
PB1_50	75	0.96	67.8	5.0	67.3	5.7	150.0	120.0	67.7	5.0	100.7
PB1_39	92	0.79	67.8	4.8	61.7	4.7	150.0	110.0	67.8	4.8	109.9
PB1_36	77	1.20	79.5	7.2	200.0	18.0	2170.0	140.0	69.0	6.2	39.8
PB1_34	130	0.78	69.7	5.4	67.2	4.9	230.0	100.0	69.5	5.3	103.7
PB1_43	87	1.07	69.2	5.4	60.9	5.1	-10.0	110.0	69.6	5.5	113.6
PB1_1	72	0.71	73.7	6.3	99.9	8.1	820.0	130.0	71.2	6.2	73.8
PB1_63	97	0.96	77.2	6.4	139.0	10.0	1430.0	120.0	71.8	6.0	55.5
PB1_47	87	1.28	72.0	5.6	65.0	5.3	140.0	110.0	72.1	5.6	110.8
PB1_40	138	0.95	73.4	5.9	68.4	5.5	150.0	100.0	73.4	6.0	107.3
PB1_48	192	0.83	75.3	6.5	67.0	5.3	120.0	100.0	74.8	6.4	112.4
PB1_60	107	0.90	74.6	6.6	70.0	5.8	110.0	110.0	74.9	6.4	106.6
PB1_49	89	1.07	76.0	6.7	71.9	6.6	180.0	130.0	75.9	7.0	105.7

Table A2. Detrital zircon U-Pb geochronologic analyses by using LA-ICP-MS analysis (continued)

Analysis	U (ppm)	U/Th	Apparent ages (Ma) $^{206}Pb^*/^{238}U$	± 2σ (Ma)	$^{207}Pb^*/^{235}U$	± 2σ (Ma)	$^{207}Pb^*/^{206}Pb^*$	± 2σ (Ma)	Preferred age ± 2σ (Ma)		conc (%)
PB1_28	109	1.28	77.9	6.7	72.5	6.1	210.0	120.0	77.7	7.0	107.4
PB1_25	116	0.89	78.3	6.9	73.1	6.1	210.0	120.0	78.2	7.0	107.1
PB1_54	111	1.00	79.0	7.3	69.5	6.0	170.0	120.0	79.1	7.6	113.7
PB1_22	370	0.43	79.4	9.6	76.6	7.6	120.0	120.0	79.1	9.5	103.7
PB1_61	81	1.14	78.9	8.4	69.4	7.1	150.0	150.0	79.2	8.3	113.7
PB1_52	132	0.80	79.5	7.1	75.1	6.3	210.0	110.0	79.6	7.0	105.9
PB1_44	225	0.61	81.7	7.4	75.9	6.3	160.0	100.0	81.5	7.6	107.6
PB1_56	88	0.92	81.7	7.4	73.3	6.9	140.0	130.0	81.6	7.6	111.5
PB1_46	84	1.14	82.8	8.8	88.5	9.1	470.0	150.0	81.7	8.8	93.6
PB1_18	107	0.80	82.3	7.7	72.3	6.5	230.0	130.0	81.8	7.6	113.8
PB1_19	118	0.81	82.5	7.8	74.4	6.2	210.0	120.0	82.2	7.6	110.9
PB1_6	63	1.43	82.8	8.2	76.7	7.7	180.0	160.0	82.8	8.3	108.0
PB1_41	61	1.61	83.6	7.9	73.9	7.3	90.0	150.0	83.4	7.6	113.1
PB1_45	40	1.29	83.8	8.6	68.6	9.5	190.0	190.0	83.8	8.9	122.2
PB1_8	68	1.21	84.1	8.0	76.8	7.7	230.0	150.0	83.9	8.2	109.5
PB1_35	99	1.11	84.7	8.1	72.9	6.6	210.0	120.0	84.6	8.2	116.2
PB1_4	72	1.20	86.1	8.0	81.9	7.5	370.0	140.0	85.3	8.2	105.1
PB1_27	112	0.80	86.0	11.0	70.0	8.9	30.0	180.0	86.0	11.5	122.9
PB1_24	121	0.90	86.9	8.2	69.3	6.3	50.0	120.0	87.1	8.3	125.4
PB1_55	51	1.21	90.0	12.0	99.0	14.0	530.0	220.0	88.0	11.8	90.9
PB1_3	78	1.22	89.0	8.6	76.0	7.7	50.0	140.0	88.9	8.3	117.1
PB1_29	123	0.80	89.8	8.5	77.6	6.7	200.0	130.0	89.0	8.2	115.7
PB1_10	117	0.68	93.6	9.6	127.0	11.0	1020.0	130.0	89.4	9.1	73.7
PB1_58	73	0.96	89.0	10.0	77.3	8.7	190.0	170.0	89.8	10.2	115.1

PB1_31	108	1.16	91.0	8.6	75.3	6.9	110.0	130.0	90.7	8.9	120.8
PB1_32	127	1.02	92.3	9.1	78.6	7.2	130.0	130.0	92.1	8.9	117.4
PB1_20	93	0.96	94.5	9.1	100.6	9.0	600.0	140.0	92.9	8.7	93.9
PB1_30	76	1.06	93.0	10.0	77.5	8.8	130.0	160.0	93.1	10.2	120.0
PB1_5	106	1.10	99.0	17.0	121.0	19.0	1010.0	280.0	93.9	16.4	81.8
PB1_57	117	0.91	95.0	10.0	78.0	8.0	140.0	140.0	94.4	10.7	121.8
PB1_17	58	0.98	98.0	12.0	77.6	9.6	320.0	190.0	97.3	12.0	126.3

Table A2. Detrital zircon U-Pb geochronologic analyses by using LA-ICP-MS analysis (continued)

Analysis	U (ppm)	U/Th	Apparent ages (Ma) $^{206}Pb^*/^{238}U$	± 2σ (Ma)	$^{207}Pb^*/^{235}U$	± 2σ (Ma)	$^{207}Pb^*/^{206}Pb^*$	± 2σ (Ma)	Preferred age ± 2σ (Ma)		conc (%)
PB1_13	130	0.93	98.0	10.0	78.9	7.8	110.0	130.0	97.7	10.7	124.2
PB1_59	78	1.00	101.0	13.0	121.0	15.0	720.0	180.0	98.7	13.0	83.5
PB1_11	109	1.09	99.1	9.9	81.8	7.8	140.0	130.0	99.1	10.1	121.1
PB1_26	80	1.21	100.0	12.0	88.0	10.0	210.0	170.0	99.3	11.4	113.6
PB1_7	99	0.98	99.0	10.0	78.4	7.9	140.0	140.0	99.7	10.1	126.3
PB1_53	81	0.95	103.0	13.0	102.0	12.0	330.0	160.0	102.7	12.6	101.0
PB1_33	80	1.38	110.0	12.0	87.7	9.2	190.0	160.0	110.7	12.0	125.4
PB1_23	119	0.93	112.0	15.0	100.0	12.0	310.0	180.0	111.3	15.0	112.0
PB1_21	92	0.95	120.0	15.0	88.0	10.0	90.0	160.0	119.8	14.5	136.4
PB1_14	88	0.96	121.0	15.0	95.0	11.0	110.0	170.0	120.8	15.1	127.4
PB1_15	71	1.27	131.0	18.0	99.0	15.0	260.0	210.0	131.2	18.2	132.3

Table A2. Detrital zircon U-Pb geochronologic analyses by using LA-MC-ICP-MS analysis

Analysis	U (ppm)	U/Th	Apparent ages (Ma) $^{206}Pb^*/^{238}U$	± 2σ (Ma)	$^{207}Pb^*/^{235}U$	± 2σ (Ma)	$^{207}Pb^*/^{206}Pb^*$	± 2σ (Ma)	Preferred age ± 2σ (Ma)		conc (%)
Sample RB1-Chorrillo Chico Formation											
B531_53	113	0.43	64.4	1.3	67.9	1.8	161.0	41.0	64.4	1.3	94.9
B531_44	197	0.40	64.7	1.4	66.1	1.7	141.0	33.0	64.7	1.4	97.8
B531_43	115	0.45	64.9	1.4	67.9	1.9	198.0	47.0	64.9	1.4	95.6
B531_36	438	0.96	65.0	1.4	65.1	1.6	82.0	22.0	65.0	1.4	99.8
B531_35	140	0.40	65.2	1.4	68.7	1.9	183.0	44.0	65.2	1.4	94.9
B531_49	105	0.48	65.5	1.5	67.2	1.9	128.0	46.0	65.5	1.5	97.5
B531_27	139	0.36	65.6	1.4	68.5	1.9	139.0	36.0	65.6	1.4	95.8
B531_48	397	0.67	65.8	1.4	67.7	1.6	141.0	23.0	65.8	1.4	97.2
B531_41	93	0.41	66.0	1.4	67.4	2.2	132.0	48.0	66.0	1.4	97.9
B531_47	58	0.39	66.3	1.4	74.5	2.5	359.0	59.0	66.3	1.4	89.0
B531_33	96	0.41	66.6	1.4	71.8	1.9	233.0	36.0	66.6	1.4	92.8
B531_31	108	0.53	66.9	1.4	73.0	2.2	273.0	52.0	66.9	1.4	91.7
B531_16	259	0.47	67.0	1.4	68.1	1.7	103.0	31.0	67.0	1.4	98.3
B531_22	166	0.44	67.1	1.4	68.6	1.9	122.0	47.0	67.1	1.4	97.9
B531_42	261	0.60	67.2	1.5	67.8	1.8	96.0	31.0	67.2	1.5	99.1
B531_30	124	0.43	67.2	1.4	69.7	1.9	167.0	45.0	67.2	1.4	96.4
B531_28	636	1.12	67.3	1.4	67.6	1.5	78.0	17.0	67.3	1.4	99.6
B531_39	101	0.45	67.8	1.4	70.8	2.0	186.0	45.0	67.8	1.4	95.7
B531_24	91	0.49	68.1	1.5	68.5	2.2	97.0	53.0	68.1	1.5	99.3
B531_23	189	0.68	68.5	1.5	70.2	1.6	123.0	29.0	68.5	1.5	97.6
B531_20	117	0.46	68.6	1.4	71.3	2.1	175.0	50.0	68.6	1.4	96.2

B531_34	106	0.46	68.6	1.4	71.6	2.0	167.0	35.0	68.6	1.4	95.9

Table A2. Detrital zircon U-Pb geochronologic analyses by using LA-MC-ICP-MS analysis (continued)

Analysis	U (ppm)	U/Th	Apparent ages (Ma) $^{206}Pb^*/^{238}U$	± 2σ (Ma)	$^{207}Pb^*/^{235}U$	± 2σ (Ma)	$^{207}Pb^*/^{206}Pb^*$	± 2σ (Ma)	Preferred age ± 2σ (Ma)		conc (%)
B531_26	71	0.45	69.2	1.5	73.5	2.4	222.0	56.0	69.2	1.5	94.1
B531_21	436	1.07	69.5	1.5	70.4	1.8	121.0	21.0	69.5	1.5	98.8
B531_51	597	0.60	74.1	1.6	76.1	1.8	133.0	25.0	74.1	1.6	97.3
B531_15	669	0.71	74.7	1.6	75.0	1.7	94.0	17.0	74.7	1.6	99.7
B531_32	802	0.59	74.9	1.5	75.0	1.7	68.0	23.0	74.9	1.5	99.8
B531_9	723	0.61	75.7	1.6	76.7	1.7	107.0	17.0	75.7	1.6	98.7
B531_4	1061	0.47	76.4	1.6	77.1	1.7	106.0	17.0	76.4	1.6	99.1
B531_1	342	0.55	76.7	1.6	77.9	1.8	134.0	22.0	76.7	1.6	98.5
B531_45	745	0.51	76.9	1.6	77.0	1.7	84.0	18.0	76.9	1.6	99.8
B531_6	825	0.72	77.4	1.6	77.8	1.8	101.0	17.0	77.4	1.6	99.5
B531_0	1043	0.51	77.6	1.6	77.9	1.8	95.5	11.0	77.6	1.6	99.5
B531_3	359	0.67	77.6	1.7	78.5	1.8	142.0	18.0	77.6	1.7	98.8
B531_29	426	0.53	78.0	1.6	78.9	1.8	113.0	21.0	78.0	1.6	98.9
B531_17	156	0.45	78.8	1.7	79.7	2.2	114.0	35.0	78.8	1.7	98.9
B531_38	405	0.48	78.9	1.6	80.6	1.9	145.0	27.0	78.9	1.6	97.9
B531_7	427	0.56	80.1	1.7	80.8	2.0	105.0	20.0	80.1	1.7	99.2
B531_46	234	0.36	86.3	1.8	92.0	2.5	240.0	40.0	86.3	1.8	93.8
B531_5	1432	1.65	91.2	1.9	91.8	2.0	113.8	12.0	91.2	1.9	99.3
B531_37	1571	0.68	93.9	2.0	94.7	2.0	104.0	13.0	93.9	2.0	99.2
B531_19	284	0.70	94.9	1.9	94.9	2.3	106.0	28.0	94.9	1.9	100.0
B531_14	624	0.49	94.9	1.9	95.2	2.1	105.0	14.0	94.9	1.9	99.7
B531_11	1484	1.11	95.1	2.0	95.8	2.1	121.0	12.0	95.1	2.0	99.3
B531_50	541	0.61	95.2	1.9	96.2	2.1	113.0	18.0	95.2	1.9	99.0
B531_18	285	0.66	96.7	2.0	96.6	2.3	115.0	25.0	96.7	2.0	100.1
B531_8	376	0.28	97.8	2.0	99.8	2.4	144.0	23.0	97.8	2.0	98.0
B531_13	147	0.47	108.0	2.2	110.2	2.8	166.0	30.0	108.0	2.2	98.0
B531_12	213	0.34	109.3	2.2	112.1	2.8	172.0	30.0	109.3	2.2	97.5
B531_40	563	0.27	113.1	2.3	113.1	2.4	116.0	15.0	113.1	2.3	100.1
B531_25	152	0.58	113.8	2.4	114.8	3.0	124.0	31.0	113.8	2.4	99.1
B531_52	124	0.73	134.7	2.9	145.5	3.5	319.0	34.0	134.7	2.9	92.6
B531_10	139	0.59	528.3	11.0	526.3	9.8	533.0	13.0	528.3	11.0	100.4

Table A2. Detrital zircon U-Pb geochronologic analyses by using LA-MC-ICP-MS analysis (continued)

Analysis	U (ppm)	U/Th	Apparent ages (Ma) $^{206}Pb^*/^{238}U$	± 2σ (Ma)	$^{207}Pb^*/^{235}U$	± 2σ (Ma)	$^{207}Pb^*/^{206}Pb^*$	± 2σ (Ma)	Preferred age ± 2σ (Ma)		conc (%)
B531_2	25	0.02	655.3	13.0	647.2	12.0	643.0	17.0	655.3	13.0	101.3

Table A2. Detrital zircon U-Pb geochronologic analyses by using LA-ICP-MS analysis

Analysis	U (ppm)	U/Th	Apparent ages (Ma) $^{206}Pb^*/^{238}U$	± 2σ (Ma)	$^{207}Pb^*/^{235}U$	± 2σ (Ma)	$^{207}Pb^*/^{206}Pb^*$	± 2σ (Ma)	Preferred age ± 2σ (Ma)		conc (%)
Sample CC1-Dorotea Formation											
CC1_34	75	1.19	44.9	1.6	54.7	3.4	420.0	110.0	44.3	1.6	82.1

CC1_48	276	0.73	78.1	2.6	79.0	3.4	79.0	61.0	78.1	2.6	98.9
CC1_31	99	1.01	88.2	1.9	87.7	3.9	84.0	75.0	88.3	1.9	100.6
CC1_26	221	1.13	89.0	2.0	91.3	3.3	179.0	58.0	88.8	2.0	97.4
CC1_11	286	0.80	91.9	2.6	92.5	3.6	99.0	53.0	91.9	2.7	99.4
CC1_29	94	0.56	94.1	2.0	97.3	4.1	202.0	67.0	93.8	2.0	96.7
CC1_49	183	1.55	95.3	2.2	94.3	3.7	129.0	61.0	95.2	2.2	101.1
CC1_40	132	1.04	96.5	2.1	95.6	3.7	117.0	60.0	96.4	2.2	100.9
CC1_37	44	0.96	96.6	2.2	94.1	5.3	103.0	94.0	96.6	2.3	102.7
CC1_42	50	1.47	97.0	2.6	100.3	5.4	179.0	97.0	96.8	2.6	96.7
CC1_22	155	0.69	97.2	2.3	94.7	3.7	97.0	60.0	97.2	2.3	102.6
CC1_46	69	0.99	98.6	2.6	97.9	4.6	166.0	77.0	98.5	2.6	100.7
CC1_39	513	0.54	99.1	2.2	107.4	3.9	278.0	51.0	98.7	2.2	92.3
CC1_24	87	1.19	100.6	2.3	103.6	4.3	200.0	67.0	100.3	2.2	97.1

Table A2. Detrital zircon U-Pb geochronologic analyses by using LA-ICP-MS analysis (continued)

Analysis	U (ppm)	U/Th	Apparent ages (Ma) $^{206}Pb^*/^{238}U$	± 2σ (Ma)	$^{207}Pb^*/^{235}U$	± 2σ (Ma)	$^{207}Pb^*/^{206}Pb^*$	± 2σ (Ma)	Preferred age ± 2σ (Ma)		conc (%)
CC1_45	40	0.98	102.4	2.5	100.6	5.9	88.0	98.0	102.5	2.6	101.8
CC1_1	112	0.72	107.0	2.2	105.8	4.0	149.0	63.0	106.8	2.2	101.1
CC1_25	131	1.52	107.8	2.7	115.5	4.6	200.0	66.0	107.3	2.7	93.4
CC1_18	207	1.74	108.7	2.7	108.0	4.1	122.0	57.0	108.8	2.7	100.6
CC1_19	179	1.33	111.7	3.3	116.6	4.4	169.0	52.0	111.5	3.2	95.9
CC1_9	283	2.14	112.2	2.4	111.9	3.9	137.0	51.0	112.1	2.5	100.2
CC1_30	134	2.06	113.5	3.0	111.4	4.6	39.0	61.0	113.7	3.1	101.9
CC1_44	101	0.98	122.6	3.3	123.4	5.1	168.0	65.0	122.5	3.3	99.4
CC1_36	81	1.37	128.6	4.7	147.0	7.5	460.0	95.0	127.3	4.7	87.5
CC1_8	130	1.17	130.8	3.3	139.4	5.3	287.0	61.0	130.1	3.3	93.8
CC1_20	384	0.99	144.2	3.1	142.9	4.7	164.0	50.0	144.2	3.1	101.0
CC1_41	169	1.17	148.5	3.8	148.2	5.3	189.0	53.0	148.3	3.8	100.2
CC1_38	257	0.83	153.1	3.3	158.3	5.5	211.0	53.0	152.8	3.4	96.7
CC1_3	1528	1.08	155.6	3.6	158.6	5.2	159.0	46.0	155.6	3.6	98.1
CC1_5	1395	1.57	157.7	3.0	159.0	4.8	177.0	38.0	157.6	3.0	99.2
CC1_2	256	0.90	160.8	3.7	161.3	5.4	206.0	56.0	160.6	3.8	99.7
CC1_14	416	1.28	162.6	3.9	164.8	5.7	216.0	58.0	162.3	3.9	98.7
CC1_6	127	0.64	277.2	6.5	276.3	8.9	314.0	55.0	276.8	6.9	100.3
CC1_27	36	0.88	282.0	6.0	290.4	11.0	287.0	72.0	281.2	6.1	97.1
CC1_33	149	1.09	301.9	6.9	307.4	9.6	320.0	53.0	301.7	6.8	98.2
CC1_43	34	0.68	305.0	7.2	298.2	11.0	295.0	69.0	304.8	7.5	102.3
CC1_12	143	1.06	321.0	9.4	343.4	12.0	473.0	58.0	319.0	9.3	93.5
CC1_16	71	0.68	346.8	7.8	336.0	11.0	291.0	58.0	347.0	8.1	103.2
CC1_13	550	2.82	384.0	7.8	399.4	12.0	464.0	51.0	382.7	8.0	96.2
CC1_7	147	0.94	480.2	11.0	481.1	14.0	466.0	41.0	480.1	10.9	99.8
CC1_35	137	1.19	483.8	11.0	488.8	14.0	491.0	57.0	483.5	11.0	99.0
CC1_32	126	2.38	511.3	11.0	529.0	15.0	571.0	54.0	509.7	11.5	96.7
CC1_47	168	1.33	532.2	10.0	533.9	15.0	522.0	50.0	532.0	10.3	99.7
CC1_4	109	0.77	538.1	16.0	538.1	16.0	489.0	54.0	538.4	16.3	100.0
CC1_50	132	22.00	1018.8	23.0	1023.9	26.0	1058.0	56.0	1016.4	24.2	99.5
CC1_17	103	1.24	1473.8	29.0	1452.0	26.0	1439.0	46.0	1476.3	31.3	101.5

Table A2. Detrital zircon U-Pb geochronologic analyses by using LA-ICP-MS analysis (continued)

Analysis	U (ppm)	U/Th	Apparent ages (Ma) $^{206}Pb^*/^{238}U$	± 2σ (Ma)	$^{207}Pb^*/^{235}U$	± 2σ (Ma)	$^{207}Pb^*/^{206}Pb^*$	± 2σ (Ma)	Preferred age ± 2σ (Ma)		conc (%)
CC1_28	48	0.69	2676.0	61.0	2708.8	37.0	2658.0	43.0	2658.0	43.0	98.8

* indicates radiogenic Pb (corrected for common Pb).

All errors are reported at the 2σ level of uncertainty

ANEXO B1

COMPILACIÓN FORAMINÍFEROS BENTÓNICOS CON EDADES Y RANGOS BATIMÉTRICOS

Table B1. Compilation of benthic and planktonic foraminifera recorded in the Cenozoic formations of the Magallanes-Austral Basin, showing their first appearance date (FAD), last appearance date (LAD) and bathymetric ranges.

Benthic/Planktonic Foraminifera	Formation	Min. Depth	Max. Depth	FAD (Ma)	LAD (Ma)
Globigerina triloculinoides	Agua Fresca	101	964	48.6-55.8	
Globigerina aquiensis		30	625		
Globigerina spiralis		95	949		
Globorotalia compressa		92	963		
Globorotalia cf. *quadrata*		101	102		
Acarinina triplex Subbotina		182	801		
Globorotalia membranacea (Ehrenberg)		144	551		
Elphidium		50	203		
Allomorphina conica		122	122		
Dorothia principensis		385	385		
Pseudohastigerina wilcoxensis			1186		
Deflandrea antarctica		17	620		
Alterbidinium distinctum		33	525		
Achilleodinium biformoides		195	741		
Globanomalina australiformis			967	55.5	44.2
Acarinina esnaensis		50	409		51
Cyclammina	Chorrillo Chico		4097	47.8-56	
Allomorphina		200	938		
Trochammina		50	4706		
Ammobaculites			4096		
Haplophragmoides			4097		
Alabamina wilcoxensis		65	385		
Deflandrea cygniformis		162	162		
Eisenackia crassitabulata			430		
Palaeocystodinium golzowense		47	1034		
Palaeoperidinium pyrophorum		433	659		

Spiniferites membranaceous			535		
Spinidinium macmurdoense		17	919		
Spiroplectammina spectabilis		28	1087		56
Globigerinatheka index	Tres Brazos		1025	43.7	34.3
Acarinina sp.		181?	1139	56	33.9
Globigerina triloculinoides		101	964		
Elphidium patagonicum		103	103		
Acarinina bullbrooki	Leña Dura	181?	1132		41.8
Plectina elongata		181	331		
Spiroplectammina			1850		
Cibicides	Los Ciervos (Loreto)	31	3062		
Kolesnikovella severini		182	332		
Virgulina			3354		
Marginulina			2182		
Elphidium		50	203	48.6-55.8	

ANEXO C1

PUBLICACIÓN COMO CO-AUTOR: TECTONOPHYSICS

Tectonophysics 695 (2017) 76–99

Contents lists available at ScienceDirect

Tectonophysics

journal homepage: www.elsevier.com/locate/tecto

Tectonic events reflected by palaeocurrents, zircon geochronology, and palaeobotany in the Sierra Baguales of Chilean Patagonia

Nestor M. Gutiérrez [a], Jacobus P. Le Roux [a,b,*], Ana Vásquez [a,c], Catalina Carreño [a,d], Viviana Pedroza [a], José Araos [a,e], José Luis Oyarzún [f], J. Pablo Pino [g], Huber A. Rivera [a,b], L.F. Hinojosa [g,h]

[a] Departamento de Geología, FCFM, Universidad de Chile, Plaza Ercilla 803, Santiago, Chile
[b] Centro de Excelencia en Geotermia de los Andes, Plaza Ercilla 803, Santiago, Chile
[c] FCC Servicios Ciudadanos, Av. Vitacura 2771, Of. 403, Santiago, Chile
[d] Codelco, Calama, Chile
[e] Departamento de Geografía, Facultad de Cs. Sociales, Universidad Alberto Hurtado, Cienfuegos 41, Santiago, Chile
[f] Miraflores 863, Puerto Natales, Chile
[g] Instituto de Ecología y Biodiversidad (IEB), Santiago, Chile
[h] Departamento de Ciencias Ecológicas, Universidad de Chile, Ñuñoa, Santiago, Chile

ARTICLE INFO

Article history:
Received 23 August 2016
Received in revised form 6 December 2016
Accepted 9 December 2016
Available online 13 December 2016

Keywords:
Andean tectonics
Patagonian Transgression
Zircon provenance
Gondwana reconstruction
Antarctic Peninsula

ABSTRACT

The Sierra Baguales, situated north of the Torres Del Paine National Park in the Magallanes region of southern Chile, shows a well-exposed stratigraphic sequence ranging from the Late Cretaceous to late Pliocene, which presents a unique opportunity to study the evolution of sedimentological styles and trends, palaeoclimate changes, and tectonic events during this period. The depositional environment changed from a continental slope and shelf during the Cenomanian-Campanian (Tres Pasos Formation) to deltaic between the Campanian-Maastrichtian (Dorotea Formation) and estuarine in the Lutetian-Bartonian (Man Aike Formation). During the Rupelian, a continental environment with meandering rivers and overbank marshes was established (Río Leona Formation). This area was flooded in the early Burdigalian (Estancia 25 de Mayo Formation) during the Patagonian Transgression, but emerged again during the late Burdigalian (Santa Cruz Formation). Measured palaeocurrent directions in this Mesozoic-Cenozoic succession indicate source areas situated between the northeast and east-southeast during the Late Cretaceous, east-southeast during the middle Eocene, and southwest during the early Oligocene to early Miocene. This is confirmed by detrital zircon age populations in the different units, which can be linked to probable sources of similar ages in these areas. The east-southeastern provenance is here identified as the Antarctic Peninsula or its northeastern extension, which is postulated to have been attached to Fuegian Patagonia during the Eocene. The southwestern and western sources were exhumed during gradual uplift of the Southern Patagonian Andes, coinciding with a change from marine to continental conditions in the Magallanes-Austral Basin, as well as a decrease in mean annual temperature and precipitation indicated by fossil leaves in the Río Leona Formation. The rain shadow to the east of the Andes thus started to develop here during the late Eocene-early Oligocene (~34 Ma), long before the "Quechua Phase" of Andean tectonics (19–18 Ma) that is generally invoked for its evolution at lower latitudes.

1. Introduction

The Southern Patagonian Andes resulted from collision of the Nazca Plate with southernmost South America, which was manifested in various pulses of uplift during the Late Cretaceous, Eocene and late Miocene (Ramos and Kay, 1992; Ramos, 2005). Such changes in the source topography can have important effects on hydrodynamic conditions and sedimentation styles within the adjoining depocenters (Ruddiman et al., 1997; Bossi et al., 2000), which in this case are represented by the Magallanes-Austral Basin (Fig. 1A).

The link between Andean tectonics and the sedimentology of Cenozoic successions in the Magallanes-Austral Basin has only been partially investigated to date. Palaeocurrent measurements in the Última Esperanza Province of Patagonia have been restricted mostly to the Upper Cretaceous Cerro Toro and Dorotea Formations (Scott, 1966; Fildani and Hessler, 2005; Crane and Lowe, 2008; Romans et al., 2010; Schwartz and Graham, 2015), the middle – upper Eocene Man Aike Formation (Le Roux et al., 2010), and the lower Miocene Santa Cruz Formation (Bostelmann et al., 2013). Similarly, relatively few zircon ages have been published (Bernhardt, 2011; Fosdick et al., 2011, 2015a, 2015b;

* Corresponding author at: Departamento de Geología, FCFM, Universidad de Chile, Plaza Ercilla 803, Santiago, Chile.

http://dx.doi.org/10.1016/j.tecto.2016.12.014
0040-1951/

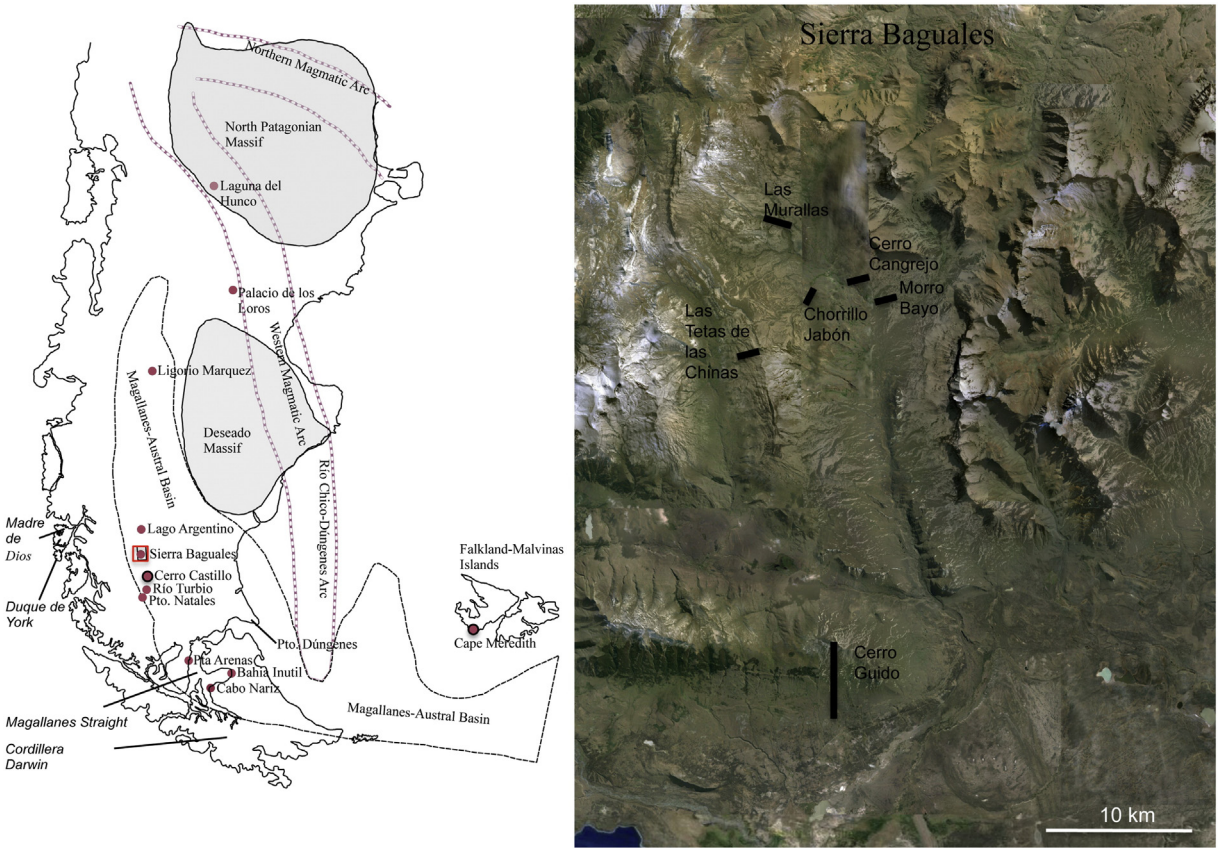

Fig. 1. Locality map of South America and the Sierra Baguales showing tectonic elements and Tertiary fossil leaf localities.

Bostelmann et al., 2013; Schwartz et al., 2016, and references therein), and only one provenance study based on zircon populations was carried out for the post-Cretaceous formations in the southernmost part of the basin (Barbeau et al., 2009). A comprehensive provenance study based on zircon populations has therefore been lacking for the post-Cretaceous formations. As a result, most previous authors (e.g., Bernhardt et al., 2008; Hubbard et al., 2010; Cuitiño, 2011; Schwartz and Graham, 2015) considered the provenance areas of the Magallanes-Austral Basin to have been located to the north, west, and southwest (Barbeau et al., 2009; Zahid and Barbeau, 2010) thus ignoring the existence of possible sources to the east.

In the Sierra Baguales, located about 100 km north of Puerto Natales (Fig. 1A), the stratigraphic succession includes all the formations mentioned above as well as the Rupelian Estancia 25 de Mayo Formation, but with the exception of the Cerro Toro Formation. In spite of previous studies in this and surrounding areas (Feruglio, 1938; Piatnitzky, 1938; Cecioni, 1957; Hoffstetter et al., 1957; Furque, 1973; Malumián, 1990; Marenssi et al., 2000, 2002, 2005; Le Roux et al., 2010; Malumián and Nañez, 2011; Cuitiño et al., 2012; Bostelmann et al., 2013), there has been no consensus about the geographic distribution of the different stratigraphic units and their contact relationships. For the Sierra Baguales, in fact, the most detailed geological map presently existing is at a scale of 1:100,000, showing obsolete nomenclature such as the "Río Bandurrias", "Calafate" and "Las Flores" Formations (Muñoz, 1981). Here we present a new geological map at a scale of 1:10,000 (Fig. 2), updating the nomenclature according to international stratigraphic principles and correcting the spatial distribution of the different stratigraphic units. However, our main objective has been to determine the link between sedimentation in the Magallanes-Austral Basin and its tectonic context. With this in mind, we investigated the depositional environments of the different units and their palaeocurrent patterns, backed up by a study of zircon age populations. Six new detrital zircon U-Pb ages are presented, of which three are from the Dorotea Formation, one from the Man Aike Formation, and two from the Río Leona Formation. Bearing in mind the well-established relationship between tectonics and local climate, we also carried out a palaeobotanical analysis based on fossils leaves from the Río Leona Formation, comparing these results with those of similar studies on older successions in Patagonia.

2. Methodology

Field work in the Sierra Baguales consisted of geological mapping, the measurement of stratigraphic columns and palaeocurrent directions, sampling for petrographic work and detrital zircon dating, and the collection of fossil leaves for palaeobotanical and palaeoclimatic studies.

Geological mapping of the Sierra Baguales was carried out on a scale of 1:10,000 between Cerro Cono in the north, Cerro Ciudadela and the Chilean-Argentinean border in the east, Cerro Guido in the south, and the Río Las Chinas in the west (Fig. 2).

Seven stratigraphic columns (some composite) were measured at 10 different localities (Fig. 1B). In the Tres Pasos Formation, a 380 m thick composite section was surveyed at Cerro Guido and Estancia Las Chinas. Towards the west, at Las Tetas de las Chinas, a 200 m thick profile was surveyed in the Dorotea Formation. The stratigraphy of the Man Aike Formation was described in 3 different sections comprising its basal, middle and upper parts, respectively. The basal section, measured in the vicinity of Las Tetas de las Chinas, has a thickness of 40 m, while the middle section comprised 240 m measured by Le Roux et al. (2010) on Estancia 3R, which was correlated with the section described by Ugalde (2014) and Cecioni (1957) in the sector Las Flores. The upper part has a thickness of 50 m measured at Chorrillo Jabón. In the Río Leona Formation, two 115 m thick profiles were surveyed. The basal

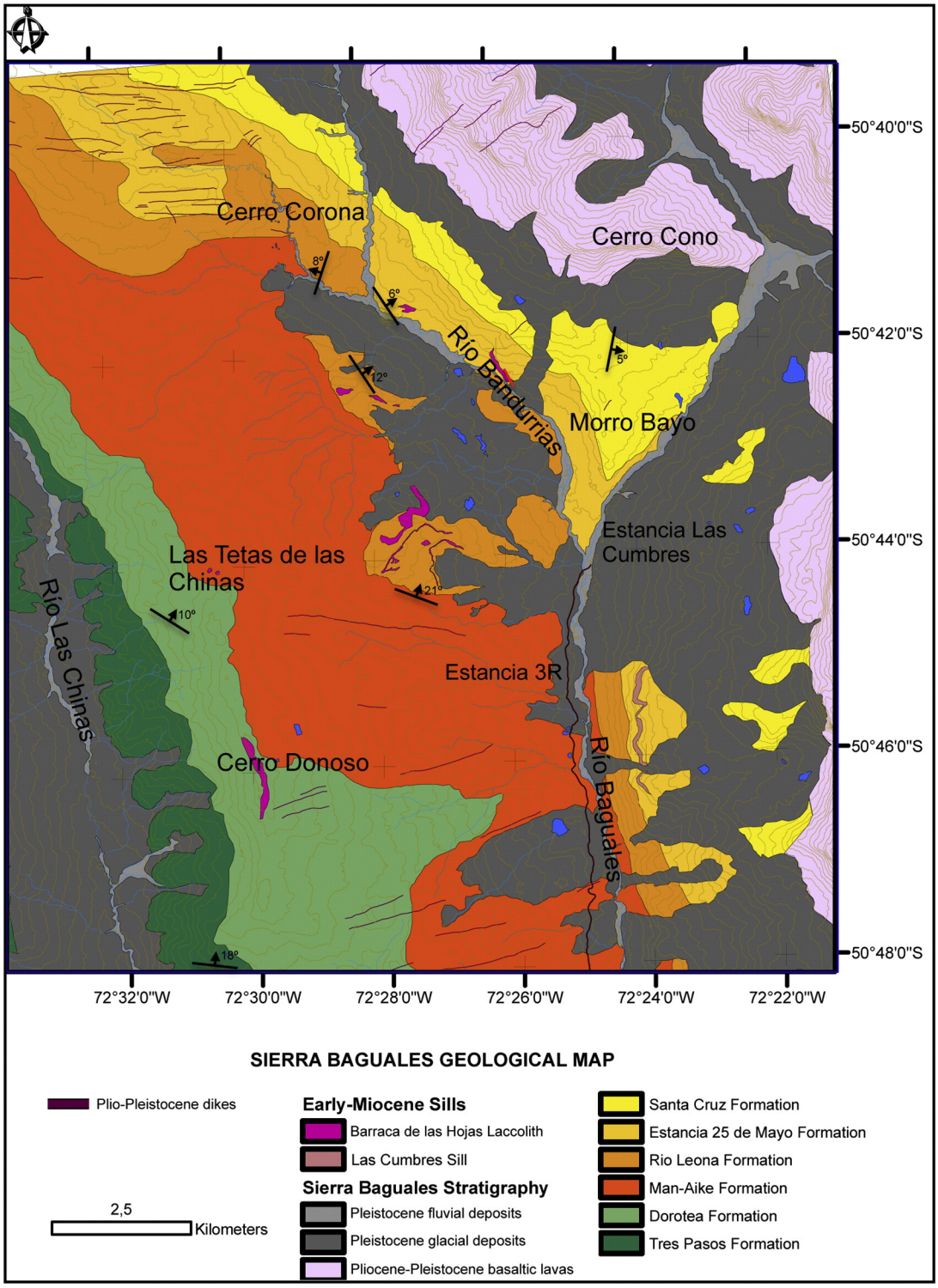

Fig. 2. Geological map of the Sierra Baguales.

part of this formation, which conformably overlies the Man Aike Formation in this area, was measured in the sectors Barranca de las Hojas and Chorrillo Jabón, whereas the upper part was measured at Las Murallas west of the Bandurrias River (Fig. 2). Two stratigraphic columns were also measured in the Estancia 25 de Mayo Formation, the first at the locality of Las Murallas and the second at Cerro Cangrejo. The profile of the Santa Cruz Formation at Cerro Cono, measured by the first four authors of this paper and published in Bostelmann et al. (2013), was included as part of the data base.

A total of 192 palaeocurrent directions were measured, including planar and trough cross-lamination, streaming and parting lineation, rib-and-furrow structures, ripple marks, and the elongation of nodules and concretions where such structures showed a preferred orientation at any particular locality. The growth of concretions is controlled by the grain orientation of their host beds and like streaming and parting lineation do not yield vectors, but can be used in conjunction with other associated structures such as cross-bedding to find the palaeocurrent trends. The recorded directions were distributed as

follows: 55 in the Dorotea Formation, 9 in the Man Aike Formation, 18 in the Río Leona Formation, 37 in the Estancia 25 de Mayo Formation, and 73 in the Santa Cruz Formation. Although the beds in this particular area are generally sub-horizontal, tilt corrections were carried out to obtain the original palaeocurrent directions using the methodology of Le Roux (1991). These were further analyzed by directional statistics (Le Roux, 1992, 1994), to obtain the vector mean azimuth, magnitude, and channel sinuosity of each data set. In the Tres Pasos and Estancia 25 de Mayo Formations no measurable directions were encountered. However, published palaeocurrent data from the Estancia 25 de Mayo Formation at Lago Argentino (Cuitiño, 2011) were also incorporated into this data set.

Eight samples from the Sierra Baguales succession were selected for detrital zircon dating. The first of these was taken from the Dorotea Formation close to its basal contact with the Tres Pasos Formation near Cerro Guido (Fig. 1B), whereas the second and third are from the upper part of the Dorotea Formation at Las Tetas de las Chinas. One sample was dated from near the top of the overlying Man Aike Formation at Chorrillo Jabón (Fig. 1B). For the Río Leona Formation, two samples were dated, one from Chorrillo Jabón close to its basal contact with the Man Aike Formation, and the other from Cerro Ciudadela, where it was previously attributed to the "Las Flores Formation" and correlated with the Man Aike Formation (Ugalde, 2014). These 6 samples were analyzed in the Mass Spectrometry Laboratory of the Andean Geothermal Centre of Excellence (CEGA) at the University of Chile. Two other samples, previously dated at the Australian National University in Canberra (Bostelmann et al., 2012) were collected from near the base and top of the Santa Cruz Formation, respectively.

More than 3700 fossil leaves recovered from the Río Leona Formation were identified, classified, and subjected to multi- and univariate analysis to determine temperature and precipitation conditions as well as their morphospecies diversity. Palaeoclimatic analysis was performed using the models and datasets of Hinojosa and collaborators (Hinojosa, 2005; Hinojosa et al., 2006, 2011).

3. Geological setting

The Rocas Verdes Basin, a predecessor of the Magallanes-Austral Basin, developed as a backarc or marginal basin during a Middle to Late Jurassic extensional episode associated with the initial breakup of Gondwanaland (Dalziel et al., 1974; Gust et al., 1985; Biddle et al., 1986; Pankhurst et al., 2000; Calderón et al., 2007). Inversion converted its eastern part into a foreland basin and caused flexural loading, thus creating the north-south orientated Magallanes-Austral Basin (Natland et al., 1974; Dalziel, 1986).

The Sierra Baguales represents the region in the Magallanes-Austral Basin with the most complete, uninterrupted Mesozoic-Cenozoic stratigraphic succession, reaching a total approximate thickness of 1300 m. It includes the Tres Pasos and Dorotea Formations, both of Late Cretaceous age, as well as the Man Aike Formation (middle to late Eocene), Río Leona Formation (early Oligocene), Estancia 25 de Mayo Formation (early Miocene), and the Santa Cruz Formation (middle Miocene).

The basal part of the Tres Pasos Formation is partly contemporaneous with the underlying Cerro Toro Formation, which represents large, conglomerate-filled submarine channels prograding towards the south along the Magallanes-Austral axis (Katz, 1963; Natland et al., 1974; Hubbard et al., 2008). The Tres Pasos Formation is of late Campanian age in its uppermost part, as indicated by the ammonites *Hoplitoplacenticeras plasticus* and *H. semicostatus* at Cerro Cazador (Paulcke, 1907). Its contact with the overlying Dorotea Formation is concordant, as revealed in the upper part of Cerro Guido (Fig. 1B). The latter formation reaches a thickness of about 200 m in the study area, consisting mainly of medium to coarse sandstones. The Man Aike Formation, previously referred to as the Río Baguales or Las Flores Formation in different parts of the study area (Le Roux et al., 2010; Ugalde, 2014), overlies the Dorotea Formation paraconformably to unconformably, consisting of about 300 m of medium- to coarse-grained sandstones and conglomerates. Apart from fossils clearly reworked from the underlying Dorotea Formation, late Eocene shark teeth, fish fossils and invertebrates are present (Otero et al., 2013). The Río Leona Formation overlies the Man Aike Formation concordantly at Chorillo Jabón, where it reaches an approximate thickness of 200 m. It is here composed mainly of mudstones and medium-grained sandstones with intraformational conglomerate lenses. Thin lignite beds, as well as fossil wood and leaves are common (Barreda et al., 2009; Torres et al., 2009). The Estancia 25 de Mayo Formation concordantly overlies the Río Leona Formation and represents the Patagonian or "Superpatagonian" Transgression (Feruglio, 1949; Malumián, 1999), which took place during the early Miocene between 20 and 18 Ma (Parras et al., 2012; Bostelmann et al., 2013; Cuitiño et al., 2013). Its fossil assemblage includes oyster banks (*Ostrea hatcheri*), bivalves, typical Leonenses gastropods such as *Perissodonta ameghinoi*, and crabs (*Chaceon peruvianum*) (Gutíerrez et al., 2013). A prominent, 2 m thick pyroclastic horizon of rhyodacitic composition is present in the middle of this unit at Cerro Corona (Figs. 2, 3). It was also reported in the Lago Argentino succession, where it was identified as "LPL" and dated by U—Pb at 19.14 ± 0.5 Ma (Cuitiño et al., 2013). The Santa Cruz Formation lies conformably upon the Estancia 25 de Mayo Formation (Bostelmann et al., 2013) at Cerro Cono (Fig. 2), where it reaches a thickness of about 100 m. It consists of multi-coloured mudstones with medium to coarse sandstones and conglomerates. Terrestrial vertebrate fossils indicate a post-Colhuehuapense to pre-Santacrucian age, which is supported by a population of detrital zircons with a mean age of 18.23 ± 0.26 Ma (Bostelmann et al., 2013). However, the dated sample also contained several zircons with ages of about 16 Ma, which indicated that the latter may have to be revised downward.

Olivine-rich dolerite intrusions are common in the Sierra Baguales, forming huge, laccolite-like sills reaching many tens of meters in thickness, as well as dikes up to 3 m thick (Fig. 3). Field evidence shows that none of these sills penetrates the Santa Cruz Formation, suggesting that their intrusion occurred before the deposition of this unit.

The "Andesitic Lavas of Sierra Baguales" (Muñoz, 1981) are of late Pliocene age and overlie the Santa Cruz Formation, forming prominent cliffs in the high mountains to the north and east of the Río Baguales. These lavas, as well as all the Cretaceous and Miocene successions below, have been intruded by younger dioritic and basaltic dikes with an E-W trend.

In spite of its location close to the fold-and-thrust belt of the Rocas Verdes Basin, the Sierra Baguales area is relatively undeformed, with very gentle folding and faults being almost absent. Our measurements throughout the study area indicate a mean strike and dip of 303°/10°NE.

4. Lithostratigraphy and depositional environments

4.1. Tres Pasos Formation

This formation is described by Bernhardt (2011) and Macauley and Hubbard (2013) as a continental slope system. In the vicinity of the Río Las Chinas and Cerro Guido the succession consists of decimeter-scale intercalations of fine-grained sandstones, siltstones, and organic-rich shales (Fig. 4A) in occasional fining-upward cycles. The sandstones show lower flow regime horizontal lamination and rare flutes at the base (facies 11 in Table 1). *Rusophycus* trace fossils, probably formed by arthropods, are abundant. This facies is typical of distal turbidites and suggests a continental slope environment. Towards the top of this formation there is a coarsening-upward trend with fine- to very coarse sandstone beds showing high-angle tabular and trough cross-lamination, in which trace fossils of *Rusophycus*, *Palaeophycus* (Fig. 4B), *Cruziana* (Fig. 4C), fish trails or undichnia (Fig. 4D), *Psilonichnus* (Fig. 4E), and *Skolithos* (Fig. 4F) are present. This facies assemblage (mainly facies 10 in Table 1, but elements of facies 9 are also present)

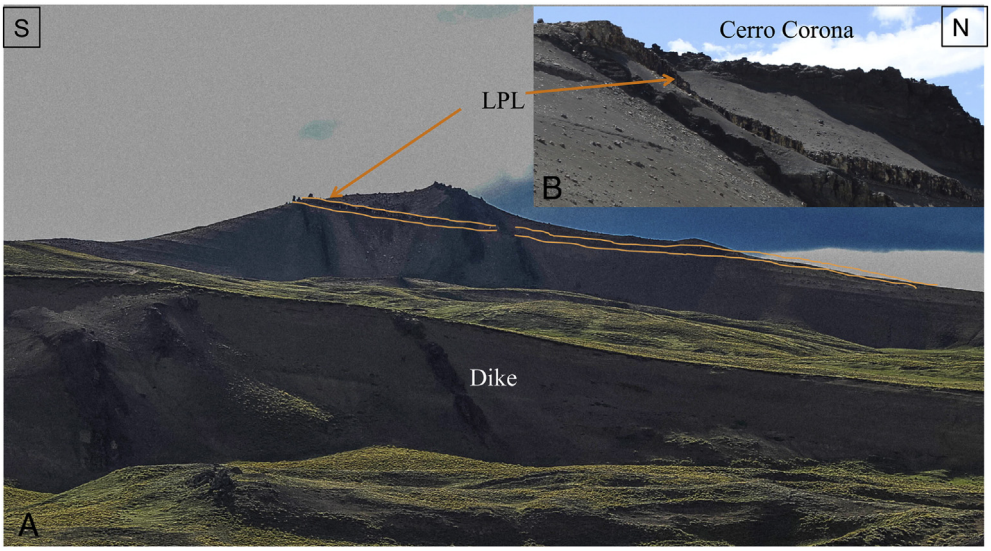

Fig. 3. A) Vertical dike intruding Estancia 25 de Mayo Formation. B) Pyroclastic bed (LPL) in the Estancia 25 de Mayo Formation.

suggests a transition to shallow marine conditions ranging from the shelf or lower shoreface to an upper shoreface with ridges and runnels. There is a thus a gradual transition into the deltaic facies of the Dorotea Formation.

4.2. Dorotea Formation

According to previous authors (Katz, 1963; Riccardi and Rolleri, 1980; Schwartz and Graham, 2015), this formation was deposited in a

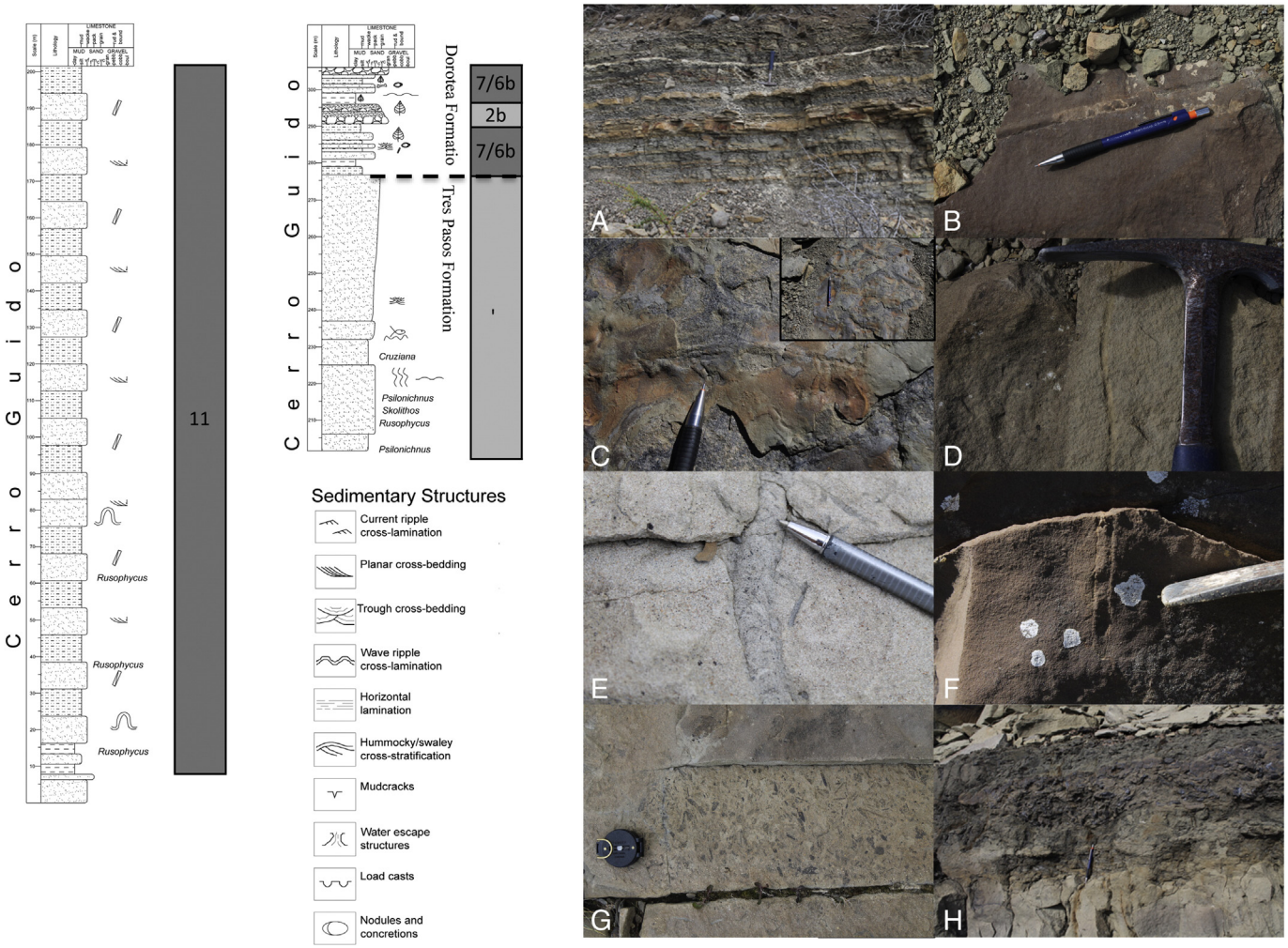

Fig. 4. Measured stratigraphic column of the Tres Pasos and Dorotea Formations in Cerro Guido. A) Turbidites; B); Palaeophycus; C) Cruziana; D) Fish trails (undichnia); F) Oyster bank; G) Wood and leaf fragments; H) *Psilonichnus*; H) *Skolithos*.

Table 1
Depositional facies recognized in the Upper Cretaceous to middle Miocene stratigraphic succession of the Sierra Baguales.

Id	Facies	Formation	General description
1	1a. Braided rivers with abandoned channels. 1b. Braided rivers proximal to ocean.	Santa Cruz, Río Leona. Man Aike	**Lithology:** Fining- and coarsening-upward, medium- to coarse, greenish sandstones and conglomerates with mud clasts; mudstone and calcareous, very fine-grained sandstone lenses within sandstones. **Sedimentary structures:** High-angle tabular and trough cross-lamination. **Fossils:** High content of tree trunks and poorly preserved leaf fragments; shark teeth in 1b.
2	2a. Point bars in meandering rivers. 2b. Point bars in meandering distributary channels.	Río Leona, Santa Cruz. Tres Pasos, Dorotea, Man Aike.	**Lithology:** Three types of fining-upward cycles: Medium-grained sandstone to nodular mudstone; coarse- and medium-grained sandstone to fine- and very fine-grained sandstone; coarse, clast-supported, monomictic conglomerate to fine conglomerate. Conglomerates contain very fine-grained sandstone lenses. **Sedimentary structures:** High-angle tabular and trough cross-lamination; upper flow regime parallel lamination; rib-and-furrow structures; current ripple marks in 2a; wave ripples in 2b. **Fossils:** Bivalves, oysters, shark teeth in 2b, vertebrates, arthropods, tree trunks and leaves in 2a. **Ichnofossils:** *Arenicolites*, arthropod trails in 2b.
3	Levees	Santa Cruz	**Lithology:** Thin, intercalated beds of siltstone and very fine-grained sandstone.
4	Subaerial flood plains.	Dorotea, Río Leona, Santa Cruz.	**Lithology:** Multicoloured mudstones with thin, grey to brown shale, reddish siltstone and fine-grained sandstone beds and lenses. **Fossils:** Wood fragments, leaves, pollen, vertebrates.
5	Overbank swamps.	Río Leona.	**Lithology:** Sapropelite interbedded with black mudstone. **Fossils:** Wood fragments and leaves.
6	6a. Crevasse splays on flood plains. 6b. Crevasse splays in interdistributary bays	Río Leona, Santa Cruz. Tres Pasos, Dorotea, Man Aike, Estancia 25 de Mayo.	**Lithology:** Fine- to medium-grained sandstone; quartz and chert clasts; calcareous sandstone beds with $CaCO_3$ nodules in 6b. **Fossils:** Tree trunks, leaves, vertebrate fragments in 6a. Bivalves, gastropods, oysters, shark teeth, leaves, tree trunks, vertebrate fragments in 6b.
7	Estuaries and interdistributary bays.	Dorotea, Man Aike, Estancia 25 de Mayo.	**Lithology:** Greenish grey mudstones and grey to brown shales with thin interbeds of siltstone and fine-grained sandstone. **Fossils:** Wood fragments, leaves, bivalves, oysters, shark teeth.
8	8a. Low-sinuosity meandering rivers. 8b. Tidal channels	Santa Cruz. Dorotea, Man Aike.	**Lithology:** Coarse- to medium-grained sandstones and clast-supported, monomictic conglomerates; beds and lenses have erosional bases; $CaCO_3$ nodules. **Sedimentary structures: U**pper flow regime horizontal lamination; high-angle tabular and trough cross-lamination; herringbone cross-lamination in 8b. **Fossils:** Burnt wood fragments in 8a. Burnt wood fragments, shark teeth in 8b. **Trace fossils:** *Skolithos* in 8b.
9	Upper shoreface with shoals, ridges and runnels, occasional distributary mouth bars.	Tres Pasos, Dorotea, Man Aike, Estancia 25 de Mayo.	**Lithology:** Coarse- to very coarse-grained sandstones and conglomerates in coarsening-upward cycles; sandstones contain fine-grained sandstone lenses. **Sedimentary structures:** High-angle tabular and trough cross-lamination. **Fossils:** Wood and leaf fragments, *Turritella*, gastropods, oysters, crabs. **Ichnofossils:** Fish trails (undichnia), *Psilonichnus*, *Skolitos*, *Rusophycus*, *Palaeophycus*, *Cruziana*
10	Shelf to lower shoreface	Estancia 25 de Mayo.	**Lithology:** Fine- to medium-grained sandstone interbedded with shale; $CaCO_3$ nodules and concretions. **Sedimentary structures:** Lower flow regime horizontal lamination. **Fossils**: Gastropods, brachiopods, crabs, leaves.
11	Continental slope, turbidity currents	Tres Pasos.	**Lithology:** Medium- to fine-grained sheet sandstones interbedded with thin, organic-rich shales; occasional fining-upward cycles. **Sedimentary structures:** Lower flow regime horizontal lamination, rare flute marks. **Ichnofossils:** *Rusophycus*.

transitional, shallow marine to deltaic environment. It contains invertebrate, vertebrate, insect and plant fossils, while traces of *Skolithos* and *Thalassinoides* are common.

In the Cerro Guido section (Fig. 4, left) this formation concordantly overlies the Tres Pasos Formation, consisting of greenish grey mudstones and grey to brown shales with thin interbeds of siltstone and fine-grained sandstone (facies 7 in Table 1). Fining-upward conglomerates filling channels also occur (facies 2), while fossils are represented by wood and leaf fragments (Fig. 4G), bivalves, shark teeth and oyster accumulations (Fig. 4H). This section is interpreted as representing estuaries or interdistributary bays with oyster banks.

Five depositional facies were recognized in the profile of the Dorotea Formation measured at Las Tetas de las Chinas (Fig. 5). The first (facies 4; Table 1) consists of up to 40 m of reddish to greenish and grey mudstones with bed thicknesses between 10 and 30 cm, intercalated with cm-scale horizons of grey to brown shale. Thin lenses of fine- to medium-grained sandstone are also present. These deposits contain fossil wood and leaves, pollen, and vertebrate fragments, being interpreted as representing overbank flood plains with small channels and shallow ponds.

The second (facies 2; Table 1) is represented by 2–5 m thick, grey, medium- to coarse-grained sandstones with erosional bases, separated by mudstones. The sandstones display trough and high-angle planar cross-lamination as well as upper flow regime parallel lamination (Fig. 5K), rib-and-furrow structures (Fig. 5I), and wave ripples (Fig. 5G). Trace fossils are represented by *Arenicolites* (Fig. 5C, D) and arthropod trails (Fig. 5E, F). Meter-scale lenses of brown, very coarse-grained sandstones with high-angle planar cross-lamination are also present. This facies reflects low-sinuosity distributary channels with lunate and straight-crested bars under the influence of wave action.

The third (facies 6; Table 1) is up to 5 m thick, being composed of brown, calcareous, fine- to medium-grained sandstones with chert and quartz clasts as well as carbonate nodules. Bivalves and gastropods are present. They are interpreted as crevasse splay deposits partially filling interdistributary bays, as they are interbedded with facies 7.

The fourth (facies 9; Table 1) consists of up to 5 m thick cycles of coarse to very coarse sandstones grading upward into conglomerates with chert and quartz clasts reaching 14 cm in diameter. The sandstones display trough- and high-angle planar cross-lamination (Fig. 5J) and contain fine-grained sandstone lenses. Fossil leaves and wood fragments are present. These characteristics suggest prograding upper shoreface deposits with ridges and runnels, or possibly distributary mouth bars.

The fifth association (facies 2b; Table 1), displays three types of fining-upward cycles: up to 8 m of medium sandstone grading into mudstone with calcareous nodules; medium sandstone grading into fine

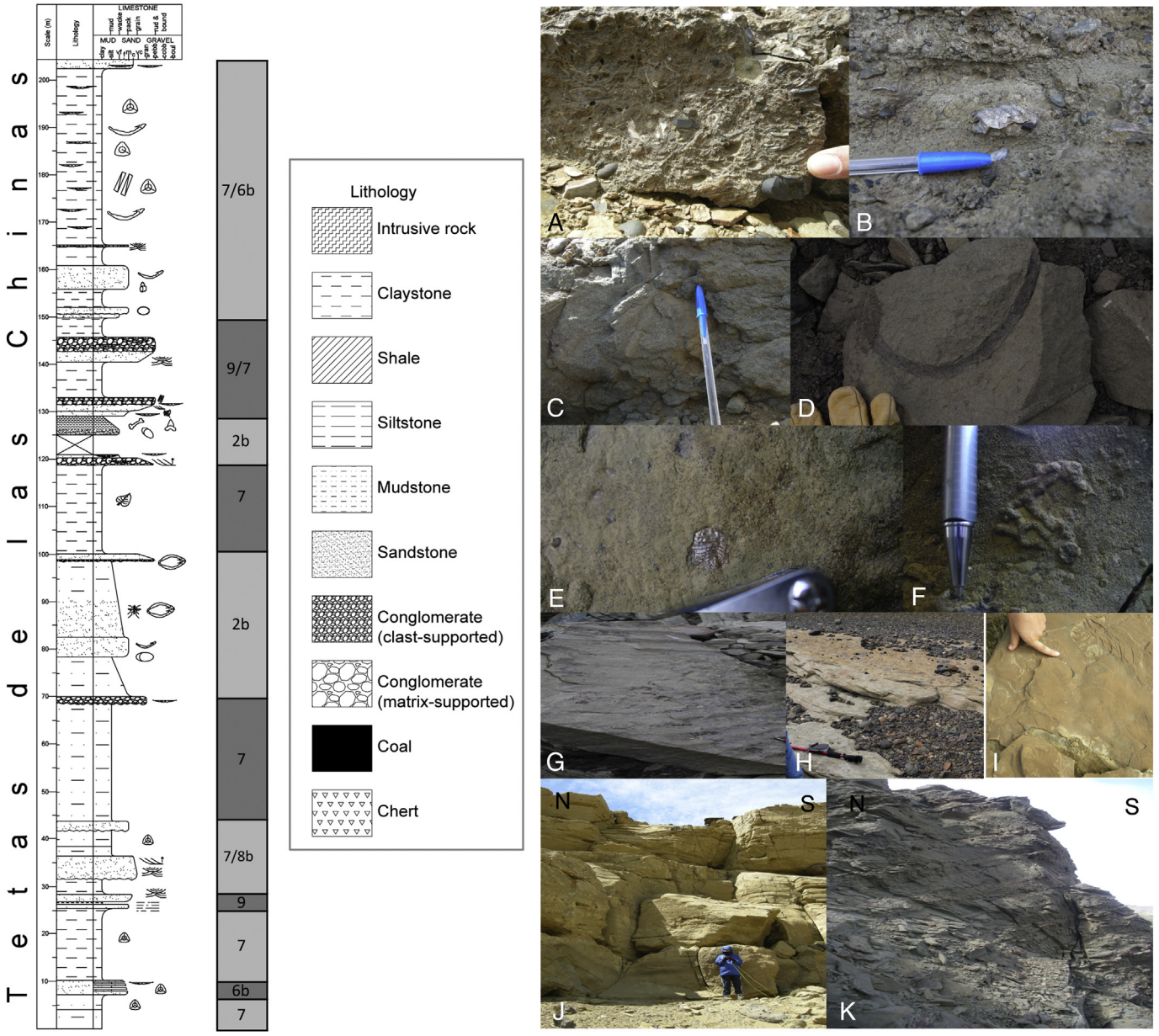

Fig. 5. Measured stratigraphic column of Dorotea Formation at Las Tetas de las Chinas. A) Bivalves; B) Oysters; C and D) *Arenicolites*; E) Arthropod; F) Arthropod trails; G) Wave ripples; H) Trough cross-lamination; I) Rib-and-furrow structures; J) High-angle tabular and trough cross-lamination; K) upper flow regime horizontal lamination.

sandstone over a total thickness of 20 m; and up to 2 m thick cycles of coarse conglomerate grading into monomictic, clast-supported conglomerates with rounded chert clasts reaching 10 cm in diameter. In the latter cycles, the conglomerates show high-angle cross-bedding and contain fine-grained sandstone lenses. Fossils include shark teeth, vertebrate fragments, insects, bivalves and oysters. This facies is interpreted as representing meandering distributary channels directly connected to the open sea.

The characteristics described above therefore indicate a shallow marine, deltaic environment for the Dorotea Formation, in which subaerial delta plains with low to higher sinuosity distributary channels and overbank sediments graded laterally into interdistributary bays with crevasse splays. Distributary mouth bars developed on the upper shoreface where the channels entered the underwater platform. This interpretation coincides with those of Gutíerrez et al. (2013), González (2015), and Schwartz and Graham (2015), based on other profiles measured in the Dorotea Formation.

4.3. Man Aike Formation

The middle part of the Man Aike Formation was deposited in a mainly wave-dominated estuary, but with extensive tidal flats (Le Roux et al., 2010). A 50 m thick profile was measured in the Chorrillo Jabón sector and 40 m in the Las Tetas de las Chinas sector (Fig. 6). The first is complementary to the top of the Man Aike Formation measured by and referred to as the Río Baguales Formation by Le Roux et al. (2010), whereas the second corresponds to the base of this column. In the measured base and top of the Man Aike Formation, three different facies were recognized, all containing shark teeth. The first (facies 1a; Table 1) consists of medium to coarse sandstone with both coarsening- and fining-upward trends, displaying high-angle tabular and trough cross-lamination and decimeter-scale mudstone lenses. Poorly preserved wood and leaf fragments are present. It is interpreted as representing braided streams in a general estuary environment. The presence of shark teeth indicates proximity to the ocean. The second

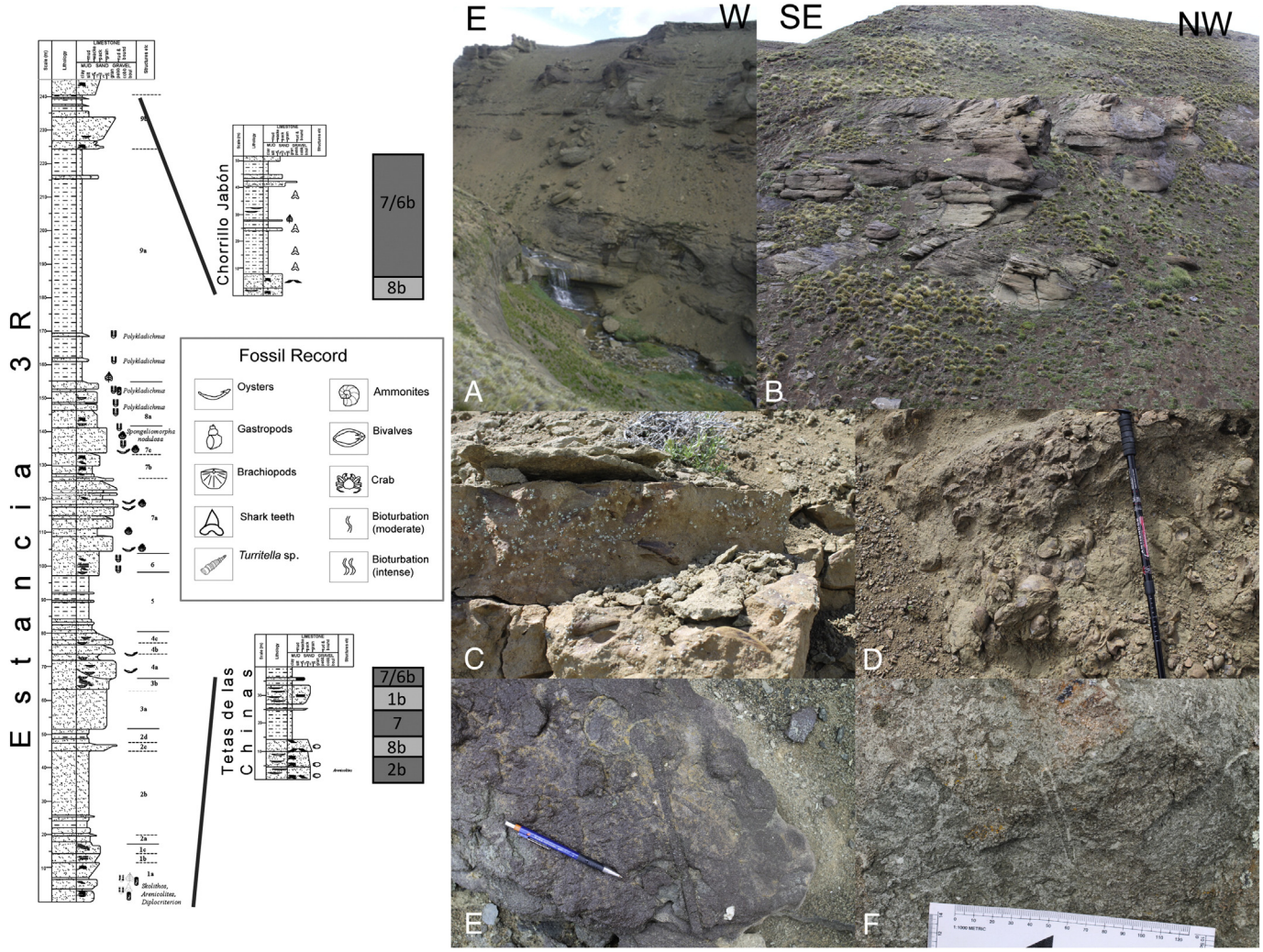

Fig. 6. Measured stratigraphic columns of Man Aike Formation at Las Tetas de las Chinas and Chorrillo Jabón. A) Outcrop of Man Aike Formation at Chorillo Jabón; B) Herringbone cross-lamination; C) Bivalves; D) Gastropods; E) and F) *Skolithos*.

facies (facies 7; Table 1) is dominated by mudrocks interbedded with fine- to medium-grained sandstone beds and lenses. Bivalves and gastropods are present (Fig. 6C, D) in addition to shark teeth. This facies is considered to reflect an estuary. The third facies (facies 8b; Table 1) is represented by medium- to coarse-grained sandstones with erosional bases showing herringbone (Fig. 6B) and trough cross-lamination. Trace fossils are represented by *Skolithos* (Fig. 6E, F). This facies reflects tidal channels subjected to ebb and flow. The association is thus typical of tide-dominated estuaries, which is consistent with the interpretation of Le Roux et al. (2010).

4.4. Río Leona Formation

The Río Leona Formation was deposited in a fluvial environment characterized by meandering and anastomosing rivers with wide overbank flood plains (Marenssi et al., 2000, 2005).

A composite section of the Río Leona Formation was measured at Chorrillo Jabón and Las Murallas, respectively (Fig. 7), in which 6 depositional facies were identified. The first (facies 4; Table 1) consists of brown to greenish, massive mudstones interbedded with siltstones and very fine-grained, grey to dark grey sandstones. Its thickness varies between 5 and 20 m. Fossil tree trunks and leaves were also recorded. This facies is attributed to a subaerial, overbank environment.

Buff, fine to medium-grained sandstones up to 1 m thick intercalated with buff to brown mudstones compose the second facies (facies 6a, Table 1). Fossil roots, trunks and leaves (Fig. 7C–F) are present, indicating a subaerial environment. This facies reflects crevasse splays in an overbank environment.

The third association (facies 2a, Table 1) is composed of coarse- to fine-grained sandstones forming 2–5 m thick, fining-upward cycles. Current ripple marks occur at the top of some cycles, with fossil wood fragments and leaves also present. These are interpreted as point bars in meandering channels.

The fourth facies (facies 1a; Table 1) displays greenish, medium- to coarse-grained sandstones with intraformational mud-clast conglomerates. Both coarsening- and fining-upward cycles are present. Sedimentary structures include trough and high-angle tabular cross-lamination. Mudstone lenses with erosional basal and upper contacts and some calcareous sandstone lenses were also recorded. There are abundant, but poorly preserved fossil tree trunks and leaves. This facies represents braided streams with abandoned channels.

Facies 5 (Table 1) consists of sapropelite interbedded with black mudstones, indicating a high organic content that coincides with the presence of abundant fossil wood fragments and leaves. It is interpreted as representing swampy, reducing conditions within an overbank environment.

The overall sedimentological characteristics of the Río Leona Formation thus suggest a coastal plain with meandering and locally braided channel systems. Flood plain swamps created reducing conditions in which wood and leaf fragments were well preserved. This

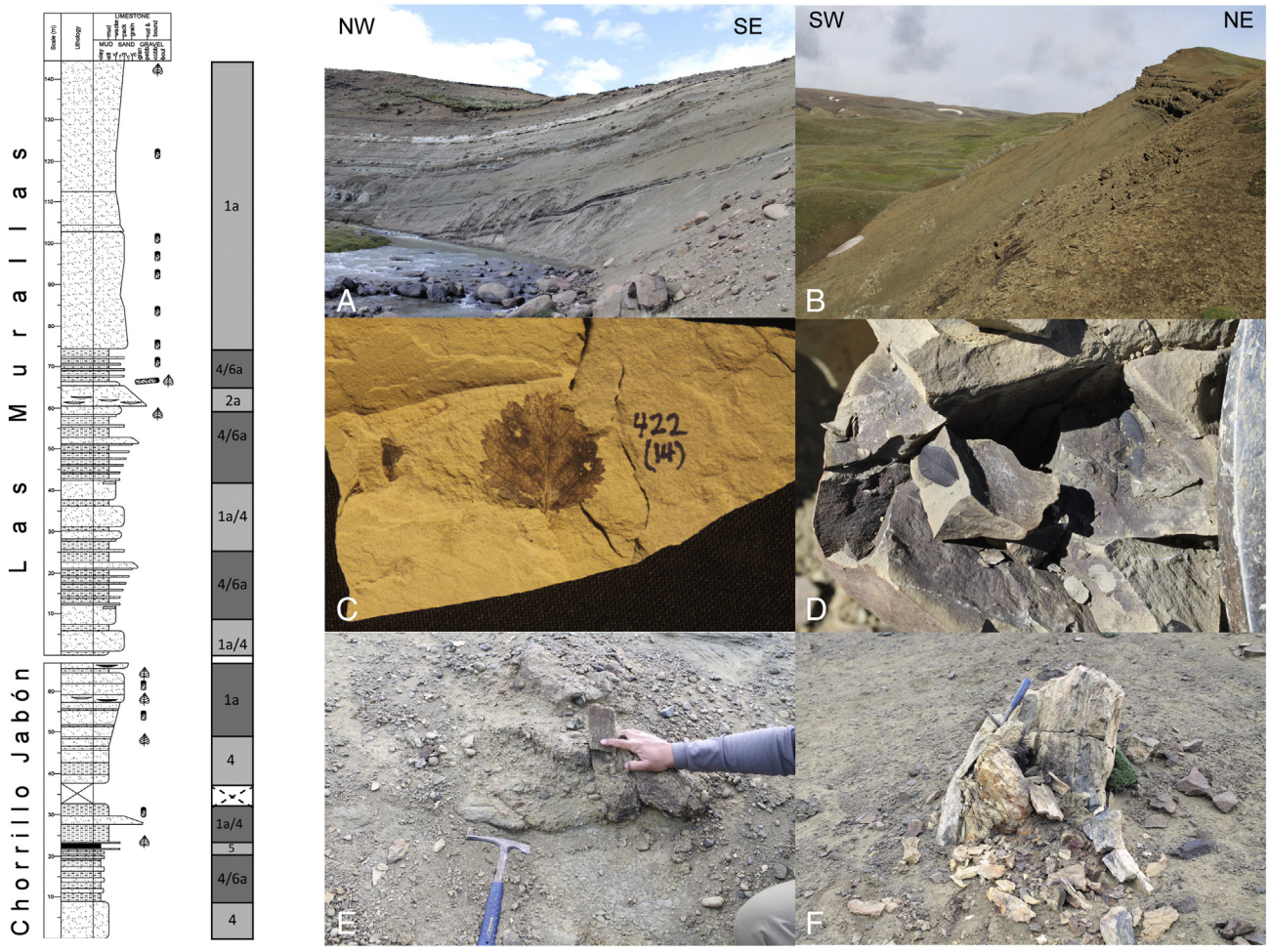

Fig. 7. Measured stratigraphic columns of Río Leona Formation at Las Murallas and Chorrillo Jabón. A) and B) Outcrops of Río Leona Formation at Las Murallas and Chorillo Jabón; C) and D) Well preserved fossil leaves; E) Wood fragment in conglomerate; F) tree trunk in life position.

interpretation of the Río Leona Formation is consistent with previous studies of this formation in Argentina and Chile (Malumián, 1990; Marenssi et al., 2000, 2002, 2005; Le Roux et al., 2010; Malumián and Nañez, 2011; Cuitiño et al., 2013).

4.5. Estancia 25 de Mayo Formation

Two facies were recognized in this formation. The first (facies 10, Table 1) consists of thin (1–2 m), sheet-like beds of greenish, fine- to medium-grained, calcareous sandstones. These are intercalated with ochre to brown, calcareous shales, also between 1 and 2 m thick, in which cm-scale, calcareous nodules and fossiliferous concretions are present. Among the fossils are gastropods and crabs, as well as brachiopods and leaves. This facies represents a lower shoreface environment.

The second facies (facies 9; Table 1) is composed of massive, medium- to coarse-grained, calcareous sandstones showing ochre to greenish colours, calcareous nodules and concretions containing gastropods (including *Turritella*), crabs (Fig. 9B), articulated brachiopods (Fig. 8B), and oysters (Fig. 8F). The presence of *Turritella* and oysters suggests a nearshore environment in the vicinity of river mouths, so that this facies is interpreted as representing sandy shoals in an upper shoreface environment.

4.6. Santa Cruz Formation

This formation was deposited in meandering rivers on a flood plain with local small lakes. No new stratigraphic profiles were measured in the Santa Cruz Formation, as this had already been done by the present authors in a previous publication (Bostelmann et al., 2013). The facies recognized in that study (Morro Bayo section; Fig. 9A) included 2–10 m thick units of multicoloured mudstones with abundant vegetal remains, showing metric-scale, reddish siltstone lenses in the thicker units. Vertebrate fossils (Fig. 9B) and pollen are abundant, with occasional insect traces (Fig. 9D). This association (facies 4; Table 1) represents overbank flood plain deposits. Fine- to medium-grained sandstones reflecting crevasse splays (facies 6a; Table 1) are between 1 and 1.5 m thick and interbedded with the mudstone. Meandering channels with point bar deposits (facies 2a; Table 1) are represented by 2–5 m thick, fining-upward, coarse- to fine-grained sandstone with epsilon (Fig. 9F), high-angle tabular (Figs. 9C, 10) and trough cross-lamination (Fig. 9E, H), whereas levees (facies 3; Table 1) are indicated by thin beds (less than 1 m) of siltstone intercalated with very fine sandstone. Somewhat straighter channels (facies 8a; Table 1) are represented by clast-supported, monomictic conglomerates showing erosional basal contacts and trough cross-bedding. Burnt wood fragments are also present. These characteristics indicate a fluvial system dominated by meandering streams, with local minor braided systems.

5. Palaeocurrent directions

5.1. Tres Pasos Formation

Previous palaeocurrent studies in the Cerro Toro and lower parts of the Tres Pasos Formation indicated a consistent southward-directed

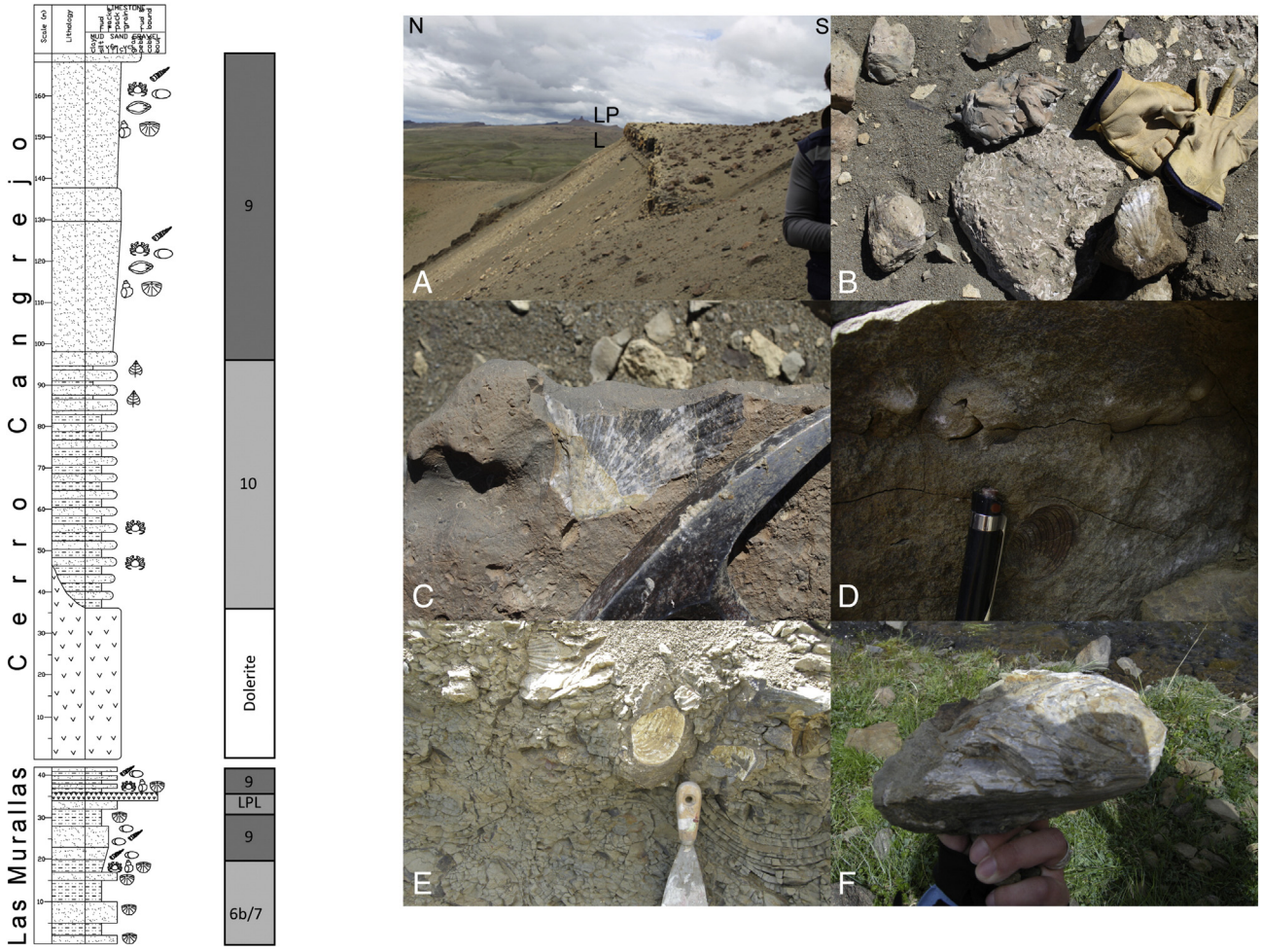

Fig. 8. Measured stratigraphic columns of Estancia 25 de Mayo Formation at Las Murallas and Cerro Cangrejo. A) Outcrop of Estancia 25 de Mayo Formation and LPL bed at Las Murallas. B) Gastropods, *Turritella* and crabs; C)–E) Brachiopods; F) Oysters.

dispersal pattern (Scott, 1966; Fildani and Hessler, 2005; Crane and Lowe, 2008; Hubbard et al., 2008, 2010; Bernhardt et al., 2008, 2011; Jobe et al., 2010; Romans et al., 2010). Palaeocurrent directions in the Tres Pasos Formation were mainly derived from the inclination direction of slope clinoforms, lateral facies changes indicating southward progradation, and sole structures such as tool and flute marks. Measured directions vary between 160 and 180° (Hubbard et al., 2010). Our identification of shelf to lower shoreface facies in the upper part of the Tres Pasos Formation in the Sierra Baguales concurs with these studies, in that it represents a more proximal, shallow marine environment in comparison with the continental slope facies identified further south by Bernhardt (2011) and Macauley and Hubbard (2013). The source area was therefore located mainly to the north.

5.2. Dorotea Formation

In the Dorotea Formation (Campanian to Maastrichtian), the 55 measured palaeocurrent directions in the Sierra Baguales are towards the west with a range between southwest and northwest (Fig. 10A). This is consistent with the type of depositional environment, being a tide-dominated delta. However, the vector mean is 269° with a vector magnitude of 84%, suggesting that the source area was situated mainly to the east. Forty-one palaeocurrents measured by us further south at Cerro Castillo (Fig. 1) gave a vector mean of 241° with a vector magnitude of 32%.

5.3. Man Aike Formation

Only 9 measurements were taken in the Man Aike Formation (Lutetian to Bartonian) in the Sierra Baguales, which display two trends. The main trend is towards the west-northwest and the second towards the east (Fig. 10B). The vector mean is 295° with a magnitude of 43%. This coincides with an estuary environment (Le Roux et al., 2010) subjected to ebb and flow tides as shown by herringbone cross-lamination. We also measured 32 palaeocurrent directions in the time-equivalent Loreto Formation west of Punta Arenas (Fig. 1), yielding a vector mean of 291° with a vector magnitude of 18%. This set also shows two modes, one with a vector mean of 289° ($n = 19$) and another ($n = 13$) with a vector mean of 104°.

5.4. Río Leona Formation

The Río Leona Formation (Rupelian) yielded 18 measurements with three preferential directions towards the south, northwest and northeast, respectively (Fig. 10C). The last concentrates the majority of readings, with a vector mean of 56° and a magnitude of 63%.

5.5. Estancia 25 de Mayo Formation

In the Estancia 25 de Mayo Formation (early Burdigalian), 37 palaeocurrent directions were recorded, which are dominated by two

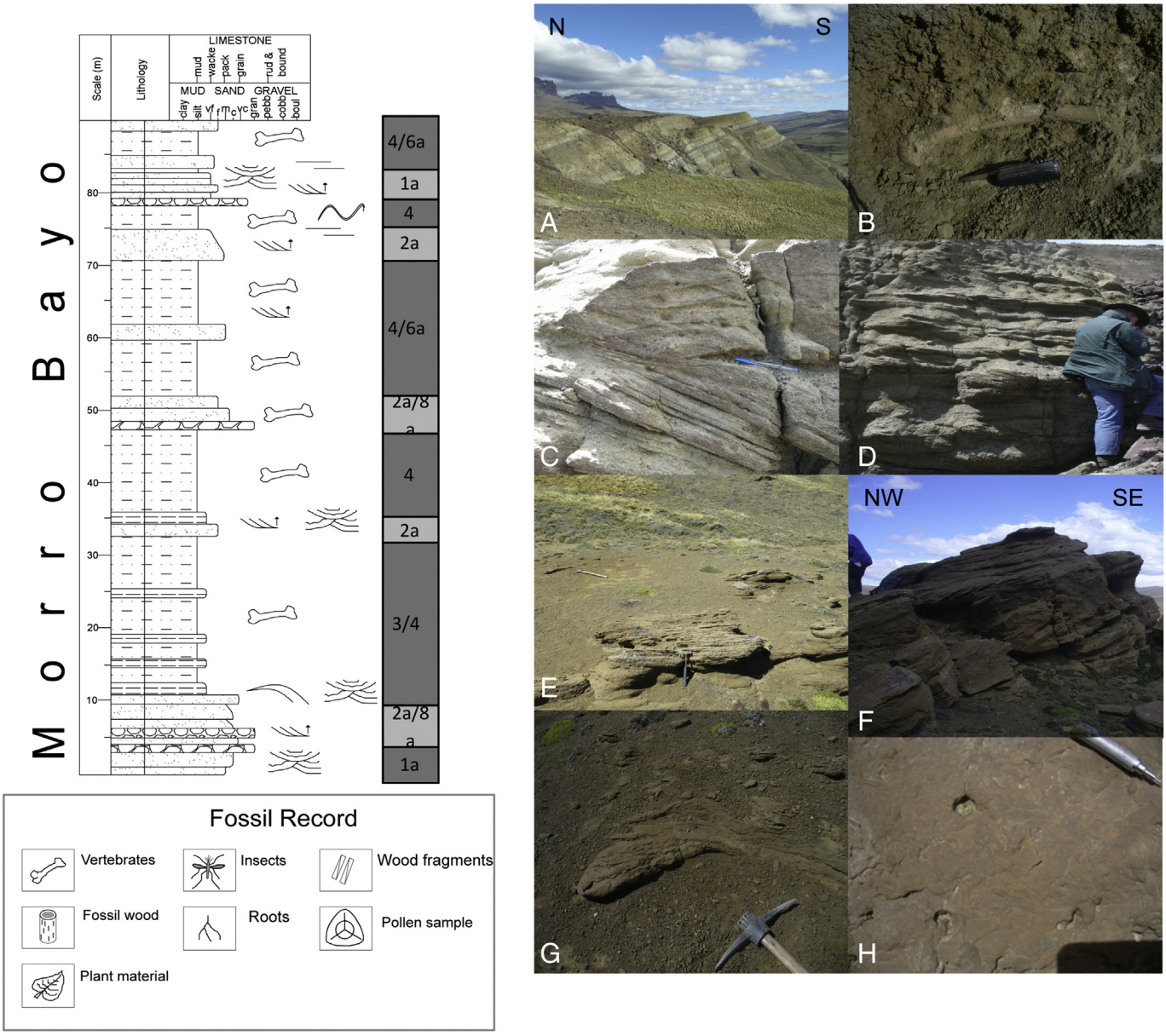

Fig. 9. Measured stratigraphic column of Santa Cruz Formation in Morro Bayo (after Bostelmann et al., 2013). A) Outcrops of the Santa Cruz Formation; B) Vertebrate bone; C–D) Tabular cross-lamination; E–F) Trough cross-lamination; G) Epsilon cross lamination; H) Insect trails.

trends, namely north and southeast (Cuitiño, 2011). The vector mean is 55° with a magnitude of 36% (Fig. 10D).

5.6. Santa Cruz Formation

In the Santa Cruz Formation (late Burdigalian), 73 palaeocurrents were recorded with a vector mean of 65° and a magnitude of 83% (Fig. 10E).

5.7. Summary of palaeocurrent directions

Our measured palaeocurrent directions and vector magnitudes in the Sierra Baguales indicate that they were directed mainly towards the west (269°) between the Cenomanian and Maastrichtian, varying from southwest to west-northwest. This is consistent with 86 palaeocurrent directions measured by us in the Thanetian (57.6 ± 1 Ma; Sánchez et al., 2010) "Cabo Nariz Beds" on Tierra del Fuego in the southern part of the Magallanes-Austral Basin, which gave a vector mean of 300°. The northwesterly trend was maintained at least until the Bartonian-Priabonian, when a vector mean of 295° was recorded in the Man Aike Formation. However, during the Rupelian and early Chattian an abrupt swing to the northeast (055°) occurred, shifting to east-northeast (065°) during the Burdigalian. Additionally, the data show a decrease in the vector magnitude between the Río Leona and Estancia 25 de Mayo Formations, changing from 63% to 36%. This decrease coincides with a change in the depositional environment, passing from meandering and braided rivers in the Río Leona Formation to a shoreface environment in the Estancia 25 de Mayo Formation. After deposition of the latter, there was an increase in the vector magnitude from 36% to 86%, which coincides with a new change in depositional environment from shoreface to continental, fluvial conditions in the Santa Cruz Formation.

6. Detrital zircons and radiometric ages

6.1. Tres Pasos Formation

The Tres Pasos Formation was dated by Bernhardt (2011) in the Silla Syncline to the south of the Sierra Baguales between 89.5 ± 1.9

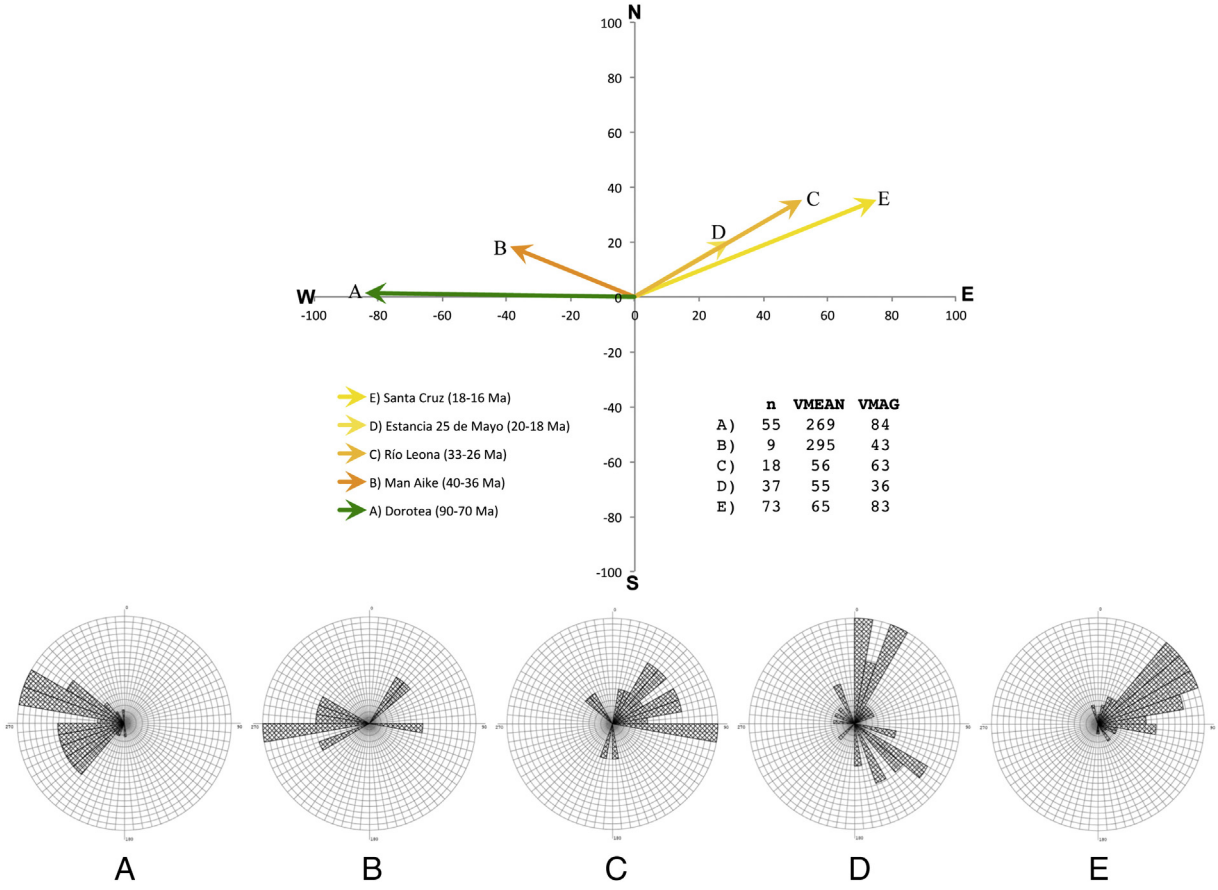

Fig. 10. Rose diagrams of palaeocurrent directions in the different formations of the Sierra Baguales. A) Dorotea Formation; B) Man Aike Formation; C) Estancia 25 de Mayo Formation; D) Río Leona Formation; E) Santa Cruz Formation.

(Turonian) and 81.7 ± 1.7 Ma (Campanian), using Sr isotopes as well as detrital and volcanic zircons. The last age is supported by the presence of *Hoplitoplacenticeras plasticus* and *H. semicostatus* ammonites at Cerro Cazador (Paulcke, 1907). Her sample SdT-Wc, collected from just north of Lago del Toro about 40 km south of the Sierra Baguales, contained 2 detrital zircons with ages exceeding 1000 Ma, 13 with ages between 672 and 251 Ma, and 16 between 155 and 93 Ma. These are here assigned to groups I, IIe and IIIe, respectively.

6.2. Dorotea Formation

Sample Zr-PTO-123 (Fig. 11, top) was collected from the base of the Dorotea Formation at Cerro Guido. The results of detrital zircon dating show 5 populations with ages ranging from 636–480 Ma, 423–310 Ma, 270–171 Ma, 151–139 Ma, and finally 127–84 Ma. The latter population has a mean maximum depositional age of 92.78 ± 0.76 Ma. However, the youngest zircon yielded a date of 83.9 ± 2.6 Ma (late Santonian). Two further samples, Zr-FB-1 (Fig. 11, bottom) and Zr-FB-2 (Fig. 12, top), were collected in the sector Las Tetas de las Chinas, from the middle and upper part of the Dorotea Formation, respectively. Detrital zircon dating of sample Zr-FB-1 shows 3 populations: the first with ages ranging from 578 to 390 Ma, the second with dates between 158 and 123 Ma, and the third group of 31 zircons varying between 112 and 71 Ma. The mean maximum depositional age is 95.1 ± 1.5 Ma (Cenomanian). Similarly, 3 populations were also identified in sample Zr-FB-2, the first between 512 and 406 Ma, the second from 380 to 268 Ma, and the final group ranging from 152 to 72 Ma. In this case the mean maximum depositional age is 93.7 ± 1.2 Ma. However, two zircons in sample Zr-FB-1 have ages of 74.9 ± 2.1 and 71.0 ± 1.2 Ma (Campanian), respectively, whereas one zircon in sample Zr-FB-2 has an age of 71.7 ± 1.2 Ma. The latter dates are supported by the presence of *Gunnarites sp.*, *Pachydiscus aff. gollevilensis*, and *Pachydiscus cazadoriana* in the Dorotea Formation in the vicinity of Las Tetas de las Chinas (González, 2015). The first two fossils are of Maastrichtian age (Martínez-Pardo, 1965), while the last is from the Campanian-Maastrichtian (Otero et al., 2009). A vertebrate fragment of an *Aristonectes* sp. (Plesiosauria, Elasmosauridae) reported by Otero et al. (2015) at the same locality also indicates a late Maastrichtian age, while the presence of *Hoplitoplacenticeras* ammonite species at Cerro Cazador suggests a Campanian age for the basal part of the Dorotea Formation (Macellari et al., 1989). In addition, in the Cordillera Chica and Sierra Dorotea, where the Dorotea Formation also crops out, maximum depositional ages between 72 Ma and 67 Ma were obtained from detrital zircons (Hervé et al., 2004; Fosdick et al., 2015a, 2015b). Therefore, although the possible age of the Dorotea Formation ranges from the late Cenomanian to Maastrichtian (Late Cretaceous), the youngest zircons as well as ammonite fossils indicate a Campanian-Maastrichtian age.

Taking account of the overlapping ages of the populations from different samples, two general groups can be distinguished, namely IIe, between 636 and 171 Ma, and IIIe, between 158 and 67 Ma.

6.3. Man Aike Formation

A sample from the top of this formation, Zr-PTO-77 (Fig. 12, bottom), from the locality of Chorrillo Jabón shows 3 zircon age populations ranging from 550–450 Ma, 143 Ma–72 Ma, and 49 Ma–35 Ma, respectively. The first two populations therefore correspond to the broad groups IIe and IIIe defined in the Dorotea Formation, while the third, here referred to as IV, is younger. The maximum depositional age of a population with 39 zircons is 40.30 ± 0.47 Ma. A mean maximum zircon age of 40.48 ± 0.37 Ma was also reported by Le Roux (2012a), Bostelmann et al. (2012)

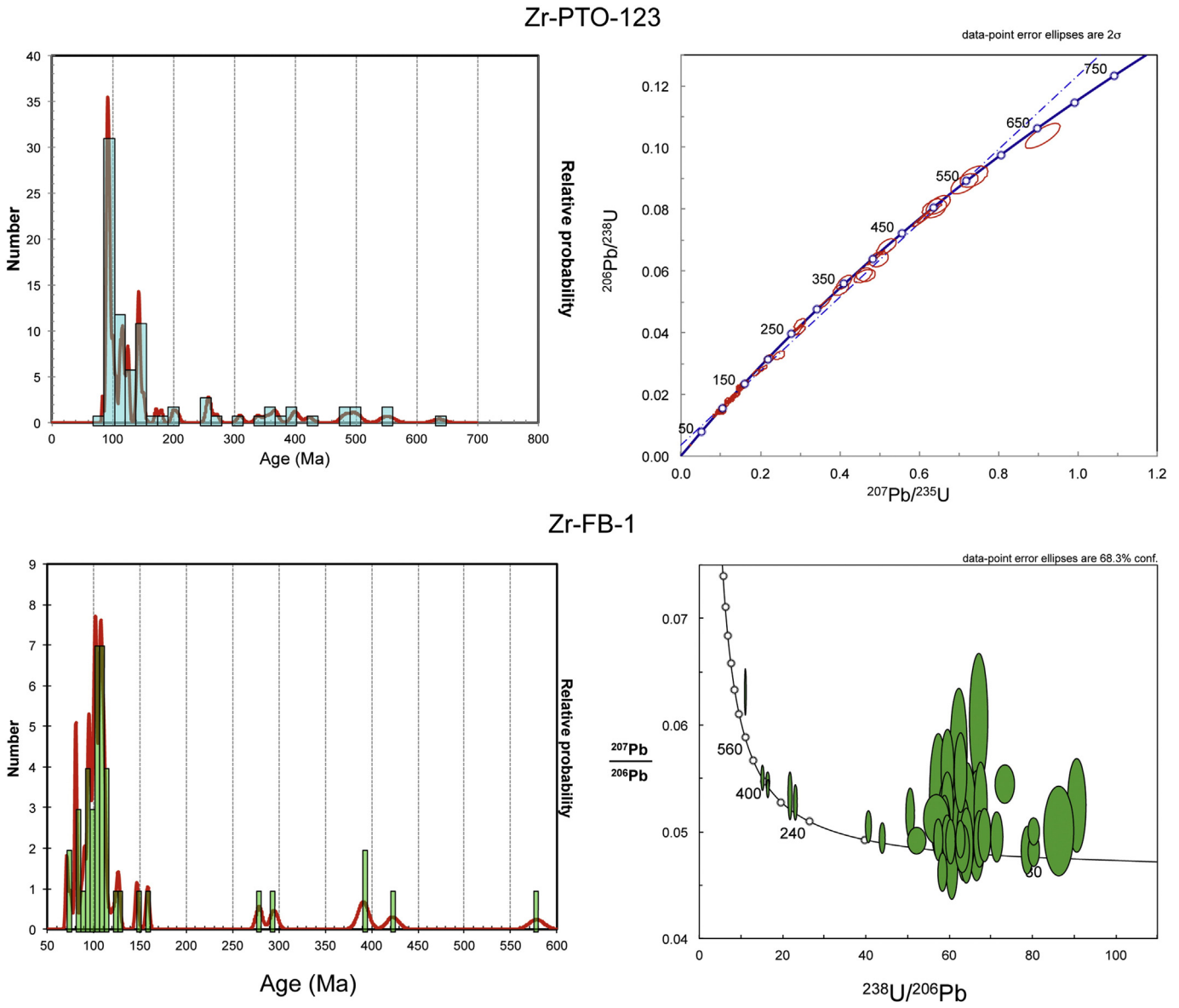

Fig. 11. U-Pb detrital zircon ages in sample PTO-123 and ZR-FB-1 from the Dorotea Formation.

and Otero et al. (2013), so that a latest Lutetian to Bartonian (middle Eocene) age can be accepted. Although Le Roux (2012a) and Bostelmann et al. (2012) never published the details of this sample collected from the top of the Man Aike Formation in a stratigraphic profile measured on Estancia 3R (Le Roux et al., 2010), the results are consistent with those of sample Zr-PTO-77.

6.4. Río Leona Formation

Sample Zr-PTO-81 (Fig. 13, top) was collected from Chorrillo Jabón, being a feldspathic wacke located at the base of the Río Leona Formation. The zircons show three populations, the first with ages exceeding 120 Ma and the second dating between 100 Ma and 76 Ma. Both populations belong to group IIIw. The third population has ages between 43 Ma and 30.8 Ma, therefore belonging to group IV, with a mean calculated age of 35.33 ± 0.57 Ma. Again, the 17 youngest zircons have ages less than 35 Ma, forming a sub-population with a mean of 33.0 ± 2.8 Ma, which is thus taken as the maximum depositional age.

Sample Zr-BAG-25 (Fig. 13, bottom) was collected from Chorrillo las Flores (Fig. 1B) by Ugalde (2014) in the stratotype section of the former Las Flores Formation of Cecioni (1957), which was redefined by the first author as being from the top of the Man Aike Formation. The sample is a feldspathic wacke. The detrital zircon dates show 4 populations, the first with ages exceeding 117 Ma, the second with dates between 108 Ma and 93 Ma, and the third with ages ranging from 80 Ma to 68 Ma. These therefore correspond to group IIIw. The final population lies between 46 Ma and 30 Ma, extending the lower range of group IV by 5 Ma. Although the calculated maximum depositional age for the latter population is 37.0 ± 0.27 Ma (Priabonian), the 16 youngest zircons are all less than 35 Ma old. Taking these as a sub-population, they yield a mean age of 32.83 ± 0.65 Ma, which is here taken to represent the maximum depositional age, i.e. Rupelian (early Oligocene). The presence of fossil leaves of Nothofagaceae, fossil wood belonging to the Araucariaceae, and palynological records of pollen, spores and organic material of plant origin, deposited in an environment of tidal bars and flats (Ugalde, 2014), suggests that this section in fact corresponds to the base of the Río Leona Formation (see Fig. 13, modified from Ugalde, 2014).

The lithological similarity between samples Zr-PTO-81 and Zr-BAG-25, together with the fact that they show very similar zircon population groups and have coinciding maximum depositional ages of 33 Ma, supports the idea that both are from the base of the Río Leona Formation, which is therefore considered to be of Rupelian age.

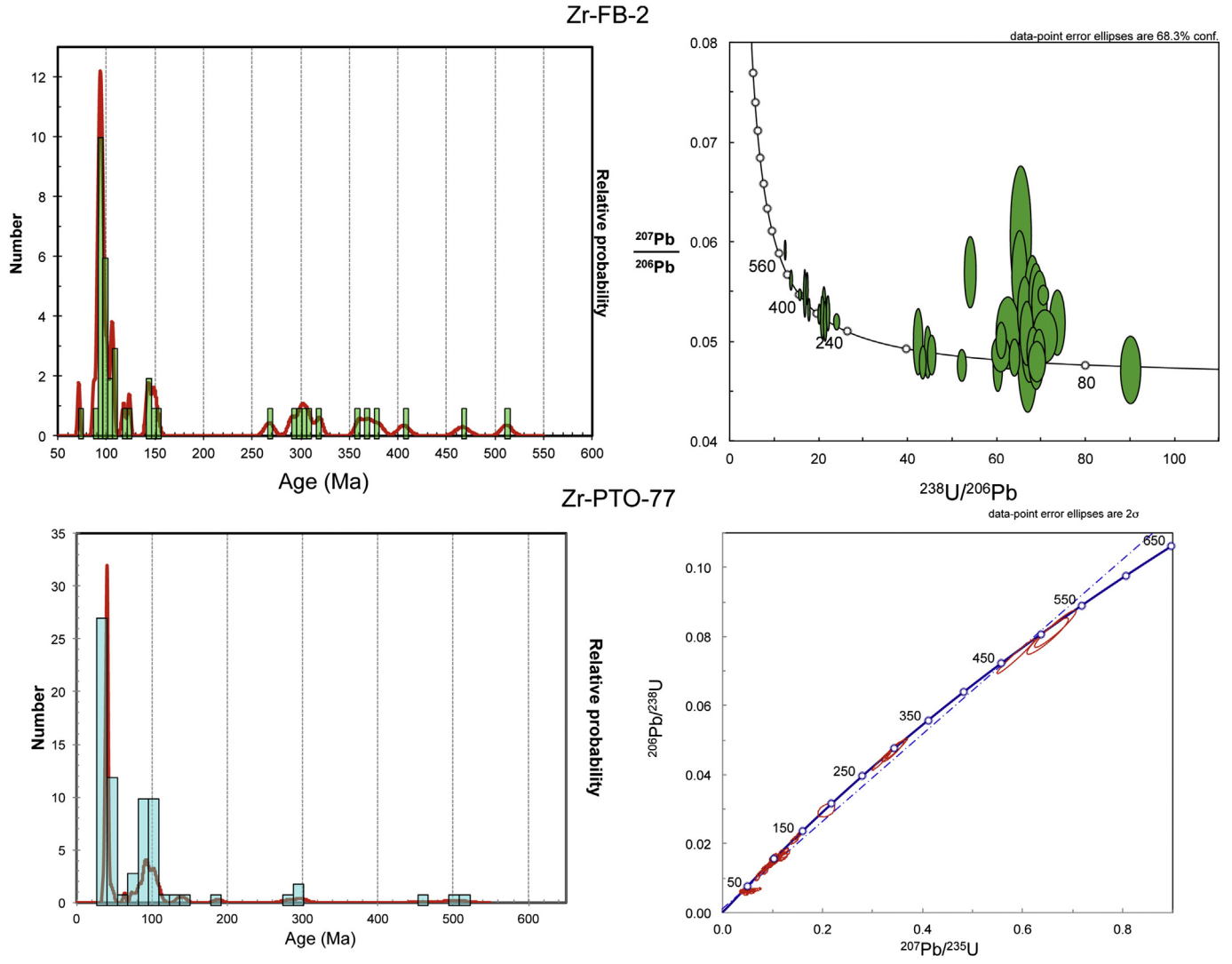

Fig. 12. U-Pb detrital zircon ages in sample Zr-FB-2 from the Dorotea Formation and U-Pb detrital zircon ages in sample Zr-PTO-77 from the Man Aike Formation.

6.5. Estancia 25 de Mayo Formation

It was not possible to date the Estancia 25 de Mayo Formation using detrital zircons in Sierra Baguales. Nevertheless, in the middle part of the stratigraphic section measured in the Alto Río Bandurrias sector, a 2 m-thick pyroclastic bed with a rhyodacitic composition was identified. This pyroclastic event was also recorded in the Quien Sabe Member of the Lago Argentino sector, where it was referred to as "LPL" by Cuitiño et al. (2012), and yielded a zircon U-Pb age of 19.14 ± 0.5. Cuitiño et al. (2015) subsequently dated the stratigraphically equivalent El Chacay Formation in the northern Magallanes-Austral Basin at 20.3–18.1 Ma using strontium isotopes. The Estancia 25 de Mayo Formation is therefore of early Burdigalian age.

6.6. Santa Cruz Formation

Two samples were dated from this formation by Bostelmann et al. (2013) using the SHRIMP U-Pb method. Sample Zr-LF-002 (Fig. 14), located stratigraphically 65 m below Zr-LF-001, yielded 70 zircons. The oldest population showed ages exceeding 1000 Ma, here classified into group I. The second ranged from 700 Ma to 500 Ma, in this paper being considered as part of group IIw because palaeocurrents indicate a source to the southwest instead of the east. The third population, with an age range between 450 Ma and 250 Ma, and the fourth showing ages clustered around 200 Ma, would also form part of group IIw. The fifth population, with ages of 154 Ma – 130 Ma, together with the sixth between 92 Ma and 88 Ma, would belong to group IIIw, distinguished from group IIIe because palaeocurrents indicate a different source area. No younger zircons were present (Fig. 14).

Sample Zr-LF-001 (Fig. 15) was collected from near the top of the exposed Santa Cruz Formation. It contained a total of 70 zircons, of which the oldest 42 could be grouped into 6 populations. The first group has ages between 2927 Ma and 1656 Ma and is here classified into group I. The second population lies between 695 Ma and 560 Ma, the third between 397 Ma and 303 Ma, and the fourth between 299 Ma and 270 Ma, all belonging to group IIw. The fifth population consists of 4 zircons ranging in age between 153 Ma and 142 Ma, and the sixth has 18 zircons dating from 108 Ma to 79 Ma. Both populations belong to group IIIw. For the youngest population of 28 zircons, all falling in group V (with ages less than 25 Ma), Bostelmann et al. (2013) reported a mean calculated age of 18.23 ± 0.22 Ma. However, a new interpretation of these data suggests that the maximum depositional age of the Santa Cruz Formation in the Última Esperanza Province is in fact 16.8 ± 0.22 Ma (late Burdigalian), which is the mean age of a subpopulation of the 8 youngest zircons.

Except for the absence of zircons younger than 25 Ma from sample Zr-LF-001, there is a clear similarity between the population groups of

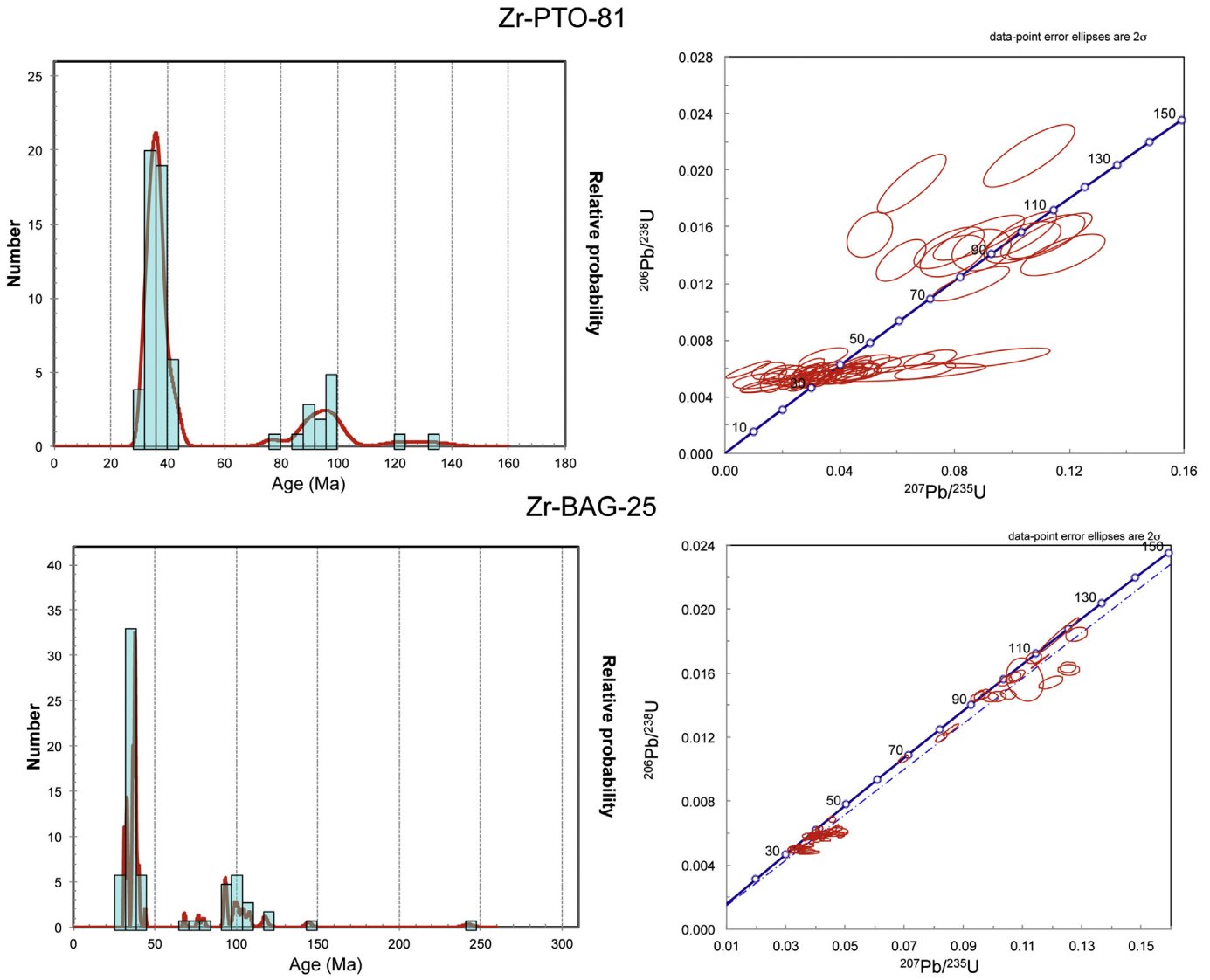

Fig. 13. U-Pb detrital zircon ages in sample Zr-PTO-81 from the Río Leona Formation and U-Pb detrital zircon ages in sample Zr-Bag-25 from the Río Leona Formation (after Ugalde, 2014).

samples Zr-LF-001 and Zr-LF-002, suggesting that the source of the Santa Cruz Formation did not change, but that the younger plutons had either not been exhumed when the base of the formation was being deposited or were not specifically eroded by the rivers delivering detritus to the basin.

7. Zircon provenance areas

Romans et al. (2010) summarized the available evidence from detrital zircon ages that indicate potential source areas for the Late Cretaceous deposits in the Magallanes-Austral Basin, based mostly on the work of Pankhurst et al. (2000), Hervé and Fanning (2003) and Hervé et al. (2007). According to the latter authors, detrital zircons older than 168 Ma were derived from metasediments of the Eastern Andean Metamorphic Complex and the Duke de York Complex, both located to the west of the Magallanes-Austral Basin, while Pankhurst et al. (2000) proposed that volcanic rocks of the Tobífera Formation contributed Early to Late Jurassic zircons (201–145 Ma). The Southern Patagonian Batholith along the southwestern and western side of the basin experienced 3 plutonic episodes dating between 144 and 137 Ma, 136–127 Ma, and 126–75 Ma, providing zircons of these ages (Hervé et al., 2007).

Zircon populations in the Sierra Baguales can be broadly classified into 7 groups, namely I, between 3000 and 1000 Ma; IIe, between 700 and 250 Ma; IIw, between 700 and 200 Ma; IIIe, between 160 and 65 Ma; IIIw, between 155 and 75 Ma; IV, between 50 and 30 Ma; and V, between 25 and 15 Ma. The designations e (east) and w (west) indicate zircons of similar age ranges but different source areas as suggested by palaeocurrent directions. In the western source area groups, there are gaps between 1000–700 Ma, 200–155 Ma, 75–50 Ma, and 30–25 Ma, whereas the eastern provenance area groups show gaps between 250–160 Ma, and 65–50 Ma. In the southern part of the Magallanes-Austral Basin, the zircons dated by Sánchez et al. (2010) from the "Cabo Nariz Beds" range between 165 and 57 Ma, thus roughly coinciding with group IIIe zircons. Three zircon ages fall in group II and two in group I. In the Chorillo Chico Formation near Punta Arenas, which is chronostratigraphically equivalent to the "Cabo Nariz Beds", we only found group IIIe zircons.

The Tres Pasos Formation hosts zircons belonging to groups I, IIe and IIIe, which according to palaeocurent studies and lateral facies changes were derived from source areas to the north of the Magallanes-Austral Basin. Bernhardt (2011) also considered some input from the Andean Fold-and-Thrust Belt to the west. As far as group I zircons is concerned, outcrops of basement rocks with ages exceeding 1000 Ma are scarce in southern South America, currently only known to be present northeast

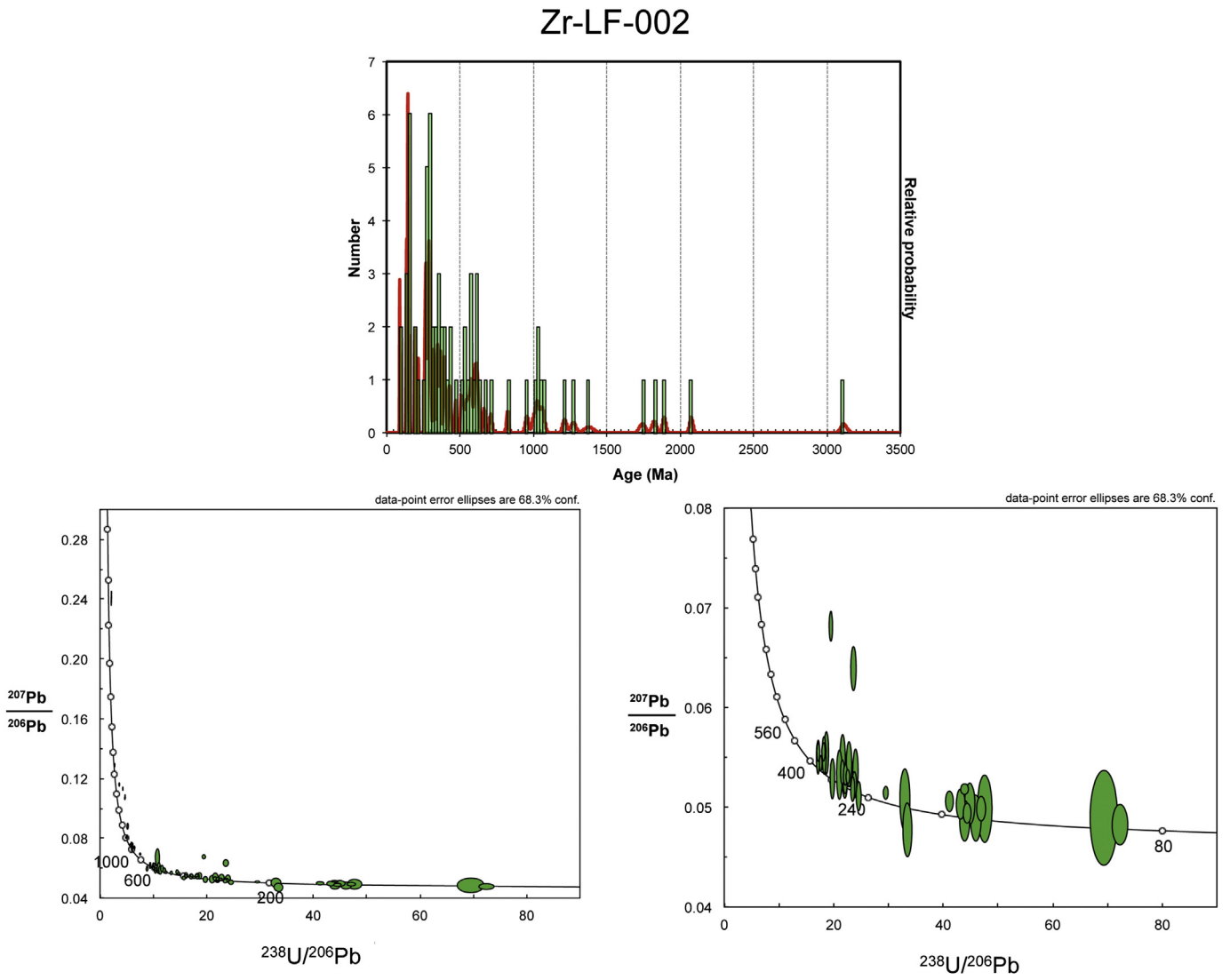

Fig. 14. U-Pb detrital zircon ages in sample ZR-LF-002 from the Santa Cruz Formation (after Bostelmann et al., 2013).

of the Magallanes-Austral Basin in the Río de la Plata Craton where ages between 2200 and 2000 Ma are recorded (Santos et al., 2003; Ramos et al., 2014a, 2014b), and in the North Patagonia Massif where relatively high-grade schists and gneisses with Rb-Sr ages of up to 1190 Ma (Linares et al., 1988) are intruded by Paleozoic granites (Pankhurst et al., 1998). The Kalahari Craton of southern Africa also has Mesoproterozoic rocks (1600–1000 Ma), whereas the Proto-Kalahari Craton dates back to the Archaean (Jacobs et al., 2008). The Magallanes-Austral Basin was at about the same distance from the Kalahari and Río de la Plata Cratons during the Jurassic, so that detritus derived from the northeast could have been diverted into its north-south trending axis.

Some of the group IIe zircons in the Tres Pasos Formation could have been sourced by the Deseado Massif (Fig. 1; 16), where small windows in the Jurassic sequence reveal micaceous and amphibolitic schists of very late Precambrian or Cambrian age, as well as Permo-Triassic plutonic rocks located to the north of the Magallanes-Austral Basin at 40°S (Pankhurst et al., 1998).

The Dorotea Formation, despite being the oldest unit for which zircon data are available in the Sierra Baguales, did not yield zircons representing group I, and obviously also lacks groups IV and V. However, 3 zircons belonging to group I were dated by us in samples from Cerro Castillo. This formation therefore contains groups I, IIe and IIIe. On the other hand, group I zircons do appear to be absent from the Man Aike Formation, as we found only groups IIe, IIIe and IV in Sierra Baguales, whereas the time-equivalent Loreto Formation in the vicinity of Punta Arenas yielded only groups IIIe and IV. It therefore seems that the Dorotea Formation still received some detritus from the Río de la Plata Craton or time-equivalent rocks to the north-northeast, but that this source area became obsolete during deposition of the Man Aike Formation, in which groups IIe, IIIe, and IV are strongly represented.

Although group IIe zircon ages (636–268 Ma) partially overlap with the maximum recorded ages (451–267 Ma) in the Eastern Andes Metamorphic Complex, 62% of the published ages of metamorphic complexes west of the Magallanes-Austral Basin (Hervé et al., 2008; fig. 1) fall in the gap of 250–160 Ma between groups IIe and IIIe. Moreover, zircons between 636 and 451 Ma are represented neither in these metamorphic complexes nor in the Southern Patagonian Batholith. Although group IIIe (160–65 Ma) zircons could have been derived from the latter, where the oldest recorded intrusion age is 157 Ma (Hervé et al., 2007), a source located to the west would contradict the majority of measured palaeocurrent directions.

The region northeast and east of the Magallanes-Austral Basin has a magmatic and metamorphic belt with Paleozoic basement and sedimentary rocks as well as granitoid intrusions, which could have contributed some of the group IIe zircons to the Dorotea and Man Aike Formations (Fig. 16). This prominent geomorphological feature, the

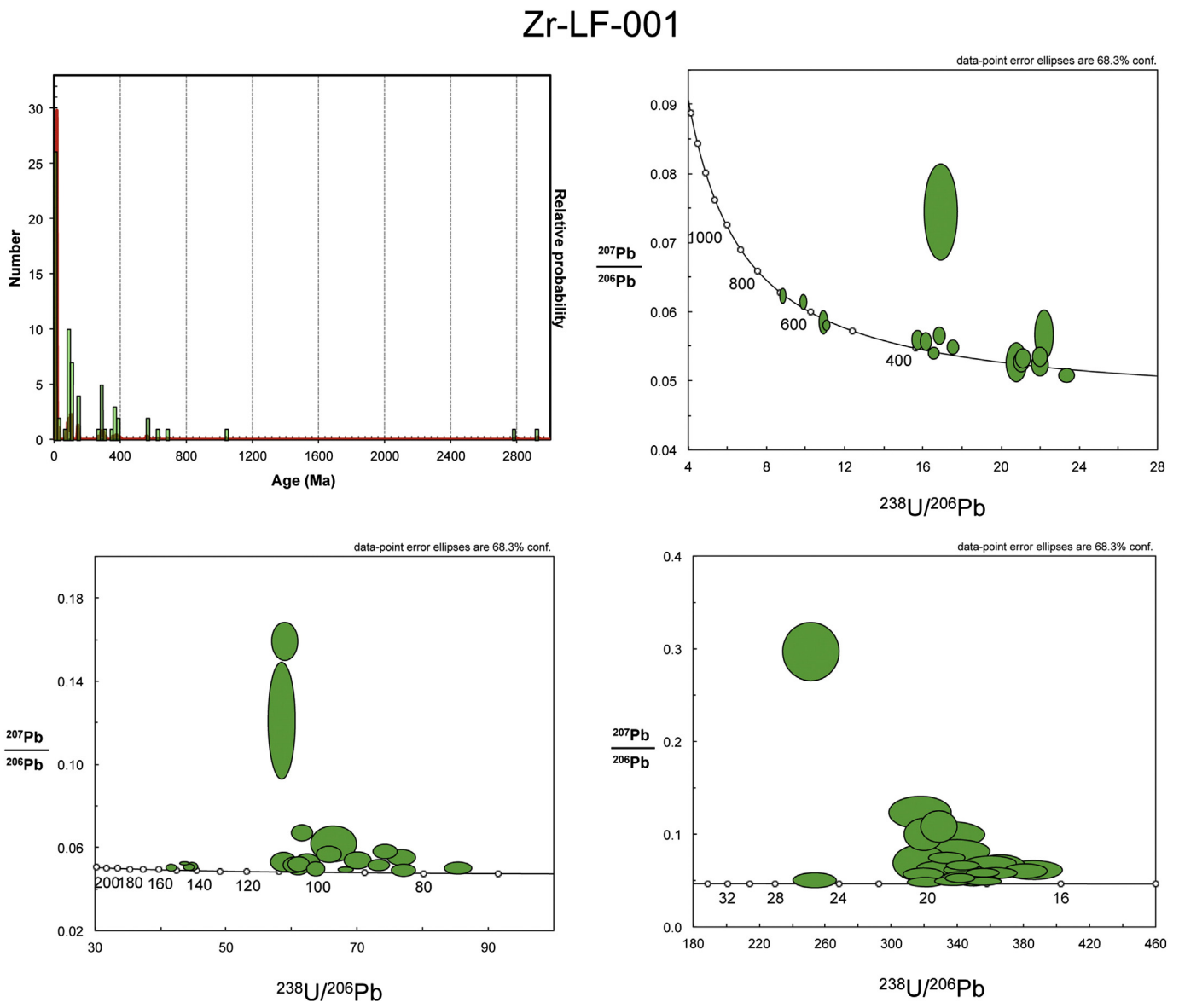

Fig. 15. U-Pb detrital zircon ages in sample ZR-LF-001 from the Santa Cruz Formation (after Bostelmann et al., 2013).

Western Magmatic Arc (e.g. Ramos, 2008), is known as the Río Chico-Punta Dúngenes Arc in its offshore, southeastern extension (Galeazzi, 1996; fig. 1; 16). The Western Magmatic Arc has plutonic and metamorphic rocks in which ages between 476 Ma and 344 Ma have been recorded (Ramos, 2008), and according to this author (Fig. 10) shed detritus westward into the Magallanes-Austral Basin. Another granite pluton in the Western Magmatic Arc with an age of 280 Ma (Ramos, 2008) could have contributed some of the younger zircons to group IIe. On the other hand, older zircons could have been derived from the Deseado Massif, which is situated between the Western Magmatic Arc and Magallanes-Austral Basin (Fig. 16) and where ages between 580 and 346 Ma have been recorded (Permuy Vidal et al., 2014). Basement rocks with ages between 536 and 527 Ma also occur to the southwest of Puerto Dúngenes (Fig. 16) (Hervé et al., 2008; Dickinson, 2009).

Alternatively, Jurassic and Cretaceous zircon populations identified in the Dorotea and Man Aike Formations could have been eroded from the rhyolitic Chon-Aike Province (Fig. 16), which overlaps with the Magallanes-Austral Basin and has plutons with the same ages (Gust et al., 1985; Pankhurst and Rapela, 1995). Some of the zircons in the Man Aike Formation could also have been reworked from the underlying Dorotea Formation, because it shows ample evidence of reworked fossils (e.g. shark teeth) from the latter formation and their contact is a prominent erosional unconformity.

The origin of group IIIe zircons (160–65 Ma) in the Dorotea, Man Aike, and Chorillo Chico Formations is more problematic if sources southeast of the Magallanes-Austral Basin are to be considered because of the recorded palaeocurrent directions. The basin does extend southeastward to the Magallanes-Fagnano Fault System in Fuegian Patagonia where it links up with the Falkland-Malvinas Basin, so that transport could easily have taken place along the basin axis (Fig. 16). However, this implies the existence of a hitherto unidentified point source in the vicinity of the present Cape Horn.

Finally, group IV zircons (50–30 Ma) in the Man Aike Formation were possibly eroded from intrusions of this age around the western exit of the Magellan Strait (Hervé et al., 2007), as some palaeocurrents suggest a possible source to the southwest (Fig. 10B).

In the Río Leona Formation both groups I and II zircons are absent, while groups IIIw and IV are well represented. Plutons with Jurassic-Cretaceous ages that could have provided group IIIw zircons (155–75 Ma) to the Río Leona Formation are common west of the Magallanes-Austral Basin (Fildani et al., 2003; Hervé et al., 2007). The majority are emplaced into the western flank of the Southern Patagonian

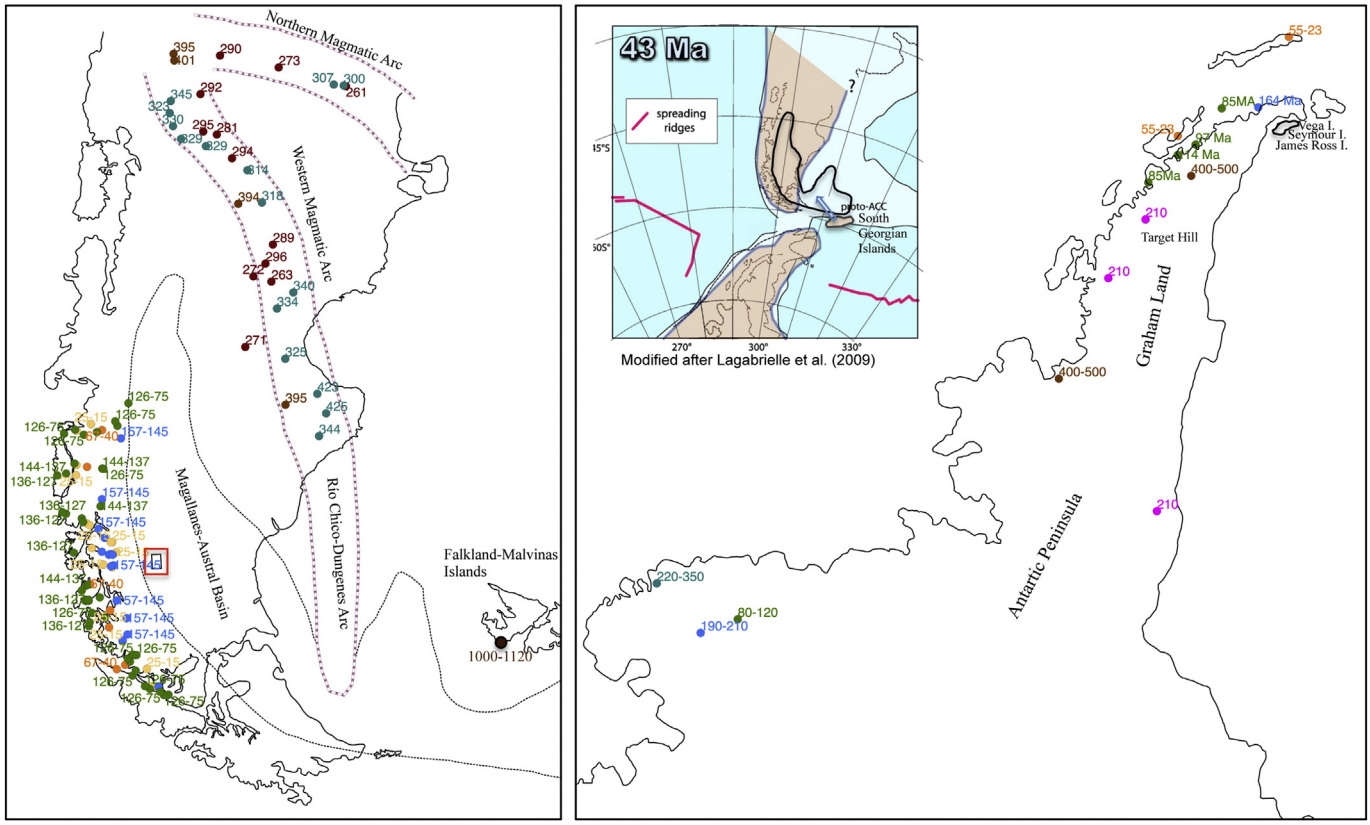

Fig. 16. Distribution of possible detrital zircon source rocks in southern South America and the Antarctic Peninsula. See text for references.

Andes where they form part of the Southern Patagonian Batholith, for example east of the Madre de Dios Archipelago and Duke de York Island around 50°–51°S, at the same latitude as the Sierra Baguales (Fig. 16). In this sector the vast majority of the plutons are of Jurassic to Cretaceous and Neogene age, with only one Paleogene date, which coincides with the zircon age gap between 67 and 49 Ma in the Río Leona Formation.

The absence of group IIe, having been replaced by group IIw in the Río Leona Formation, suggests that the source area had begun to shift by this time, but that group IV was still being contributed. The source of the latter was probably situated between the Pacific end of the Magallanes Strait and the Guadalupe Channel to the north, i.e. to the southwest of the Sierra Baguales (Fig. 16).

The Estancia 25 de Mayo Formation lacks groups I, IIw and IIIw, hosting only group IV, which reflects the dominance of the southwestern provenance that contributed to the Río Leona Formation.

The Santa Cruz Formation has zircons of group I, IIw, IIIw and V, being the only formation in the Sierra Baguales with group I zircons. In this case the Kalahari and Río de la Plata Cratons can be discarded as direct sources due to the recorded northwesterly palaeocurrent trend in the Santa Cruz Formation. However, the reworking of Jurassic and Cretaceous successions, such as the Tobífera, Zapata, Punta Barrosa and Cerro Toro Formations, which do have outcrops to the southwest and west of the Sierra Baguales, could have provided detrital zircons of Precambrian age, as such zircons are known to be present within these rocks. The erosion of these successions implies significant uplift and probably folding to the southwest and west of the Sierra Baguales, which would coincide with the observed change in palaeocurrent directions.

Finally, zircons of Neogene age ranging from 25 Ma to 15 Ma (group V) coincide with early to middle Miocene plutons dated by Hervé et al. (2007) in the Southern Patagonian Batholith between 50° and 51°S, directly to the west of the Sierra Baguales (Fig. 16).

8. Palaeobotany and palaeoclimate

A quantitative reconstruction of terrestrial paleoclimate can be made using fossil leaf morphology (e.g. Wolfe, 1995; Wilf, 1997; Mosbrugger and Utescher, 1997; Mosbrugger, 1999; Kowalski, 2002; Uhl et al., 2007). Estimations of the mean annual precipitation (MAP), mean annual temperature (MAT), and diversity according to the number of morphospecies, were based on 3746 fossil leaves collected at the localities of Barranca de las Hojas and Alto Río Bandurrias in the Río Leona Formation (Fig. 1). The fossil flora of this formation were compared to 4 fossil flora sites (Fig. 1) in Patagonia ranging in age from Paleocene to Eocene, which had been used previously to estimate the MAP and MAT as well as the diversity conditions (Wilf et al., 2005; Hinojosa et al., 2006; Iglesias et al., 2007). The Palacio de los Loros fossil flora of Paleocene age (61.7 Ma) represent a MAP of 166.3 cm, a MAT of 12.2 °C, and a diversity of 39 morphospecies (Hinojosa et al., 2006; Iglesias et al., 2007). The Early Eocene fossil flora of Ligorio Marquez (Hinojosa et al., 2016) indicate a MAP of 108–153 cm and a MAT between 17.2 °C and 20.9 °C, with a diversity of 55 morphospecies (Hinojosa et al., 2006, 2016). At Laguna el Hunco, the fossil floras are of early Eocene age (52 Ma), reflecting a MAP of 193.8 cm, a MAT between 14.8° and 17.7 °C, and a diversity of 122 morphospecies (Wilf et al., 2005; Hinojosa et al., 2011; Peppe et al., 2011; Quattrochio et al., 2013). Finally, the fossil flora of Río Turbio, with a middle Eocene age (45 Ma) indicate a MAP of 152.5 cm, a MAT between 16.1 and 18 °C, and a diversity of 45 morphospecies (Hinojosa, 2005; Hinojosa et al., 2011; Peppe et al., 2011; Quattrochio et al., 2013).

Our data indicate that the Río Leona Formation, with a Rupelian (early Oligocene) age, reflects a MAP of 55–74 cm based on multivariate analysis, and 92–96 cm according to the univariate method. As concerns the MAT, we estimate a range of 6.7 °C–7.7 °C according to the standard equations for Chile (MAT = 18.85 ∗ pE + 3.83) and South America (MAT = 26.03 ∗ pE + 1.31) (Hinojosa et al., 2011) and between 7.6

and 11 °C according to CLAMP (Climate Leaf Analysis Multivariate Program) (Wolfe, 1993, 1995; Kovach and Spicer, 1995; Wolfe and Spicer, 1999; Spicer, 2000; Spicer et al., 2004) including the CLAMP3bSA dataset (Hinojosa, 2005). Diversity in the Río Leona Formation includes a total of 24 dicotyledoneous morphospecies, in which the families *Nothofagacea*, *Mirtaceae*, *Cunoniacea*, *Sapindaceae*, *Gesneriaceae*, *Leguminosae*, *Monimiaceae*, *Grosulariaceae*, *Berberidaceae*, *Blechnaceae*, and *Podocarpaceae* stand out. These have a typical Mixed Flora phytogeographic character and indicate the oldest cold and dry forests in Patagonia.

The MAP, MAT and diversity conditions mentioned above illustrate the palaeoclimatic evolution and composition of forests in Patagonia, where Paleocene-Eocene, high-diversity forests flourishing under high precipitation and temperature conditions during the Eocene were replaced by low-diversity forests with low MAP and MAT conditions during the early Oligocene (Fig. 17).

The decrease in temperature recorded in the fossil flora of the Río Leona Formation between the Lutetian/Bartonian and early Oligocene coincides with the opening of the Drake Passage, which caused the first influx of Pacific sea-water into the Atlantic Ocean (Scher and Martin, 2006) and the development of the Antarctic Circumpolar Current (Barker, 2001). This event rang in the start of glaciation in Antarctica, as manifested in the global Oi-1 sea level fall (Zachos et al., 1996), an increase in deep-sea $\delta^{18}O$, and a decrease in atmospheric CO_2 (Zachos et al., 2001; Beerling and Royer, 2011). This cooling period, referred to as the Bartonian-Rupelian Cooling by Le Roux (2012a, 2012b), was not only subcontinent-wide but global. Independent records of palynomorph species diversity in the Río Leona Formation (Barreda et al., 2009) also indicate a decrease in temperature, and a similar trend is observed during the Cenozoic at tropical latitudes (Jaramillo et al., 2006).

On the other hand, the precipitation registers a decrease from 150 to 200 cm during the Paleocene and Eocene to less than 80 cm (55–70 cm) during the Oligocene. This decrease in precipitation went hand-in-hand with a decrease in morphospecies diversity in Patagonia, passing from 39 to 131 in the Paleocene fossil flora of Palacio de los Loros and the Eocene fossil flora of Laguna el Hunco, to only 29 morphospecies in the palaeoflora of the Río Leona Formation. The decrease in precipitation and morphospecies diversity in the Sierra Baguales can be related to the rise of the Southern Patagonian Andes as an orographic barrier to the Westerly Winds and creating a rain shadow to the east thereof, which is consistent with the abrupt change in palaeocurrent directions and zircon source areas between the Priabonian and Rupelian (~34 Ma). Topographic forcing on climate only begins to take effect at around 1000 m (Browning, 1980), so that this amount of uplift would have represented a major pulse in the Andean tectonic cycle. Palaeocurrents from the southwest at this time also agree with the present strike and dip of the Sierra Baguales strata, which are mainly tilted towards the northeast. It can therefore be postulated that tectonic compression at this time was directed from the southwest. At Cabo Nariz in Bahía Inútil (Fig. 1), our measured mean strike of 292° is consistent with this trend.

9. Discussion and conclusions

The different lines of evidence presented above, including the recorded changes in depositional environments, palaeocurrent directions, zircon source areas, and palaeoclimate, all coincide in the following sequence of tectonic events:

During the Late Cretaceous the depositional environment changed from a continental slope system with turbidites in the Tres Pasos Formation to deltaic conditions in the overlying Dorotea Formation. This shallowing-upward succession suggests that tectonic uplift started during the late Campanian. Palaeocurrents were rather variable with a full range between northeast and southeast, but being mainly from the east. The most probable source consisted of the Western Magmatic and Río Chico-Punta Dúngenes Arcs (as previously proposed by Ramos, 2008), as well as the rhyolitic Chon-Aike Province.

Tectonic uplift continued after deposition of the Dorotea Formation, causing a 30 m.y.-long period of erosion that lasted throughout the Paleocene and most of the Eocene (~70–40 Ma), ending with the deposition of the Man Aike Formation. The latter succession still received its detritus from the east and southeast, suggesting that the erosion was caused by tectonic uplift focused in this area. Although the eastern provenance can possibly still be attributed to the Río Chico-Punta Dúngenes Arc, the southeastern source needs another explanation. We propose that a local continental plate fragment was attached to the eastern end of Fuegian Patagonia and immediately to the south of the Falkland-Malvinas Plateau Basin. Our zircon data suggest that it may have formed part of the Antarctic Peninsula and/or its northeastern extension.

Zircon ages between 120 Ma and 80 Ma have been registered from the northern tip of the Antarctic Peninsula (Fig. 16) (Pankhurst, 1990). This area could also have contributed some group IIe zircons, as crystalline basement crops out at Target Hill and elsewhere in Graham Land (Fig. 16), where whole-rock ages of 410 ± 15 and 426 ± 12 Ma have been obtained (Milne and Millar, 1989).

The relative position of the Antarctic Peninsula with respect to southern South America during the Mesozoic and Cenozoic is still problematic (Miller, 2007), although many accept that it was located west of South America from the Middle to Late Jurassic (e.g., Grunow et al., 1987; Lawver and Scotese, 1987; Hanson and Wilson, 1991; Ghidella et al., 2002; Hervé and Fanning, 2003; Hervé et al., 2008; Breitsprecher and Thorkelson, 2009) and from there drifted southward along the South American Plate boundary. A problem with this interpretation is that Late Cretaceous and Cenozoic strike-slip faults in the Southern Patagonian Andes as well as on the eastern side of the Antarctic Peninsula are dominantly right-lateral (Storey and Nell, 1988; Diraison et al., 2000), which contradicts this notion. On the other hand, Seton et al. (2012; figs. 18–22) show the position of the Antarctic Peninsula as essentially unchanged to the south-southwest of Patagonia between 200 and 120 Ma, from where it drifted north and east, almost becoming a southward continuation of Fuegian Patagonia by 60 Ma. Diraison et al. (2000; fig. 3b and c) indicate this position to have been reached between 90 and 50 Ma, and that by the latter date, South Georgia was located along the northern boundary of the Scotia Plate. Several other authors have also indicated the position of the Antarctic Peninsula immediately to the south of Fuegian Patagonia during the Late Cretaceous (Barker and Lawver, 1988; Lagabrielle et al., 2009; Eagles, 2016a). It has also been suggested that the Antarctic Peninsula was a continuation of Fuegian Patagonia and Cordillera Darwin (Veevers et al., 1984; Pankhurst, 1990; Reguero et al., 2013) extending southeast of the Magallanes-Austral-Falkland-Malvinas Basin even during the Jurassic. However, Eagles (2016b) disputed the proximity of South Georgia to Tierra del Fuego during the Early Cretaceous.

An alternative northeastern extension of the Antarctic Peninsula is the small subsided banks of the Scotia Sea, including Terror Rise, Pirie Rise, and Bruce Bank, which Eagles and Jokat (2014) referred to as Omond Land. Given their present proximity to the Antarctic Peninsula and the South Orkney microcontinent, these could perhaps be more easily reconciled with the postulated southeastern source, which would have been removed by extension, rupture and subsidence during the Eocene.

If our proposal is correct that the northernmost tip of the Antarctic Peninsula and/or its northeastern extension was located immediately southeast of the Magallanes-Austral Basin during the Lutetian, this could have provided detritus to the Man Aike Formation along the northwest-trending basin axis. Uplift here could have been caused by the development of a transform fault with accompanying shoulder elevation, which can easily reach more than 1 km (Buck, 1986; Basile and Allemand, 2002). The most likely candidate here is the North Scotia Ridge, a left-lateral transform boundary forming the eastward extension

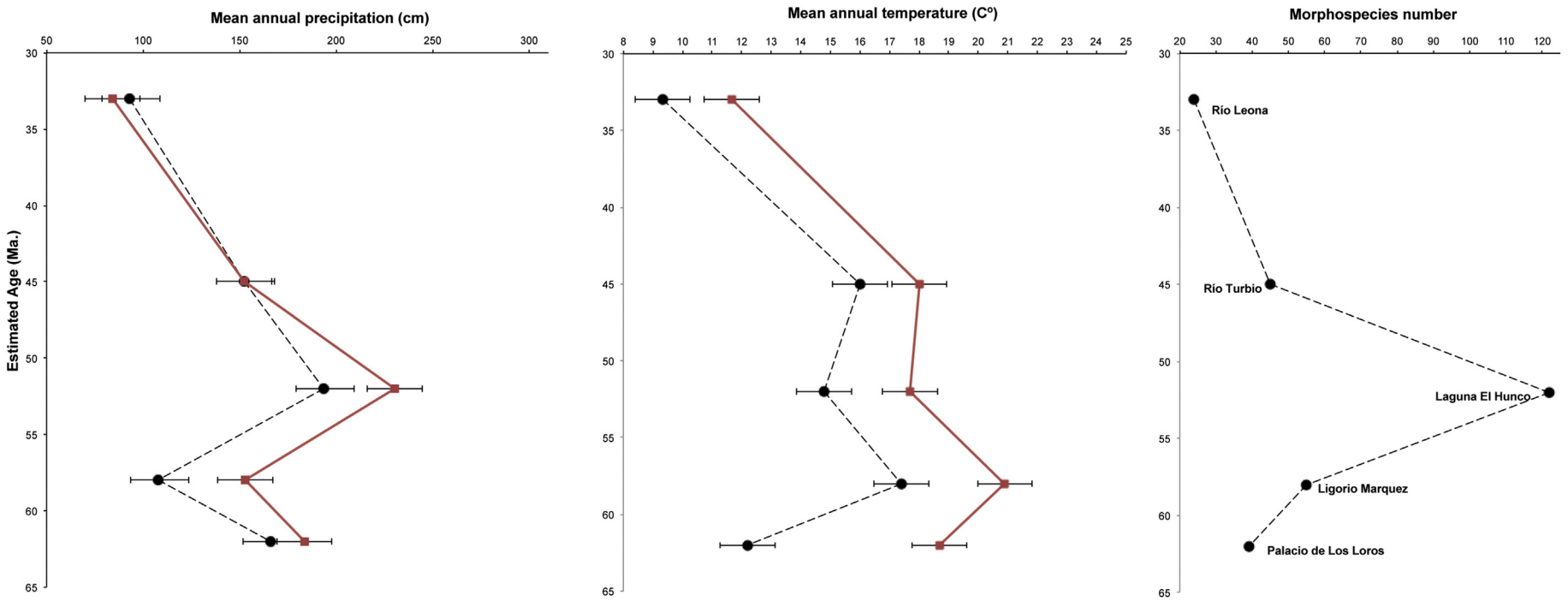

Fig. 17. Palaeoclimatic and palaeodiversity evolution in Patagonia as derived from fossil leaf morphology.

of the Magallanes-Fagnano Fault System in Fuegian Patagonia and stretching east to South Georgia, with a series of shallow banks in between (Eagles and Jokat, 2014). Geophysical surveys indicate that this ridge consists of mainly continental blocks, suggesting post-Cretaceous fragmentation of a formerly continuous continental area (Barker and Griffiths, 1972). It is still unclear whether the South Georgian Islands, presently located on the South American side of the plate boundary, are part of the Scotia Plate or have been recently accreted to the South American Plate (Thomas et al., 2003), but they could present vestiges of such an uplift shoulder. The original position of the South Georgia microcontinent was south of the Burdwood Bank and south of the Falkland-Malvinas Islands, from where it moved further east during the ongoing lengthening of the North Scotia Ridge (Dalziel et al., 2013). Considering the left-lateral movement along this ridge, this would imply that it was originally part of the Antarctic/Scotia Plate and could thus have formed, together with the submerged banks mentioned above, the northeastern extension of the Antarctic Peninsula. The Scotia Plate was formed mainly since a change in relative motion between the South American and Antarctic Plates during the Ypresian (~50 Ma) according to Pelayo and Wiens (1989). Marine geophysical data indicate that motion between the South American and Antarctic Plates at that time shifted from N-S to WNW-ESE, which was accompanied by an eightfold increase in the separation rate (Livermore et al., 2005).

There are many palaeontological similarities between the Antarctic Peninsula and the Magallanes-Austral Basin. For example, Aristonectinae (Plesiosauria) found in the Sierra Baguales are also found on Seymour Island (Gasparini et al., 1984; Chatterjee and Small, 1989; Fostowicz-Frelik and Gaździcki, 2001), James Ross Island (Otero et al., 2014) and Vega Island (O'Gorman et al., 2010) of the Antarctic Peninsula. South Pacific records are so far restricted to the Quiriquina Basin of central Chile, which according to Cecioni (1970) and Le Roux (2012a) was connected to the Magallanes-Austral Basin during the Late Cretaceous. However, plesiomorphic elasmosaurids were present in both the latter basin and the Antarctic Peninsula during the early Campanian, but only appeared in the Quiriquina Basin during the early Maastrichtian (Otero et al., 2015). Furthermore, palaeoichtyofauna of North Atlantic affinity present in both the Magallanes-Austral Basin and on Seymour Island include the chondrichtyan genera *Squatina*, *Pristiophorus*, and *Carcharocles* (Otero et al., 2013; Kriwet et al., 2016). Chondrichthyans were dominant elements in the Antarctic fish fauna during the Paleogene, but decreased in abundance from the middle to late Eocene, during which time bony fishes increased. This decline of chondrichthyans as registered in the Eocene La Meseta Formation on Seymour Island was related to the sudden cooling of seawater, reduction in shelf area, and increasing shelf depth according to Kriwet et al. (2016). Although these authors attributed their disappearance during the late Eocene to climatic conditions rather than plate tectonics, it could also be due to the development of a transform fault and ridge between southernmost South America and the northern tip of the Antarctic Peninsula. Lagabrielle et al. (2009) in fact show the latter immediately to the south of Patagonia at 43 Ma, from where it drifted to the east until 32 Ma, accompanied by strengthening of the Antarctic Circumpolar Current. Up to 25 Ma it was still drifting eastward along the Magallanes-Fagnano Transform Fault-Northern Scotia Ridge stretching from Fuegian Patagonia to the southern border of the Falkland-Malvinas Plateau, from where it began to move south with the development of an ocean ridge in the Drake Passage.

Palaeomagnetic studies indicate that the Antarctic Peninsula-block was located at or near its present-day position with respect to East Antarctica by ~130 Ma, while Antarctic Peninsula-block ~110 and ~85 Ma poles are similar to equivalent age poles from the East Antarctica-block, indicating that little or no relative motion between these two blocks occurred (Grunow, 1993). Poblete et al. (2011) also concluded from their palaeomagnetic studies in the Antarctic Peninsula that the small displacement between the latter and the East Antarctica-block during the Tertiary is probably not discernible by palaeomagnetism. Furthermore, Mid-Cretaceous poles in the northern and southern parts of the Antarctic Peninsula are alike, suggesting that the "S" shape of the peninsula was not due to oroclinal bending since 110 Ma (Grunow, 1993). Fitting the Antarctic Peninsula along the western border of the South American Plate during the Late Cretaceous would therefore require considerable counterclockwise rotation of both the former and East Antarctica to bring them into their present position and orientation. This should also be manifested in left-lateral instead of the observed right-lateral strike-slip faulting along the western side of South America and the eastern side of the Antarctic Peninsula. However, if the Antarctic Peninsula was initially located south-southwest of South America and then drifted north-northeast to become attached to the southeastern tip of Patagonia, it would explain the left-lateral strike-slip direction along the Magallanes-Fagnano Fault System and North Scotia Ridge. The right-lateral strike-slip faulting observed at the eastern side of the Antarctic Peninsula could be due to its southwestward drift along the South Scotia Ridge after separation from the South Georgian-Falkland-Malvinas continental fragment. This whole process would require very little rotation to bring it into its present orientation, which would agree with the 10° postulated by Poblete et al. (2011).The Man Aike Formation was deposited in a coastal (estuarine) environment, which indicates that uplift of the postulated ridge shoulder between the Scotia and South American Plates had come to an end by 40 Ma and that denudation or minor subsidence brought the region closer to base level.

Renewed uplift followed during deposition of the Río Leona Formation, maintaining a continental environment close to base level until the Rupelian (early Oligocene). The source areas by now had shifted to the southwest, reflecting the initial uplift of the Southern Patagonian Andes at around 34 Ma. This uplift led to the development of a rain shadow to the east of the latter, causing a marked decrease in precipitation. It was accompanied by a drop in temperature and a decrease in morphospecies diversity, which was also reflected globally at the time. This can be attributed to the complete separation of the Antarctic Peninsula from South America, with the final opening of the Drake Passage that allowed the generation of the Antarctic Circumpolar Current and the Bartonian-Rupelian Cooling period leading to the glaciation of Antarctica (Le Roux, 2012a).

A period of crustal subsidence occurred at around 19 Ma that caused the Patagonian Transgression, as reflected in the marine Estancia 25 de Mayo Formation. This was followed by a period of accelerated plate convergence together with slab detachment at around 17 Ma, causing another period of rapid uplift in the Southern Patagonian Andes. Apatite fission track ages from the western flank of the Andean segment suggest that 3–4 km of denudation occurred in this region since 17 Ma (Blisniuk et al., 2006). This uplift bought the Sierra Baguales area above base-level and led to the establishment of the continental depositional environment of the Santa Cruz Formation. Zircons probably derived from older, underlying formations were now being exposed to the west, suggesting that folding accompanied this uplift.

Acknowledgements

This research was financially supported by Project ANILLOS ATC-105 and Projects FONDECYT 1130006 and 1150690, being carried out under the auspices of Project CONICYT/FONDAP 15090013. N.M.G. is grateful for the grant "Beca CONYCYT de Estudios de Doctorado para Extranjeros en Chile". Detrital zircon dating was carried out by Mathieu Leisen in the Mass Spectrometry Laboratory of the Andean Geothermal Centre of Excellence. Victor Ramos and an anonymous reviewer provided much-appreciated comments which helped to improve this manuscript considerably.

References

Barbeau Jr., D.L., Olivero, E.B., Swanson-Hysell, N.L., Zahid, K.M., Murray, K.E., Gehrels, G.E., 2009. Detrital-zircon geochronology of the eastern Magallanes foreland basin:

implications for Eocene kinematics of the northern Scotia Arc and Drake Passage. Earth Planet. Sci. Lett. 284, 489–503.
Barker, P.F., 2001. Scotia regional tectonic evolution: implication for the mantle flow and paleocirculation. Earth-Sci. Rev. 55, 1–39.
Barker, P.F., Griffiths, D.H., 1972. The evolution of the Scotia Ridge and Scotia Sea. Philos. Trans. R. Soc. A Math. Phys. Eng. Sci. 271, 1213.
Barker, P.F., Lawver, L.A., 1988. South American-Antarctic plate motion over the past 50 Myr, and the evolution of the South American-Antarctic ridge. Geophys. J. Int. 94, 377–386.
Barreda, V., Palazzesi, L., Marenssi, S., 2009. Palynological record of the Paleogene Río Leona Formation (southernmost South America): stratigraphical and paleoenvironmental implications. Rev. Palaeobot. Palynol. 154, 22–33.
Basile, C., Allemand, P., 2002. Erosion and flexural uplift along transform faults. Geophys. J. Int. 151, 646–653.
Beerling, D.J., Royer, D.L., 2011. Convergent Cenozoic CO_2 history. Nat. Geosci. 4, 418–420.
Bernhardt, A., 2011. Paleogeography and Sedimentary Development of Two Deep-marine Foreland Basins: The Cretaceous Magallanes Basin, Southern Chile, and the Tertiary Molasse Basin, Austria. Unpubl. Ph.D. thesis. Stanford University (218 pp.).
Bernhardt, A., Jobe, Z.A., Lowe, D.R., 2008. The evolution of an elongate foreland basin: the deep to shallow-marine filling of the Cretaceous Magallanes Basin, Chile. 28th Annual GCSSEPM Foundation, Bob F. Perkins Research Conference, pp. 268–310.
Bernhardt, A., Jobe, Z.A., Lowe, D.R., 2011. Stratigraphic evolution of a submarine channel-lobe complex system in a narrow fairway within the Magallanes foreland basin, Cerro Toro Formation, southern Chile. Mar. Pet. Geol. 28, 785–806.
Biddle, K.T., Uliana, M.A., Mitchum Jr., R.M., Fitzgerald, M.G., Wright, R.C., 1986. The stratigraphic and structural evolution of the central and eastern Magallanes Basin, southern South America. In: Allen, P.A., Homewood, P. (Eds.), Foreland Basins. International Association of Sedimentologists, Special Publication 8, pp. 41–63.
Blisniuk, P.M., Stern, L.A., Chamberlain, C.P., Zeitler, P.K., Ramos, V.A., Sobel, E.R., Haschke, M., Strecker, M.R., Warkus, F., 2006. Links between mountain uplift, climate, and surface processes in the southern Patagonian Andes. The Andes, Active Subduction Orogeny. Ch. 20, Frontiers in Earth Sciences. Springer Verlag, Berlin, pp. 429–440.
Bossi, G.E., Vides, M.E., Ahumada, A.L., Georgieff, S.M., Muruaga, C.M., Ibañez, L.M., 2000. Análisis de las paleocorrientes y de la varianza de los componentes a tres niveles, Neógeno del valle del Cajón, Catamarca, Argentina. Rev. Asoc. Argent. Sedimentol. 7, 23–47.
Bostelmann, E., Le Roux, J.P., Oyarzún, J.L., Gutiérrez, N., Vasquez, A., Carreño, C., 2012. A new continental Late-Early Miocene (Burdigalian) fossil fauna from the Sierra Baguales, Magallanes, Chile. III Simposio – Paleontología en Chile, Punta Arenas, Chile.
Bostelmann, J.E., Le Roux, J.P., Vasquez, A., Gutiérrez, N.M., Oyarzún, J.-L., Carreño, C., Torres, T., Otero, R., Llanos, A., Fanning, C.M., Hervé, F., 2013. Burdigalian deposits of the Santa Cruz Formation in the Sierra Baguales, Austral (Magallanes) Basin: age, depositional environment and vertebrate fossils. Andean Geol. 40, 458–489.
Breitsprecher, K., Thorkelson, D.J., 2009. Neogene kinematic history of Nazca–Antarctic–Phoenix slab windows beneath Patagonia and the Antarctic Peninsula. Tectonophysics 464, 10–20.
Browning, K.A., 1980. Structure, mechanism and prediction of orographically enhanced rain in Britain. In: Hide, R., White, P.W. (Eds.), Orographic Effects in Planetary Focus. Global Atmospheric Research Programme Series 23, pp. 85–114.
Buck, W.R., 1986. Small-scale convection induced by passive rifting: the cause for uplift of rift shoulders. Earth Planet. Sci. Lett. 77, 362–372.
Calderón, M., Fildani, A., Herve, F., Fanning, C.M., Weislogel, A., Cordani, U., 2007. Late Jurassic bimodal magmatism in the northern sea-floor remnant of the Rocas Verdes basin, southern Patagonian Andes. J. Geol. Soc. Lond. 162, 1011e1022.
Cecioni, G., 1957. Età della flora del Cerro Guido e stratigrafía del Departamento Última Esperanza. Boll. Soc. Geol. Ital. 76, 3–16.
Cecioni, G., 1970. Esquema de Paleogeografia Chilena. Editorial Universitaria, Santiago (144 pp.).
Chatterjee, S., Small, B.J., 1989. New plesiosaurs from the Upper Cretaceous of Antarctica. In: Crame, J. (Ed.), Origins and Evolution of the Antarctic Biota. Geological Society, London Special Publication 47, pp. 197–215.
Crane, W.H., Lowe, D.R., 2008. Architecture and evolution of the Paine channel complex, Cerro Toro Formation (Upper Cretaceous), Silla Syncline, Magallanes basin, Chile. Sedimentology 55, 979–1009.
Cuitiño, J.I., 2011. Registro sedimentológico e isotópico de paleoambientes marinos y transicionales en el patagoniano (Mioceno) del Lago Argentino. Unpubl. Ph.D. thesis. Facultad de Ciencias Exactas y Naturales, Universidad de Buenos Aires.
Cuitiño, J.I., Pimentel, M.M., Ventura Santos, R., Scasso, R.A., 2012. High resolution isotopic ages for the early Miocene "Patagoniense" transgression in Southwest Patagonia: stratigraphic implications. J. South Am. Earth Sci. 38, 110–122.
Cuitiño, J.I., Ventura Santos, R., Muruaga, P.J.A., Scasso, R.A., 2015. Sr-stratigraphy and sedimentary evolution of early Miocene marine foreland deposits in the northern Austral (Magallanes) Basin, Argentina. Andean Geol. 42, 364–385.
Cuitiño, J.I., Ventura Santos, R., Scasso, R.A., 2013. Insights into the distribution of shallow marine/estuarine early Miocene oysters from Southwestern Patagonia: Sedimentologic and stable isotope constraints. PALAIOS 28, 583–598.
Dalziel, I.W.D., 1986. Collision and cordilleran orogenesis: An Andean perspective. In: Coward, M.P., Ries, A.C. (Eds.), Collision Tectonics. Geological Society, London Special Publication 19, pp. 389–404.
Dalziel, I.W.D., De Wit, M.J., Palmer, K.F., 1974. Fossil marginal basin in the southern Andes. Nature 250, 291–294.
Dalziel, I.W.D., Lawver, L.A., Norton, I.O., Gahagan, L.M., 2013. The Scotia Arc: genesis, evolution, global significance. Annu. Rev. Earth Planet. Sci. 41, 767–793.
Dickinson, W.R., 2009. Anatomy and global context of North American Cordillera. In: Kay, S.M. (Ed.), Backbone of the Americas: Shallow Subduction, Plateau Uplift, and Ridge and Terrane Collision. Geological Society of America, Memoir 204, pp. 1–60.
Diraison, M., Cobbold, P.R., Gapais, D., Rossello, E.A., Le Corre, C., 2000. Cenozoic crustal thickening, wrenching and rifting in the foothills of the southernmost Andes. Tectonophysics 316, 91–119.
Eagles, G., 2016a. Plate kinematics of the Rocas Verdes Basin and Patagonian orocline. Gondwana Res. 37, 98–109.
Eagles, G., 2016b. Tectonic reconstructions of the southernmost Andes and the Scotia Sea during the opening of the Drake Passage. In: Ghiglione, M.C. (Ed.), Geodynamic Evolution of the Southernmost Andes. Springer Int. Publ. AG, Switzerland, pp. 75–108.
Eagles, G., Jokat, W., 2014. Tectonic reconstructions for paleobathymetry in Drake Passage. Tectonophysics 611, 28–50.
Feruglio, E., 1938. El Cretácico superior del lago San Martín (Patagonia) y de las regiones adyacentes. Physis 12, 293–342.
Feruglio, E., 1949. Descripción Geológica de la Patagonia. Ministerio de Industria y Comercio de la Nación. Dirección General de Yacimientos Petrolíferos Fiscales 2, pp. 1–349.
Fildani, A., Hessler, A.M., 2005. Stratigraphic record across a retroarc basin inversion: Rocas Verdes- Magallanes Basin, Patagonian Andes, Chile. Geol. Soc. Am. Bull. 117, 1596–1614.
Fildani, A., Cope, T., Graham, S.A., Wooden, J., 2003. Initiation of the Magallanes foreland basin: timing of the southernmost Patagonian Andes orogeny revised by detrital zircon provenance analysis. Geology 31, 1081–1084.
Fosdick, J.C., Bostelmann, J.E., Leonard, J., Ugalde, R., Oyarzún, J.L., Griffin, M., 2015a. Timing and rates of foreland sedimentation: new detrital zircon U/Pb geochronology of the Cerro Dorotea, Río Turbio, and Río Guillermo formations, Magallanes Basin. XIV Congreso Geológico Chileno, La Serena, Chile.
Fosdick, J.C., Grove, M., Graham, S.A., Hourigan, J.K., Lovera, O., Romans, B.W., 2015b. Detrital thermochronologic record of burial heating and sediment recycling in the Magallanes foreland basin, Patagonian Andes. Basin Res. 27, 546–572.
Fosdick, J.C., Romans, B.W., Fildani, A., Calderón, M.N., Bernhardt, A., Graham, S.A., 2011. Kinematic history of the Cretaceous-Neogene Patagonia fold-thrust belt and Magallanes foreland basin, Chile and Argentina (51°30′S). Geol. Soc. Am. Bull. 123, 1679–1698.
Fostowicz-Frelik, Ł., Gaździcki, A., 2001. Anatomy and histology of plesiosaur bones from the Upper Cretaceous of Seymour Island, Antarctic Peninsula. In: Gaździcki, A. (Ed.), Palaeontological Results of the Polish Antarctic Expeditions. Part III. Palaeontologia Polonica 60, pp. 7–32.
Furque, G., 1973. Descripción geológica de la Hoja 58b Lago Argentino. Boletín del Servicio Nacional Minero y Geológico 140. Servicio Nacional Minero y Geológico, Buenos Aires, pp. 1–49.
Galeazzi, J.S., 1996. Cuenca de Malvinas. In: Ramos, V.A., Turic, M.A. (Eds.), Geología y Recursos Naturales de la Plataforma Continental Argentina. 13° Congreso Geológico Argentino y 3° Congreso de Exploración de Hidrocarburos, Buenos Aires, Relatorio 15, pp. 273–309.
Gasparini, Z., Del Valle, R., Goñi, R., 1984. An *Elasmosaurus* (Reptilia, Plesiosauria) of the Upper Cretaceous in the Antarctic. Boletín Del Instituto Antártico Argentino 305, pp. 1–24.
Ghidella, M.E., Yañez, G., LaBrecque, J.L., 2002. Revised tectonic implications for the magnetic anomalies of the Western Wedell Sea. Tectonophysics 347, 65–86.
González, E., 2015. Estratigrafía secuencial y sedimentología de la Formación Dorotea (Maastrichtiano), sector Río de las Chinas, Región de Magallanes y Antártica Chilena, Chile (50°S). Memoria, Departamento de Geología, Universidad de Chile.
Grunow, A.M., 1993. New paleomagnetic data from the Antarctic Peninsula and their tectonic implications. J. Geophys. Res. 98 (13815-13813).
Grunow, A.M., Kent, D.W., Dalziel, I.W.D., 1987. Mesozoic evolution of West Antarctica and the Weddell Sea Basin: new paleomagnetic constraints. Earth Planet. Sci. Lett. 86, 16–26.
Gust, D.A., Biddle, K.T., Phelps, D.W., Uliana, M.A., 1985. Associated Middle to Late Jurassic volcanism and extension in southern South America. Tectonophysics 116, 223–253.
Gutíerrez, N.M., Le Roux, J.P., Bostelmann, J.E., Oyarzún, J.L., Vásquez, A., Araos, J., Carreño, C., Ugalde, R., Otero, R., Fanning, C.M., Hervé, F., 2013. Geology and stratigraphy of Sierra Baguales, Última Esperanza Province, Magallanes, Chile. Geosur 2013, Viña del Mar, Chile.
Hanson, R.E., Wilson, T.J., 1991. Submarine rhyolitic volcanism in a Jurassic proto-marginal basin; southern Andes, Chile and Argentina. Geol. Soc. Am. Spec. Pap. 265, 13–28.
Hervé, F., Fanning, C.M., 2003. Early Cretaceous subduction of continental crust at the Diego de Almagro Archipelago, southern Chile. Episodes 26, 285–289.
Hervé, F., Calderón, M., Faúndez, V., 2008. The metamorphic complexes of the Patagonian and Fuegian Andes. Geol. Acta 6, 43–53.
Hervé, F., Massonne, H.-J., Calderón, M., Theye, T., 2004. Metamorphic P-T conditions of rhyolites in the Magallanes fold and thrust belt, Patagonian Andes. Bollettino di Geofísica teórica ed applicata, Extended Abstracts, International Symposium on the Geology and Geophysics of the Southermost Andes, the Scotia Arc and the Antartic Peninsula, Trieste, pp. 15–18.
Hervé, F., Pankhurst, R.J., Fanning, C.M., Calderón, M., Yaxley, G.M., 2007. The South Patagonian batholith: 150 my of granite magmatism on a static plate margin. Lithos 97, 373–394.
Hinojosa, L.F., 2005. Cambios climáticos y vegetacionales inferidos a partir de Paleofloras Cenozoicas del sur de Sudamérica. Rev. Geol. Chile 32, 95–115.
Hinojosa, L.F., Gaxiola, A., Perez, M.F., Carvajal, F., Campano, M.F., Quattrocchio, M., Nishida, H., Uemura, K., Yabe, A., Bustamante, R., Kalim, M.T., 2016. Non-congruent fossil and phylogenetic evidence on the evolution of climatic niche in the Gondwana genus *Nothofagus*. J. Biogeogr. 43, 555–567.
Hinojosa, L.F., Pérez, F., Gaxiola, A., Sandoval, I., 2011. Historical and phylogenetic constraints on the incidence of entire leaf margins: insights from a new South American model. Glob. Ecol. Biogeogr. 20, 380–390.
Hinojosa, L.F., Pesce, O., Yabe, A., Uemura, K., Nishida, H., 2006. Physiognomical analysis and paleoclimate of the Ligorio Márquez fossil flora, Ligorio Márquez Formation,

46°45′S, Chile. In: Nishida, H. (Ed.), Post Cretaceous Floristic Changes in Southern Patagonia, Chile. Chuo University, Tokyo, pp. 45–55.
Hoffstetter, R., Fuenzalida, H., Cecioni, G., 1957. Lexique Stratigraphique International, Amérique Latine. Fascicule 7, Chili. Centre National de la Recherche Scientifique, Paris (444 pp.).
Hubbard, S.M., Fildani, A., Romans, B.W., Covault, J.A., McHargue, T.R., 2010. High-relief slope clinoform development: insights from outcrop, Magallanes Basin, Chile. J. Sediment. Res. 80, 357–375.
Hubbard, S.M., Romans, B.W., Graham, S.A., 2008. Deep-water foreland basin deposits of the Cerro Toro Formation, Magallanes Basin, Chile: architectural elements of a sinuous basin axial channel belt. Sedimentology 55, 1333–1359.
Iglesias, A., Wilf, P., Johnson, K.R., Zamuner, A.B., Cúneo, N.R., Matheos, S.D., Singer, B.S., 2007. A Paleocene lowland macroflora from Patagonia reveals significantly greater richness than North American analogs. Geology 35, 947–950.
Jacobs, J., Pisarevsky, S., Thomas, R.J., Becker, T., 2008. The Kalahari Craton during the assembly and dispersal of Rodinia. Precambrian Res. 160, 142–158.
Jaramillo, C., Rueda, M., Mora, G., 2006. Cenozoic plant diversity in the Neotropics. Science 311, 1893–1896.
Jobe, Z.R., Bernhardt, A., Lowe, D.R., 2010. Facies and architectural asymmetry in a conglomerate-rich submarine channel fill, Cerro Toro Formation, Sierra del Toro, Magallanes Basin. J. Sediment. Res. 80, 1085–1108.
Katz, H.R., 1963. Revision of Cretaceous stratigraphy in Patagonian Cordillera of Última Esperanza, Magallanes Province, Chile. Am. Assoc. Pet. Geol. Bull. 47, 506–524.
Kovach, W.L., Spicer, R.A., 1995. Canonical correspondence analysis of leaf physiognomy: a contribution to the development of a new palaeoclimatological tool. Palaeoclimates 1, 125–138.
Kowalski, E.A., 2002. Mean annual temperature estimation based on leaf morphology: a test from tropical South America. Palaeogeogr. Palaeoclimatol. Palaeoecol. 188, 141–165.
Kriwet, J., Engelbrecht, A., Mörs, T., Reguero, M., Pfaff, C., 2016. Ultimate Eocene (Priabonian) chondrichthyans (Holocephail, Elasmobranchii) of Antarctica. J. Vertebr. Paleontol. http://dx.doi.org/10.1080/02724634.2016.1160911.
Lagabrielle, Y., Goddéris, Y., Donnadieu, Y., Malavieille, J., Suarez, M., 2009. The tectonic history of Drake Passage and its possible impacts on global climate. Earth Planet. Sci. Lett. 279, 197–211.
Lawver, L.A., Scotese, C.R., 1987. A revised reconstruction of Gondwanaland. Gondwana Six: Structure, Tectonics, and Geophysics. Geophysical Monograph Series 40. American Geophysical Union, pp. 17–23.
Le Roux, J.P., 1991. Paleocurrent analysis using Lotus 1-2-3. Comput. Geosci. 17, 1465–1468.
Le Roux, J.P., 1992. Determining the sinuosity of ancient fluvial systems from paleocurrent data. J. Sediment. Petrol. 62, 283–291.
Le Roux, J.P., 1994. The angular deviation in circular statistics as applied to the calculation of channel sinuosities. J. Sediment. Res. A64, 86–87.
Le Roux, J.P., 2012a. A review of Tertiary climate changes in southern South America and the Antarctic Peninsula. Part 1: oceanic conditions. Sediment. Geol. 247–248.
Le Roux, J.P., 2012b. A review of Tertiary climate changes in southern South America and the Antarctic Peninsula. Part 2: continental conditions. Sediment. Geol. 247-248, 21–38.
Le Roux, J.P., Puratich, J., Mourgues, A., Oyarzún, J.L., Otero, R.A., Torres, T., Hervé, F., 2010. Estuary deposits in the Río Baguales Formation (Chattian-Aquitanean), Magallanes Province, Chile. Andean Geol. 37, 329–344.
Linares, E., Cagoni, M.C., Do Campo, M., Ostera, H.A., 1988. Geochronology of metamorphic and eruptive rocks of southeastern Neuquen and northern Rıo Negro Provinces, Argentine Republic. J. S. Am. Earth Sci. 1, 53–61.
Livermore, R., Nankivel, A., Eagles, G., Morris, P., 2005. Paleogene opening of Drake passage. Earth Planet. Sci. Lett. 236, 459–470.
Macauley, R.V., Hubbard, S.M., 2013. Slope channel sedimentary processes and stratigraphic stacking, Cretaceous Tres Pasos Formation slope system, Chilean Patagonia. Mar. Pet. Geol. 41, 146–162.
Macellari, C.E., Barrio, C.A., Manassero, M.J., 1989. Upper Cretaceous to Paleocene depositional sequences and sandstone petrography of southwestern Patagonia (Argentina and Chile). J. S. Am. Earth Sci. 2, 223–239.
Malumián, N., 1990. Foraminíferos de la Formación Man Aike (Eoceno, Sureste Lago Cardiel), Provincia de Santa Cruz, Argentina. Rev. Asoc. Geol. Argent. 45, 365–385.
Malumián, N., 1999. La sedimentación en la Patagonia Extraandina. In: Caminos, R. (Ed.)- Instituto de Geología y Recursos Minerales, Geología Argentina, Anales Vol. 29, pp. 557–578.
Malumián, N., Nañez, C., 2011. The Late Cretaceous-Cenozoic transgressions in Patagonia and the Fuegian Andes: Foraminifera, paleoecology and paleogeography. Biol. J. Linn. Soc. 103, 269–288.
Marenssi, S.A., Casadio, S., Santillana, S.N., 2002. La Formación Man Aike al sur de El Calafate (Provincia de Santa Cruz) y su relación con la discordancia del Eoceno medio en la cuenca Austral. Rev. Asoc. Geol. Argent. 57, 341–344.
Marenssi, S.A., Limarino, C.O., Tripaldi, A., Net, L.I., 2005. Fluvial systems variations in the Rio Leona Formation: tectonic and eustatic controls on the Oligocene evolution of the Austral (Magallanes) Basin, southernmost Argentina. J. S. Am. Earth Sci. 19, 359–372.
Marenssi, S.A., Santillana, S.N., Net, L.I., Rinaldi, C.A., 2000. Facies conglomerádicas basales para la Formación Río Leona al sur del lago Argentino, Provincia de Santa Cruz, Argentina. Resúmenes, II Congreso Latinoamericano de Sedimentología y VIII Reunión Argentina de Sedimentología. Mar del Plata, pp. 109–110.
Martínez-Pardo, R., 1965. *Bolivinoides draco dorreeni* FINLAY from the Magellan Basin, Chile. Micropaleontology 11, 360–364.
Miller, H., 2007. History of views on the relative positions of Antarctica and South America: a 100-year tango between Patagonia and the Antarctic Peninsula. In: Cooper, A.K., Raymond, C.R. (Eds.), Antarctica: A Keystone in a Changing World – Online Proceedings of the 10th ISAES, USGS Open-File Report 2007-1047, Short Research Paper 041, p. 4.
Milne, A.J., Millar, I.L., 1989. The significance of mid-Palaeozoic basement in Graham Land, Antarctic Peninsula. J. Geol. Soc. Lond. 146, 207–210.
Mosbrugger, V., 1999. The nearest living relative method. In: Jones, T.P., Rowe, N.P. (Eds.), Fossil Plants and Spores: Modern Techniques. Geological Society, London, pp. 261–265.
Mosbrugger, V., Utescher, T., 1997. The coexistence approach—a method for quantitative reconstructions of Tertiary terrestrial palaeoclimate data using plant fossils. Palaeogeogr. Palaeoclimatol. Palaeoecol. 134, 61–86.
Muñoz, J., 1981. Geología y petrología de las rocas ígneas e inclusiones ultramáfcas del sector SW de Meseta Las Vizcachas, Ultima Esperanza, Magallanes, XII Región, Chile. (M.Sc. Thesis), Universidad de Chile, Departamento de Geología, Santiago.
Natland, M., González, E., Canon, A., Ernst, M., 1974. A system of stages for correlation of Magallanes Basin sediments. Geol. Soc. Am. Mem. 39 (126 pp.).
O'Gorman, J.P., Gasparini, Z., Reguero, M., 2010. *Aristonectes parvidens* Cabrera (Sauropterygia, Plesiosauria) from Cape Lamb, Vega Island (Upper Cretaceous), Antarctica. Scientific Committee on Antarctic Research (SCAR), Open Science Conference, No. 31, Abstract 557, Buenos Aires (1 pp.).
Otero, R., Oyarzún, J.-L., Soto-Acuña, S., Yury-Yáñez, R.E., Gutiérrez, N.M., Le Roux, J.P., Torres, T., Hervé, F., 2013. Neoselachians and Chimaeriformes (Chondrichthyes) from the latest Cretaceous-Paleogene of Sierra Baguales, southernmost Chile. Chronostratigraphic, paleobiogeographic and paleoenvironmental implications. J. S. Am. Earth Sci. 48, 13–30.
Otero, R.A., Soto-Acuña, S., Salazar, C., Oyarzún, J.-L., 2015. New elasmosaurids (Sauropterygia, Plesiosauria) from the Late Cretaceous of the Magallanes Basin, Chilean Patagonia: evidence of a faunal turnover during the Maastrichtian along the Weddellian Biogeographic Province. Andean Geol. 42, 237–267.
Otero, R.A., Soto-Acuña, S., Vargas, A.O., Rubilar-Rogers, D., Yury-Yáñez, R., Gutstein, C.S., 2014. Additions to the diversity of elasmosaurid plesiosaurs from the Upper Cretaceous of Antarctica. Gondwana Res. 26, 772–784.
Otero, R.A., Suárez, M.E., Le Roux, J.P., 2009. First record of elasmosaurid plesiosaurs (Sauropterygia: Plesiosauria) in upper levels of the Dorothea Formation, Late Cretaceous (Maastrichtian), Puerto Natales, Chiulean Patagonia. Andean Geol. 36, 342–350.
Pankhurst, R.J., 1990. The Paleozoic and Andean magmatic arcs of West Antarctica and southern South America. Geol. Soc. Am. Spec. Pap. 241, 1–7.
Pankhurst, R.J., Rapela, C.W., 1995. Production of Jurassic rhyolite by anatexis of the lower crust of Patagonia. Earth Planet. Sci. Lett. 134, 23–36.
Pankhurst, R.J., Leat, P.T., Sruoga, P., Rapela, C.W., Marquez, M., Storey, B.C., Riley, T.R., 1998. The Chon Aike province of Patagonia and related rocks in West Antarctica: a silicic large igneous province. J. Volcanol. Geotherm. Res. 81, 113–136.
Pankhurst, R.J., Riley, T.R., Fanning, C.M., Kelley, S.P., 2000. Episodic silicic volcanism in Patagonia and Antarctic Peninsula: chronology of magmatism associated with the breakup of Gondwana. J. Petrol. 41, 605–e625.
Parras, A., Dix, G.R., Griffin, M., 2012. Sr-isotope chronostratigraphy of Paleogene-Neogene marine deposits: Austral Basin, southern Patagonia (Argentina). J. S. Am. Earth Sci. 37, 122–135.
Paulcke, W., 1907. Die Cephalopoden de oberen Kreide Südpatagoniens. Berichte der Naturforschenden Gesellschaft zu Freiburg 15, pp. 1–82.
Pelayo, A.M., Wiens, D.A., 1989. Seismotectonics and relative plate motion in the Scotia sea region. J. Geophys. Res. 94, 7293–7320.
Peppe, D.J., Royer, D.L., Cariglino, B., Oliver, S.Y., Newman, S., Leight, E., Enikolopov, G., Fernandez-Burgos, M., Herrera, F., Adams, J.M., Correa, E., Currano, E.D., Erickson, J.M., Hinojosa, L.F., Hoganson, J.W., Iglesias, A., Jaramillo, C.A., Johnson, K.R., Jordan, G.J., Kraft, N.J.B.V., Lovelock, E.C., Lusk, C.H., Niinemets, Ü., Peñuelas, J., Rapson, J., Wing, S.L., Wright, I.J., 2011. Sensitivity of leaf size and shape to climate: global patterns and palaeoclimatic applications. New Phytol. 190, 724–739.
Permuy Vidal, C., Moreira, P., Guido, D.M., Fanning, C.M., 2014. Linkages between the southern Patagonia Pre-Permian basements: new insights from detrital zircons U-Pb SHRIMP ages from the Cerro Negro District. Geol. Acta 12, 137–150.
Piatnitzky, A., 1938. Observaciones geológicas en el oeste de Santa Cruz (Patagonia). Boletín de Informaciones Petroleras 165, pp. 45–85.
Poblete, F., Arriagada, C., Roperch, C., Astudillo, N., Hervé, F., Kraus, S., Le Roux, J.P., 2011. Paleomagnetism and tectonics of the South Shetland Islands and the northern Antarctic Peninsula. Earth Planet. Sci. Lett. 302, 299–313.
Quattrochio, M., Martínez, M., Hinojosa, L.F., Jaramillo, C., 2013. Quantitative analysis of Cenozoic palynofloras from Patagonia (southern South America). Palynology 37, 246–258.
Ramos, V.A., 2005. Seismic ridge subduction and topography. Foreland deformation in the Patagonian Andes. Tectonophysics 399, 73–86.
Ramos, V.A., 2008. Patagonia: a Paleozoic continent adrift? J. S. Am. Earth Sci. 26, 235–251.
Ramos, V.M., Kay, S.M., 1992. Southern Patagonian plateau basalts and deformation: back-arc testimony of ridge collisions. Tectonophysics 205, 261–282.
Ramos, V.A., Chemale, F., Naipauer, M., Pazos, P.J., 2014a. A provenance study of the Paleozoic Ventania System (Argentina): transient complex sources from Western and Eastern Gondwana. Gondwana Res. 26, 719–740.
Ramos, V.A., Litvak, V.D., Folguera, A., Spagnuolo, M., 2014b. An Andean tectonic cycle: from crustal thickening to extension in a thin crust (34°–37°SL). Geosci. Front. 5, 351–367.
Reguero, M., Goin, F.J., Acosta Hospitaleche, C., Dutra, T., Marenssi, S., 2013. West Antarctica: TECTONICS and paleogeography. Late Cretaceous/Paleogene West Antarctica Terrestrial Biota and Its Intercontinental Affinities. Springer Briefs in Earth System Sciences, pp. 10–17.
Riccardi, A.C., Rolleri, E.O., 1980. Cordillera Patagonia Austral. Segundo Simposio Geológico Regional Argentino, Cordoba, pp. 1163–1306.

Romans, B., Fildani, A., Graham, S., Hubbard, S., 2010. Importance of predecessor basin history on the sedimentary fill of a retroarc foreland basin: provenance analysis of the Cretaceous Magallanes Basin, Chile (50–52°S). Basin Res. 22, 640–658.
Ruddiman, W.F., Raymo, M.E., Prell, W.L., Kutzbach, J.E., 1997. The uplift-climate connection: a synthesis. In: Ruddiman, W.F. (Ed.), Tectonic Uplift and Climate Change. Plenum Press, New York, pp. 383–397.
Sánchez, A., Pavlishina, P., Godoy, E., Hervé, F., Fanning, C.M., 2010. On the presence of Upper Paleocene rocks in the foreland succession at Cabo Nariz, Tierra del Fuego, Chile: geology and new palynological and U-Pb data. Andean Geol. 37, 413–432.
Santos, J.O., Hartmann, L.A., Bossi, J., Campal, N., Schipilov, A., Pifieiro, McNaughton, N.J., 2003. Duration of the TransAmazonian Cycle and its correlation within South America b ased on U-Pb SHRIMP geochronology of the La Plata craton, Uruguay. Int. Geol. Rev. 45, 27–48.
Scher, H.D., Martin, E.E., 2006. Timing and climatic consequences of the opening of the Drake Passage. Science 312, 428–430.
Schwartz, T.M., Graham, S.A., 2015. Stratigraphic architecture of a tide-influenced shelf-edge delta, Upper Cretaceous Dorotea Formation, Magallanes-Austral Basin, Patagonia. Sedimentology 62, 1039–1077.
Schwartz, T.M., Fosdick, J.C., Graham, S.A., 2016. Using detrital zircon U-Pb ages to calculate Late Cretaceous sedimentation rates in the Magallanes-Austral Basin, Patagonia. Basin Res. http://dx.doi.org/10.1111/bre.12198, 1-22.
Scott, K.M., 1966. Sedimentology and dispersal pattern of a Cretaceous flysch sequence, Patagonian Andes, southern Chile. AAPG Bull. 50, 72–107.
Seton, M., Müller, R.D., Zahirovic, S., Gaina, C., Torsvik, T., Shephard, G., Talsma, A., Gurnis, M., Turner, M., Maus, S., Chandler, M., 2012. Global continental and ocean basin reconstructions since 200 Ma. Earth Sci. Rev. 113, 212–270.
Spicer, R.A., 2000. Leaf physiognomy and climate change. In: Culver, S.J., Rawson, P. (Eds.), Biotic Response to Global Change: The Last 145 million Years. Cambridge University Press, Cambridge, pp. 244–264.
Spicer, R.A., Herman, A.B., Kennedy, E.M., 2004. Foliar physiognomic record of climatic conditions during dormancy: Climate Leaf Analysis Multivariate Program (CLAMP) and the cold month mean temperature. J. Geol. 112, 685–702.
Storey, B.C., Nell, P.A.R., 1988. Role of strike-slip faulting in the tectonic evolution of the Antarctic Peninsula. J. Geol. Soc. Lond. 145, 333–337.
Thomas, C., Livermore, R., Pollitz, F., 2003. Motion of the Scotia Sea plates. Geophys. J. Int. 155, 789–804.
Torres, T., Cisterna, M., Llanos, A., Galleguillos, H., Le Roux, J.P., 2009. Nuevos registros de Nothofagus Bl. en Sierra Baguales, Última Esperanza, Patagonia, Chile. Extended Abstracts, XII Congreso Geológico Chileno, Santiago, Chile, pp. S12–S19.
Ugalde, R.A., 2014. Contribución al conocimiento de la estratigrafía cenozoica de la Sierra Baguales: la formación Man Aike ("Las Flores"). Provincia de Última Esperanza, Magallanes. Memoria de Título. Universidad de Chile (82 pp.).
Uhl, D., Klotz, S., Traiser, C., Thiel, C., Utescher, T., Kowalski, E., Dilcher, D.L., 2007. Cenozoic paleotemperatures and leaf physiognomy – a European perspective. Palaeogeogr. Palaeoclimatol. Palaeoecol. 248, 24–31.
Veevers, J.J., Powell, C.M.A., Collinson, J.W., López-Gamundí, O.R., 1984. Synthesis. In: Veevers, J.J., Powell, C.M.A. (Eds.), Permian-Triassic Pangean Basins and Foldbelts along the Pantalassian Margin of Gondwanaland. Geological Society, America, Memoir Vol. 184, pp. 331–352.
Wilf, P., 1997. When are leaves good thermometers? A new case for leaf margin analysis. Paleobiology 23, 373–390.
Wilf, P., Johnson, K.R., Cúneo, N.R., Smith, M.E., Singer, B.S., Gandolfo, M.A., 2005. Eocene plant diversity at Laguna del Hunco and Río Pichileufú, Patagonia, Argentina. Am. Nat. 165, 634–650.
Wolfe, J.A., 1993. A method of obtaining climatic parameters from leaf assemblages. U.S. Geol. Surv. Bull. 2040, 1–71.
Wolfe, J.A., 1995. Paleoclimatic estimates from Tertiary leaf assemblages. Annu. Rev. Earth Planet. Sci. 23, 119–142.
Wolfe, J.A., Spicer, R.A., 1999. Fossil leaf character states: multivariate analysis. In: Jones, T.P., Rowe, N.P. (Eds.), Fossil Plants and Spores: Modern Techniques. Geological Society, London, pp. 233–239.
Zachos, J., Pagani, H., Sloan, L., Thomas, E., Billups, K., 2001. Trends, rhythms, and aberrations in global climate: 65 Ma to present. Science 292, 686–693.
Zachos, J.C., Quinn, T.M., Salamy, S., 1996. High-resolution (104 years) deep-sea foraminiferal stable isotope records of the Eocene-Oligocene climate transition. Paleoceanography 11, 251–266.
Zahid, K., Barbeau Jr., D.L., 2010. Provenance of eastern Magallanes foreland basin sediments: heavy mineral analysis reveals Paleogene tectonic unroofing of the Fuegian Andes hinterland. Sediment. Geol. 229, 64–74.

ANEXO C2

PUBLICACIÓN EN PRIMER SIMPOSIO DE TECTÓNICA SUDAMERICANA

THRUST PROPAGATION AND SEDIMENTARY RESPONSE IN THE THRUST-BELT-FOREDEEP DEPOZONE SYSTEM OF THE PALEOGENE MAGALLANES BASIN, SOUTHERN CHILE

Huber Rivera [1], Jacobus P. Le Roux [2], Marcelo Farías [3]
1,2,3-Departamento de Geología, Universidad de Chile, Plaza Ercilla 803, Santiago, Chile;
1,2-Andean Geothermal Centre of Excellence, Plaza Ercilla 803, Santiago, Chile.

The progressive time-space eastward migration of the Magallanes (Austral) fold-belt-foredeep system, has been widely discussed and interpreted by over two decades as consequence of lithospheric plates-convergence. Nevertheless, the structural architecture of the deformation front and its strongly influence on the configuration of adjacent foredeep sedimentary basin does not seem to have been a subject of exhaustive research. Therefore, a reliable predictive model regarding to a thrust-related depositional sequences is still lacking. In this way, this work dealing with the relationship between active compressional tectonics and sedimentation at the foredeep depozone system of the foreland Magallanes basin, by using a detailed sedimentological study of the Paleogene rocks outcropping in the Brunswick Peninsula-Skyring Sound area, integrated with 2D seismic reflection survey, in order to construct a solid structural and seismic-stratigraphic model. We propose a new sedimentological framework that explains the stratigraphic architecture of the foreland basin and its sedimentary evolution during the Paleogene. In addition, the structural domains of the fold-thrust-belt can be described in terms of the tectono-stratigraphic setting of the basin, highlighting that the facies distribution, paleobathymetry and basin configuration reflects an overwhelming heritage from the predecessor Jurassic extensional events, where at least two different depocenters with independent sedimentation histories within the whole basin can be identified. Finally, this research shed light about the important potential for the presence of oil and gas reservoirs linked to deep-water turbidites in response to the growth and forward migration of the Patagonian Andes frontal thrust system which creates and/or enhanced stratigraphic and structural traps in the foredeep during the progressive deformation, in turn, the characterization of the deep-water sedimentation mechanisms, allows us a better understanding of the critically tapered wedge dynamics (=steep frontal ramp system) and its role in the development of the adjacent basin and sedimentary environments associated.